

Faculty of Mechanical Engineering

Department of Engineering Processes Automation
and Integrated Manufacturing Systems

Doctoral thesis

Modelling, testing, and optimisation of the efficiency of electric energy recovery systems from mechanical vibrations operating with the use of non-classical piezoelectric transducers

A thesis submitted in fulfilment of the requirements for the degree of

Doctor of Philosophy (PhD) in the Faculty of Mechanical Engineering,

Department of Engineering Processes Automation
and Integrated Manufacturing Systems

Demeke Girma Wakshume (M.Sc.)

Supervisor: Assoc. Prof. Marek Płaczek, Ph.D., DSc.

Co-supervisor: Dr Eng. Gabriela Fojt-Dymara

Gliwice 2026

Abstract

In recent years, technologies that capture energy from mechanical vibrations have advanced, offering an alternative for continuously powering small electronic devices and those with low power requirements. The energy harvested from mechanical vibrations is quite limited compared to other energy generation techniques. Utilising waste energy from environmental vibrations around a system presents a promising approach for creating self-powered electronic devices, which currently rely on batteries. This method can also be compactly integrated at the MEMS design level, ensuring high sensitivity to mechanical vibrations of low amplitude. The primary objective of this thesis is to design a model, then validate and optimise the performance of converting mechanical vibrations into electrical energy using non-classical Macro Fiber Composite (MFC-P2) piezoelectric materials for powering small electronic devices.

The key scientific contribution is an integrated framework that combines analytical modelling, finite element simulations, experimental verification, and numerical optimisation for vibration-based piezoelectric energy harvesters employing non-classical MFC materials. The first objective was to develop an analytical model of a unimorph aluminium cantilever beam that includes MFC piezoelectric material using Euler–Bernoulli beam theory together with the constitutive relations of piezoelectric materials. This model was used to determine the mode shapes, fundamental natural frequency, harvested voltage amplitude, and power output of the harvester, yielding a resonance frequency of 10.69 Hz, a maximum voltage of 0.265 V, and a corresponding power output of 0.00291 mW. The result of the analytical model was then verified through finite element modelling in COMSOL Multiphysics; by finite element modelling, the maximum output voltage was 0.28 V and a power output of 0.0032 mW at a resonance frequency of 10.96 Hz. After all, the model was validated against experimental tests. From the experimental validation, the maximum output voltage of 0.245 V and a power output of 0.00272 mW at a resonance frequency of 10.2 Hz were obtained. The result obtained from the theoretical, numerical, and experimental models shows that the energy harvester model has confirmed the validity of the developed modelling approach. The simulated and model-developed energy harvester results were compared with previously reported work; the results are highly correlated.

After experimental validation, the first improvement in harvester performance was through geometric variations of the energy harvester. For the tapered beam geometry, the FEM model

obtained a voltage of around 0.45 V compared to 0.28 V for the conventional rectangular beam, which was an increase of 60.71%. The maximum output power of 0.0065 mW as compared to the conventional rectangular beam of 0.0032 mW. This is a 103.13% increase in power output at the first natural frequency of 12.42 Hz.

Another model considered a tapered beam with a tip mass and MFC patches attached at different locations, which gave a higher voltage and power for the same applied force compared to the rectangular beam-with-tip-mass configuration. The improvement was attributed to a larger bending moment near the clamped end and a more uniform strain distribution over the tapered region. The configuration generated 40.6% more voltage at an input point force of 0.5 N, and the maximum power near the root was improved by 131.57% compared to a rectangular beam harvester with tip mass. An additional important aspect in improving the harvesting efficiency was the parametric optimisation of the MFC patch placement, along with the tip mass and beam thickness. The combined optimisation of the MFC placement, tip mass and beam thickness resulted in maximum power outputs of 0.0095 mW and 0.022 mW for the rectangular and tapered beam configurations, respectively. Across all configurations modelled, the combination of tapered beam geometry with optimised MFC patch placement consistently produced the highest harvested energy compared with the conventional rectangular cantilever energy harvester, a result that held across all three optimisation criteria: beam geometry, tip mass, and MFC patch placement.

In the last phase of the work, algorithm-based optimisation was carried out over the entire range of the geometric and electromechanical parameters that influence the performance of the harvester: shape of the beam (rectangular versus tapered rectangular), position of the MFC patch from the fixed support (X_p), thickness of the beam (t_b), size of the tip mass (t_m), value of the load resistance (R_{Load}) and magnitude of the applied force (F), all of which influence the mode shape, natural frequency, voltage and power output. The electromechanical coupling behaviour was simulated in COMSOL Multiphysics, and the *BOBYQA* (Bound Optimisation BY Quadratic Approximation) algorithm was used to optimise. The first optimisation algorithm (*BOBYQA*) modelled a rectangular beam with an MFC, yielding a maximum power of 0.028 mW and a voltage of 0.95 V, with a resonant frequency of approximately 10.61 Hz. The MFC patch was placed about 5 mm from the fixed support, where the bending strain is maximum. The corresponding beam thickness and tip mass dimension for the parametric optimisation were 2.2 mm and 1.26 mm, respectively.

The same BOBYQA algorithm optimisation applied to the tapered rectangular beam resulted in a peak harvested power of 0.065 mW, an output voltage of 2.3 V and a resonant frequency of 12 Hz. Compared with the rectangular beam harvester, this configuration resulted in a twofold increase in the output voltage and a 2.4-fold increase in the harvested power. The corresponding design optimum parameters were X_p = 5.46 mm, t_b = 2.17 mm, t_m = 1.12 mm, R_{Load} = 12 kΩ, and F = 0.26 N. The mechanical advantage of the tapered geometry is that it distributes the bending strain more uniformly along the beam, thus increasing the average strain experienced by the MFC patch and therefore the overall electromechanical energy conversion efficiency.

As a whole, the combined effect of tapered geometry and systematic algorithm-based optimisation of MFC patch placement, tip mass, beam thickness and load resistance is significantly more effective than relying on geometric modification or parametric variation alone. Future work should extend this work to bimorph configurations, the effects of temperature, nonlinear deformation and novel machine-learning or surrogate-modelling approaches to reduce the computational cost of exploring large design spaces covering material composition, geometry, and circuit parameters.

Streszczenie

W ostatnich latach nastąpił postęp w dziedzinie technologii pozyskujących energię z drgań mechanicznych, co stanowi alternatywę w odniesieniu do ciągłego zasilania małych urządzeń elektronicznych oraz tych o minimalnym zapotrzebowaniu na energię. Chociaż energia pozyskiwana z drgań mechanicznych jest dość ograniczona w porównaniu z innymi technikami wytwarzania energii, zastosowanie energii odpadowej pochodzącej z drgań otoczenia wokół systemu stanowi obiecujące podejście do tworzenia urządzeń elektronicznych z własnym zasilaniem, które obecnie opierają się na bateriach. Metodę tę można również kompaktowo zintegrować na poziomie projektowania układów MEMS, zapewniając wysoką czułość na drgania mechaniczne o małej amplitudzie.Głównym celem niniejszej pracy jest opracowanie modelu, a następnie weryfikacja i optymalizacja wydajności systemu przekształcania drgań mechanicznych w energię elektryczną z zastosowaniem nieklasycznych materiałów piezoelektrycznych typu Macro Fibre Composite (MFC-P2) w celu zasilania niewielkich urządzeń elektronicznych. Kluczowym wkładem naukowym pracy jest zintegrowana struktura łącząca modelowanie analityczne, symulacje metodą elementów skończonych, weryfikację eksperymentalną oraz optymalizację numeryczną piezoelektrycznych urządzeń pozyskujących energię z drgań, w których zastosowano nieklasyczne materiały MFC.

Głównym celem było opracowanie modelu analitycznego jednorodnej aluminiowej belki wspornikowej zawierającej materiał piezoelektryczny typu MFC z zastosowaniem teorii belek Eulera–Bernoulliego w połączeniu z zależnościami konstytutywnymi materiałów piezoelektrycznych. Model ten użyto do określenia postaci drgań, częstotliwości drgań własnych, amplitudy napięcia pozyskanego oraz mocy wyjściowej urządzenia pozyskującego energię, uzyskując pierwszą częstotliwość rezonansową wynoszącą 10,69 Hz, maksymalne napięcie 0,265 V oraz odpowiadającą mu moc wyjściową 0,00291 mW. Wyniki modelu analitycznego zweryfikowano następnie za pomocą modelowania metodą elementów skończonych w programie COMSOL Multiphysics. Modelowanie to wykazało maksymalne napięcie wyjściowe wynoszące 0,28 V oraz moc wyjściową 0,0032 mW przy częstotliwości rezonansowej 10,96 Hz. Ostatecznie model zweryfikowano w oparciu o testy eksperymentalne. W wyniku walidacji eksperymentalnej uzyskano maksymalne napięcie wyjściowe wynoszące 0,245 V oraz moc wyjściową wynoszącą 0,00272 mW przy częstotliwości rezonansowej 10,2 Hz. Wyniki uzyskane z modeli teoretycznych, numerycznych i eksperymentalnych wskazują, że model urządzenia do pozyskiwania energii potwierdził słuszność opracowanego podejścia

modelowego. Wyniki symulacji i opracowanego modelu systemu do pozyskiwania energii porównano z wynikami opublikowanymi wcześniej, wykazując wysoką korelację.

Po walidacji eksperymentalnej, pierwszą poprawę wydajności harvestera zaobserwowano dzięki zmianom geometrycznym w jego konstrukcji. W przypadku analizowanej belki stożkowej (o zmniejszającej sie szerokośći), w wyniku analizy MES uzyskano napięcie 0,45 V w porównaniu z 0,28 V w przypadku konwencjonalnej belki prostokątnej, co stanowi wzrost o 60,71%. Maksymalna moc wyjściowa wyniosła 0,0065 mW w porównaniu z konwencjonalną belką prostokątną o mocy 0,0032 mW. Stanowi to wzrost mocy wyjściowej o 103,13% przy pierwszej częstotliwości drgań własnych 12,42 Hz.

W kolejnym modelu uwzględniono belkę stożkową z masą skupioną na swobodnym końcu i przetwornikiem MFC przymocowanym w różnych pozycjach, przez co uzyskano wyższe napięcie i moc przy tej samej przyłożonej sile w porównaniu z konfiguracją belki prostokątnej z masą skupioną na swobodnym końcu. Poprawę przypisano większemu momentowi zginającemu w pobliżu utwierdzonego końca i bardziej równomiernemu rozkładowi odkształceń w obszarze stożkowym. Konfiguracja wygenerowała o 40,6% więcej napięcia przy sile wzbudzającej 0,5 N, a maksymalna uzyskiwana moc układu została poprawiona o 131,57% w porównaniu z belką o stałym przekroju prostokątnym i z masą skupioną. Dodatkowym ważnym aspektem poprawy wydajności systemu była parametryczna optymalizacja rozmieszczenia przetwornika MFC, masy skupionej i grubością belki, w wyniku której uzyskano maksymalną mocą wyjściową układu wynoszącą 0,0095 mW i 0,022 mW odpowiednio w przypadku prostokątnej i stożkowej konfiguracji zastosowanej belki wspornikowej. We wszystkich modelowanych konfiguracjach, stosując połączenie stożkowej geometrii belki ze zoptymalizowanym rozmieszczeniem przetwornika MFC uzyskiwano najwyższą energię w porównaniu z konwencjonalnym układem belki prostokątnej.

W ostatniej fazie prac przeprowadzono optymalizację opartą na algorytmie w całym zakresie parametrów geometrycznych i elektromechanicznych mających wpływ na wydajność systemu odzysku energii z drgamechanicznych: kształt belki (prostokątny kontra zwężający się), odległość przetwornika MFC od utwierdzonego końca belki wspornikowej (Xp), grubość belki (t_b), wymiary masy końcówki (t_m), wartość oporu obciążenia (R_{Load}) oraz wielkość przyłożonej siły (F) – wszystkie te parametry mają wpływ na postacie drgań, częstotliwość drgań własnych, napięcie oraz moc wyjściową. Zachowanie sprzężenia elektromechanicznego zasymulowano w programie COMSOL Multiphysics, a do optymalizacji zastosowano algorytm BOBYQA (Bound Optimisation BY Quadratic Approximation). Początkowo algorytm

optymalizacyjny (BOBYQA) zastosowano do prostokątnej belki z ogniwem MFC, co dało maksymalną moc 0,028 mW i napięcie 0,95 V przy częstotliwości rezonansowej wynoszącej około 10,61 Hz. Przetwornik MFC umieszczono w odległości 5 mm od utwierdzenia belki, gdzie odkształcenie zginające jest największe. Odpowiednie wartości grubości belki i masy skupionej dodanej na jej końcu po optymalizacji parametrycznej wynosiły odpowiednio 2,2 mm i 1,26 mm. Tę samą metodę optymalizacji zastosowana do zwężającej się belki, otrzymując szczytową moc pozyskaną wynoszącą 0,065 mW, napięcie wyjściowe 2,3 V oraz częstotliwość rezonansową 12 Hz. Prowadzi to do wzrostu napięcia i mocy – dwukrotnego w przypadku napięcia i 2,4-krotnego w przypadku mocy – w porównaniu z ukadem odzysku energii opartym na belce prostokątnej. Odpowiednie parametry projektowe tej konfiguracji to: Xp = 5,46 mm, t_b = 2,17 mm, t_m = 1,12 mm, R_{Load} = 12 kΩ oraz F = 0,26 N. Zaletą zastosowanej geometrii stożkowej jest to, że rozkłada ona odkształcenie zginające bardziej równomiernie wzdłuż belki, zwiększając w ten sposób średnie odkształcenie odczuwane przez płatek MFC, a co za tym idzie ogólną sprawność konwersji energii elektromechanicznej.

Zastosowanie geometrii stożkowej oraz systematycznej optymalizacji pozycji przetwornika MFC, masy skupionej, grubości belki i nośności jest znacznie skuteczniejszy niż poleganie wyłącznie na modyfikacjach geometrycznych lub zmianach parametrów. W zakresie dalszych prac należy rozszerzyć niniejsze badania o konfiguracje bimorficzne, uwzględnić wpływ temperatury oraz odkształceń nieliniowych, a także zastosować podejścia oparte na uczeniu maszynowym lub modelowaniu zastępczym w celu zmniejszenia wymaganego nakładu czasu i mocy obliczeniowej związaneych z badaniem rozległych przestrzeni projektowych, obejmujących rodzaj materiałów, geometrię i parametry obwodów elektrycznych.

Acknowledgements

This thesis is the result of my four years as a research student. I wish to express my sincere gratitude to those who have accompanied me in achieving my goal. First, I would like to express my thanks to my supervisor Professor Marek Płaczek for his continuous guidance, encouragement, and support throughout my PhD studies at the Silesian University of Technology Faculty of Mechanical Engineering. This dissertation would not have been possible without his guidance. He gave me the freedom to develop my research ideas and was a valuable source of insightful advice when asked.

Working with such an informed and supportive scholar has been a truly rewarding experience. I deeply appreciate his sense of responsibility towards his students and his guidance for my future in research and life. The past four years under his supervision have been among the most memorable of my academic life, and I could not have asked for a better research experience. I would also like to thank my co-supervisor Dr Eng. Gabriela Fojt Dymara for her time and help and for generously sharing her knowledge and experience.

I would like to express my thanks to Dr DSc Eng. Andrzej Wróbel, Prof. PŚ and Dr Eng. Jacek Harazin for their valuable suggestions and continuous support during my PhD studies. Their expertise and considered feedback enhanced the quality and rigour of this research. I am also very thankful to the staff members of the Faculty of Mechanical Engineering, Department of Engineering Processes, Automation, and Integrated Manufacturing Systems, for giving me the opportunity to conduct this research successfully. It has been an honour to begin my career at SUT.

Finally, I would like to thank my family and friends sincerely for their love, support, and encouragement during my PhD studies. Without their understanding and continued support this dissertation could not have been completed.

Table of Contents

Abstract I
Streszczenie IV
Acknowledgements VII
Table of Contents VIII
List of Figures XI
List of Tables XIII
Abbreviations and Symbols XIV
Chapter 1 Introduction 1
1.1. Piezoelectric energy harvesting and modelling mechanism 1
1.2. Research gaps 3
1.3 Objective 4
1.4 Motivation 5
1.5. Original contribution and significance of the thesis 7
1.6. Outline of the thesis structure 9
Chapter 2 Literature review 11
2.1. Vibration energy harvesting mechanism 11
2.2. Mechanical vibration-based energy harvesting mechanism 14
2.3. Sources of vibration 18
2.4. Piezoelectricity 18
2.4. Piezoelectric Materials 20
2.5. Piezoelectric mode of operation 26
2.6. Fundamentals of piezoelectricity 30
2.7. Piezoelectric Energy Harvesting working mode and Configuration 36
2.8. Modelling mechanical vibration based piezoelectric energy harvesters 41
2.8.1 Analytical modelling of piezoelectric based energy harvesting 41
2.9 Optimizing performance of energy harvesting systems 43
2.9.1 Optimisation Methods for PEH in COMSOL Multiphysics 45
2.9.2 Choosing the appropriate Method for a parametric optimisation 48
2.9.3 Local and global parametric optimization selection 48
2.10. Applications of energy harvested from piezoelectric materials 49
Chapter 3 Analytical modelling 53
3.1. Analytical linear modelling of MFC Piezo with cantilever beam 53

3.1.1 Modelling method 54
3.2. Modelling of electromechanical coupling equation 55
3.3. Mechanical equation 59
3.4. Mode shape and natural frequency analysis for the electrotechnical coupling 69
3.5. Voltage and power for the analytical model 74
Chapter 4 Finite Element Modelling 77
4.1 Numerical modelling using finite element method 78
4.2 Geometric and material properties of the Substrate and energy harvester 80
4.2.1 Design parameter of substrate and energy harvester 81
4.2.2 Mechanical damping model 83
4.3 Analysis of simulation results for the finite element method model 83
4.4.1 Natural Frequencies and modal analysis of a Cantilever Beam 84
4.4 Comparison between theoretical and numerical models 92
Chapter 5 Experimental validation 95
5.1. Sample preparation 95
5.2. Description of experimental procedures and system identification 99
5.3 Result and discussion of experimental model 101
5.4. Comparison of the theoretical, FEM and experimental model 104
Chapter 6 Parametric optimisation of piezoelectric harvesters 109
6.1. Improving the efficiency of the piezoelectric energy harvesting systems 109
6.1.1 Geometric parametric optimization 111
6.1.2 The effect of adding tip mass at the free end of the energy harvester 115
6.1.2.1 Tip mass with rectangular beam 115
6.1.2.2 Tip mass with tapered rectangular beam 119
6.2. The effect of MFC patch location on energy harvesting efficiency 122
6.2.1 MFC placement for the rectangular beam without tip mass 122
6.2.2 MFC placement on the rectangular beam with tip mass 126
6.2.3 MFC placement on the tapered rectangular beam without tip mass 128
6.2.4 MFC Pach placement on the tapered rectangular beam with tip mass 130
6.3. Parametric optimization EH based on the variable thickness of the substrate 133
6.3.1 Effect of substrate thickness on the efficiency of EH from a rectangular beam 134
6.3.2 Influence of variable substrate thickness on a tapered beam 138
6.4. Optimisation by algorithm including parameters and constraints 144
6.4.1 Algorithm optimisation rectangular cantilever beam with MFC 145

6.4.2 Optimisation of a tapered rectangular cantilever beam with MFC configuration..151
Chapter 7 Conclusions and Future Work 160
7.1. Conclusion 160
7.2. Future work recommendation 164
List of scientific achievements 166
A. Publication related with my PhD thesis: 166
B. Book chapter/ monograph and international conference participation 166
C. Internship and mobility participation 167
References 169
Appendix :1 MAT LAB script 182
MATLAB script for the analytical mode shapes and natural frequencies 182
Analytical Voltage and Eigenfrequencies Model 184
Voltage and frequency obtained from the experimental work 185
Experimental, theoretical, and numerical voltage and power with Eigenfrequency 186

List of Figures

Figure 2-1 Block diagram for EH from mechanical vibration of piezoelectric materials 12
Figure 2-2.Mechanism of piezoelectric effect [1,73]..... 19
Figure 2-3 Macro Fiber Composite Material (type P2) structural component [117]..... 25
Figure 2-4 PEH mode: a) piezoelectric mode 3-1, (b) piezoelectric mode 3-3 27
Figure 2-5 The basic summary of piezoelectric categories based on different properties..... 30
Figure 2-6 Schematic of the MFC piezoelectric with rectangular cantilever beam EH 39
Figure 3-1 Geometry of the aluminium cantilever beam with unimorph MFC PEM 54
Figure 3-2 The first four modes' shapes and natural frequency by line graph 74
Figure 3-3 Analytical frequency Response with Voltage for linear vibration energy harvester 75
Figure 3-4 Analytical power and resonance frequencies of energy harvester 75
Figure 4-1 COMSOL Multiphysics coupling for simulation..... 78
Figure 4-2 schematic Aluminium cantilever beam unimorph patched with MFC..... 80
Figure 4-3 The components of Macro fiber Composites from model on COMSOL Multiphysics 80
Figure 4-4 Schematic of the EH MFC with a unimorph rectangular substrate model and mesh .. 85
Figure 4-5 The mode shapes and natural frequencies for numerical model..... 86
Figure 4-6 Displacement amplitude versus frequency for analytical model 88
Figure 4-7 3D mode shape and natural frequency, COMSOL Multiphysics modelled..... 89
Figure 4-8 Von Mises stress of EH at MFC is 65 mm from the fixed support end 90
Figure 4-9 Voltage and Power versus Eigen frequency of the for rectangular EH..... 90
Figure 4-10 Voltage and power under with different external resistances..... 91
Figure 4-11 The theoretical and numerical models of voltage and power..... 94
Figure 5-1 Unmorphed MFC-P2 sample prepared for experimental testing..... 96
Figure 5-2 Schematic model of the experiment for validation 97
Figure 5-3 The overall experimental setup for MFC vibration energy harvester 100
Figure 5-4 Experimental voltage versus frequency response at constant resistance load 103
Figure 5-5 The experimental frequency responses vs power harvester with a load resistor 103
Figure 5-6. Experimental, theoretical, and numerical voltage with frequency..... 106
Figure 5-7 Comparison of power for experimental, theoretical, and numerical model..... 106
Figure 6-1 Schematic of a tapered beam with unimorph MFC energy harvester geometry..... 113
Figure 6-2 Mode shape and eigenfrequency and 3D Model for tapered beam EH 114
Figure 6-3 The FE simulation of the MFC with the tapered beam..... 114
Figure 6-4 A schematic representation of EH integrated with a tip mass..... 115
Figure 6-5 The model and the first mode shape and eigenfrequency when a tip mass is applied 118

Figure 6-6 Mode shape and natural frequency by line graph with tip mass 119
Figure 6-7 The effect of adding tip mass on the voltage and power..... 119
Figure 6-8 Geometrical model and resonance frequency of tapered beam with the tip mass 121
Figure 6-9 Voltage and output power for tapered EH within tip mass added free end..... 121
Figure 6-10 Mode shape and natural frequency when MFC attached at different place 123
Figure 6-11 3D mode shape and natural frequency when MFC placed at different location 124
Figure 6-12 The von Mises stress along the rectangular cantilever energy harvester 124
Figure 6-13 The voltage versus frequency response for various placements of MFC 125
Figure 6-14 The power output and resonance frequency with various placements of the MFC .. 125
Figure 6-15 Mode shape versus resonance frequency with tungsten tip mass 127
Figure 6-16 Frequency versus Voltage for a rectangular cantilever beam shape with a tip mass 127
Figure 6-17 Frequency versus power for a rectangular cantilever beam with a tip mass..... 128
Figure 6-18 Mode shape and natural frequency by line graph for tapered beam 129
Figure 6-19 Frequency and voltage magnitude at the resonance modes for tapered beam 129
Figure 6-20 Frequency and power for the tapered beam 130
Figure 6-21 Mode shape and eigen frequency by Line Graph for tapered beam with tip mass ... 132
Figure 6-22 Frequency versus Voltage, for tapered beam with tip mass 132
Figure 6-23 Power output versus frequency for tapered beam with tip mass..... 133
Figure 6-24 The mode shape, natural frequency, and displacement with different thickness 136
Figure 6-25 Variation of voltage over frequency for different substrate thicknesses 137
Figure 6-26 The power versus excitation frequency for different thicknesses 137
Figure 6-27 Mode shapes and eigenfrequencies of tapered beams with variable thickness..... 140
Figure 6-28 Eigenfrequency with the variable thickness for a tapered rectangular beam..... 141
Figure 6-29 Parametric study for displacement varying thickness for a cantilever beam EH..... 141
Figure 6-30 Parametric study for varying the thickness on Voltage and frequency 142
Figure 6-31 The effect of parametric study for varying the thickness of tapered beam EH..... 142
Figure 6-32 Flowchart for Optimisation of Energy Harvesting in COMSOL Multiphysics 146
Figure 6-33 The influence of geometric parameters on voltage and output power 148
Figure 6-34 The optimum amplitude, voltage and outputs power..... 149
Figure 6-35 Amplitude displacement and the optimised energy for tapered beam 153

List of Tables

Table 2-1 Summary of mechanical vibration energy harvesting mechanism 17
Table 2-2 The common PEM and their advantages, disadvantages, and applications..... 28
Table 2-3 PEH operation frequency, output energy, application area, and their limitations..... 50
Table 3-1 Geometry, mechanical and material properties of energy harvester..... 73
Table 3-2 Natural frequency for the theoretical model..... 74
Table 4-1 Geometric parameters and material properties of unimorph beam PEH..... 82
Table 4-2 The natural frequencies for analytical and numerical..... 93
Table 5-1 The physical dimensions, geometric characteristics, and material properties..... 98
Table 5-2 Voltage and output power from experiments with frequencies 102
Table 5-3 The comparison of the 1st natural frequencies of the model. 105
Table 5-4 Comparison of EHM for the theoretical, numerical, and experimental 105
Table 5-5 Comparison of voltage and power at fundamental frequency for all model 107
Table 6-1 Mechanical properties of the tip mass and its dimensions 116
Table 6-2 The natural frequencies' variation due to tip mass added at the free end beam 117
Table 6-3 EH performance of a rectangular beam at different substrate thicknesses..... 137
Table 6-4 Voltage and power versus frequency for tapered beam EH with substrate thickness... 143
Table 6-5 Optimisation Parameters and Control Variables rectangular beam 147
Table 6-6 Optimisation result analysis for rectangular harvester 150
Table 6-7 Design variables for the optimisation for the tapered beam..... 151
Table 6-8 Optimisation result for tapered rectangular beam with MFC..... 152
Table 6-9 Comparison of Algorism optimised EH by rectangular and tapered models 154
Table 6-10 Summary of the results from the initial model to the fully optimised design 158

Abbreviations and Symbols

EH	Energy harvesting
VEH	Vibration energy harvesting
IoT	Internet of things
WLS	Smart wireless sensor
SHM	Structural health monitoring
MVEH	Mechanical vibration energy harvesting
PEM	Piezoelectric energy materials
PZT	Lead zirconate titanate
MFC	Macro Fiber composite
IDE	Interdigitated Electrodes
PVDF	Polyvinylidene fluoride
MEMS	Micro electromechanical system
GVEH	Gravitational electromagnetic energy harvesting
V	Voltage
Al	Aluminium
Q	Charge
L_P	Length of piezo materials
W	Watt
ϕ	Magnetic flux
D	Electric displacement
S	Strain
σ	Stress
T	Matrix transposition
F	Force
t	Thickness
d	Piezoelectric strain coefficient
ε	Dielectric permittivity
v	Volume
E	Electric field
d_{31}	Piezoelectric polarisation along the thickness
d_{33}	Piezoelectric strain coefficient along the beam length
g_{33}	Piezoelectric voltage coefficient
P_{pe}	Piezoelectric polarisation vector
S_{pe}	Mechanical strain by the reverse piezoelectric effect

σ_{pe}	Stress produced by an electric field (converse effect)
${s_{11}}^{E}$	Compliance / elastic compliance at constant electric field
w_b	Width of beam
t_b	Beam thickness
L_b	Beam length
$p_{(t)}$	Concentrated point load
I_b	Second moment inertia of a beam
$\phi_{i(x)}$	Mode shape function
ω_n	Natural angular frequency
SF	Shear force
t_p	Thickness of MFC
k_{eff}	Effective stiffness
f_n	Natural frequency
V_ω	Voltage magnitude at the natural frequency
R_L	Load resistance
C_p	Capacitance
ς	Power damping ratio
P	Generated Power
A_b	Beam area
A_p	MFC area
y_b	Beam centroid from the bottom
y_p	MFC centroid from the bottom
E_b	Stiffness of beam
E_p	Stiffness of beam
E_{eq}	Equivalent flexural modulus
$\dot{m}$	Mass per unit length
ρ_{eq}	Equivalent area density
SF	Shear force
BM	Bending moment
PO	Parametric Optimisation

Chapter 1 Introduction

This chapter outlines the introductory section of the thesis, which focuses on a piezoelectric mechanism for harvesting energy from mechanical vibrations. It explains the motivation behind the research and identifies the existing gap in the literature. Then the objectives of the thesis and concludes with original contributions and overall significance of the thesis.

1.1. Piezoelectric energy harvesting and modelling mechanism

Recent developments in wireless sensor networks, wearable electronics, biomedical devices, smart infrastructure, structural health monitoring systems, the Internet of Things (IoT), and microelectromechanical systems (MEMS) have significantly increased the demand for compact, durable, and self-powered energy sources. However, these devices rely on batteries as their power supply [1–3]. Batteries have a finite lifetime and must be replaced periodically. Battery replacement can be exceedingly difficult because many wireless sensors are installed in remote or difficult-to-reach locations. This limitation disrupts the operation of wireless sensors and restricts their broader deployment [1,4–6]. Battery maintenance requirements limit the long-term operation of devices, especially in inaccessible or hazardous environments [1,7,8].

Energy harvesting (also known as 'energy scavenging' [9,10]) has emerged as a promising alternative for powering low-power electronic devices by converting ambient energy into usable electricity. Different environmental energy sources such as solar, thermal, radiofrequency, wind and mechanical vibrations can be harvested using suitable energy conversion mechanisms. Among these sources, mechanical vibration is of particular interest due to its omnipresence in industrial machines, vehicles, civil infrastructure, and human motion, which makes it a reliable source to power autonomous electronic devices [2,11–13]. Each source requires specific conversion mechanisms to efficiently convert that energy into usable electrical power for powering a wide range of applications, from small sensors and wearable devices to large-scale power generation [2,4].

There are three main transduction methods for converting mechanical vibration energy into electrical energy: electromagnetic, electrostatic, and piezoelectric. Among these, piezoelectric energy harvesting (PEH) has attracted much attention due to its simple structure, small size, high energy density, and the ability to directly convert mechanical strain to electrical energy without an external power source. Therefore, piezoelectric energy harvesters are widely used in

wireless sensor networks, structural health monitoring, biomedical devices, wearable electronics, and industrial monitoring systems [1,12,14,15].

Usually, piezoelectric energy harvesters use brittle piezoceramic materials, such as lead zirconate titanate (PZT). However, these materials are not flexible and tend to crack under repeated mechanical loading. To address these limitations, macro fibre composite (MFC) piezoelectric materials have been developed. MFC is made of piezoelectric fibres embedded in an epoxy matrix and protected with a flexible Kapton layer, which gives better flexibility, durability and electromechanical performance. These features make MFC materials particularly suitable for harvesting energy from low-frequency vibration and structures with complex geometry.

Piezoelectric energy harvesting has made great progress, but there are still some challenges. Most current harvesters output low electrical power and are efficient only around their resonant frequencies. Moreover, the influence of structural geometry, tip mass and piezoelectric patch location on the overall energy harvesting performance is not well understood, especially for harvesters based on non-classical piezoelectric materials, such as MFCs. However, complete studies including analytical modelling, finite element analysis, experimental validation, and structural optimisation are still not available.

The aim of this PhD research is thus to model, test and optimise the efficiency of electrical energy harvesting from mechanical vibrations using non-classical Macro Fibre Composite (MFC-P2) piezoelectric materials. Macro-Fiber Composites (MFC) are characterised by their flexibility of large deformation. However, the energy generated by MFC is still far smaller than that required by electronics at present. It is designed to take advantage of the d_{31} mode of vibration. In this thesis, a vibration energy harvesting system using MFC patches bonded to an aluminium cantilever beam is modelled and simulated. First, an analytical electromechanical model is developed based on Euler-Bernoulli beam theory and validated by finite element modelling in COMSOL Multiphysics and experimental measurements, respectively. Then the effects of beam geometry, tip mass and MFC patch placement on voltage output, power generation and resonant frequency are studied to find an optimal harvester configuration. The results will help to design and optimise high-performance vibration energy harvesters for self-powered sensing and other low-power electronic applications.

1.2. Research gaps

Piezoelectric energy harvesting (PEH) is commonly utilised as a power source for small electronic devices because of its high energy density and ease of integration into different systems. It produces small amounts of electrical power for applications in remote or inconvenient locations such as wireless sensor networks (WSNs) and microelectromechanical systems (MEMS) without causing disruptions of operations and maintenance [16]. However, the conventional electrochemical battery is used as an energy storage unit; however, there are limited capacity, life cycle, weight, and size limitations, as well as the leakage of chemical solutions [17]. An important aspect in the design and development of piezoelectric energy harvesters is the optimisation of the output power. Energy harvesting and power management units must be compact enough to be integrated into the host device, as small electronic devices typically consume power in the mW or μW range. There are several ways to convert the mechanical energy of vibrating or moving structures into electrical energy to power electronic devices, such as electrostatic induction, piezoelectric effect and electromagnetic induction [17–19].The increasing application of piezoelectric energy harvesting materials in different industrial fields has made the correct design and optimisation of these devices ever more important. Piezoelectric devices are widely used for actuation and sensing in applications like precision positioning systems [20]. Among available piezoelectric materials, monolithic piezoceramic materials such as lead zirconate titanate (PZT) are the most widely used materials for energy recovery. However, classical PZT material patches are very fragile and cannot support large vibration amplitudes [5,13]. Piezoelectric polymers are robust and flexible to damage; however, piezoelectric polymer materials have poor actuation capability, which limits their application [21,22]. Therefore, to overcome these limitations, a piezoelectric composite material has been developed by integrating piezoceramic fibers into a polymer matrix, such as epoxy. Such composites with high piezoelectric properties of ceramic materials combined with the flexibility and mechanical durability of polymers are suitable for energy harvesting applications. These advances in mechanical reliability, flexibility and electrical output have given a boost to the interest in piezoelectric composite materials and have spurred further studies in this field. As a result, the energy harvester's efficiency depends not only on the piezoelectric transducer but also on how well it is integrated into the electrical circuit [23–29].The development of more efficient piezoelectric transducers, such as non-classical composite and functionally graded designs, offers new opportunities to harvest electrical energy from mechanical vibrations. These developments are particularly promising for the

improvement of the electromechanical conversion efficiency and the overall performance of the piezoelectric energy harvesting systems. For energy harvesting, modelling is essential because modelling represents both forward and reverse piezoelectric effects and is integrated within a hosting geometry [30]. While piezoelectric materials can generate relatively high power density, the absolute power generated by especially MFC harvesters under low-frequency and low-amplitude excitation can still be limited. To enhance problems, different PE materials, electromechanical coupling, and electrical circuit design and modelling are interesting area [31]. Macro Fiber Composite is a new piezoelectric material; its capability of harvesting energy has not been fully investigated [32]. There are limitations to using single-phase piezoelectric materials such as PZT and PVDF in vibration energy harvesting. The monolithic piezoelectric materials have good piezoelectricity, but they are brittle. Harvesters with large vibration amplitude and large deflection may easily damage piezoelectric ceramics since they lack the required flexibility. The piezoelectric polymers are quite flexible, but they also have very weak piezoelectricity. Therefore, piezoelectric composites, which have better flexibility than monolithic materials and better piezoelectricity than polymers, are widely studied and used for vibration energy harvesting [33]. Hence, this thesis addresses a gap by investigating the MFC-P2 mode of PE transducers for energy harvesting by analytical modelling, numerical simulation, experimental validation and optimisation of MFC-based geometric configurations for energy harvesting systems. In particular, an integrated approach comprising mathematical modelling, finite element analysis, experimental investigation, numerical optimisation and sensitivity analysis is required to identify the impact of mechanical parameters on the harvested power. Filling this gap may contribute to a better understanding of the electromechanical behaviour of non-classical composite piezoelectric transducers and to the development of more efficient vibration-based energy harvesting systems for low-power electronic applications.

1.3 Objective

This thesis aims to address some fundamental gaps in research observed within the field of Macro Fiber Composite piezoelectric vibrational energy harvesting. The main objective of this thesis is to model, experimentally validate, and numerically optimise parameters for enhancing the efficiency of non-classical MFC-P2 piezoelectric materials in recovering electrical energy from mechanical vibrations, with a particular focus on determining the main parameters that affect its energy-harvesting efficiency.

The specific objectives of this doctoral thesis are as follows:

- To review the piezoelectric materials used for energy harvesting from mechanical vibrations.
- To develop mathematical models of the Macro Fiber Composite (MFC) piezoelectric transducer electromechanical coupling using constitutive equations.
- To develop a finite element model and perform numerical modelling using COMSOL Multiphysics based on geometric configuration, shape, size, boundary conditions, and material properties.
- To experimentally validate the analytical and numerical models through laboratory testing and investigate the effect of operating conditions on the performance of the energy harvesting system.
- To analyse the results from analytical and numerical simulation model and experimental testing.
- To determine the key parameters that affect the performance of the energy harvester and to optimise the finite element model to maximise the energy harvesting efficiency from mechanical vibration systems.

1.4 Motivation

Macro Fiber Composite (MFC) are smart materials widely employed in vibration control, energy harvesting, and structural health monitoring because of their high mechanical flexibility, enhanced strength, environmentally sealed construction, and strong blocking force [27]. They provide excellent performance, durability, and adaptability while remaining a cost-effective solution [27]. It was developed by NASA in 1996. Smart. Since then, the MFC has been continuously improved and tailored to the specific needs of clients. MFC technology enables the fabrication of small, perfectly matched Fiber actuators with a thickness of only
a few tenths of a millimetre. Today, power-wireless and portable electronic devices are becoming an integral part of our living environment in applications ranging from environmental control, energy harvesting, and structural health monitoring to factory automation. As these devices decrease in size and increase in number, batteries are no longer a practical energy source due to the costs of installation, replacement, and disposal. An affordable and sustainable alternative energy source for small electronic solutions is urgently needed to achieve fully self-contained and maintenance-free systems. With the advancement of autonomous, low-powered,

self-powered electronic devices, energy consumption has been reduced [15]. The first motivation of this research is to power small electronic components by converting the waste vibration energy available in their environment into electrical energy using a non-classical piezoelectric material which is called Macro Fiber Composite transducer. Vibration energy exists everywhere, and this type of energy can be converted into electrical energy through piezoelectric, electromagnetic, and electrostatic transducers. Compared with electromagnetic and electrostatic approaches, piezoelectric materials offer high electromechanical coupling, high energy density, high energy conversion efficiency, flexibility in system integration, and well-developed micro- and macro-scale manufacturing techniques. In addition, they can generate electrical charge directly when subjected to mechanical strain. Research and literature reviews have demonstrated the effectiveness of this approach [5,7,34,35].

These materials have been effectively used as actuators and sensors in recent years, in addition to energy harvesting and structural health monitoring. The direct piezoelectric effect is widely used for sensing and energy harvesting. However, the coupling between these two effects is often omitted in analyses. Due to their ease of use in creating thin-layer structures, composites based on PZT fibers are among the most extensively researched materials for mechanical energy harvesting, wireless sensor technology, and low-power portable electronics that operate without an external power source. The term "non-classical piezoelectric materials" is used here to describe piezoelectric materials that extend beyond conventional bulk lead zirconate titanate (PZT) ceramics. These materials include lead-free ceramic families such as barium titanate, potassium sodium niobate, sodium bismuth titanate-based ceramics, and bismuth ferrite-related compositions; polymer-based materials such as polyvinylidene fluoride (PVDF), PVDF copolymers, and polylactic acid; polymer-ceramic composites; nanostructured thin films; Macro Fiber Composites; and flexible piezoelectric nanogenerator materials.

The growing interest in these non-classical materials is driven not only by environmental sustainability considerations but also by their advantageous properties, including mechanical flexibility, low density, conformability, ease of processing, biocompatibility, and suitability for curved, flexible, and wearable surfaces. If the efficiency of MFC is further improved, they may become more suitable than lead zirconate titanate (PZT) for real-world applications because of their attractive flexibility. Additionally, in real industrial energy-harvesting scenarios, it is advantageous to use an off-resonance approach with MFC patches directly attached to areas of maximum stress. MFCs are particularly suitable for this approach because of their flexibility, conformability, and anisotropic force coupling characteristics.

The limitations associated with conventional power supply systems and classical piezoelectric materials have motivated increasing research into energy harvesting from non-classical materials, also referred to as energy scavenging. In this approach, insignificant amounts of ambient energy are converted into useful electrical energy for powering low-power electronic devices. The primary motivation of this thesis is to investigate the harvesting of mechanical vibration energy from waste or unused ambient sources and convert it into electrical energy capable of powering small wireless electronic sensors using Macro Fiber Composite (MFC) piezoelectric materials. Advances in conventional battery technology have not been rapid enough to meet the long-term power requirements of portable wireless electronic systems. Therefore, energy harvesting using MFC materials represents a promising and sustainable energy solution for wireless and portable electronic devices.

1.5. Original contribution and significance of the thesis

This PhD thesis contributes to the field of non-classical piezoelectric materials (MFC) energy harvesting through the development and validation of an integrated modelling, experimental and numerical optimisation framework for harvesting electrical energy from mechanical vibrations. The work addresses the problem of improving the electrical output and the conversion efficiency of piezoelectric vibration energy harvesters for self-powered low-power electronic devices. So far, the literature on piezoelectric energy harvesting has focused on conventional or PZT materials, with some mathematical and experimental models, while finite element analysis (FEA) studies on non-classical energy harvesters remain limited. The Macro-Fiber Composite (MFC), used as a sensor, actuator, or energy harvester, is a new piezocomposite developed at NASA Langley Research Centre. The thesis undertaken as part of the PhD programme aims to harvest energy and optimise the efficiency of a non-classical piezoelectric material and a system capable of scavenging vibrational energy under realistic environmental conditions. The original contributions of this thesis can be summarised as follows:

The first stage involved defining the thesis topic, entitled "Modelling, testing, and optimisation of vibration-based electric energy harvesting using MFC non-classical piezoelectric materials". The research methodology was developed based on this stage. Material selection focused on the MFC-P2 as an energy harvester and the MFC-P1 as a vibration actuator. Material characterisation, including dielectric, piezoelectric, elastic, and damping properties, was obtained from reliable datasheets. Therefore, one contribution of this work was to demonstrate that the MFC can be used not only as a sensor and actuator but also as an energy

harvester. The second stage of the research focused on developing analytical and finite element models for a cantilever beam integrated with non-classical MFC-P2 piezoelectric materials for low-power vibration energy harvesting. The proposed system was designed using flexible piezoelectric composites that can be easily bonded to structural substrates. These models are applicable not only to sensing and actuation systems but also to energy-harvesting applications involving flexible and easily integrated vibrating structures. This stage enabled the prediction of the natural frequency, mode shape, harvested voltage, and electrical energy output of a non-classical piezoelectric energy harvester operating at low frequencies under transverse excitation. The third stage involved experimental testing of a unimorph cantilever beam with MFC-P2 as the energy harvester and MFC-P1 as the vibration actuator providing external excitation for beam vibration. The tests measured the frequency response and open-circuit voltage, calculated power output as a function of load resistance, and assessed durability under repeated cycles at exceptionally low frequencies. For most power-harvesting systems using Macro Fiber Composites, the energy generated by the piezoelectric material is usually insufficient to power most electronic devices. Therefore, optimising the efficiency of the MFC to make it suitable for use as a power-harvesting device for wearable electronics was an important aspect of this research.

The experimental and FEA models of the harvester showed good agreement, indicating the applicability of the proposed modelling approach for energy-harvester design. This work provides useful reference for the design and study of energy-harvesting systems operating in low-frequency vibration environments based on both experimental results and simulation models. The output voltage of the MFC harvester is experimentally evaluated and compared with the finite element method model. Another important contribution of this thesis is to improve the efficiency of different cantilever beam geometries with an MFC piezoelectric energy harvester, compared to conventional piezoelectric structures. Enhancing the efficiency of linear PEHs by optimising the geometric parameters, such as beam length, thickness, piezoelectric patch placement, proof mass, load resistance, and excitation frequency, should be varied through simulation work on the maximum strain induced in the piezoelectric material (MFC). Developing a parametric study performed for cantilever beam energy harvesting by varying the beam geometry, proof mass, and MFC patch placement to find the best configuration for the PEH while keeping the maximum strain on the MFC below the failure limit. In general, the first contribution of this thesis is the modelling of the MFC for energy harvesting, which is important for powering small electronic devices in the system. Another significant contribution of this work is the optimization of the efficiency of the MFC

piezoelectric material to efficiently recover electrical energy from mechanical vibrations through the parametric design of the mechanical geometry. The results of this research provide useful design guidelines for the design of efficient vibration energy harvesters for powering wireless sensor networks, structural health monitoring systems, Internet of Things (IoT) devices, biomedical sensors, wearable electronics, and other autonomous low-power systems. The developed analytical, numerical, and experimental framework serves as a foundation for future research into nonlinear behaviour, advanced optimisation methods, machine learning and the design of next-generation piezoelectric energy harvesting systems.

1.6. Outline of the thesis structure

This thesis consists of seven chapters, which are organised as flows.

Chapter 1. Introduction: This chapter introduces mechanical vibration energy harvesting, particularly focusing on piezoelectric energy harvesting. It presents the research gaps, objectives, motivation, and research approach of the dissertation, and finally, contributions and significance of the dissertation are highlighted.

Chapter 2.Literature review: This chapter states the state-of-the-art in mechanical vibration energy harvesting techniques with a focus on piezoelectric transduction. The different types of piezoelectric materials and transducers, their working principles, mathematical modelling approaches, optimisation methods and applications are reviewed.

Chapter 3. Analytical modelling: This chapter describes the theoretical background and analytical modelling of a unimorph cantilever beam integrated with an MFC piezoelectric transducer for energy harvesting. The mathematical model is formulated on the basis of the Euler-Bernoulli beam theory and the linear constitutive equations of piezoelectric materials. The governing coupled electromechanical equations are obtained from the energy equations and the corresponding linear constitutive relations. Using the model, the resonance frequencies, mode shapes, frequency response, voltage output and harvested power are identified. The analytical model is coded in MATLAB to simulate the system and assess its electromechanical performance.

Chapter 4. Finite element modelling: In this chapter, the finite element modelling of the MFC-P2 piezoelectric energy harvester is presented using COMSOL Multiphysics. A coupled electromechanical finite element model is presented to investigate the performance of the MFC-P2 harvester and to predict its resonance frequency, output voltage and harvested power. The

influences of relevant material and geometry parameters on the performance of the energy harvesting system are also studied.

Chapter 5. Experimental validation: In this chapter, a prototype of an aluminium cantilever beam integrated with the MFC-P2 piezoelectric transducer is developed and experimentally evaluated. The experimental setup and measurement procedures are described, and the experimental results are compared with the analytical and numerical results presented in Chapters 3 and 4. Experimental investigation is employed to verify the proposed analytical and finite element models and to evaluate the performance of the MFC-based energy harvesting system under different operating conditions.

Chapter 6. Optimisation of the energy harvesting system: This chapter presents the optimisation methodology used in COMSOL Multiphysics to improve the performance of the MFC-based energy harvesting system. The optimisation is performed to maximise the harvested voltage and electrical power and to minimise the operating resonant frequency. The effects of some key design and operating parameters are investigated, including geometric configuration of the harvester, substrate thickness, MFC patch position, tip mass, excitation force and electrical load resistance. The BOBYQA optimisation algorithm is adopted to get the optimal combination of design parameters to improve the energy-harvesting performance.

Chapter 7. Conclusion and future work: This chapter provides a summary of the key findings and contributions of the thesis. Results of the analytical modelling, numerical simulations, experimental investigation and optimisation are presented. Recommendations and possible directions for future research are also discussed.

Chapter 2 Literature review

In this chapter, a comprehensive review of the literature concerning energy harvesting from mechanical vibrations is presented. It begins by exploring the fundamental mechanism for ambient vibration energy harvesting, followed by an overview of harvester designs and strategies for enhancing performance. The following part deals with piezoelectric materials, their properties, constitutive behaviour and integration in energy harvesting systems. The limitations and open problems in the existing modelling frameworks, experimental characterisation methods and efficiency enhancement techniques have been consistently pointed out throughout the chapter, thereby specifying the research gap that this thesis intends to model.

2.1. Vibration energy harvesting mechanism

Energy harvesting refers to the process of capturing energy from the surrounding environment and converting it into electrical energy, which can be used immediately to power small electronic devices or stored for future use. This concept has existed for more than a century in forms such as windmills, watermills, and solar power. Over the past four decades, mechanical vibration energy harvesting from ambient sources has emerged as a highly promising approach, not only because it is environmentally friendly and cost-effective but also because it helps overcome the limitations associated with conventional batteries [1,5].

In many practical applications, electronic devices do not require substantial amounts of power; however, they are expected to operate continuously for prolonged periods without human intervention. Although conventional batteries remain widely used as power sources, they present several limitations, including limited lifetime, maintenance requirements, additional weight, environmental concerns, and difficulties associated with replacement in embedded or remotely located systems [36].Vibration-based energy harvesting is now an important research area because most engineering structures and mechanical and machine systems, when operated, have dynamic motion. These mechanical vibration energies are in the form of waste. Using piezoelectric materials to convert this energy to electrical energy is a modern technology. The energy harvesting using any piezoelectric material can follow three procedures to convert mechanical vibration to electrical energy. Piezoelectric energy harvesting systems have a wide variety of applications, ranging from human wearable devices, the aerospace industry, civil infrastructure, and biomedical devices.

Figure 2-1 shows the steps of converting energy from piezoelectric materials. The complete energy harvesting process involves four main stages: mechanical input energy from ambient vibrations, mechanical strain energy developed within the structure, electrical energy generated and stored in the piezoelectric capacitance through electromechanical conversion, and finally the useful electrical power delivered to an external load or energy storage system.

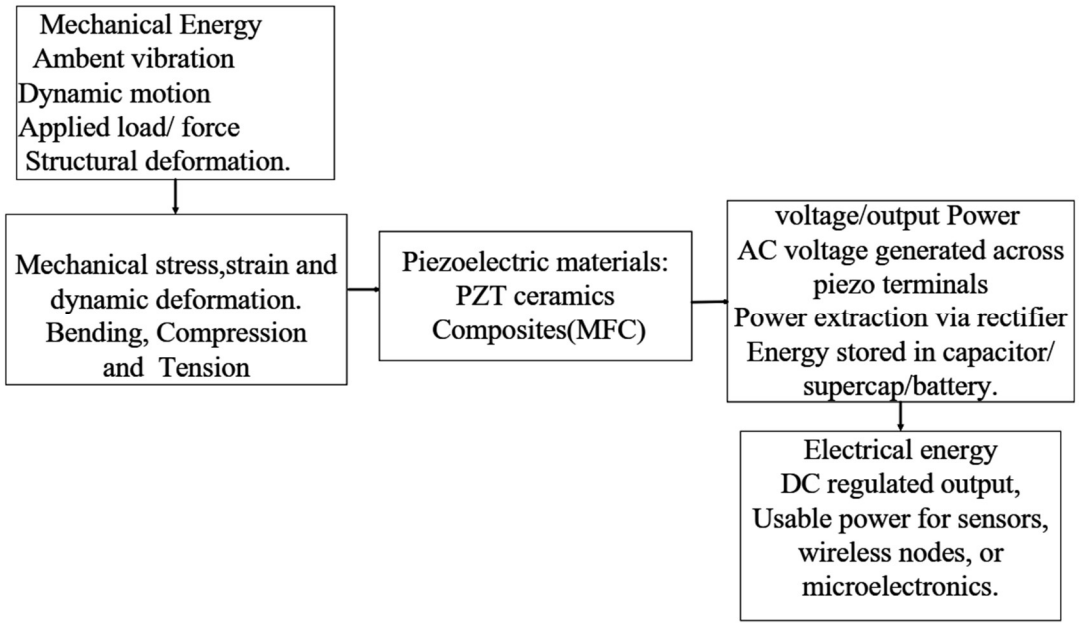


Figure 2-1 Block diagram for EH from mechanical vibration of piezoelectric materials

This chapter is devoted to the review of ambient energy harvesting, sources of mechanical vibration, piezoelectricity, piezoelectric materials, piezoelectric constitutive equations, modelling optimisation of piezoelectric energy and application of harvested energy from piezoelectric materials. Another method of harvesting energy from mechanical vibrations is by using piezoelectric materials, as mentioned in the introduction. Piezoelectric energy transduction is particularly attractive for wireless sensors and electromechanical systems because it is compact, has a high energy density, requires little maintenance, is easy to integrate into small-scale systems, and is well-suited for high-frequency vibrations.

Ambient energy harvesting method

As early explained, energy harvesting (or energy scavenging) is the process of capturing and converting energy from various ambient sources into usable electrical energy. such as high-level ambient energy sources like wind, solar, biomass, hydropower, geothermal, and tides, and low-level energy sources, like vibration, noise, and heat, are captured and stored. It is becoming an attractive clean energy alternative to conventional battery-powered systems using environmentally ambient energy sources. The energy from low-level sources may not seem like

much, but it is enough to power low-energy electronic devices. They include wireless sensor networks (WSNs), remote sensing systems, structural health monitoring (SHM) systems, wearable electronics, and microelectromechanical systems (MEMS).

Today, every task relies on electricity for communication in our daily lives, manufacturing, light, housekeeping, entertainment, etc. Most conventional energy harvesting causes environmental pollution and natural resource depletion from the earth. As a whole, energy harvesting has three main parties: the energy source, from which the initial power is harvested and converted to usable electrical energy (mechanical energy, thermal energy, light energy, electromagnetic energy, etc.); the second energy harvesting mechanism, which converts ambient energy to electrical (piezoelectric, thermoelectric, photovoltaic cells, etc.); and the load (where output electrical energy is stored) [2,19].

Researchers are finding alternative sustainable green energy by using technology with high energy efficiency conversion that is friendly to the environment. From this, energy harvesting from mechanical vibration nowadays has more attractive research for small electronic devices [37]. Many different methods are available to obtain electrical energy from mechanical vibration [5]. Among the three types of vibration energy harvesting mechanisms (electrostatic, piezoelectric, and electromagnetic), piezoelectric energy transduction is preferable for wireless sensors and electromechanical systems due to compact size, high density, minimal maintenance, easier small-scale system integration, and high-frequency fluctuation [5,22,38,39].

The energy from piezoelectric materials is the most efficient for applications due to their simple structure and the high robustness to external/internal electromagnetic waves [40]. Therefore, piezoelectric vibration-based energy harvesting can be an alternative to powering those devices because the piezoelectric energy harvester generates voltage under mechanical deformation [41]. The common and simple method for vibration energy harvesting is to use the direct piezoelectric effect [14]. Piezoelectric energy harvesters are smart materials for sensing mechanical vibrations and converting them into usable energy to empower low-power electronic materials [42]. Electromagnetic energy harvesting is based on the theory of Faraday law. The induction of electromagnetics typically involves coils, springs and magnets, which describe when a conductor (wire) is moved in a magnetic field or vice versa. Voltage is generated by mechanical vibration between the relative motion of the coil and magnet [43–45]. The electrostatic method of energy harvesting is relative movement between charged capacitor plates that are electrically isolated via air, vacuum, or dielectric insulator (capacitor) to produce energy. The structural vibration influences the capacitance distance between the parallel plates

or their effective overlap area [44]. For this work, the cantilever beam integrated with the Macro Fiber Composite transducer base was selected. This piezoelectric energy harvester consists of a mechanical substrate, piezoelectric material, and electrical interface. The mechanical structure is used as an input vibration sensor, which creates stress in the piezoelectric layer due to input vibrations. This stress is converted into voltage and power by the piezoelectric material.

2.2. Mechanical vibration-based energy harvesting mechanism

The energy harvesting mechanism consists of a structure that converts the ambient energy into electrical energy [1,2]. The fundamental aim of a vibration energy harvester (VEH) is to transform kinetic energy from a moving source into electrical energy through an electromechanical coupling mechanism. A vibration energy harvesting mechanism is one of the most promising approaches to extend the functionality life of wireless sensors and low-power electronic devices, powering an electronic watch, an accelerometer inside the tyre tread, and wireless temperature sensors, demonstrating great promise as a substitute for batteries and other portable power source devices [46–48].

Mechanical vibration-based energy produced by all manmade structures and human beings during natural activity is used for wide applications. Mechanical energy is one of the most investigated forms due to its abundance, accessibility and ubiquity in the environment, in addition to multiple possible transduction types [49,50].These sources of vibration can be diverse forms such as machine vibration, flowing water, wind, human motion, shock waves, vibrations from household appliances such as air conditioners or from rotating machines, rolling element bearings and shafts to achieve self-powered sensor networks [50,51]. Example wireless sensor networks where the battery replacement is a crucial issue. Of the three vibration energy harvesting mechanisms, piezoelectric energy harvesting (PEH) has the advantage of a simple device structure, high power density, and the ability to be integrated into a wide range of systems, from small-scale wearable devices to large-scale infrastructure or dynamic systems, to capture ambient vibrations and convert them into usable electrical power, and it has no need for an extra power supply and thus has attracted extensive investigations [52,53].

The techniques for mechanical vibrations energy harvesting are commonly classified into three categories: piezoelectric, electrostatic, and electromagnetic, applied in various energy harvesting applications [1,4,8,16,36,49,54]. Each of these methods leverages distinct principles of physics to efficiently harness energy from various sources, enabling a wide range of

applications in renewable energy systems and electronic devices. The choice between the three mechanisms is highly dependent on the application [1,2,11] .

1 Piezoelectric energy harvesting mechanism

The piezoelectric energy harvesting mechanism converts mechanical strain or stress applied to certain materials into an electrical charge via the direct piezoelectric effect [1,54,55]. It can be achieved by directly bonding piezoelectric elements or by installing harvesters as add-on systems (usually cantilever configurations with bonded piezoelectric elements) on a vibrating host structure. Piezoelectric energy harvesting technology, with its advantages of simple structure, no electromagnetic interference, and easy miniaturisation and integration, provides an effective pathway for the conversion of this type of vibration energy into electrical energy. However, the core challenge of vibration energy harvesting lies in the insufficient strain of piezoelectric elements under low-frequency micro-vibration and the limited energy conversion efficiency under low-amplitude excitation, making it difficult for traditional piezoelectric energy harvesters to achieve efficient electromechanical coupling. One common and simple method for energy harvesting is to use the direct piezoelectric effect. The effectiveness of piezoelectric vibrators, which transform impact vibration energy into electrical energy, has been extensively studied. When comparing piezoelectric energy harvesting mechanisms to the other energy harvesting techniques, the transduction capacity, the preservation of efficiency, the higher power density, scalability, and the capacity to function in high-frequency environments are very high [56]. It is also important to note that the lifetime of a piezoelectric harvester can be almost unlimited if the applied force and working temperature are kept within the material's operational range [8,36,57].

2 Electrostatic vibration energy harvesting mechanisms

The basic concept for electrostatic energy conversion is to use variable capacitors. The variable capacitor configuration consisting of dual parallel conductive plates, which are interspersed with dielectric materials or air. When the conductors are moved relative to each other, the capacitance is varied, and then the mechanical energy is converted into electrical energy [33,48].While these devices are highly compatible with micro-electro-mechanical systems (MEMS) fabrication, they generally exhibit lower power output efficiency than piezoelectric or electromagnetic counterparts and are limited by the need for a priming source [48,58]. The main advantage of this energy harvesting mechanism configuration is that it is very easy to scale down to a very small size, which facilitates seamless integration into micro-electro-mechanical systems ($MEMS$). Nevertheless, the limitation of this mechanical energy

conversion mechanism is that an external power source is required to start the harvesting process, and the power output efficiency for energy harvesting using electrostatic conversion is relatively low compared to the other transduction mechanisms [5,59].

3 Electromagnetic vibration energy harvesting mechanisms

The electromagnetic principles governing the process of vibration energy harvesting are fundamentally grounded in Faraday's law of electromagnetic induction, which asserts that "an electric current will be generated in any closed circuit when there is a variation in the magnetic flux through a surface enclosed by the conductor" [11]. In 1831, Michael Faraday discovered that when a wire and magnet move relative to one another, the cutting of the magnetic flux results in a current being induced to the wire, in turn producing a voltage [60]. Electromagnetic energy harvesters produce electricity when batches of metallic coils are cut across a magnetic field according to the law of induction [48]. These systems typically produce higher current but lower voltage less than 1V, compared to piezoelectric harvesters [61]. The advantage of the electromagnetic mechanical vibration energy harvesting mechanism is its scalability and the suitability for large or multi-directional energy harvesting. For instance, gravitational electromagnetic energy harvesters ($GVEH$) optimised for low-frequency applications (4 Hz) have achieved power levels of up to 32 mW under 0.5 g excitation [62]. Recent designs also focus on "springless" architecture or tenable magnet positions to improve performance in low-frequency ranges. Another advantage of electromagnetic energy harvesters is their good scalability, low maintenance requirements, and stable performance over extended periods of time [45,63]. This kind of conversion mechanism requires a permanent magnetic field. However, permanent magnets are usually bulky and difficult to scale into MEMS size [62, 64].

Table 2-1 Summary of mechanical vibration energy harvesting mechanism

Type of Mechanical EH	Operational principle	Advantages	Limitation	Application
Piezoelectric	Mechanical strain/stress to electrical charge due to the direct piezoelectric effect With the constitutive equation of $D = dT + \varepsilon E$ [1,64].	High energy density, simple configuration, high conversion efficiency, and precise control [8]. Compact integration with electronic and MEMS structures, direct energy or no need for an outside source conversion mechanism. Simple for fabrication, customisable shapes, and little mechanical damping [65].	Low efficiency at low frequency Very hard and brittle or rigid [47]. Classical PEM is a toxic, insufficient strain of piezoelectric elements under low-frequency micro-vibration.	Structural health monitoring (SHM) sensors, aerospace & automotive, civil infrastructure, industrial monitoring, biomedical devices, wearable electronics, and marine energy [2,50].
Electromagnetic	The relative motion between the magnet and coil, according to Faraday's law, produces voltage $V = \frac{d\Phi}{dt}$ [47,66].	High efficiency in converting mechanical-to-electrical energy, No voltage source needed, Matured technology.	bulky and complicated mechanisms, not compatible with fabrication at the microscale level, higher current but lower voltage, and magnetic interference.	Marine and Blue Energy Harvesting. larger motions and lower frequencies.
Electrostatic	The distance between capacitances changed due to mechanical vibration. The capacitance variation produces electrical energy. with initial voltage or current.	very easy to scale down to a very small size. Easier to integrate into microsystems, No smart materials needed.	An initial external voltage or a pre-charged electret material to maintain a bias, lower power output efficiency when compared to other mechanisms.	MEMS, Wireless sensor networks, structural health monitoring, industrial machinery and aerospace [67,68].

Table 2-1 summarises the comparison of three major mechanical energy harvesting mechanisms (piezoelectric, electromagnetic and electrostatic) in terms of working principle,

advantages, limitations and applications. Piezoelectric harvesting relies on direct strain-to-charge conversion, offering high energy density and high accuracy control in simple and compact designs. However, it suffers from low efficiency at low frequencies and material brittleness/toxicity. Electromagnetic harvesting is based on the relative motion between a magnet and a coil (Faraday's law) to achieve high conversion efficiency without the need for a voltage source, but it requires bulkier, more complex mechanisms that are poorly suited to the fabrication at the microscale. Electrostatic harvesting exploits capacitance changes from mechanical vibration, is readily miniaturised and integrated into MEMS, but requires an initial bias voltage and typically provides lower power output. In general, the choice of between these mechanisms is a matter of compromise between efficiency, scalability, material properties, and intended use, from structural health monitoring and wearables (piezoelectric) to marine/blue energy systems (electromagnetic), and MEMS-based wireless sensors (electrostatic).

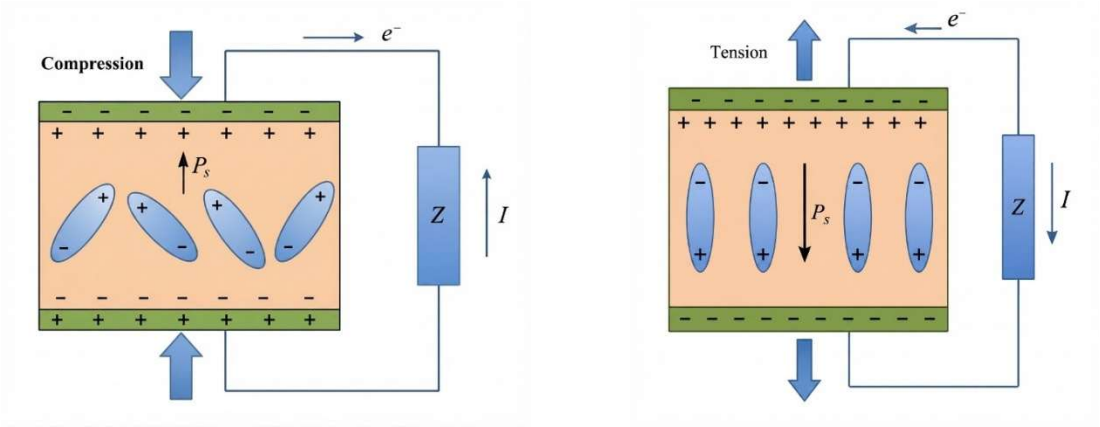
2.3. Sources of vibration

Mechanical vibration energy serves as a useful environmental source for energy harvesting, otherwise lost as heat or sound [7,69]. Vibration sources can be captured in various environments, ranging from bridges, buildings, home appliances or industrial equipment. Mechanical vibrations are widely present in rotating machinery, vehicles, railways, bridges, industrial equipment, buildings, aircraft, human motion, and structures excited by wind or ocean waves [70] Rather than allowing this mechanical energy to dissipate completely as heat through damping mechanisms, vibration-based energy harvesters capture a portion of the available vibrational energy and convert it into electrical energy. The generated power is typically within the microwatt-to-milliwatt range, which is insufficient for high-power devices but highly suitable for low-power applications such as wireless sensors, data loggers, low-duty-cycle transmitters, and structural or condition-monitoring systems. Early studies on low-level energy scavenging demonstrated that ambient mechanical vibrations could serve as a practical power source for wireless sensor nodes when the energy harvester is appropriately designed and tuned to the characteristics of the surrounding vibration environment [11,71].

2.4. Piezoelectricity

Piezoelectricity was first discovered in 1880 by Jacques and Pierre Curie [59]. The name "piezo" is derived from the Greek, meaning "to press"; hence, piezoelectricity is the generation of electricity because of a mechanical pressure [1,15,72]. This means generating electricity when external pressure or stress is applied to it, or the coupling between mechanical and

electrical fields when pressure or stress is applied to them, or the coupling between mechanical and electrical fields [19,42].When strong electric fields are applied and the temperature of the piezoelectric materials is higher than the cure temperature, the electric dipole is aligned with the direction of the applied electric field. Piezoelectric materials commonly display anisotropic traits; therefore, the material's properties [34,53]. The transduction mechanism itself can generate electricity by exploiting the mechanical strain, which is the direct piezoelectric effect from Figure 2-2(a). In another way, the piezoelectric materials are also capable of converting the electrical energy into mechanical strain energy, which is known as the converse piezoelectric effect (see Figure 2-2 (b)) [1,73].



(a) Direct piezoelectric effect (b) Converse piezoelectric effect

Figure 2-2.Mechanism of piezoelectric effect [1,73]

Figure 2-2 (a) shows the application of a mechanical compressive force in the vertical direction to the piezoelectric material. The spontaneous polarisation vector represents the electrical polarisation of the material. Compression of the material results in a change of the relative positions of the positive and negative charges in the piezoelectric domains. This deformation induces an electric displacement and charge separation at the electrode [74]s. This results in a potential difference developing between the two electrodes. In the second figure, Figure 2-2 (b), the mechanical loading is reversed, and the piezoelectric material is stretched. The tensile force alters the internal polarisation and charge distribution of the piezoelectric domains. This results in an electric potential being generated between the electrodes and a charge flowing through the external circuit. What is important is that the direction of the generated electrical response depends on the direction of mechanical stress relative to the direction of polarisation of the material. Thus, an alternating mechanical load, such as vibration, produces an alternating electrical output [7,55].

2.4. Piezoelectric Materials

Piezoelectric materials are a type of smart material. Smart materials change their physical properties in a specific manner in response to an external strain or voltage applied. These materials can capture energy from ambient vibration and convert it into electrical energy, which can be stored in batteries or used to power small electronic devices which utilise the direct piezoelectric effect [50,75] batteries or to power small electronic devices which utilize the direct piezoelectric effect [75].When an external strain is applied, they generate an output voltage [76–79].These materials have a wide range of applications, including sensors, actuators, energy harvesters, artificial muscles, etc. [80–82].

Small-scale energy harvesting devices have become more viable due to the growth, development, and applications of smart materials. Smart materials function as transducers, converting one form of energy to another, making them useful for the purposes of harvesting energy. These materials are commonly utilised in applications such as energy harvesting, health monitoring, structural damage detection, and vibration damping owing to their pronounced electromechanical coupling, substantial blocking force, elevated stiffness, and rapid response characteristics [83]. These materials have been known for more than a century. They are smart materials because they exhibit unique coupling between mechanical and electrical energy and are capable of being sensors and actuators [1]. This material has two effects: direct and converse piezoelectric effects. Direct effects were discovered in 1880 by Pierre Curie and Jacques [84]. As a strain or external mechanical load, the electric voltage is applied due to a change in the polarisation of these materials, and the degree of polarisation is proportional to the externally applied load. The charge generated by mechanical stress input on the surface of piezoelectric materials. This effect in piezoelectric materials, which are used for PEHs, is a direct piezoelectric-effect method [43,53]. Similarly, in 1881, Gabriel Lippmann discovered the converse effect of external voltage or electric field applied across the surface of piezoelectric materials that induced stress across the surface. Figure 2-2 (b) below shows the converse and direct piezoelectric effect [85–87]. The direct piezoelectric effect is the primary method used for sensors and energy harvesting mechanisms [88]. Most smart wireless electronic devices exhibit energy consumption in milliwatts or microwatts. More than 200 diverse types of piezoelectric materials have been created with various piezoelectric constants. These materials are smart because they can produce mechanical and electrical energy when an external force or electric field is applied. It can be found in nature or synthetically. Naturally, materials such as quartz, Rochelle salt, and some natural organic materials such as silk, wood, rubber, dentin,

bone, hair, and enamel. The second classification is synthetics, such as polymers, ceramics, and composite materials. Under this topic, the study focuses on piezoelectric materials such as single crystals (e.g., Rochelle salt, lithium niobate, and quartz crystals); piezoelectric ceramics (e.g., barium titanate ($BaTiO_3$), lead-zirconate-titanate (PZT), and polyvinylidene fluoride (PVDF)); and piezoelectric fibers and their characteristics for energy harvesting, which can be summarised.

1. Single-crystal piezoelectric materials

Single crystals (barium titanate ($BaTiO_3$)) with the highest piezoelectric properties have an ordered orientation of positive and negative ions. The piezoelectric property depends on domain size, which significantly increases with decreasing domain size [89]. Great promise as a candidate sensor element from which to develop low-noise, high-sensitivity accelerometers when used in a novel, high-gain bandwidth, flexural accelerometer structure. crystal piezoelectric material to succeed; however, in industrial applications, future research will need to be focused on reducing the variance in the piezoelectric properties over the surface of the crystal [90].

2. Lead-zirconate-titanate (PZT) or piezoceramics

Lead zirconate titanate is a widely used piezoelectric substance. To this point, lead zirconate titanate ($Pb(Zr, Ti)O_3$, PZT)-based piezoelectric materials are, nonetheless, the most versatile and the most universally used piezo ceramics. Nevertheless, the volatilisation of toxic lead and its associated compounds during the high-temperature sintering process of PZT contributes to environmental contamination and poses significant health risks. Despite its excellent piezoelectric properties, the environmental and health implications of lead-based piezoelectric materials like PZT have prompted a search for alternative materials that offer comparable performance without the use of toxic elements. This quest has led to significant research into lead-free alternatives to address environmental concerns while maintaining or approaching the performance characteristics of traditional lead-based materials [1].In addition, they have a very poor ability to conform to curved surfaces and are very dense and stiff, causing mass loading and localised stiffness to be a factor when working with very flexible or lightweight structures. This material is very brittle and can crack under high-frequency cyclic load. The use of lead-based piezoceramics is common in many industrial applications but is accompanied by certain limitations, such as the inherent resistance of ceramic materials, the reduced flexibility, and the limited adaptability to curved geometry [72,86].

In terms of material systems, traditional piezoelectric ceramics (such as PZT) have high piezoelectric coefficients, but they are brittle and difficult to adapt to bending deformation; piezoelectric polymers (such as PVDF) have good flexibility, but their piezoelectric activity is low. Piezoceramics have large electro-mechanical coupling constants and provide a high energy conversion rate, but they are too brittle to use as a general-shape energy transducer. Furthermore, based on piezoelectric polymers (PVDF and its co-polymers), researchers have attempted to develop alternative, suitable piezoelectric materials to circumvent the toxicity issue. By employing a phase-inversion technique to create the Gd_5Si_4-PVDF nanocomposite. The PE strain constant for polymers is much less than that of piezoceramics. However, the stress constant for polymer piezoelectric is better than that of ceramics, which makes polymers more stable than ceramics.

3. Piezoelectric polymers

Piezoelectric polymers are mechanically flexible and can endure high strain; they are a superior alternative for piezoelectric energy harvesting applications. In addition, despite their low power density, they produce a suitable voltage with adequate power output and can withstand higher driving fields due to their high dielectric breakdown and maximum functional field strength. They are also less expensive to fabricate and process faster than ceramic-based composites [84,91–93]. Due to their molecular structure and orientation, polymers are carbon-based materials that demonstrate a piezoelectric effect. They exhibit moderate strain coefficients (d_{33}) and voltage coefficients (g_{33}) and are significantly softer than ceramics. However, due to their special qualities, including design versatility, low density, and ease of processing, they are suitable for a variety of energy-collecting applications, but they have very weak piezoelectricity [94,95].

Piezoelectric polymer-based energy harvesters are particularly suitable for low-frequency and large-deformation applications, where conventional ceramic piezoelectric materials are more prone to cracking or brittle failure. Thanks to their high flexibility and biocompatibility, polymer materials are appealing for use in wearable electronics, biomedical systems, and smart textile applications. However, compared to ceramic piezoelectric materials, polymers have lower dielectric constants and smaller piezoelectric coefficients, which can limit the electrical power output achievable.

From a modelling perspective, polymer-based piezoelectric harvesters require careful consideration of viscoelastic behaviour because the mechanical properties of polymers vary with frequency, temperature, and strain rate. As a result, simple linear elastic models may not

accurately predict the dynamic response or harvested power. Such simplified models may neglect important effects such as hysteresis, energy dissipation, and phase differences between mechanical deformation and electrical response [93,96,97].To balance piezoelectricity and good toughness, NASA proposed Macro Fiber composite, which are composed of piezoelectric ceramic fibers and a continuous-phase polymer matrix. This retains the advantages of high sensitivity and high activity of the original piezoelectric materials while improving the brittleness of piezoelectric ceramics.

4. Macro Fiber Composite Piezoelectric Materials

Traditional piezoelectric materials (PZT) are widely used in the fields of energy harvesting. However, the ceramic properties of the monolithic piezoelectric material are very fragile, so they are susceptible to accidental breakage during the handling and bonding process. Therefore, as classical piezoelectric materials are brittle and lack flexibility, these materials are exposed to cracking and cannot conform to curved surfaces despite their strong piezoelectric effect. In general, single piezoelectric crystals and ceramics have better piezoelectric-constant properties but are also rigid and hard to withstand high stress, making them unsuitable for some energy harvest applications. The MFC is the leading low-profile actuator and sensor that offers high performance, flexibility on large deformation, easy handling, durability, shape, easy integration into composite laminates, and reliability in a cost-effective device. However, the energy generated by MFC is still far smaller than that required by electronics at present [28,98–101]. The MFC actuator or sensor package employs piezoceramic fibers locked in an epoxy resin matrix and sandwiched between two arrays of interdigitated electrodes. MFC has rectangular cross sections and an assembled MFC package with regular spacing and precise parallel alignment. The rectangular fiber geometry of the MFC guarantees consistent, appreciable contact between the IDEs and piezoceramic fibers, reducing attenuation of the IDE electric field due to the low dielectric constant of the epoxy matrix [14,24,47,102,103].

From a piezoelectric fibre/epoxy resin functional layer, then, interdigitated electrodes (IDE) are covered on the upper and lower surfaces of the functional layer by processes such as magnetron sputtering. First, processing piezoelectric ceramic (lead zirconate titanate PZT-5H) into millimetre-long strip fibers, arranging them in an orientation, and bonding them with epoxy resin to form a piezoelectric fibre/epoxy resin functional layer; then, covering the upper and lower surfaces of the functional layer with interdigitated electrodes (IDE) through processes such as magnetron sputtering and extracting electrical signals from inside; finally, covering the

top and bottom of the overall structure with a flexible polyimide (PI) film as an insulating encapsulation and substrate [100,104–107].

The high-volume fraction of piezoelectric fibers can enhance the overall piezoelectric and dielectric constants of the material, but excessive fiber content may lead to material brittleness or uneven electric field distribution, thereby limiting energy harvesting efficiency [108]. Composites with transversely orientated piezoelectric fibers in an epoxy matrix are developed as a means for large-scale structural actuation and sensing, as well as for energy harvesting. It has rectangular piezo ceramic rods sandwiched between layers of adhesive, electrodes, and polyimide film. The flexibility of PZT composites can realise the mechanical impedance matching easily, and recently, advanced experimental results demonstrated that MFC has a high energy conversion transducer [50]. The Macro Fiber composite was invented in 1996 by NASA [1,19,32,83,91,94,106,109] as 10^{09} cycles as an actuator and 10^{10} cycles as sensors [110,111]. In 2002, Smart Material started commercialising this invention worldwide as NASA's licensed manufacturer and distributor. MFC allows for easy non-resonant and resonant energy harvesting applications through the integration of electronic components. The development of transducers has enabled new applications of piezoelectric materials, including solutions such as the recovery of electrical energy from mechanical vibration (energy harvesting systems), and has improved the operation of existing equipment [32]. In 2002, Smart Material began promoting the invention worldwide as a licensed manufacturer and distributor of NASA. Since then, MFC has constantly improved and been customised to meet specific customer needs and new application requirements. In 2021, more than 1,300 MFC publications worldwide documented various applications, MFC characteristics, and reliability, which can solve the problems of the application of classic, monolithic piezoelectric transducers that are heavy and fragile [8]. However, the energy generated by MFC is still far smaller than that required by electronics at present [112]. As a new piezoelectric material, the MFC energy harvest capacity has not been fully studied [51]. Macro Fiber Composites (MFCs) of the P_2 type operate based on the d_{31} piezoelectric effect, where the material is polarised along the z-axis and the resulting strain occurs along the x-axis. This configuration allows P_2 MFCs to produce substantial actuation, reaching strains of up to 750 parts per million (ppm) under an applied voltage between –60 V and +360 V.

Because of their high flexibility and efficiency, P_2 MFCs are well-suited for energy harvesting and strain-sensing applications. In energy harvesting, they convert ambient mechanical vibrations into usable electrical energy, making them a reliable source for powering

low-energy electronic devices. For strain sensing, their high sensitivity enables the detection of very small structural deformations, which is crucial for structural health monitoring in engineering systems. Their combination of mechanical robustness, sensitivity, and adaptability makes P_2 MFCs valuable in a wide range of technologies, including aerospace systems, civil infrastructure, and wearable electronics, where precision, reliability, and energy efficiency are essential.

There are several excitation conditions and operating environments in which monolithic piezoceramic configurations cannot be used due to their extremely brittle nature. The Macro-Fiber composite (MFC) piezoelectric configuration is an alternative because of its flexibility and robust nature [44,81,113]. It consists of rectangular piezoceramic rods sandwiched between layers of adhesive, electrodes, and polyimide film, primarily used in industrial and research applications for vibration monitoring and dampening; noise control, health monitoring, morphing of structures, directional actuation, and conforming to curved surfaces or irregularly shaped surfaces, and it can generate power at the mW level [83,114–117]. The structure and components of MFC are detailed in Figure 2-3. As a conclusion, MFC piezoelectric composites, which have better flexibility, robustness, and reliability than monolithic materials and better piezoelectricity than polymers, are widely used for vibration energy harvesting [47,100].

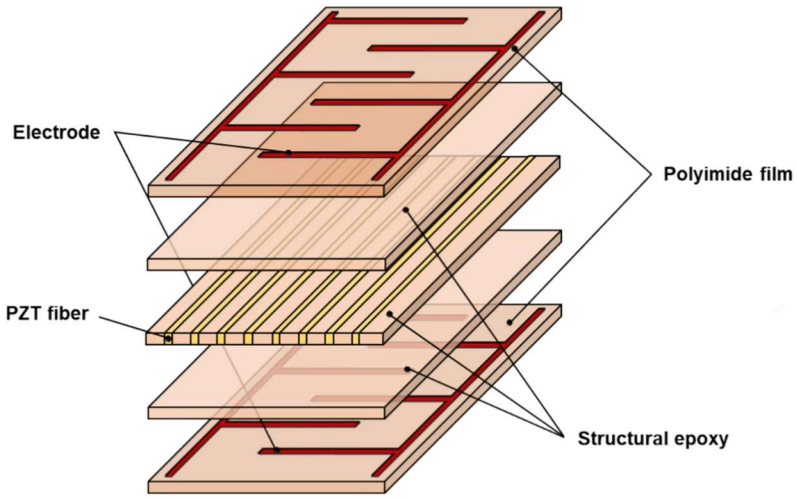


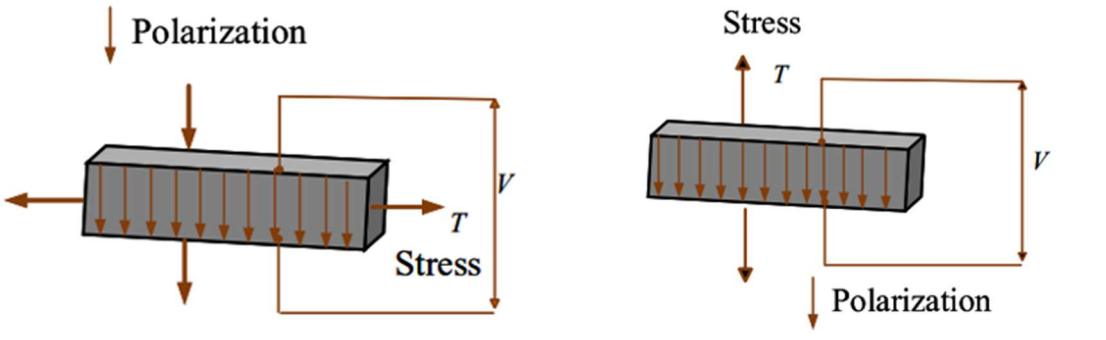
Figure 2-3 Macro Fiber Composite Material (type P2) structural component [117]

Figure 2-3 illustrates the layered structure of an MFC piezoelectric transducer, comprising aligned PZT fibres embedded in a structural epoxy matrix sandwiched between patterned electrodes and polyimide films.

2.5. Piezoelectric mode of operation

Piezoelectric transducers have two coupling modes of operation (polling direction); these are modes d_{33} and d_{31}. Their difference is the polarisation direction with a corresponding resonant frequency. $P2$-type using the d_{31} effect (bending mode), which is the transverse mode, the direction of mechanical pressure T is perpendicular to the direction of electric or polaris ation [102]. Figure 2-4 (a) [94,100,102]. All piezoelectric fibers are poled in the through-thickness direction, and it is assumed that in-plane electric fields vanish in the direction $E_1 = E_2 = 0$.This mode, d_{31} [103,114] was evaluated under a small mechanical vibration source to generate enough current for battery charging. Nelson [115], who was the first to investigate the bending mode of piezoelectric energy harvesting, suggested using a small piezoelectric element on the underside of the rail. The optimised average power was about 0.053 mW at a load resistance of 387 kΩ. Then, a cantilever beam with a proof mass at its free end and attached piezoelectric material was used and extensively studied. A classical PZT material was proposed to be clamped at the rail track with a cantilever. The maximum output power of 4.9 mW was achieved for a load impedance of 100 kΩ under rail acceleration of 5 g, displacement of 0.2-0.4 mm, and frequency of 7 Hz, which also confirmed the potential of the piezoelectric energy harvesters for railway applications [110,118]. Mode 3-3 is 3 to 5 times greater in power generation than mode 3-1. With an equivalent d_{31} parameter calculated as 1.87×10^{-10}^$10\frac{C}{N}$; however, this mode is difficult to manufacture (fabricate) and too stiff to couple [14,100,101,112]. Mode 3-1 has greater material efficiency with uniform electric potential through it but has too low a piezoelectric constant and output voltage, which is still too low. Mode d_{33} (compression) type or P1 (longitudinal mode, the direction of the mechanical stress, T, is parallel to the direction of the current or polarisation) as shown Figure 2-4 (b), the d_{33} mode has a stronger piezoelectric coefficient, which gives greater actuator and sensor functions than the d31 mode (transverse mode). However, because of the non-uniform electric field in the direction of fibers these materials cannot be used to their full potential, and this mode did not produce a high current due to its construction even if a high value of voltage was generated [47,114]. Therefore, Mode d_{31} Macro Fiber Composite is well-suited to harvest energy directly from waste vibration present in the environment without additional mechanical fixtures due to its flexibility, robustness, and long lifetime [110,112,119]. In addition, mode d_{31} is transverse, primarily applied in sensor measurement and vibration energy capture, while mode d_{33} is the longitudinal operation focused on achieving precise displacement actuation [79,108].

The MFCs with item numbers M2814P2, M8514P2, M8528P2, M8557P2, and M8585P2 are the preferred components used in many vibration energies harvesting applications. The P2 type MFCs feature a high electric source capacitance and increased electric charge generation. The MFCs are based on piezoelectric fibres and are environmentally sealed, which yields increased flexibility and robustness compared with standard, monolithic piezoceramic harvesters. The MFC-P2 cantilever PEHs allow for energy harvesting from bending motions & vibrations. The MFC cantilevers are comprised of a glass fiber composite (FR4, which is PZT fibers with top and bottom electrodes obtained by dicing metallised PZT wafers) as the base material with an integrated P2-type MFC. The P1-type MFCs use the d_{33} effect for actuation and will elongate up to 1800 ppm if operated at the maximum voltage rate of from -500V to +1500V [102]. The P1-type MFCs are also overly sensitive strain sensors. The P_2 uses the d_{31} effect for actuation and will contract up to 750 ppm if operated at the maximum voltage rate of minus (-) 60V to +360 V. The P_2 and P_3 type MFCs are mostly used for energy harvesting (PEH) and as strain sensors. In general, MFC has the potential for use in intelligent clothing with a flexible piezoelectric energy harvesting system aiming at a general power source for charging portable equipment such as a health monitoring unit, cellular phone, or medical drug delivery device; to model this device, a detailed description of the layer sequence and thickness and homogenous mechanical, piezoelectric, and dielectric properties of the layer is needed [1,114]. In general, the overall summary of common piezoelectric materials, advantages, disadvantage and applications is listed in Table 2-2.



(a) d_{31} mode (b) d_{33} mode

Figure 2-4 PEH mode: a) piezoelectric mode 3-1, (b) piezoelectric mode 3-3

d_{31} modes: Polarisation is applied in the thickness (Z-direction), and stress/force is applied in the longitudinal axis (*X*-direction), perpendicular to the direction of polarisation. The resulting voltage is generated along the polarisation axis, which gives a lower coupling coefficient but a larger strain for a given force.

d_{33} modes: Polarisation and applied stress are on the same axis (X-direction, according to the interdigitated electrode pattern), so the direction of mechanical loading is the same as the polarisation direction. d_{33} mode: Polarisation and applied stress are on the same axis (X-direction, according to the interdigitated electrode pattern), so the direction of mechanical loading is the same as the polarisation direction. This alignment leads to a higher electromechanical coupling coefficient of d_{33}-mode transducers (e.g., MFC-P2) than d_{31}-mode devices, which makes them more efficient for energy harvesting. This alignment leads to a higher electromechanical coupling coefficient of d_{33}-mode transducers (e.g., MFC-P2) than d_{31}-mode devices that makes them more efficient for energy harvesting.

Table 2-2 The common PEM and their advantages, disadvantages, and applications

Materials	Example	Advantages	Disadvantages	Application
Ceramics	PZT	Good piezoelectric, mechanical, and thermal properties; easy fabrication; easy shaping; good stability; and low cost.	However, PZT is brittle, which causes limitations in the power harvesting applications. When subjected to large deflections and high-frequency cyclic loading, the piezoelectric ceramics are susceptible to the initiation and growth of cracks and fatigue failure.	Widely used in harvesting applications in recent years. The cost of a PZT is relatively low in comparison with other piezoelectric materials. It is highly manufacturable; bulk, film, or composite with different dimensions and shapes can be fabricated relatively easily and at a reasonable cost [120] characterised by large electromechanical coupling factors, dielectric, and piezoelectric coefficients.
Polymers	PVDF	Good mechanical flexibility; higher chemical resistance. Mechanically flexible and can withstand high strain. They have a low fabrication cost, and the processing is faster compared with ceramic-based composites.	One order lower piezoelectric coefficient than PZT. narrow working temperature range. Low power density.	Wearable, biocompatible: •The most popular piezoelectric polymer materials. •Polymers are different from PZT, with lower piezoelectric coefficients (strain coefficients (d_{33}) and voltage coefficients (g_{33})), larger mechanical flexibilities, lower stiffness, and higher chemical resistance, which makes polymers have high fatigue resistance and a

				good service lifetime [2,20]. •It can be used as a sensor, actuator, and energy-harvesting device.
Lead-free	BT, BNT, KNN	Comparable piezo-electric property with PZT in the same composition.	Overall, lower piezoelectric property than PZT, lower thermal stability, and more difficulties in processing.	Environmentally compatible; diverse application.
Nanomaterials	ZnO	Easy to form nanostructure, no poling is required, chemically stable, biologically safe, and low cost.	Lower piezoelectric properties.	Nano generator compatible
Single crystals	PMT-PT PZN-PT	Very good piezoelectric performance.	Toxic lead: lower mechanical properties, higher cost, and difficult to fabricate and process.	Single-crystal materials provide much better piezoelectric properties than the conventional PZT materials. More expensive and not applicable for energy harvesters[114].
Composites	PTZ+PVDF (Composite materials) [121].	Possibility to have the advantages of both phases in the compounds.	Complicated processing required.	Composite materials are studied for energy harvesting and health monitoring. Macro Fibre Composites (MFCs) consist of thin, unidirectionally aligned $Pb(Zr–Ti)O_3$ (PZT) fibres embedded between printed electrode patterns on a polyimide film.
Macro Fiber Composite Piezoelectric Materials	MFC-P2, MFC-P1	The structure of MFCs is more flexible than that of monolithic piezoceramic. suitable for smart structures, curved surfaces, thin beams, and vibration energy harvesters.	Their anisotropies and electrode geometries make them more complex.	Macro Fiber composite piezoelectric materials are effective applications in vibration control, noise suppression, precision alignment control, energy harvesting, sensing, and damage detection.

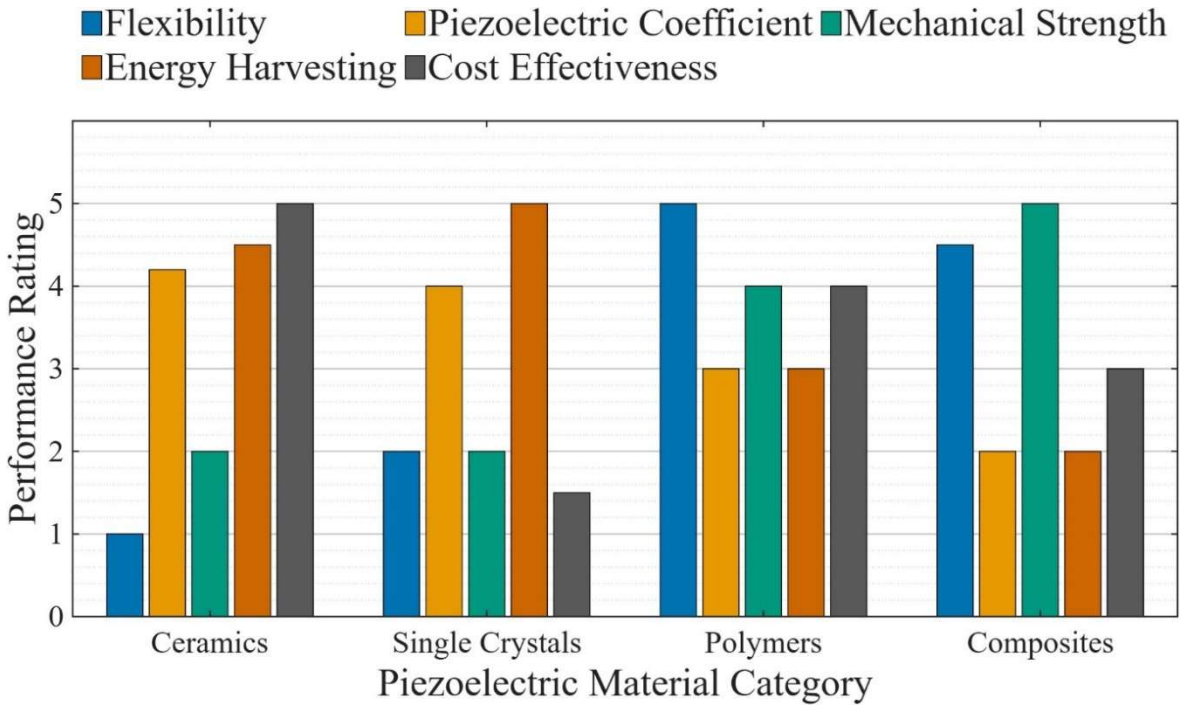


Figure 2-5 The basic summary of piezoelectric categories based on different properties

As shown in Figure 2-5, the choice of a piezoelectric material depends not only on its piezoelectric properties and the functionality of the application sector but also on parameters such as design flexibility, application frequency, available volume, cost-effectiveness, and mechanical strength.

2.6. Fundamentals of piezoelectricity

Piezoelectricity is the property of certain materials to generate an electric charge in response to mechanical stress. There are two types of piezoelectric effects: these are the direct and the converse piezoelectric effects. The ability of a piezoelectric material to convert mechanical strain into electrical energy is defined by the direct piezoelectric effect, whereas the converse effect describes the ability to convert applied electrical potential into mechanical strain energy, as shown in Figure 2-4. Once the piezoelectric material is chosen for a particular application, it is important to set the mechanical and electrical axes of operation. These axes are set during "poling", the process that induces piezoelectric properties in the piezoelectric material. This polarisation generates an electric field that can be used to transform the mechanical energy used in the material's deformation into electrical energy. Polarisation generates an electric field which in turn causes the flow of the free charges existing in the conductor. Figure directions and orientation axes of the piezoelectric material. Axes *X, Y* and Z represent an orthogonal

coordinate system, and axes 4, 5 and 6 are axes of rotation. There are two commonly known piezoelectric modes of operation to harvest energy, i.e., 3-1 loading mode (P_2) and 3-3 loading modes (P_1). In the 3-1 loading mode, the direction of the electric field is perpendicular to the direction of force applied, and in the 3-3 mode, the external stress direction generates a voltage in the same direction. In the 3-1 loading mode, the direction of the electric field is perpendicular to the direction of force applied, and in the 3-3 mode, the external stress direction generates a voltage in the same direction [1,116].

Piezoelectric parameter coefficient

Piezoelectricity has a physical property of anisotropy (a physical property which has a different value when measured in different directions). The constants depend on both the direction of applied mechanical or electric force and the direction perpendicular to the applied force. Each constant has two subscripts to indicate the direction of the two related quantities, such as stress (F/A) and strain ($\frac{\Delta L}{L}$), and elasticity. The directions *X, Y* and *Z* are represented by 1, 2 and 3, respectively [1,78,122–124].

Piezoelectric charge constant ($\boldsymbol{d_{ij}}$)

The piezoelectric constant coefficient is a fundamental parameter in piezoelectric materials that describes the relationship between mechanical stress and electrical charge generation (or vice versa). The polarisation obtained per unit of mechanical stress (σ) applied to a piezoelectric material or the mechanical strain (S) experienced by a piezoelectric material per unit of electric field applied. External voltage is applied to the piezoelectric transducer polarised along the direction of *Z* (3), electric field along the thickness (t) and strain produced along the direction of *X* (1). voltage is directly proportional to electric field, and thickness along the direction of the harvester can be described by the equation (2.1):

$$V = E_3\, t. \tag{2.1}$$

From Hook's law, strain (S) is given by the following:

$$S = \frac{\Delta l}{l}, \tag{2.2}$$

and the magnitude of the induced strain ε by an external electric field E_3 is represented by (2.1) into (2.2):

$$S = d_{31}E_3 = d_{31}\frac{V}{t}, \tag{2.3}$$

$$\frac{\Delta l}{l} = d_{31}.\frac{V}{t}. \tag{2.4}$$

When an external force *(F)* is applied to the transducer and the generated electric field is in the longitudinal direction, which is Z (3), it generates the stress and electric change (direct piezoelectric effect, d_{33}) respectively:

$$Q = DA = d_{33}\sigma A, F = \sigma A. \quad (2.5)$$

Therefore

$$Q = d_{33}F = d_{33}\sigma A. \quad (2.6)$$

Piezoelectric Voltage Constant (g_{ij})

The piezoelectric voltage constant, g, is the mechanical strain experienced by piezoelectric materials per unit electric displacement applied or the electric field generated by piezoelectric materials per unit mechanical stress applied. It describes the electric field or voltage generated per unit of mechanical stress applied to the material. Electric field E is related to an external stress σ through the piezoelectric voltage constant g (an important figure of merit for sensor applications) [116].

$$E = g\,\sigma. \quad (2.7)$$

Considering the relation, $P = d\,\sigma$, we obtain an important relation between g and d.

Permittivity or dielectric constant ($\boldsymbol{\varepsilon}$)

Permittivity is the piezoelectric property of dielectric displacement per unit electric field.

E^T electric field at constant stress and ε^S permittivity and constant strain.

Elasticity and Compliance

Elastic compliance, s, is the strain produced in a piezoelectric material per unit of stress applied and, for the 11 and 33 directions, is the reciprocal of the modulus of elasticity (Young's modulus, Y*).*s^D Is the compliance under a constant electric displacement; s^E is the compliance under a constant electric field. The first subscript indicates the direction of strain; the second is the direction of stress.

Electromechanical Coupling Factor (k)

Electromechanical coupling is the indicator for which piezoelectric materials effectively convert the conversion of mechanical energy to electrical or the conversion of electrical to mechanical energy by piezoelectric materials.

The IEEE standard assumes that piezoelectric materials are linear. When a poled piezoelectric material is mechanically strained, it becomes electrically polarised, producing a

fixed electric charge on the surface of the material (piezoelectric transducer). In piezoelectric materials, the energy density generated is directly proportional to the external applied force.

The fundamental equations delineating the piezoelectric characteristics are predicated on the premise that the aggregate strain within the transducer is the cumulative result of the mechanical strain elicited by the applied mechanical stress and the modifiable actuation strain instigated by the exerted electric voltage.

$$\mathrm{P}_{\mathrm{pe}} = d\sigma, \tag{2.8}$$

where P_{pe} is the piezoelectric polarisation vector (piezoelectric material under stress polarised and surface charge appears), d is the piezoelectric strain coefficient and σ is the stress to which the piezoelectric material is subjected.

For the indirect piezoelectric effect, the strain produced by the reverse effect is given by:

$$S_{pe} = d\mathrm{E}, \tag{2.9}$$

where S_{pe} is the mechanical strain produced by the reverse piezoelectric effect, and what E is the magnitude of the applied electric field.

The direct and reverse piezoelectric effects can alternatively be formulated as:

$$P_{pe} = d\sigma = dSY, \tag{2.10}$$

$$\sigma_{pe} = Y\,S_{pe} = Y\,d\mathrm{E} = e \cdot \mathrm{E}, \tag{2.11}$$

when piezoelectric materials are subjected to strain, they will have two effects. The first will generate elastic stress (σ_e = *Y.S*) and the second will generate piezoelectric polarization

($Pe = e \cdot S$), Polarisation creates an internal electric field in the material Ep_{e}.

The stress $\sigma_{pe} = e \cdot E_{pe}$ is produced by the electric field E_{pe}.

The total stress generated by strain, S, is given by the following:

$$E_{pe} = \frac{P_e}{\epsilon}, \tag{2.12}$$

where ϵ is the dielectric constant of the material.

The constitutive equations of the piezoelectric materials assume that the total strain in the transducer is the sum of mechanical strain induced by the mechanical stress and the controllable actuation strain caused by the applied electric voltage.

From Hooke's law, stress causes strain (S):

$$S = \frac{\sigma}{Y}, \tag{2.13}$$

in special materials such as piezoelectric materials (reverse piezoelectric effect), electric field E causes strain as well:

$$S = d\mathrm{E}, \tag{2.14}$$

from the linear electrical behaviour of the material [2] electric displacement is given by:

$$D = S\,\mathrm{E}, \tag{2.15}$$

when stress is applied to piezoelectric materials, charge is developed on the surface; therefore, the polarisation is directly proportional to both strain (S) and piezoelectric constant (d).

$$P = d\,\sigma, \tag{2.16}$$

normally, polarisation$(P) = Q.A$ and stress are $\frac{F}{A}$

$$Q = d\,F. \tag{2.17}$$

Piezoelectric materials have a coupled electromechanical response in which a mechanical deformation induces an electric response and vice versa an electric field induces a mechanical deformation. The behaviour of a piezoelectric material can be described by a linear constitutive theory for small strains and electric fields. The constitutive equations relate the mechanical stress, mechanical strain, electric field and electric displacement via material dependent coefficients. The constitutive equations for the linear piezoelectric material can be written in a number of equivalent forms, depending upon the choice of the independent variables. The usual forms are strain-charge, stress-charge, strain-voltage and stress-voltage [125,126].In the following, S_{ij} is the strain tensor, $\sigma_{ij}$is the stress tensor, while the electrical behaviour is described by the electric field vector E_i and D_i is the electric-displacement vector. The assumption that the strain, stress and electric field are aligned along the one direction. Which is the strain-charge or the stress-charge form. Now add equation (2.15) to equation (2.14) and equation (2.17) to equation (2.16).

The strain-charge equation [115,116,127]:

$$S = s^{\mathrm{E}}\sigma + d^{T}\mathrm{E}, \tag{2.18}$$

$$D = d\sigma + \epsilon^{\sigma}\mathrm{E}. \tag{2.19}$$

The equation (2.18) represents the converse piezoelectric effect, i.e., the strain of the sample under the electric field load. This corresponds to the device being used as an actuator, and

equation (2.19) deals with the opposite case when the transducer is being used as a sensor (direct piezoelectric effect).

Strain voltage from or sensor/energy-harvesting form:

$$S = s^D\sigma + g^T D, \tag{2.20}$$

$$E = g^\sigma + (\varepsilon^\sigma)^{-1} D. \tag{2.21}$$

Where s is a 6 × 1 mechanical strain (m/m), σ is a 6 × 1 mechanical stress (Pa), E is a 3 × 1 electric field (V/m), D is a 3 × 1 electric displacement field (C/m²), g is a 6 × 3 piezoelectric voltage or pressure constant matrix ($\frac{m^2}{C}$ or $\frac{V.m}{N}$), ε^σ is a 3 × 3 dielectric permittivity matrix ($\frac{F}{m}$), s^E is a 6 × 6 elastic compliance coefficient matrix ($\frac{m^2}{N}$), d is a 3×6 piezoelectric strain (charge) coefficient ($\frac{C}{N}$ or $\frac{m}{V}$), and T denotes the transposed matrix.

$$S_{ij} = s^E{}_{ijkl}\,\sigma_{kl} + d_{kij}\,E_{\mathrm{k}}, \tag{2.22}$$

$$D_i = d_{ijk} + \epsilon^\sigma{}_{ij}\mathrm{E}_{\mathrm{kj}}, \tag{2.23}$$

in the stress-charge form:

$$\sigma_{ij} = C^E{}_{ijkl}S_{kl} - e_{kij}\mathrm{E}_k, \tag{2.24}$$

$$D_i = e_{ijkl}S_{jk} + \epsilon^S{}_{ik}E_{\mathrm{k}}, \tag{2.25}$$

stress voltage form

$$\sigma_{ij} = C^D{}_{ijkl}S_{kl} - h_{kij}\,D_k, \tag{2.26}$$

$$E = -h_{ijk}S_{jk} + (\epsilon^S)^{-1}D_j. \tag{2.27}$$

Equitation 2.18 and 2.19 in matrix form are the following:

$$\begin{bmatrix} S_1 \\ S_2 \\ S_3 \\ S_4 \\ S_5 \\ S_6 \end{bmatrix} = \begin{bmatrix} d_{11} & d_{12} & d_{13} \\ d_{21} & d_{22} & d_{23} \\ d_{31} & d_{32} & d_{33} \\ d_{41} & d_{42} & d_{43} \\ d_{51} & d_{52} & d_{53} \\ d_{61} & d_{62} & d_{63} \end{bmatrix} \begin{bmatrix} E_1 \\ E_2 \\ E_3 \end{bmatrix} + \begin{bmatrix} s_{11}{}^E & s_{12}{}^E & s_{13}{}^E & s_{14}{}^E & s_{15}{}^E & s_{16}{}^E \\ s_{21}{}^E & s_{22}{}^E & s_{23}{}^E & s_{24}{}^E & s_{25}{}^E & s_{26}{}^E \\ s_{31}{}^E & s_{32}{}^E & s_{33}{}^E & s_{34}{}^E & s_{35}{}^E & s_{36}{}^E \\ s_{41}{}^E & s_{42}{}^E & s_{43}{}^E & s_{44}{}^E & s_{45}{}^E & s_{46}{}^E \\ s_{51}{}^E & s_{52}{}^E & s_{53}{}^E & s_{54}{}^E & s_{55}{}^E & s_{56}{}^E \\ s_{61}{}^E & s_{62}{}^E & s_{63}{}^E & s_{64}{}^E & s_{65}{}^E & s_{66}{}^E \end{bmatrix} \begin{bmatrix} \sigma_1 \\ \sigma_2 \\ \sigma_3 \\ \sigma_4 \\ \sigma_5 \\ \sigma_6 \end{bmatrix}, \tag{2.28}$$

$$\begin{bmatrix} \mathrm{D}_1 \\ \mathrm{D}_2 \\ \mathrm{D}_3 \end{bmatrix} = \begin{bmatrix} \varepsilon_{11}{}^\sigma & \varepsilon_{12}{}^\sigma & \varepsilon_{13}{}^\sigma \\ \varepsilon_{21}{}^\sigma & \varepsilon_{22}{}^\sigma & \varepsilon_{23}{}^\sigma \\ \varepsilon_{31}{}^\sigma & \varepsilon_{32}{}^\sigma & \varepsilon_{33}{}^\sigma \end{bmatrix} \begin{bmatrix} \mathrm{E}_1 \\ \mathrm{E}_2 \\ \mathrm{E}_3 \end{bmatrix} + \begin{bmatrix} \mathrm{d}_{11} & \mathrm{d}_{12} & \mathrm{d}_{13} & \mathrm{d}_{14} & \mathrm{d}_{15} & \mathrm{d}_{15} \\ \mathrm{d}_{21} & \mathrm{d}_{22} & \mathrm{d}_{23} & \mathrm{d}_{24} & \mathrm{d}_{25} & \mathrm{d}_{26} \\ \mathrm{d}_{31} & \mathrm{d}_{32} & \mathrm{d}_{33} & \mathrm{d}_{34} & \mathrm{d}_{35} & \mathrm{d}_{36} \end{bmatrix} \begin{bmatrix} \mathrm{E}_1 \\ \mathrm{E}_2 \\ \mathrm{E}_3 \end{bmatrix}. \tag{2.29}$$

Where $c^{E/D}$ is a 6×6 elastic stiffness coefficient matrix (for $\frac{E}{D}$ = 0) in $\frac{N}{m^2}$, h is a 3×6 piezoelectric deformation coefficient matrix in $\frac{N}{C}$ or $\mathrm{V/m}$ (the matrix for the direct piezoelectric

effect), and d^t is the matrix for the converse piezoelectric effect. The superscripts E, T, and t indicate a zero or constant electric field, stress field, and the transposition of a matrix, respectively. dij represents the polarisation generated by applied mechanical stress or strain developed in piezoelectric materials per electric field applied. Equation 2.28 and 2.29 are the core general for piezoelectric modeling as they are used for comprehensive, multi-axis, high-fidelity simulations where 1D approximations are insufficient. But for one dimension equation, the 2.18 and 2.19 or 2.24 and 2.25 are the appropriate. In an Euler-Bernoulli cantilever beam model (the standard approach for MFC harvesters, e.g., Erturk & Inmanstyle formulations [77,125]), the strain is given by the bending kinematics of the beam. At any point strain is directly prescribed by the beam curvature and the distance from the neutral axis, and once a mode shape is assumed or the beam PDE is solved it is a known function.

2.7. Piezoelectric Energy Harvesting working mode and Configuration

Piezoelectric energy harvesting facilitates the advancement of eco-friendly, complete, battery-free devices and apparatuses that are energised through microwatt-scale energy conversion and low-frequency movements within the body system. The main target of this innovative technology enhances the sustainability of small electronic devices and electronic medical equipment and opens new avenues for continuous health monitoring and data collection without the need for frequent battery replacements. The configuration of a piezoelectric energy harvester can be broadly classified into classical and non-classical structures. The classical PEH structure is based on well-defined regular shapes, such as trapezoids and triangular shapes, and the non-classical PEH structure is based on specific applications and is largely influenced by irregular shapes [128]. Various strategies exist to improve the performance of energy harvesting systems, such as selecting piezoelectric materials, their structural modifications, hybridisation, selecting proper substrates, and selecting preparation methods for piezoelectric materials [1,86]

In the design of piezoelectric energy harvesters, the creation layer of the piezoelectric structure is critical. Mechanical structures and geometries that have been employed for energy harvesting, including cantilever beams, stacks, cymbals, and diaphragms, are designed to capture energy from stress and frequency vibrations [50]. The cantilevered PEH has attracted the most attention of the researchers, as the ambient vibrations occur at a low frequency (below 200 Hz), and a cantilever beam has the lowest stiffness for a given size; thus, it is easier to design a low-frequency PEH by using a cantilever beam [1,129].The power output is proportional to the average strain in the PEH, and the cantilever beam generates the highest average strain for a given mechanical load. MFC patches were typically bonded to cantilever

beam structures in various configurations. A piezoelectric transducer on the rectangular beam could be either a unimorph [112,127] that is, the substrate covered with a piezoelectric patch on its lower or upper surface, or a bimorph, which has two surfaces layered with the smart material.

The unimorph configuration can be designed in 31-mode or 33-mode, depending on electrode arrangements concerning the piezoelectric layer. In the 31-mode, the layered piezoelectric material is sandwiched between two electrodes, while in the 33-mode, the electrode is on top of the transducer with an inter-digital electrode pattern. Mode 31 simplifies manufacturing because piezoelectric materials are easier to polarise in the thickness direction than along the length. On the other hand, the bimorph configuration is commonly designed to operate in the bending mode to have the top layer in tension and the bottom layer in compression, or vice versa, when the system vibrates, hence generating an electric charge under the piezoelectric effect. The charge poling of the top and bottom layers can be made in the same direction or in the opposite direction, which is commonly known as parallel or series poling. The essence is to induce an accumulated current in parallel poling or voltage in series poling from each layer. The bimorph configuration has the advantage of producing higher output when implemented in an energy harvesting scenario. However, the unimorph configuration is preferable for MEMS applications due to the lower cost incurred for production [128]. It is a piezoelectric material perfectly bonded to a lower substrate layer. In the figure below, x_2 refers to the piezoelectric material length, x_1 is the offset distance of the piezoelectric material from the clamped end, and x_3 is the distance from the end of the piezoelectric material to the cantilever tip.

Cantilever beam

Piezoelectric vibration energy harvesters are commonly designed in the form of beams, plates, membranes, or shell structures. Among these configurations, cantilever beams are the most widely used because they generate relatively high strain under low-frequency vibration [12]s. In addition, their dynamic characteristics can be effectively tuned by adjusting parameters such as beam length, thickness, proof mass, materials' stiffness, and boundary conditions.

The rectangular cantilever beam is among the most used structures in piezoelectric energy harvesting, as it experiences large deflections under vibration and is therefore well-suited for power generation. This structure also has relatively low working frequency, suitable for low-frequency energy harvesting. There were also other novel geometric designs, but their manufacturing complexity increases the costs and probability of failure; hence, the rectangular cantilever configuration is often used [37,100,130].

It can be deformed by force due to external vibration to achieve different vibration states and produce matching outputs. An electrode layer, a piezoelectric layer, and an epoxy are substrate layers that are easy to integrate into this type of energy harvester [50,131]. In addition, piezoelectric energy-harvesting devices use a cantilever beam structure because they can operate in both the d_{33} and d_{31} modes and achieve the maximum deflection among other beam boundary conditions. This configuration has wide applications in the field of sensors, actuators, structural health monitoring systems, and energy harvesters [132,133] . The un-morph, Bimorph series, or Bimorph parallel are types of cantilever configurations that can be used for energy harvesting.

In Figure 2-6 the MFC unmorphed configuration is modelled based on the Euler-Bernoulli beam theory, and it is assumed to be excited by the translation of its base in the transverse direction with a superimposed small rotation. A resistive load is considered in the electrical circuit for simplicity. After deriving the governing differential equations, closed-form solutions for the coupled vibration response and the voltage response are obtained for harmonic base excitations. Model predictions are first verified for an MFC unmorphing with an Al substrate, and then validations are given for MFC unmorphing with numerical simulation and experimental model [29].The strain generated on the substrate is transferred to the piezoelectric layers as the cantilevered harvester oscillates around the natural frequency. The configurations include the piezoelectric cantilever harvesters that follow the piezoelectric direct effect, i.e., mechanical input results in electrical output. When these harvesters are subjected to mechanical loading, i.e., vibrations, the charge is collected on the surface of the MFC, causing a voltage difference across the thickness of the patch [128]. To save energy, harvesters are generally designed to operate in the first resonant mode. The resonant frequency of the cantilever beam structure is often much higher than the frequency of external excitation from the local environment [47]. The strain is at maximum in the clamped end of the cantilever, and when the piezoelectric element goes further away from the clamped end, the voltage decreases. Thus, not the entire length of the piezoelectric element participates in power generation, and the power output also depends on the location of the MFC placement and applied force. Therefore, cantilever beam energy harvesters faced the challenge of relatively low energy conversion efficiency, which can be improved by modifying their shape and structure. Figure 2-6, the rectangular-type cantilever is a common type of structure, but this design has an important level of stress at the fixed end and uneven strain distribution along the length. These issues not only lead to low energy extraction efficiency of the device but also cause material fatigue-induced damage at the cantilever root. Standing on this structure, researchers have developed a

cantilever beam energy harvester with various configurations, including trapezoidal, tapered, and bionic structures. This type of shape and structure has optimised stress distribution and enhanced power output performance; simultaneously, it poses challenges regarding mass distribution and overall structural integrity [1,2,50].

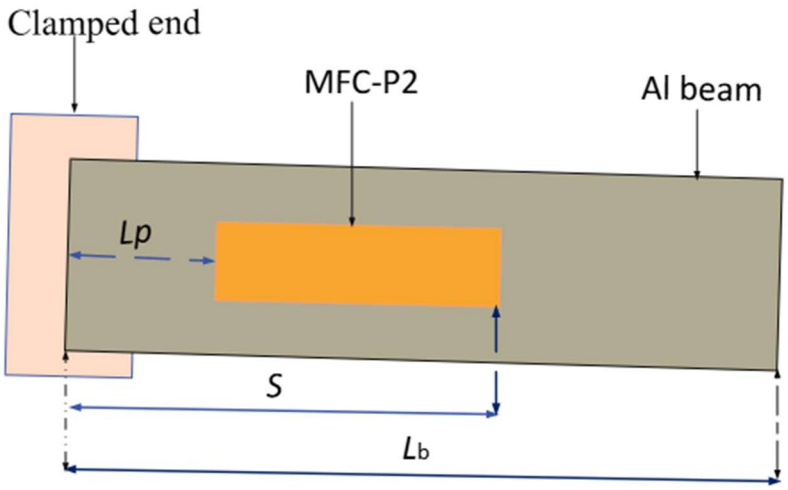


Figure 2-6 Schematic of the MFC piezoelectric with rectangular cantilever beam EH

Cymbal type

Cymbal-type energy harvesters have been developed for applications involving high-impact forces. Typically, this energy harvesters consist of a piezoelectric disc sandwiched between two metallic end caps, which are bonded using epoxy. The feasibility of energy harvesting from asphalt pavement using a traditional piezoceramic cymbal has recently been demonstrated. The results showed that a single piezoceramic cymbal can recover up to 16 μW of power from the passage of one heavy-vehicle wheel [134]. The author of this work explored a new type of radially layered cymbal piezoelectric energy harvester by combining cymbal metal end caps with a radially layered piezoelectric structure for energy harvesting from road traffic-induced low-frequency vibrations. The cantilever beam configuration has several disadvantages compared with the cymbal type in terms of efficient stress transfer. Furthermore, the maximum displacement of the cantilever beam is limited by the maximum force applied to the beam, and the generated voltage is also limited and lower than that of the cymbal type. Repeated bending over time weakens the piezoelectric element and, consequently, reduces its lifetime [1,2].The most important disadvantage of the cymbal type, despite their ability to generate high voltage, is their low sensitivity to ambient sources due to their low vibrations.

Circular Diaphragms

The piezoelectric circular diaphragms are very similar to the cantilever beam configurations. A thin circular disc of the piezoelectric crystal is manufactured and then bonded to a metal shim. Then it is clamped to an edge so that the vibration of the edge can supply the required vibration for the piezoelectric material to get excited. Chen and Yang [135] designed power up to 12 mW across a 33 kΩ resistor using piezoelectric circular diaphragms with a prestress of 1.2 N at 113 Hz. Some applications of MEMS and wireless sensors can be satisfied with this amount of power. The study shows that increasing the proof mass increases the interaction between the mass and the piezoelectric disc, which results in the enhancement of the harvested power. This design reached an increment of about 2 mW of the maximum power output when compared with previous research where the maximum output power ranged from 2 to 10 mW [2,135]. To increase the output power even more, multiple circular diaphragms can be connected in series. However, the relationship between the number of connected harvesters and the output power is nonlinear. Another key factor influencing the output power is the thickness of the piezoelectric material. Like in the case of cantilever beam and cymbal configurations, the energy harvesting ability depends on the bending behaviour of the piezoelectric element. The thicker the piezoelectric material, the more resistant it is to bend and the lower the deflection. Thus, power conversion efficiency is reduced. Thus, the thickness of piezoelectric material should be matched to the required deflection for optimum power generation.

Stack geometric configuration

The stacked energy harvesting structure is formed by stacking piezoelectric sheets in either series or parallel [136]Stacked piezoelectric transducers are formed by stacking multiple piezoelectric layers on top of each other so that the poling direction of the layers is aligned with the applied force and are used in applications where high pressure is required [1,136,137].

Consequently, there has been a significant increase in research focused on enhancing the efficiency of piezoelectric energy harvesting. Enhancing the efficiency of piezoelectric energy harvesting, including material composition, innovative mechanisms for more efficient motion conversion, amplifier frame structural (mechanical) designs, the frequency tuning method, and improvements in electronic components such as electrode polarisation methods and energy storage methods [23,51,138].

To design efficient harvesters, it is essential to establish accurate mathematical and computational models that couple the mechanical vibration behaviour of the host structure with

the electrical output of the piezoelectric element. Analytical models based on Euler–Bernoulli beam theory and linear piezoelectric constitutive equations are often used to predict the voltage and power output under harmonic or random excitations [139,140].However, analytical formulations are limited to simple geometries and boundary conditions. Despite a significant reduction in the power consumption of electronic devices, the power generated from the energy harvesting solutions is not sufficient for replacing the batteries in WSNs. Moreover, the conventional linear harvesters suffer from a narrow operational bandwidth while the ambient vibrations are scattered over a frequency range. Many research attempts have been reported for the performance and efficiency enhancement of harvesters, which can be categorised into four groups: (1) advanced piezoelectric and structural configurations; (2) sophisticated energy harvesting circuits; (3) frequency up-conversion in ultra-low-frequency scenarios; and (4) broadband energy harvesting [141].

2.8. Modelling mechanical vibration based piezoelectric energy harvesters

The modelling of piezoelectric energy harvesters based on mechanical vibration is necessary to understand and predict the coupled mechanical and electrical behaviour of the harvesting system. Typically, the modelling approach couples the dynamic response of the host structure with the piezoelectric constitutive relations to describe the conversion of the mechanical strain into electrical energy. Depending on the purpose of the analysis, analytical models based on beam theory can be used to determine the natural frequencies, mode shapes, displacement, voltage and harvested power. Finite element models provide a more detailed representation of the geometry, material properties, boundary conditions and electromechanical coupling. The harvester's electrical behaviour can be coupled also to an external load so that it can evaluate the voltage and power produced under different excitation conditions. Thus, an appropriate electromechanical model is the basis for analysing the influence of structural, material and electrical parameters and for identifying optimal operating conditions to improve the energy-harvesting performance [142].

2.8.1Analytical modelling of piezoelectric based energy harvesting

Mathematical equations are used in analytical models to describe the dynamics of piezoelectric systems. These models often employ electrical analogies to represent mechanical systems, providing the ability to analyse voltage and power output under different operating conditions. However, these modelling approaches are limited by assumptions and simplifications, which may not capture all the complexities of real-world systems [10].

Nevertheless, analytical models are valuable for the initial design and optimization of energy harvesters, providing insights into the influence of parameters such as electrical load on energy conversion efficiency [143].

Finite element modelling piezoelectric energy harvesting

While analytical models are highly effective for simple geometries, such as uniform rectangular structures, practical engineering applications often involve more complex geometries, non-uniform material layers, and localised stress concentrations that cannot be accurately captured using simplified analytical approaches. Finite element modelling (FEM) provides a full simulation of piezoelectric energy harvesters, considering the material properties, geometry, and boundary conditions [100,144,145].

It is a powerful method for accurately predicting the behaviour of complex piezoelectric systems, including the influence of proof mass and substrate materials on resonance frequencies and energy harvesting performance parameters [144]. In addition, advanced FEM techniques, such as monolithic mixed-hybrid formulations, enable the simulation of strongly coupled electromechanical systems and provide deeper insight into the interaction between the mechanical and electrical domains [42,145]. Among the commercially available software packages for simulating piezoelectric energy harvesters (PEHs), ANSYS and COMSOL Multiphysics are the most widely used. COMSOL is widely preferred because its built-in Piezoelectricity Multiphysics interface provides seamless coupling between the Solid Mechanics and Electrostatics modules, enabling efficient and accurate modelling of the electromechanical behaviour of piezoelectric energy harvesters. Analytical models are attractive due to their simplicity and ease of implementation, but they often fail to capture all the complexities of piezoelectric systems. Finite element models, on the other hand, are more detailed and accurate in their predictions, though at the cost of increased computational effort and specialised expertise. Thus, the two approaches are complementary: analytical models are useful for the initial design and understanding of the system behaviour, while finite element modelling is used to refine the design and validate its performance by means of detailed numerical simulations. In the next chapter these methods are detailed with their model assumptions.

2.9 Optimizing performance of energy harvesting systems

Energy harvesting converts ambient mechanical, thermal, or any other form of energy into usable electrical energy for low-power electronics. Among the various transduction mechanisms, piezoelectric harvesters stand out because of their strong electromechanical coupling, compact form factor, and straightforward integration into lightweight or miniaturised systems [1,23,131,138]. Despite their material advantages, piezoelectric harvesters rarely reach their theoretical output potential. The intrinsic properties of the piezoelectric materials such as electromechanical coupling coefficients, compliance, dielectric permittivity, and loss factors directly determine the achievable energy conversion. However, material quality alone is not enough. Without an optimised structural configuration, the usable strain in the piezoelectric layer remains low, resonance frequencies are mismatched with ambient excitation, and electrical power output is severely limited. Real performance gains come from tuning geometry, boundary conditions, electrode configuration, placement, and mechanical electrical load matching. Only when the material properties and structural configuration are jointly optimised can the harvester deliver power close to its physical limits.

Structural optimization plays a critical role in determining how effectively vibration energy is converted into mechanical strain within the piezoelectric material. In cantilever-based energy harvesters, beam geometry strongly influences the natural frequency, strain distribution, concentration of stress, and overall structural durability. In addition to the geometry of the harvester, the maximum achievable voltage amplitude is obtained by optimising several key system parameters, including the attachment position, attachment mass, mass moment of inertia, external excitation force location, and piezoelectric patch placement [146].

Increasing the beam length generally reduces the natural frequency, which is advantageous for harvesting low-frequency ambient vibrations; however, excessively long beams may decrease mechanical stability and robustness. Similarly, the addition of a tip mass can lower the resonant frequency and increase bending strain, thereby improving electrical output, although it may also lead to excessive deflection and higher stress levels. Beam shape also affects energy conversion efficiency. For example, tapered cantilever beams can produce a more uniform strain distribution along the structure, leading to improved utilisation of the piezoelectric material. The resonance frequency of these shape harvesters has been extracted using modal analysis, at which the harvester can achieve maximum power efficiency. In this paper [41] shows that

triangular-shaped bimorph piezoelectric energy harvesters generate more power than trapezoidal harvesters. Also, the lower resistance is required for the triangular bimorph harvester to achieve maximum power at resonance, leading to higher efficiency and lower loss in sensing applications than the rectangular harvester. In addition, the length and placement of the piezoelectric patch can be optimised so that the active material is positioned in regions of maximum strain. Therefore, the triangular and trapezoidal cantilever beam is the optimum design compared to the rectangular harvester.

Recent analytical, numerical, and experimental studies have therefore focused on optimising cantilever thickness profiles, piezoelectric patch placement, and proof-mass configurations to enhance power output and achieve improved resonance matching with ambient vibration sources [1,129,138,146–148]. Since vibration energy harvesters typically operate near resonance, matching the natural frequency of the harvester to the dominant environmental excitation frequency is essential for maximising energy conversion efficiency. Several tuning approaches have been developed for this purpose, including adjustment of the proof mass, modification of beam geometry, application of axial preload, introduction of magnetic stiffness, variation of boundary conditions, and the use of adaptive electrical circuits. However, many practical vibration sources are broadband, random, intermittent, or time-varying in nature. Under such conditions, conventional narrowband resonant tuning may not provide satisfactory performance. To address this limitation, various broadband energy harvesting strategies have been proposed, including the use of harvester arrays with staggered resonance frequencies, multimodal beam structures, nonlinear stiffness mechanisms, bistable systems, frequency up-conversion techniques, and active or passive self-tuning approaches.

The selection of an appropriate strategy depends on factors such as the predictability of the excitation source, the required operating system complexity, and the practical trade-off between energy harvesting performance and implementation cost [130,146].In practical applications, energy vibration harvesters are typically designed to operate at a specific frequency determined by the target environment. Optimal performance is generally achieved when the harvester operates near its resonance frequency, where the vibration amplitude and the resulting strain are significantly amplified, leading to increased electrical energy.

The vibration energy harvester must meet several requirements at the same time, including high power output, sufficient voltage generation, wide operating bandwidth, low weight, low cost, environmental friendliness, mechanical reliability, ease of manufacturing, and compatibility with the intended application. In many cases, improving one characteristic can

negatively affect another. For example, increasing the thickness of a ceramic piezoelectric layer may improve electromechanical coupling, but it can also increase the structural stiffness and shift the resonance frequency to a higher range. Similarly, adding a larger proof mass may enhance strain and electrical output while reducing structural durability and stability. In polymer-based materials such as PVDF composites, increasing the filler concentration can improve the dielectric properties, but it may also increase brittleness and electrical leakage.

Because of these trade-offs, harvester design should be approached as a multi-objective optimization problem rather than focusing on a single parameter. To achieve unbiased comparisons between different harvester design geometries, parameter studies are performed by changing multiple parameters simultaneously while holding the natural frequency near the excitation frequency. Another performance enhancement was observed using the placement of the piezoelectric positions as compared to the conventional design, in which the piezoelectric and substrate have equal geometric structures [52,130,141].

Recent analytical and experimental studies are being further refined, considering factors such as cantilever thickness, placement of the piezoelectric patches, and tip mass configuration to enhance power output and achieve better frequency matching. Consequently, the non-classical PE energy harvesting optimization approach adopted in this thesis is founded on the finite element method, which proves to be more robust and cost-effective than alternative techniques. The results show that a tapered, geometry-based optimization strategy can improve energy harvesting efficiency by up to 50% compared to conventional rectangular harvesters. This enhancement arises from the influence of the beam width profile, which is particularly advantageous because tapered beams promote a more uniform strain distribution and more efficient use of the material [1,8,78].

2.9.1 Optimisation Methods for PEH in COMSOL Multiphysics

Design optimisation has become an established phase in the development of piezoelectric vibration energy harvesters (PVEHs) because the electrical performance of cantilever-based devices depends strongly on their geometry, the distribution of active piezoelectric material, and the characteristics of the connected electrical load. COMSOL Multiphysics is frequently employed for this task, as it integrates structural mechanics and the piezoelectric constitutive relations within a unified finite element framework, and its Optimization Module offers three conceptually distinct optimisation categories: shape optimisation, topology optimisation, and parametric optimisation. Choosing between these is not a subjective decision; it is dictated by

the type of design variable to be adjusted, whether an unconstrained boundary shape, a spatial material layout, or a limited set of geometric or sizing parameters.

Parametric (size) optimisation

Parametric optimisation assumes that the harvester's topology and general shape class are fixed and seeks optimal values for a finite set of scalar design variables, including beam length, thickness, taper ratio, patch position, tip mass, and load resistance, to maximise a chosen performance metric such as power or voltage. This strategy is by far the most reported for cantilever-type PVEHs, primarily because the design variables correspond directly to quantities that are both manufacturable and straightforward to interpret physically. Hashim, Mahmoud and Ridha, for instance, used COMSOL Multiphysics to compare rectangular, triangular, circular, and trapezoidal cantilever cross-sections and showed that a multi-faceted trapezoidal cross-section can yield significantly higher output power than a standard rectangular beam, thereby illustrating how systematic variation of size and cross-sectional geometry can reveal superior designs. In related work, [149] integrated COMSOL finite element simulations, eigenfrequency analyses, and MATLAB-based analytical models with a genetic algorithm to optimise five different cantilever geometries: T-shaped, rectangular, L-shaped, variable-width, and triangular, again keeping the basic beam topology fixed and varying only its parametric description. At the material and circuitry scale, [150,151] formulated an analytical model for a piezoelectric cantilever with an in-span attachment and employed a genetic algorithm, assisted by a neural network surrogate trained to predict the natural frequency, to optimise the attachment mass, moment of inertia, attachment location, and patch position so that the beam's natural frequency coincided with the excitation frequency. In a similar spirit,[152] posed the choice of piezoelectric material and fiber volume fraction in a macro Fiber composite (MFC) harvester as a parametric optimisation problem, while a more recent contribution combined artificial neural network surrogates with a genetic algorithm to jointly optimise geometric and circuit parameters, patch location, tip mass, and load resistance of an MFC cantilever. Taken together, these works underscore that parametric optimisation is the standard approach when the overall beam shape family (uniform rectangular, tapered, stepped, etc.) is predetermined by the designer and only the dimensions and material distribution are adjusted.

Shape optimization

Shape optimisation, in contrast, permits the boundary or outer contour of a structure to vary continuously using control points, spline-based parameterisations, or mesh morphing without requiring the designer to commit in advance to a particular geometric class such as "rectangular"

or "trapezoidal". In the PVEH literature, this approach is most employed to identify an optimal, smoothly varying taper along the beam's length, rather than to compare
a small set of predetermined shapes. A representative case is the wind-driven energy harvester examined by [153] Zhao, Zhang, Wang, Han and Hao, who modelled the cantilever's non-uniform cross-section with a piecewise cubic Hermite interpolation and coupled an enhanced piecewise Galerkin discretisation with particle swarm optimisation to evolve the beam profile. They reported that this yielded more than a three-and-a-half-fold increase in output power compared with a prismatic beam. Although the authors refer to their procedure as a topological optimisation, the actual design variable is the continuous external boundary of the beam's cross-section, not a discrete material void layout. Conceptually, this aligns the work more closely with shape optimisation as framed in the COMSOL Optimization Module. This distinction is important when choosing methods: shape optimisation is the suitable strategy when the taper profile itself is the unknown to be identified, rather than a limited set of fixed geometric parameters describing that profile.

Topology Optimization of Piezoelectric Energy Harvesters

Topology optimisation operates at a more fundamental level again: instead of merely reshaping a boundary or resizing a predefined geometry, it distributes material freely within
a given design domain (typically modelled as a density field between 0 and 1 using a Solid Isotropic Material with Penalisation, or SIMP, formulation), enabling the algorithm to identify structural layouts that were not specified beforehand. This technique has been widely employed in piezoelectric energy harvesting, particularly for two-dimensional plate-type harvesters and for determining the optimal placement of piezoelectric patches and electrodes within an otherwise passive structure [154–156] Homayouni-Amlashi, Mohand-Ousaid and Rakotondrabe used topology optimisation for multi-directional piezoelectric plate harvesters and, in a related study, for a two-degree-of-freedom plate harvester under external in-plane loading, explicitly addressing the charge-cancellation issue that occurs when different regions of a plate undergo strains of opposite sign. In a broader review of their work, they clearly differentiate three main design strategies for piezoelectric energy harvesters' parametric optimisation, a hybrid scheme, and topology optimisation, thereby offering a useful methodological framework for researchers deciding among them. In a separate line of work, [153], Zhang and Xia applied topology optimisation to the through-thickness distribution of piezoelectric material in plate-type harvesters, aiming to increase open-circuit voltage while reducing voltage cancellation due to phase inconsistencies. Their studies build on early

contributions by [157] Zheng, Chang and Gea, generally recognised as the first to introduce topology optimisation in the context of piezoelectric energy harvester design, and by [153–157], who investigated both static and harmonic dynamic loading conditions. Further extended the approach to folded-beam and broadband, multi-resonant harvester configurations, searching for topologies that maintain a more uniform power output over a spread of excitation frequencies. Consequently, topology optimisation is most appropriate when the spatial distribution of piezoelectric or structural material, rather than only the external dimensions, is itself the primary design unknown, and it usually requires a carefully defined design domain, a suitable material interpolation model, and mesh-independent regularisation, all of which go beyond what is needed in a straightforward beam-sizing problem.

2.9.2 Choosing the appropriate Method for a parametric optimisation

Taken as a whole, this literature points to a clear correspondence between design objectives and the appropriate optimisation strategy. When the beam topology and overall shape class are prescribed by the designer and the unknowns are limited to scalar dimensions, spatial locations, or electrical properties as in the rectangular and tapered-rectangular MFC cantilever layouts examined in a sizing study, researchers consistently adopt parametric optimisation. This is illustrated by the works of [149] Hashim et al., Mohamed et al., and the in-span attachment study by [150] Homayouni-Amlashi et al. Shape optimisation only comes into play when the taper or boundary profile itself must be determined, rather than a small, predefined set of parameters describing it, as in the continuously varying cross-sections reported by [153] Zhao et al. Topology optimisation is reserved for cases where the material distribution within a design domain is not known in advance, such as the plate-type harvesters investigated by [155] Homayouni-Amlashi et al. and He et al.

2.9.3 Local and global parametric optimization selection

Once parametric optimisation has been identified as the suitable approach, a second decision concerns whether to employ local or global search algorithms. The parametric (sizing) optimisation solvers built into COMSOL are mainly local, relying on gradient-based or model-based strategies that typically converge efficiently to the nearest optimum from a chosen initial guess, but they cannot guarantee discovery of a global optimum when the objective landscape is multi-modal. BOBYQA (Bound Optimisation BY Quadratic Approximation), introduced by Powell, is a representative example: a derivative-free trust-region algorithm that constructs successive quadratic interpolation models of the objective function, enforcing bound constraints

on the design variables and avoiding the need for explicit gradient evaluations. Follow-up work by [158] Cartis, Fiala, Marteau and Roberts generalised and enhanced the robustness of these model-based derivative-free approaches, while later contributions proposed heuristic modifications that improve BOBYQA's ability to escape local minima, albeit still without rigorous guarantees of global optimality.

2.10. Applications of energy harvested from piezoelectric materials

Piezoelectric vibration harvesters play an increasingly significant role in wireless sensor networks and structural health-monitoring systems. These sensors are often installed on bridges, buildings, aircraft, wind turbines, pipelines, railways, and rotating machinery environments where continuous high-power operation is rarely required. Instead, the system typically performs periodic sensing and wireless data transmission. In such cases, the harvested energy is stored in a capacitor and released intermittently to power sensing and communication tasks. In some designs, the same piezoelectric element can function simultaneously as both the sensor and the energy harvester, enabling compact and fully self-powered monitoring systems.

Structural applications, however, impose demanding requirements. long-term durability, environmental resistance, stable bonding between the harvester and the host structure, and reliable electrical output under variable vibration conditions are all essential. These constraints become even more pronounced in wearable and biomedical applications, where traditional brittle piezoelectric ceramics are often unsuitable [5,159]. Human motion typically involves low-frequency, irregular, and mechanically compliant excitation. Because of this, flexible and non-classical piezoelectric materials such as PVDF, P(VDF-TrFE), flexible lead-free composites, and biodegradable piezoelectric materials have gained significant attention. These materials can be integrated into shoes, clothing, wearable patches, joint supports, and even implantable medical devices. Although the electrical output is modest compared to ceramic-based harvesters, it is generally sufficient to power low-energy sensors and intermittent wireless communication [160].

In wearable and biomedical contexts, additional design considerations become critical: biocompatibility, user comfort, washability, mechanical fatigue resistance, and low-temperature fabrication processes. These factors ultimately determine whether a piezoelectric energy harvesting system can operate reliably and comfortably in real-world human-centred environments [79,161].There are several authors who have also targeted their devices for application. Energy harvesting technologies have advanced to practical power levels. The

authors Wacharasindhu and Kwon [162] designed and evaluated the device which integrated under the keyboard, with a maximum power of 40μW generated by the piezoelectric transducer. Renaud et al. have presented human limb motion energy harvesting. Due to the low frequencies that exist in this application, he developed an impact-based energy harvester. His experiment results indicated that the device could generate 47 μW when it is rotated with frequency 1 Hz [163].Table 2-3 review of previous research shows the wide range of applications for vibration energy harvesting. The power levels these devices achieve are practical and sufficient, especially for applications such as condition monitoring with wireless sensors. Some of the general applications of piezoelectric energy harvesting: Pedestrian footsteps energy harvesting MEMS devices, transportation infrastructure, wearable electronics, automotive suspension systems, and hybrid vibration energy harvesters. These applications demonstrate the potential of piezoelectric materials to convert ambient mechanical energy to electrical energy for self-powered electronic devices.

Table 2-3 PEH operation frequency, output energy, application area, and their limitations.

Piezoelectric materials for energy harvesting using cantilever beams.	Operation frequency range	Output voltage (V)	Output power (mW)	Application area	Limitation
Lead Zirconate Titanate (PZT-5A, 5H) Ceramics [1,87,164,165].	10 Hz–150 Hz	10-45	5-300	High-power sensors, actuators, industrial machinery, and bridge health monitoring.	Rigid, easy to brittle. Contains lead element; toxic, very limited strain and requires bulky device.
PVDF (polymer) [52,87,166]	1–50	1–10	0.01-10	Wearable electronics, flexible devices, low-frequency vibration, smart textiles, and insoles.	Low piezoelectric coefficient, high impedance requirements, and poor thermal stability.
$BaTiO_3$ (Lead-Free Piezoelectric Ceramics)[165,167,168]	30–200 Hz	1-15	0.1-10	Lead-free energy harvesters Implantable bio, flexible EH and wireless IoT nodes.	Brittle; moderate output; often needs high stress. Lower efficiency than PZT, low Curie

					temperature (120℃).
PZT Single Beam with Tip Mass [3]	1.5-4	0.6-0.8	0.01-0.4	Civil structures (e.g., vehicle vibrations in suspension bridges).	Fatigue cracking is often initiated early due to heavy strain and stress concentration at the root block.
M8514-P2 Transverse Type MFC [100]	Near 10.78	0.1952	0.0031	Embedded self-powered mechatronic systems and structural health monitoring (SHM).	Generates very low power in unamplified low-strain ambient structural vibrations.
Flexible d31-Type MFC Array [169]	Low frequency, water flow vortex	42.2 (peak-to-peak)	0.6337-0.9639	Wearable electronics, watch-sized bio-motion harvesters.	The metal sphere impact mechanism creates structural noise and localised material stress over time.
Bicylinder Fluid-Coupled MFC Bimorph [170]	Low speed	Variable AC output	0.02186	Marine environmental monitoring using vortex-induced vibrations.	Sensitive to the slight change of spacing ratio (L/D) between cylinders.

Table 2-3 shows the types of piezoelectric materials, operation frequency, output energy, application area, and their limitations in energy harvesting. In general, vibration energy harvesting is no longer just a theory. Current power output is more than enough for wireless industrial sensors, infrastructure monitors, and low-power medical implants. Design optimization and miniaturisation are the last boundaries for widespread commercial adoption.

As a conclusion, this literature review is the state-of-the-art energy harvesting technologies with a focus on piezoelectric energy harvesting, which can significantly affect the power conversion efficiency and applicability of the harvester. The first starts with an introduction of energy harvesting mechanisms that have been presented, including electromagnetic, electrostatic, and piezoelectric methods. The wasted or unused mechanical energy from ambient vibration can be used to convert mechanical energy into electrical energy by designing a self-powered electromechanical system to support the development of smart wireless sensor devices for future technology applications. The conventional wired/wireless sensor devices still depend

on the power supply from the battery, which is a tedious task to replace and time-consuming for maintenance during the system operation.

This section provides the main contributions which fill the limitations of classical PEH to power small electronics. Since the major work of this thesis has been focused on the comprehensive review of PEH, theoretical modelling and numerical modelling, experimental testing and, finally, geometrical optimisation, the details were discussed. The important thing to note is that when external stress or vibrations, or structural deformation, are applied to piezoelectric materials or Macro Fiber composites (MFC), electric energy can be harvested to power very small electronic devices. The configuration of a harvester determines its modal shape, fundamental frequency, output energy, and the efficiency of energy harvesting. At the last part of the literature review, the application of energy harvesting from some piezoelectric materials, as well as the amount of output energy modelled by some researchers, is briefly discussed.

The literature for this thesis underpins three key conclusions for the chosen optimisation methodology. First, when dealing with cantilever-type piezoelectric harvesters whose beam topology and shape family are preselected by the designer, and for which the design variables are bounded scalar dimensions, spatial locations, and electrical parameters, the prevailing approach in the literature is parametric optimisation rather than shape or topology optimisation. This scenario aligns exactly with the rectangular and tapered rectangular MFC configurations analysed in this work. Second, COMSOL's built-in parametric optimisation algorithms, such as BOBYQA, operate as local optimisation methods.

Chapter 3 Analytical modelling

This chapter presents the development of a linear analytical model for MFC piezoelectric material integrated with a uniform rectangular cantilevered beam. The energy harvester considered here is a unimorph structure with a single MFC piezoelectric layer bonded to the top surface of the aluminium substrate. Figure 3-1 shows the cross-section of the unimorph harvester. The linear energy harvester model developed in this thesis is based on the model of the Euler-Bernoulli beam theory. The model takes the backward coupling effect into account to get a more accurate performance response of piezoelectric energy harvesters. A coupled distributed parameter model predicated on the Euler-Bernoulli beam theory was formulated by focusing on a uniform cantilevered piezoelectric energy harvester linked to a resistive load [1,100,171].

The analytical model developed in this chapter provides the theoretical foundation for predicting the dynamic behaviour, the output voltage and the harvested power of the proposed MFC-based energy harvester before experimental validation [7,100,115,172].The model is used to predict both the mechanical and electrical responses of a non-classical piezoelectric energy harvester, which is crucial. The output power can also be increased by the mechanical setup of the harvesting system. Therefore, tremendous efforts have been put into developing different models of energy harvesters. Modelling a piezoelectric harvester includes modelling the mechanical configuration of the harvester, which is a structure that the piezoelectric element is mounted on to be able to vibrate. Also, the modes of piezoelectric material, which are the direction of the mechanical stress applied on the element, are part of the mechanical structure of the piezoelectric energy harvesters.

3.1. Analytical linear modelling of MFC Piezo with cantilever beam

In the literature, a PEH is usually designed as a unimorph, a cantilever beam bonded with piezoelectric transducers, and its frequency response is dominated by the first vibration mode. One of the commonly used theories, which is both computationally simple and reasonably accurate for a thin beam, is the Euler-Bernoulli beam theory. This has served as the foundation for MVEH using piezoelectric beam modelling (PEM) [31,173,174].

3.1.1 Modelling method

A cantilever beam energy harvester has a very simple structure and can produce a large deformation under vibration . Figure 3-1 the MFC of width w $_p$, thickness $t_p$and length, $L_p$is attached to the aluminium beam of width w_b, thickness $t_b$and length L_b. Considering the bond between substrate and energy harvester is perfect, and polarisation is along the thickness of the MFC piezoelectric material.

The model assumes that the beam undergoes bending vibrations caused by a transverse excitation acting at the free end. A mathematical model is important to obtain the electrical voltage when the resistor is connected to one MFC piezoelectric transducer terminal. The geometrical parameters and materials of the piezoelectric transducer influence the output voltage. Harmonic variable electric voltage U_p(t) with specific capacitance (C_p) is an electrical substituent diagram used to develop a model. In Figure 3.1, X_2 refers to the piezoelectric material length, X_1 is the distance of the MFC piezoelectric material from the clamped end, and X or L is the total length of the cantilever beam. There are three parts to the beam, and each part has elements in it. Only substrate material makes up sections X_1 and X_3-(X_1+X_2). Section X_2, on the other hand, has both piezoelectric and substrate materials. Upper and lower surfaces of the piezoelectric layer are fully coated with electrode material, whose thickness is assumed negligible, along with the adhesive layer thickness [100].

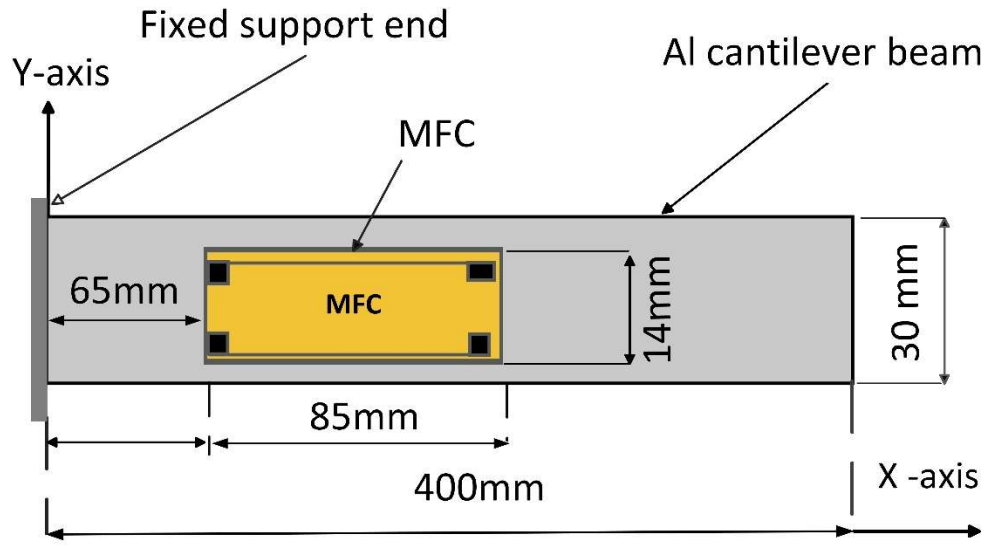


Figure 3-1 Geometry of the aluminium cantilever beam with unimorph MFC PEM

The analytical electromechanical model is based on Euler–Bernoulli beam theory and was employed to model an MFC laminated with composite epoxy fiber and a single MFC attached to an aluminium cantilever beam. It is assumed that the beam is slender, and the rotary inertia

of the beam is negligible, allowing Euler-Bernoulli beam theory to be used [171]. The transverse assumption to model is that the cross-section does not deform significantly because the tip dynamic transverse load remains normal to the deformed axis of the sample during deformation. i.e., there is no deformation along the transverse axis. Here, an essential element is to model the energy harvester for electrical energy recovery from mechanical vibration with varied materials and geometric configurations to maximise the efficiency of output power. The transverse point force, which is a harmonic function, will be applied at the centre of the beam width and at the position of the free end of the cantilever beam.

The piezoelectric body is considered homogeneous and transversely isotropic in a cantilever beam in the Cartesian coordinate system (*X, Y, Z),* and before any load is applied, the beam is unstressed and unstrained, and the electric potential is zero. The relationship between the mechanical and electrical constitutive equations of piezoelectric transducers can be expressed by Hamilton's variational principle or the constitutive equations of piezoelectric materials for a mathematical model. The constitutive equations describe the properties of piezoelectric materials based on the assumption that the total strain in the transducer is the summation of strain caused by applied electric voltages and strain induced by mechanical stress [107,109,127,175]. The formulated equation is in the form of a pair of matrices [1,176].

The model assumes negligible thickness of the piezoelectric electrodes and adhesive, with perfect bonding between the piezoelectric layer and the substrate. A constant, uniform electric field is assumed through the piezoelectric thickness in the (d_{31}) mode. Proportional damping is used for all harvester configurations, and the beam is modelled as a rectangular layer of constant width and thickness. These assumptions simplify the governing equations while maintaining sufficient accuracy to predict the piezoelectric harvester's dynamic and electromechanical behaviour.

3.2. Modelling of electromechanical coupling equation

The coupled mechanical and electrical fields in a piezoelectric material are given by the piezoelectric constitutive relations. They provide the mathematical foundation for the prediction of stress, strain, electric displacement, and electric field within the coupled electromechanical system. The linear modelling of electromechanical coupling equation assumes small deformation and linear material behaviour and thus uses the linear constitutive equations. Piezoelectric energy harvesting operates based on the direct piezoelectric effect. When a piezoelectric material is subjected to mechanical strain, electric charges are generated on its

electrodes. If these electrodes are connected to an external electrical load, the generated charges produce an electric current, allowing useful electrical power to be harvested. The linear constitutive equations of piezoelectric materials involve linear coupling between stress (σ), strain (S), electric field (E) and electric displacement (D) (or between force, displacement, electric charge, and electric potential) [177].

From Figure 3-1, showing the energy harvester, there are three different domains, where each one has its own constitutive equations. These three domains are the piezoelectric, the substrate and the epoxy layer. It is assumed that both piezoelectric and substrate layers are orthotropic materials, meaning that there are two orthogonal planes of the material's property symmetry. On the other hand, the epoxy layer is considered an isotropic material. The piezoelectric domain has electromechanically coupled constitutive relations, while the substrate and epoxy layer domains have only mechanical relations.

The relationship between electric displacement and stress can be altered in:

$$\begin{cases} D = SE \quad and\ S = \frac{\sigma}{Y} = c\sigma. \\ \{\sigma\} = [c_s]\{S\} \end{cases} \tag{3.1}$$

The MFC-P2 transducer is mounted on the surface of an aluminium cantilever beam and operates mainly in the transverse d_{31} piezoelectric mode. The MFC and beam longitudinal direction is defined as x_1 and x_3 is taken through the thickness and is the principal direction of the electric field. The Euler–Bernoulli beam assumption neglects the transverse shear deformation where the dominant mechanical deformation relevant to bending is the longitudinal normal strain S_{11} Therefore, the longitudinal stress σ_{11} is supposed to be the main mechanical stress in the piezoelectric layer. The electric field is assumed through in the thickness direction, (E_3). The direct effect of piezoelectricity can be described by equation (2.19), the generation of electric displacement or charge under mechanical stress.

$$D_3 = \epsilon_{33}^{\sigma} E_3 + d_{31}\sigma_{11}. \tag{3.2}$$

The inverse effect of piezoelectricity can be described by the general equation and given by equation (3.1)

$$S_1 = d_{31}E_3 + s_{11}^{E}\sigma_{11}. \tag{3.3}$$

Where S_1 is strain, σ_1 Voigt stress component along axis 1, E is the electric field; D is the electric displacement; d is the piezoelectric strain coefficient; $s_{11}{}^{E}$ For the specific case of a 31-mode piezoelectric coupling (mechanical stress and strain along the 1-axis, electric field and

displacement along the 3-axis) the general 3D Voigt constitutive relations reduce to the following scalar forms, where ${s_{11}}^{E} = \frac{1}{Y^E}$ is the elastic compliance to avoid dimensional ambiguity.; and ε epsilon is the dielectric permittivity measured at constant stress.

From the above equation (3.2), the direct piezoelectric effect when the transducer is being used as a sensor, and equation (3.3), the converse piezoelectric effect (actuator), the strain is produced by the induced electric field. As a piezoelectric material is polarised in the 3-direction and the electrical field are applied in the same direction, while the predominant mechanical stress and strain is in the 1-direction, the constitutive equations can be reduced to [2,15]:

$$S_{11} = {s_{11}}^{E}\sigma_{11} + d_{31}E_3, \tag{3.4}$$

$$D_3 = d_{31}\sigma + \varepsilon_{33}^{\sigma}E_3. \tag{3.5}$$

Where $\sigma = \frac{S}{s^E}$, S = longitudinal normal strain, σ= stress, ${s_{11}}^{E} = \frac{1}{Y_p}$ = elastic compliance at constant electric field, ϵ^{σ} = dielectric permittivity in the 3-direction at constant mechanical stress ($\frac{N}{m.V} = \frac{C}{m^2}$.

In the considered energy harvesting configuration for this study, the direct piezoelectric term $d_{31}\sigma_{11}$ is particularly important since mechanical bending of the MFC-integrated beam leads to an electric displacement and, hence, an electrical voltage developed across the electrodes.

The electric field E_3 and stress $\sigma_1$in terms of strain S_1 and charge are given by:

$$\sigma_1 = \frac{S_{11} - d_{31}E_3}{{s^E}_{11}}. \tag{3.6}$$

By substituting (3.6) into (3.5)

$$D_3 = d_{31}\frac{S_{11} - d_{31}E_3}{{Y^E}_{11}} + {\epsilon^{\sigma}}_{33}E_3 = \frac{d_{31}S_{11}}{{s^E}_{11}} + \left({\epsilon^{\sigma}}_{33} - \frac{{d^2}_{31}}{{s^E}_{11}}\right)E_3 = \frac{d_{31}S_{11}}{{s^E}_{11}} + {\epsilon^{S}}_{33}E_3, \tag{3.7}$$

where ${\epsilon^{\sigma}}_{33} - \frac{{d^2}_{31}}{{s^E}_{11}}$ dielectric permittivity at constant strain.

The linear piezoelectric constitutive equations are written in the strain-charge form for the one-dimensional bending mode. This formulation, widely used to describe the electromechanical behaviour of piezoelectric energy harvesters, can be expressed in the following two-by-two matrix form:

$$\begin{bmatrix} S_1 \\ D_3 \end{bmatrix} = \begin{bmatrix} {s_{11}}^{E} & d_{31} \\ d_{31} & {\epsilon^{\sigma}}_{33} \end{bmatrix}\begin{bmatrix} \sigma_1 \\ E_3 \end{bmatrix}. \tag{3.8}$$

Where S, σ, E and 'd' are strain, stress, electric field through thickness (poling direction) and piezoelectric strain constant, respectively.

The electric displacement of the MFC is simplified as:

$$D_z = [d_{31}, d_{31}\ d_{33}] \left[\begin{bmatrix} \sigma_1 \\ \sigma_2 \\ \sigma_3 \end{bmatrix} \right] + \varepsilon_{33}^{\sigma} E_3. \tag{3.9}$$

The differences in the coefficients d_{31} and d_{32}, where the 1-axis is the fiber direction and the 2-axis is the transverse to the fibres, is due to the orthotropic nature of the Macro Fibre Composite patch as described in (3.10). The MFC has d_{31} different from d_{32} due to the composite layup and interdigitated electrode geometry, unlike standard bulk PZT (where $d_{31} = d_{32}$). All numerical values employed in this work are taken from the manufacturer datasheet.

For MFC with dominant d_{31}effect and polarisation along the z-axis:

$$\mathrm{d} = \begin{bmatrix} \mathrm{d}_{31} & 0 & 0 & 0 & 0 & 0 \\ 0 & \mathrm{d}_{32} & 0 & 0 & 0 & 0 \\ 0 & 0 & \mathrm{d}_{33} & 0 & 0 & 0 \end{bmatrix}, \tag{3.10}$$

and Permittivity Matrix is given by:

$$\epsilon^{\sigma} = \begin{bmatrix} \varepsilon^{\sigma}{}_{11} & 0 & 0 \\ 0 & \varepsilon^{\sigma}{}_{22} & 0 \\ 0 & 0 & \varepsilon^{\sigma}{}_{33} \end{bmatrix}. \tag{3.11}$$

The stress charge for FE modelling, the linear constitutive equation, has the form of:

$$\begin{bmatrix} \sigma_1 \\ D_3 \end{bmatrix} = \begin{bmatrix} C_{11}{}^{E} & -e_{31} \\ e_{31} & \epsilon^{S}{}_{33} \end{bmatrix} \begin{bmatrix} S_1 \\ E_3 \end{bmatrix}. \tag{3.12}$$

The elastic stiffness constant $C_{11}{}^{E}$ equal to:

$$c_{11}^{E} = \frac{1}{s_{11}^{E}}. \tag{3.13}$$

Piezoelectric stress constant (e_{31}) is given by:

$$e_{31} = \frac{d_{31}}{s_{11}{}^{E}} = d_{31} c_{11}{}^{E}. \tag{3.14}$$

The clamped dielectric permittivity (ϵ_{33}^{S}) to the free dielectric permittivity (ϵ_{33}^{σ}) is given by :

$$\epsilon^{S}{}_{33} = \epsilon^{T}{}_{33} - \frac{d_{31}}{s_{11}{}^{E}}. \tag{3.15}$$

For modelling a cantilever beam under an external excitation load, Euler-Bernoulli beam theory is used because it has the highest modelling accuracy since the model assumes both the beam and piezo-electric materials are perfectly bonded together, and a common neutral axis

represents their deformation. Macro Fiber Composite piezoelectric materials are flexible piezoelectric devices composed of piezoceramic fibers embedded within a polymer matrix and covered by electrode layers. Unlike conventional monolithic piezoceramic plates, their composite structure provides greater flexibility and improved resistance to cracking, making them suitable for smart structures, curved surfaces, thin beams, and vibration-based energy harvesting applications. Their patches can operate using either the effective d_{33} or d_{31} piezoelectric coupling mode, depending on the electrode configuration and product type. In many MFC designs employing interdigitated electrodes, the electric field is applied along the fiber direction, resulting in an effective d_{33}operating mode. For simplified beam-based energy harvesting models, the MFC layer is commonly represented using equivalent material properties such as effective elastic modulus, density, capacitance, dielectric permittivity, and piezoelectric coefficients.

The integration of an MFC patch with an aluminium cantilever beam provides significant advantages for vibration energy harvesting. The aluminium substrate contributes structural flexibility and mechanical support, while the MFC layer performs the electromechanical energy conversion. This hybrid configuration is particularly suitable for low-frequency vibration harvesting and structural health monitoring applications. The general equation for the beam within the excitation force is given by the transverse vibration based on Euler-Bernoulli beam theory, starting from the force and momentum equations [71,127,178]. The transverse displacement of the beam is represented by w,ρ the density of the beam,A the cross-sectional area and the external force P applied to the beam per unit length. From the Figure 3-1 configuration, the MFC patch is positioned between $Lp = 65$ mm and $S = 150$ mm along the 400 mm aluminium cantilever beam. Consequently, the patch is placed near the fixed end, where bending strain is relatively high, but it does not extend into the clamped region. This arrangement helps reduce the risk of mechanical damage and stress concentration near the clamp while still enabling the MFC layer to experience significant bending deformation for effective energy harvesting.

3.3. Mechanical equation

The integration of Macro Fiber Composite materials with an aluminium cantilever beam offers significant advantages for vibration-based energy harvesting applications. The aluminium substrate provides structural flexibility and favourable dynamic characteristics, while the MFC patch enables efficient electromechanical energy conversion.

As a result, this hybrid configuration is well-suited for low-frequency vibration energy harvesting and structural health monitoring applications. To simplify the analysis, it is assumed that the bonding between the layers is perfect and the poling direction of the MFC mode of the d_{31} piezoelectric layer is along its thickness direction. The concentrated force, P, is applied perpendicularly to the cantilever surface at the tip of the cantilever, as shown in Figure 3-1. The electrical load can be connected to the MFC patches in a series.

Consider an infinitesimal beam element of length dx as shown in Figure 3-1. The transverse deflection of beam is denoted by $w(x,t)$, where x is a spatial coordinate along the beam axis. The mass of the element is $dm = \rho A\, dx$ where ρ is the density and A is the cross-sectional area. The net vertical shear on the element is $\left(\frac{\partial s_f}{\partial x}\right) dx$. The external transverse applied load is $p(x,t)\, dx$. By second newtons law in the vertical direction:

$$\left(\frac{\partial s_f}{\partial x}\right) dx - p(x,t)dx = \rho A \frac{d^2 w}{dt^2},$$

where ρ density , v volume, shear force(s_f) at distance from the fixed support.

Dividing through by dx yields the equation of motion:

$$dF = \frac{\partial s_f}{\partial x} - p(x,t) = m\frac{d^2 w}{dt^2} = \rho A \frac{d^2 w}{dt^2}. \tag{3.16}$$

The relation between shear force and bending moment is given by :

$$\mathrm{s_f} = \frac{\partial \mathrm{M}}{\partial \mathrm{x}}. \tag{3.17}$$

The Euler-Bernoulli beam theory is widely used for modelling slender cantilever-based piezoelectric energy harvesters. The theory assumes that plane cross-sections remain plane and perpendicular to the neutral axis during bending deformation. As a result, the effects of shear deformation and rotary inertia are neglected. These assumptions are generally valid for slender beams operating at relatively low vibration frequencies, where bending deformation dominates the structural response [1,100,148,179–182].

These relationships transform the equation of motion to a differential equation between the beam deformation, external load, and material properties. To solve this differential equation for the beam deformation, the physical coordinates are transformed to the modal coordinates, and the beam deformation is expressed as the summation of the vibration modes.

From the Euler-Bernoulli beam theory assumption, the relation between the bending moment and curvature is:

$$M = \frac{-YI}{1/k} = -YIk. \tag{3.18}$$

Let *w(x,t)* represent the transverse beam deflection, where t is time and x is the spatial coordinate along the beam axis. The second spatial derivative of the deflection approximates the curvature *κ(x,t)* for small deflections:

$$k(x,t) = \frac{\partial w^2}{\partial^2 x}. \tag{3.19}$$

The relation between momentum and deflection is given by :

$$M = \frac{EI}{1/k} = \mathrm{YIk} = -YI\frac{\partial^2 w}{\partial x^2} \tag{3.20}$$

Assuming that the bending stiffness YI is constant along the beam, this reduces to the standard Euler-Bernoulli beam equation. Then it is easy to obtain by Substituting (3.20) into (3.17):

$$\mathrm{s_f} = \frac{\partial \mathrm{M}}{\partial \mathrm{x}} = \frac{\partial}{\partial \mathrm{x}}\left(\mathrm{YI}\frac{\partial^2 \mathrm{w}}{\partial \mathrm{x}^2}\right) = -\mathrm{YI}\frac{\partial^3 \mathrm{w}}{\partial \mathrm{x}^3}. \tag{3.21}$$

Again, substituting equation (3.21) into (3.16) and rearranging :

$$\frac{\partial}{\partial x}\left(-YI\frac{\partial^3 w}{\partial x^3}\right) - p(x,t) = m\frac{d^2x}{dt^2} == -YI\frac{\partial^4 w}{\partial x^4} - p(x,t) = m\frac{d^2x}{dt^2} = \rho A dx\frac{d^2x}{dt^2}, \tag{3.22}$$

$$m\frac{d^2x}{dt^2} + YI\frac{\partial^4 w}{\partial x^4} = -p(x,t), \tag{3.23}$$

let say constant c,then:

$$c^2 = \frac{\mathrm{YI}}{m} = \frac{\mathrm{YI}}{\rho A}, \tag{3.24}$$

where w(m) is the vertical or transverse displacement of the beam substituting equation (3.24) into (3.23) the following expression is obtained:

$$\frac{\partial^2 \mathrm{x}}{\partial \mathrm{t}^2} + \mathrm{c}^2\frac{\partial^4 \mathrm{w}}{\partial \mathrm{x}^4} = -\frac{1}{\rho \mathrm{A}}\,\mathrm{p(x,t)}, \tag{3.25}$$

where $\rho A\frac{\partial^2}{\partial x^2}w(x,t)$ inertial force is acting on the beam, w is the transverse beam displacement, ρ is the density of the aluminium beam, I second moment of area of the beam the cross section, A is cross section of the beam, Y is the elastic modulus of the beam material, and $P(t)$ external forces per unit length applied to the beam. The transverse deflection of the beam at point *x* and time *t*. The load *p (x, t)* is written as:

$$p(x,t) = \delta(x - x_f)P(t), \tag{3.26}$$

$$\frac{\partial^2}{\partial x^2}w(x,t) + c^2\frac{\partial^4}{\partial x^4}w(x,t) = \frac{1}{\rho A}\delta(x - x_f)P(t). \tag{3.27}$$

Equation (3.25) is a governing differential equation, $P(t)$ is the external force, L is the length of the beam x_f is the application location of the external force; and δ is the Dirac delta function. Equation (3.26) is a partial differential equation solved by the separable solution method, or the displacement can be separated into two parts, one depending on position and another on time.

According to Euler–Bernoulli beam theory, the transverse deflection of the beam can be expressed in terms of its deformation as follows:

$$w(x,t) = \phi(x)\eta(t), \tag{3.28}$$

where $\emptyset_i(x)$ and $\eta_i(t)$ are mode shape function of the beam i^{th} mode, and the generalised coordinate in the i^{th} mode, respectively. Substituting equation (3.27) into (3.26) gives:

$$\frac{\delta^2}{\delta x^2}\,\phi(x)\,\eta(t)) + c^2\,\frac{\delta^4\,\phi(x)\eta(t)}{\delta x^4} = \frac{1}{\rho A}\,P(t)\delta\big(x - x_f\big), \tag{3.29}$$

to find out the natural frequency and mode shape when the system is under free vibrations and undamped. In free undamped vibration, the natural frequencies and corresponding modes of vibration of the system are determined from (3.29). For free vibration, the external excitation and the damping terms are neglected, and the resulting equation, derived and rearranged after derivation, can be written as:

$$\begin{aligned}
c^2\,\frac{d^4\phi(x)}{dx^4}(\eta_t) &= -(\emptyset_x)\,\frac{d^2\eta(t)}{dt^2} = constant(\omega^2),\\
\frac{c^2}{\phi(x)}\frac{d^4\phi(x)}{dx^4} &= -\frac{1}{\eta(t)}\frac{d^2\eta(t)}{dt^2} = constant(\omega^2),\\
= \frac{c^2}{\phi(x)}\frac{d^4\phi(x)}{dx^4} &= (\omega^2)\ or\ \frac{1}{\eta(t)}\frac{d^2(\eta(t))}{dt^2} = -\omega^2,\\
\frac{d^4\phi(x)}{dx^4} = \frac{\phi(x)}{c^2}\omega^2\ or\ \frac{d^2\eta(t)}{dt^2} &= -\eta(t)\omega^2.
\end{aligned} \tag{3.30}$$

Equation (3.29) separates the governing equation of vibration into two ordinary differential equations: a spatial equation for the beam mode shape $\phi(x)$ and a temporal equation for the time-dependent modal response $\eta(t)$. ω is the angular natural frequency of the system:

$$\text{Let } \lambda^4 = \frac{\omega^2}{c^2} \text{ and } c^2 = \frac{YI}{\rho A} = \frac{EI}{m}, c = \sqrt{\frac{YI}{m}}, \tag{3.31}$$

$$\omega^2 = \lambda^4\,\frac{YI}{m}. \tag{3.32}$$

Where c is the wave-propagation parameter of the Euler-Bernoulli beam and is related to the bending stiffness YI and the mass per unit length m . Equation (3.31) shows the relation of the natural angular frequency ω, beam bending stiffness YI, mass per unit length m and

frequency parameter λ. This relation indicates that the natural frequency depends on the mechanical stiffness and the distributed mass of the beam.

The total mass per unit length of the composite beam, considering the contribution of the beam substrate and piezoelectric MFC, which will be used later, is given by:

$$\overline{m} = W_b \rho_b t_b + W_p \rho_p t_p. \tag{3.33}$$

The angular frequency is then obtained in the form of:

$$\omega = \frac{\lambda^2}{L}\sqrt{\frac{YI}{m}}. \tag{3.34}$$

Where ω is natural angular frequency.

The corresponding natural frequency in hertz is then obtained from the standard natural-frequency equation for a uniform Euler–Bernoulli cantilever beam, equation 3.34:

$$f_n = \frac{\omega}{2\pi} = \frac{1}{\pi}\lambda^2\sqrt{\frac{YI}{m}}. \tag{3.35}$$

The natural frequencies of the beam are the frequencies at which the beam vibrates when something disturbs it. It is allowed to swing back and forth on its own without anything pushing it or slowing it down. Each natural frequency of the beam has a mode shape of the beam, which is the way the beam bends and moves when the beam is vibrating. The mode shape of the beam is like a pattern that the beam follows when the beam is vibrating at one of its natural frequencies.

Here the mode shape $\phi(x)$ for the free transverse vibration of a uniform Euler–Bernoulli cantilever beam is solved, which is the standard starting point before coupling in the piezoelectric layer. This derivation is presented step-by-step:

$$\phi(x) = Ce^{\beta x}. \tag{3.36}$$

This is the standard approach to constant coefficient linear ODEs . Since exponentials are eigenfunctions of the differentiation operator , they reduce the equation to an algebraic equation.

$$\frac{d^4(Ce^{\beta x})}{dx^4} = \lambda^4 Ce^{\beta x} = \frac{d^4(Ce^{\beta x})}{dx^4} = \lambda^4 Ce^{\beta x},$$
$$\lambda^4 Ce^{\beta x} - \beta^4 Ce^{\beta x} = 0,$$
$$\lambda^4 - \beta^4 = 0\,, \lambda^4 = \beta^4 or\ \lambda^2 = \pm\beta^2,$$
$$\lambda_{1,2} = \pm\beta\ or\ \lambda_{3,4} = \pm i\beta,$$
$$\lambda_{1,2,3,4} = \beta, -\beta, i\beta\ and - i\beta. \tag{3.37}$$

Physically, the real roots correspond to the spatially parts of the mode shape and the imaginary roots correspond to the oscillatory parts. This has four roots: two real ($\beta = \pm\lambda$) and two imaginaries ($\beta = \pm i\lambda$).

The general expansion for superposition of all four fundamental solutions:

$$\phi(x) = C_1 e^{\beta x} + C_2 e^{-\beta} + C_3 e^{i\beta x} + C_4 e^{-i\beta x}. \quad (3.38)$$

Using Euler's identities and hyperbolic function definitions:

$$e^{\beta x} = cosh\beta x + sinh\beta x$$
$$e^{-\beta x} = cosh\beta x - sinh\beta x$$
$$e^{i\beta x} = cos\beta x + isin\beta x$$
$$e^{i\beta x} = cos\beta - isin\beta x$$
$$sinh\beta x = \frac{e^{\beta x} - e^{-\beta x}}{2}, cosh\beta x = \frac{e^{\beta x} + e^{-\beta}}{2}. \quad (3.39)$$

The real value of mode shape after regrouping the constant for the standard cantilever formulation:

$$\phi(x) = A_n cos(\lambda x) + B_n \sinh(\lambda x) + C_n \cos(\lambda x) + D_n sin(\lambda x). \quad (3.40)$$

The four cantilever beam boundary condition:

- Transverse deflection at fixed support, $w(0, t) = 0$,
- For the fixed support at x=0: slope ($w'(0, \mathrm{t}) = 0$) and zero displacement (w(0,t)),
- At the free end (x=L):then the bending moment (BM) at free end , $w''(L, t) = 0$ and shear force (SF) at free end,$w'''(L, t) = 0$.

The boundary condition in terms of mode shape is given by:

- At x=0:$\phi(0) = 0$ and $\phi'(0) = 0$,
- X= L:$\phi''(L) = 0$ and $\phi'''(L) = 0$.

These four boundary conditions give four algebraic equations for the four unknown constants A, B, C and D. This is enough to completely determine the shape of each vibration mode (up to an arbitrary scale factor).

Case 1: Transverse deflection w (0, t):

$$\phi(x = 0) = (x) = Acosh(\lambda 0) + B \sinh(\lambda 0) + Ccos(\lambda x) + Dsin(\lambda 0),$$
$$A = -C \quad (3.41)$$

Case 2: Slope at the fixed end $w'(0, t$:

$$\phi'(x) = A\lambda sinh(\lambda 0) + B\lambda \cosh(\lambda 0) - C\lambda sin(\lambda 0) + D\lambda cosh(\lambda 0). \quad (3.40)$$

At x=0

$$\phi'(0) = \lambda B + \lambda D,$$
$$0 = +\lambda B + \lambda D, B = -D,$$

substituting back $C = -A \; and \; B = -D$.

Then, finally equation 3.40 become:

$$\phi(x) = C[Acosh(\lambda x) - cos(\lambda x)] + D[Bsin(\lambda x) + sin(\lambda x)]. \quad (3.43)$$

This is the general form that satisfies both fixed-end conditions simultaneously. This is why cantilever mode shapes are always written as this particular combination of hyperbolic and trigonometric terms, rather than the full four-term form.

Applying the free-end conditions (BM = 0 and S_F = 0 at x = L), By differentiating ϕ two additional times for BM and three additional times for SF, and then setting x = L, we obtain two further linear expressions in B and D:

In matrix form:

$$\begin{bmatrix} cosh(\beta L) + cos(\beta L) & sinh(\beta L) + sin(\beta L) \\ sinh(\beta L) - sin(\beta L) & cosh(\beta L) + cos(\beta L) \end{bmatrix} \begin{Bmatrix} B \\ D \end{Bmatrix} = \begin{Bmatrix} 0 \\ 0 \end{Bmatrix} \quad (3.44)$$

Expanding the equations, the above two equations are non-trivial solutions of the equation.

$$\phi(x) = B\left\{(cos\, h(\beta x) - cos(\beta x) + \frac{D}{B}\,(sinh(\beta x) - sin(\beta x))\right\},$$
$$\frac{D}{B} = -\frac{cos\, h(\beta L) + co\;(\beta L)}{sinh(\beta L) + sin(\beta L)},$$
$$Let\; \frac{D}{B} = \alpha = -\frac{cos\, h(\beta L) + co\;(\beta L)}{sinh(\beta L) + sin(\beta L)},$$
$$\phi(x) = B\{(cos\, h(\beta x) - cos(\beta x) + \alpha\,(sinh(\beta x) - sin(\beta x))\}. \quad (3.45)$$

In general, the analytical power estimation of a cantilever beam with unimorph MFC piezoelectric material based on Euler-Bernoulli theory, when the length of the beam is much greater than the thickness and width of the beam. Perfect bonding between the MFC and the beam element is considered. For transverse forced vibration of a cantilever beam with uni-morph MFC piezoelectric material, the output power depends on numerous factors such as the geometry of the beam, frequency, and magnitude of externally applied force, material property,

and boundary condition [14]. From Euler's theory, the equation of the uni-morph MFC with a cantilever beam [110]:

$$\dot{m}\frac{\partial^2 w}{\partial t^2} + YI\frac{\partial^4 w}{\partial x^4} + c\frac{\delta w(x)}{dt} = F_{piezo}(t)\delta(x - x_f\,, \tag{3.46}$$

or

$$\frac{\delta^2}{\delta x^2}(Y_{eq}I_{eq})\,w''(x,t) + \dot{m_{eq}}(x,t) + cw''(x,t) = -\dot{p}(t)\delta[x - x_F] + M_{piezo}{}''(x,t). \tag{3.47}$$

where:

- $\dot{m}(x)$: Mass per unit length for the composite beam with non-uniform length from equation (3.33)
- $Y_{eq}I_{eq}$: Flexural rigidity,
- c: Damping coefficient,
- F_{piezo}: External applied point force,
- $p(t)\delta[x - x_f]$:is the Dirac delta distribution centred at the force application point.

From the piezoelectric linear constitutive equation: the total energy stored in a small volume dv of a piezoelectric cantilever beam is the sum of the mechanical energy and the electric field-induced energy:

$$T_p = c_{11}\,S_p + e_{31}E_3, \tag{3.48}$$

where S_p is the axial strain in the piezo, $E_3$is the local electric field in the thickness direction (or equivalently, we will relate it via voltage gradient as required by the patch electrode geometry), and $e_{31}$is there piezoelectric stress coupling.

The axial strain S_p induced in the piezoelectric patch by bending of the host beam:

$$S_p = y\frac{\delta^2 w(x,t)}{\delta t^2} = h_p\,\frac{\delta^2 w(x,t)}{\delta x^2} = h_p\frac{P(L-x)}{EI_x}, \tag{3.49}$$

- $y\frac{\delta^2 w(x,t)}{\delta t^2}$ The general Euler-Bernoulli relation between beam curvature and axial strain, where y is the distance from the neutral axis to the point at which the strain is measured.
- Replacing y with h_p as the piezoelectric (MFC) layer is glued to the surface of the beam. Strain is calculated from neutral axis to mid-plane (or surface) of piezo layer offset.

This is a standard simplification for a thin surface-bonded patch, assuming that the piezo layer itself does not shift the neutral axis significantly.

- $h_p \frac{P(L-x)}{EI_x}$ static bending relation, $\frac{\delta^2}{\delta x^2} = \frac{M(x)}{EI_x}$, $M(x) = P(L-x)$ is the bending moment at position x for a cantilever loaded by a tip force P at $x = L$.

Axial stress in the MFC piezoelectric material:

$$\sigma_p = c_{11} h_p \frac{\delta^2 w(x,t)}{\delta x^2} + e_{31} E_3, \tag{3.50}$$

where $c_{11} h_p \frac{\delta^2}{\delta x^2}$ is the purely mechanical (elastic) contribution to stress,

$e_{31}E_3$. the piezoelectric stress coupling term, which accounts for the extra stress produced (or, in actuation, induced) by the electric field, E_3 through the piezoelectric coupling coefficient e_{31}.

From the assumption that the electric field is uniform across the thickness (h_p) of the MFC (d_{31} mode):

$$E_3 = \frac{V_t}{h_p}. \tag{3.51}$$

Equation(3.46) states that, if the electric field through the thickness of the MFC patch is uniform (classical d31-mode behaviour), the field is simply the voltage across the patch electrodes, Vt, divided by the patch thickness hp.

The stress in the MFC piezoelectric layer (3.45 and 3.46)

$$T_p = c_{11} h_p \frac{\delta^2 w(x,t)}{\delta x^2} + e_{31} \frac{V_t}{h_p} = c_{11} h_p \frac{P(L-x)}{EI_x} + e_{31} \frac{V_t}{h_p}. \tag{3.52}$$

The force generated by the piezoelectric material is obtained using the piezoelectric material's constitutive equation:

$$F_{piezo} = \frac{\delta}{\delta x}\left[b h_p \left(c_{11} h_p \frac{\delta^2 w(x,t)}{\delta x^2} + e_{31} h_p V(t) \right) \right] = b h^2 c_{11} \frac{\delta^2 w(x,t)}{\delta x^3} + b h_p e_{31} \frac{\delta V(t)}{\delta x}, \tag{3.53}$$

the piezoelectric coupling equation is a partial differential equation that governs the mechanical dynamics of a beam when it is integrated with an MFC piezoelectric transducer:

$$m \frac{d^2 w}{dt^2} + YI \frac{\partial^4 w}{\partial x^4} + c \frac{\delta w(x)}{dt} = -p(t)\delta[L - X_F] + b h^2 c_{11} \frac{\delta^3 w(x,t)}{\delta x^3} + b h_p e_{31} \frac{\delta V(t)}{\delta x}. \tag{3.54}$$

After rearrangement, the governing equation of the beam and piezoelectric coupling is :

$$\rho_{eq} \frac{d^2 w}{dt^2} + YI_{eq} \frac{\partial^4 w}{\partial x^4} + c \frac{\delta w(x)}{dt} = \frac{\delta}{\delta t^2} b h_p (c_{11} \frac{\delta^2 w(x,t)}{\delta x^2} + e_{31} h_p V(t))] - p(t)\delta[L - X_F]. \tag{3.55}$$

Energy losses occur at each stage of the harvesting process. Mechanical losses arise from structural damping, air damping, support or clamping losses, and material hysteresis within the structure and piezoelectric layer. Electrical losses include dielectric dissipation, leakage currents, voltage drops across rectifier diodes, switching losses in power electronics, impedance mismatch between the harvester and the load, and inefficiencies in the power management circuitry. In FEM-based harmonic or transient dynamic analysis, damping must be included to obtain a realistic and numerically stable response, particularly near resonance, where an undamped system may exhibit excessively large amplitudes and convergence difficulties. Rayleigh damping is commonly used in structural dynamics by expressing the damping matrix as a linear combination of the mass and stiffness matrices. The total damping of the coupled system can originate from both the intrinsic material/structural damping and the electrical energy extracted by the piezoelectric MFC harvesters. However, when the MFCs are modelled under open-circuit conditions, the analysis predicts the open-circuit voltage without connecting an external load; therefore, no useful electrical power is extracted from the system. In this case, the damping contribution is assumed to arise mainly from the aluminium beam material, and Rayleigh damping is applied to represent this structural damping [120].

From the piezoelectric material constitutive equations, the charge collected on the electrode surface is the integral of displacement on the surface area from the Figure 3-1 [100].

From the equations 2.6, 3.2 and 3.3, the electric charge on the surface of MFC can be obtained:

$$Q = DA = \int_{X_1}^{X_1+X_2} D_3 \, dx. \tag{3.56}$$

Substituting equation 3.6 into equation 3.52, the charge can be described as:

$$Q = b \int_0^{L_b} ((e_{31})\varepsilon_x + {\epsilon_{33}}^{\sigma} E_z) dx = b \int_{X_1}^{X_1+X_2} ((e_{31})\varepsilon_x + {\epsilon_{33}}^{\sigma} E_z) dx, \tag{3.57}$$

where: b is the width of the MFC.

Assuming the voltage produced by the piezoelectric MFC is V, from equation 3.47 and substitute to equation 3.53:

$$Q = \frac{b t_b e_{31}}{2} [\Phi(X_1 + X_2) - \Phi(L_b)] - b L_p {\epsilon_{33}}^{\sigma} \frac{V}{h_p}, \tag{3.58}$$

Voltage, charge, and current are dependent on the time function, and the frequency of the beam is dependent on mechanical vibration:

$$I = \omega Q. \tag{3.59}$$

The relation between current and voltage with resistance is:

$$I = \frac{V}{R}, \tag{3.60}$$

combining equations (5.54), (3.55), and (3.56), the current amplitude is I_A:

$$I_A = \frac{\omega b t_b e_{31}[\Phi(0)-\Phi(L_b)]}{2\left(1+bL_p\epsilon_{33}\frac{\omega R}{t_a}\right)}. \tag{3.61}$$

From the relations of the current (I), charge (Q), voltage (V), resistance load (R_1), and capacitance (Cp) [56] can be obtained:

$$I(t) = \frac{dQ(t)}{dt} = \frac{V(t)}{R_1} = C_p\frac{dV_c(t)}{dt} = \int_{x_1}^{x_2} E_p\, d_{31} t_{pc} b_p \frac{\delta^3 w(x,t)}{\delta x^2 \delta t}dx - C_p\frac{\delta V(t)}{\delta t}. \tag{3.62}$$

After differentiation and rearrangement, the electric circuit equations become:

$$\mathrm{C_p}\frac{\mathrm{d}}{\mathrm{dt}}\mathrm{V(t)} + \mathrm{R_t V(t)} + \mathrm{e_{31} b h_p}\int_{\mathrm{x_1}}^{\mathrm{x_2}} \mathrm{E_p\, d_{31} t_{pc} b_p}\frac{\delta^2 \mathrm{w(x,t)}}{\delta \mathrm{x}^2 \delta \mathrm{t}}\mathrm{dx} = 0 \text{ or}$$

$$\frac{V_R(t)}{R_1} + \frac{\varepsilon_{33} b_p L_P}{h_p C_p}\frac{dV_R(t)}{dt} = -bh_p e_{31}\int_{x_1}^{x_2}\left(\frac{dw_n(x)}{dn}\right)\eta_n(t_p). \tag{3.63}$$

Where $=C_p = \frac{\varepsilon_{33} b_p (x_2 - x_1)}{h_p}$ is the capacitance of the piezoelectric layer,

$\eta_n(t)$ = modal coordinate,

Piezoelectric electromechanical coupling coefficient ${k_{31}}^2 = \frac{d_{31}}{{S_{11}}^E \epsilon_{33}{}^T}$,

$\frac{dv}{dt_p}$ is the derivative of the voltage generated across the MFC layer, R_{load} is the load resistance in the electrical circuit, and v(t) is the voltage across the MFC layer. The term e_{31}bhp is a scaling factor related to the piezoelectric coefficient and the MFC geometry, while $\frac{\delta^2 w(x,t)}{\delta x^2}dx$ represents the integrated curvature of the beam over the region where the MFC is applied (from x_1 to x_2). The voltage generated by the piezoelectric transducer is determined by the beam's mode response, mode shape, internal capacitance, and load resistance and the material's mechanical and electrical properties.

3.4. Mode shape and natural frequency analysis for the electrotechnical coupling

Based on the proportional damping assumption (strain-rate damping is assumed to be stiffness-proportional, whereas air damping is assumed to be mass-proportional), the

eigenfunctions of the proportionally damped system become the eigenfunctions of the respective undamped system.

The solution for equation (3.40) is solved by the governing equation using the separation of variables method [7]:

$$w(x,t) = \phi(x)\eta(t) = C_1\ cos\,\lambda\frac{x}{L} + C_2\ sin\,\lambda\frac{x}{L} + C_3\ cos\,\lambda\frac{x}{L} + C_4\ sin\,\lambda\frac{x}{L}. \quad (3.64)$$

For a cantilever beam at the clamped end, both the deflection and the rotation must be zero; at the free end, neither a bending moment nor a shear force can be present [183].

Apply the boundary condition and solve for the unknown constant C. The natural frequency of transversal vibration of a continuous composite cantilever beam can be obtained analytically from the decoupled equation (3.60) of the Euler–Bernoulli beam and is given by the following:

$$f_n = \frac{\omega}{2\pi} = \frac{1}{2\pi}\frac{\lambda^2}{L}\sqrt{\frac{E_{eq}I_{eq}}{\rho_{eq}A_{eq}}}, \quad (3.65)$$

where 'n' is the mode index, ρ_{eq} is the effective density of the composite beam, A_{eq} is the effective cross-sectional area of the beam, Eeq effective Young's modulus of the composite beam, Ieq equivalent second moment area of composite beam and L is the length of the beam.

From the above equation increasing the beam length generally decrease natural frequency whereas shorter beam length has high natural frequency. The beam's natural frequency can be estimated by the piezoelectric beam's effective stiffness and mass. where λ_n is the dimensionless frequency parameter determined by the beam's boundary conditions and vibration mode. The characteristics equation for the first five roots from the standard book for simple supported cantilever beam as follows:

λ_1=1.875104ch07,λ_2=4.69409113,λ_3=7.85475744,λ_4=10.99554073 and λ_5= 14.13716839.

The resonant frequency or eigen frequency serves as a crucial performance metric for PVEH. The device achieves its highest output power at this resonant frequency, and as the excitation frequency deviates from it, the output power will diminish.

The rate of spatial curvature of the beam's displacement expressed via its modal expansion:

$$\int_{x_1}^{x_1+x_2}\frac{\delta^2}{\delta x^2}\frac{\delta w}{\delta t}dx = \sum_n[\int_{x_1}^{x_2}\phi''_n(x)]\dot{\eta}_n(t). \quad (3.66)$$

From equation 3.62, the integration is carried out over the interval from x_1 to x_2, which represents the position of the piezoelectric transducer.

Modal coupling coefficient, also known as piezoelectric coupling:

$$\theta_n = e_{31} h_p b \int_{x_1}^{x_1+x_2} \phi''_n(x)\, dx, \tag{3.67}$$

where, θn the modal piezoelectric coupling coefficient ,which characterises the electromechanical coupling between the n_{th} mechanical vibration mode and the electrical response of the piezoelectric transducer. It is especially important because it determines the efficiency of the conversion of mechanical vibration into electrical charge. The sensitivity depends on the piezoelectric coupling coefficient e_{31}, the thickness of the piezoelectric layer h_{p} and the integrated curvature of the nth mode shape along the length of the piezoelectric patch.

Equation 3.64 describes the coupled electrical relationship in the piezoelectric energy harvester, detailing how mechanical vibrations are transformed into an electrical voltage across the external load. The electric coupling equation becomes:

$$C_p \frac{d}{dt}\dot{V}(t) + \frac{V(t)}{R_t} + \sum_n \theta_n \dot{\eta}_n(t) = 0. \tag{3.68}$$

Open-circuit voltage under curvature (d_{31} mode, 1D):

$$V_{oc} = \frac{d_{31} E_p h_p}{\varepsilon_{33}{}^T} \int_{x_1}^{x_1+x_2} S_x dx, \tag{3.69}$$

where $S(x)$ is strain distribution at the resonance frequency of composite beam.

The voltage generated by the piezoelectric transducer is determined by the beam's mode response, mode shape, internal capacitance, and load resistance and the material's mechanical and electrical properties.

For energy harvesting, the first mode usually dominates (n=1). So, Voltage magnitude at resonance (first mode) load R:

$$V_\omega = \frac{\theta_\omega \eta(\omega)}{\sqrt{(\frac{1}{R})^2 + (\omega C_p)^2}}. \tag{3.70}$$

Where;

- $V\omega$ the magnitude of the output voltage across the load resistor, evaluated at the excitation angular frequency,
- $\eta(\omega)$ is the amplitude of vibration in the first mode, which is obtained by solving the mechanical (modal) equation of motion under base or tip excitation, i.e. the magnitude of the modal coordinate (modal response amplitude) at frequency ω,
- R the external load resistance (Ω) connected across the piezoelectric patch electrodes,

- C_p is capacitance of the MFC,
- Θ electromechanical coupling coefficient at the first angular frequency.

Then average output power (peak-amplitude form) is as follows:

$$P_{ave} = \frac{V^2_{max}}{2R}, V \text{ max}=V(\omega). \quad (3.71)$$

For a linear piezoelectric constitutive equation, a small-amplitude system (aluminium cantilever + *MFC* patch), the resonance frequency equals the natural frequency of the structure.

The damping ratio is very small, having a value between 0.005 and 0.02 for Al metals.
The time-average power delivered to the resistive load $R_t$is the following:

$$P_{harvest}(\omega) = \frac{|\widetilde{V^2}_{\omega}|}{R_t}. \quad (3.72)$$

R_t A simple resistive load connected across the harvester is used to derive simplified mathematical models to predict the electrical output for a given base motion input.

The information on cantilever beam and Macro Fiber Composite piezoelectric transducer dimensions and material properties is listed in Table 3-1.

The effective cross-sectional properties for the aluminium beam with an $M8514-P2$ patch bonded to its top surface.

Assumptions

- The MFC patch starts at x = 65 mm along the beam (so the patch spans x between [x_1,x_2]= [65 to 65+85] mm = [65,150]mm),
- Patch width is centred on the beam width (beam width 30 mm, patch width 14 mm → patch covers y between [8,22]mm),
- Patch thickness $t_p = 0.38$mm sits on the aluminium beam,
- Volume fraction of PZT fibres to epoxy matrix within the: epoxy = 0.6 by 0.4 percent.
- PZT-5A properties used from the vendor datasheet: d_{31}=-175×10^(-12) C/N, E_{PZT} =6.9×10^10Pa, ρ_{PZT}=7700kg/m³, ε_{PZT} =1800,
- Epoxy resin used: E_{poxy}=3.1GPa, ρ_{epoxy} = 1150kg/m³.
- Mechanical damping of the *M*8514-*P*2 (ξ_{MFC}) = 0.01 to 0.05 which depends on the air damping and bonding layer. Voltage and Power levels are quite sensitive to damping

and excitation frequency. Mechanical damping broadens the resonance but reduces the peak voltage and power.

Table 3-1 Geometry, mechanical and material properties of energy harvester

S. No.	Property of energy harvesting	Symbol (formula)	Value (unit)
1	Beam width	b	30.0 mm
2	Beam thickness	t_b	2.0 mm
3	MFC width	w_b	14.0 mm
4	MFC thickness	t_p	0.38 mm
5	Beam area	$A_b = b \cdot h$	60.0 mm^2
6	Mass of beam	$\rho.v$	64.8g
7	MFC area	$A_p = b_m \cdot t_m$	5.320 mm^2
8	Beam centroid from the bottom	$y_b = \frac{h}{2}$	1.000 mm
9	MFC centroid from the bottom	$y_p = h + \frac{t_p}{2}$	2.190 mm
10	Neutral axis	$\bar{y} = (E_b A_b y_b + E_m A_m y_m)/((E_b A_b + E_m A_m))$	1.044mm
11	Average applied force (F_{avg})	0. to 0.5	N
12	I-beam about centroid	$I_b = b\ h^3 / 12$	20.0 mm^4
13	I MFC about the centroid.	$I_m = b_m\ t_m^3 / 12$	0.064017 mm^4
14	EI contribution (beam)	$E_b\ (I_b + A_b(y_b - \bar{y})^2)$	1.408×10^6 $N \cdot mm^2$
15	EI contribution (MFC)	$E_m\ (I_m + A_m\ (y_m - \bar{y})^2)$	2.140×10^5 $N \cdot mm^2$
16	Total bending stiffness	$EI_{total} = EI_b + EI_p$	1.528e+06 $N \cdot mm^2$
18	Equivalent flexural modulus	$E_{eq} = EI_{total}/I_{total}$	59.71GPa
19	Mass per unit length	$m' = \rho_b A_b + \rho_m A_m$	0.190728 kg/m
20	Equivalent area density	$\rho e_q = \rho_b A_b + \rho_m A_m / A_b + A_m$	2920kg/m^3

Table 3-2 Natural frequency for the theoretical model

Mode shape	characteristic equations	Natural Frequency (Hz)
1	1.875	10.69
2	4.69409113	63.96
3	7.85475744	175.41
4	10.99554073	355.02

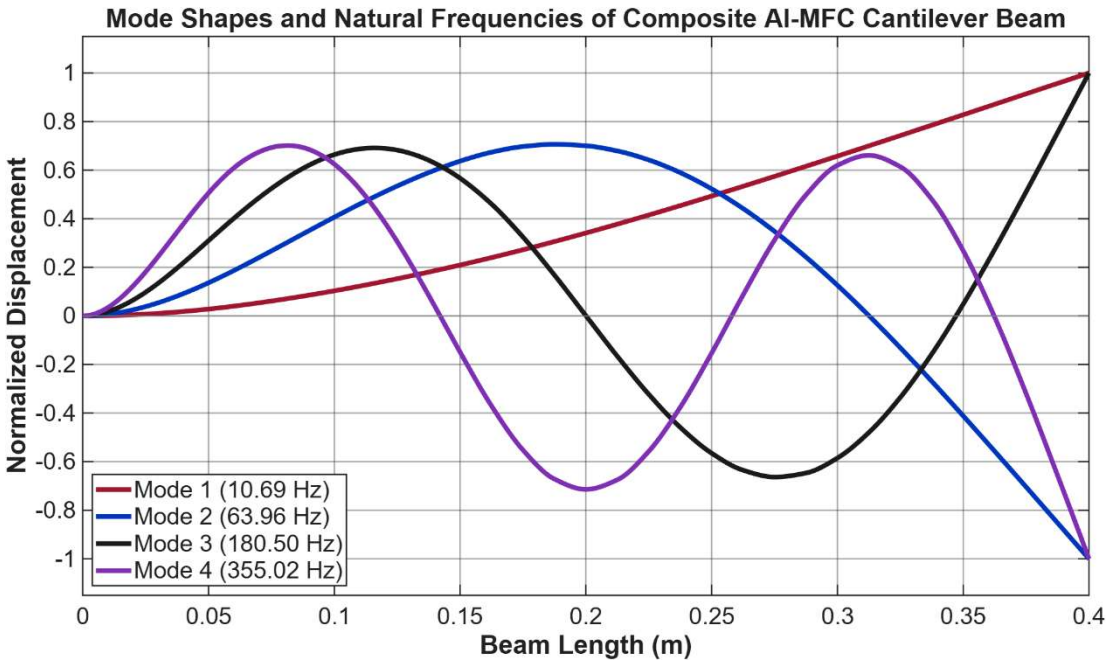


Figure 3-2 The first four modes' shapes and natural frequency by line graph

From Figure 3-2, the first model shape and natural frequency contribute to high energy harvesting; the rest contribute to a small extent. The system should effectively work in the first resonance, where the amplitude peak is the highest. In the case of the system vibrating with the second natural frequency or other higher frequencies, the effectiveness of the system significantly decreases due to a smaller amplitude of strains of the piezocomposite.

3.5. Voltage and power for the analytical model

The frequency response functions of voltage and power for the piezoelectric unimorph beam, using equations (3.64), can be used for 0.5N excitation with the load resistance of 10.5 kΩ. The resulting voltage and power frequency response results are presented in Figure 3-3 and Figure 3-4 respectively. The results shown in Figure 3-3 indicate the voltage magnitude

maximum at the fundamental frequency. The short circuit resonance for the first mode occurs at 10.37 and produces a maximum voltage of 0.265V.

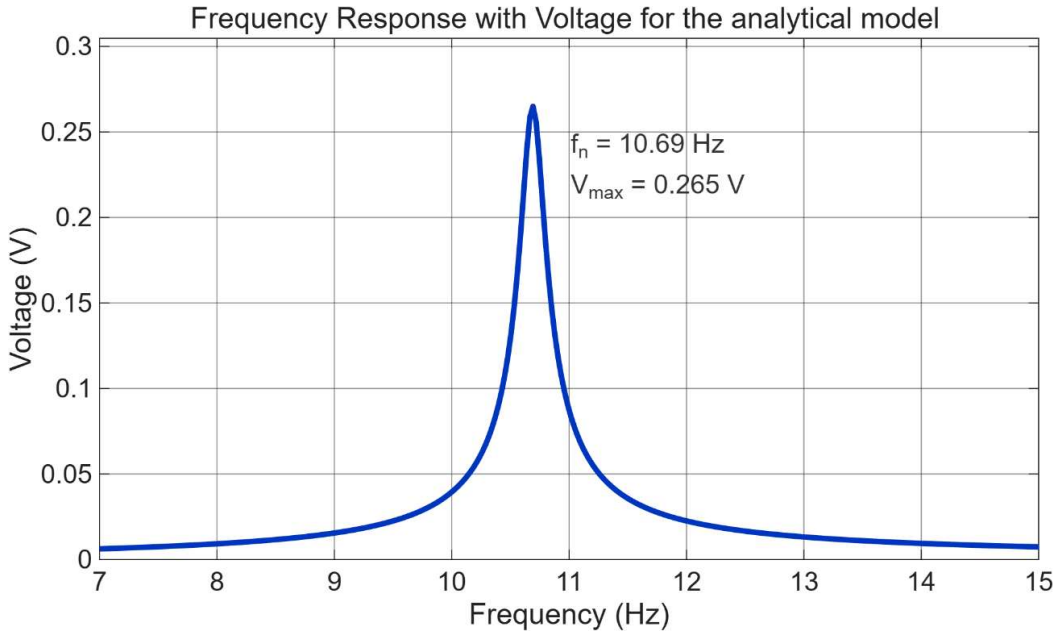


Figure 3-3 Analytical frequency Response with Voltage for linear vibration energy harvester

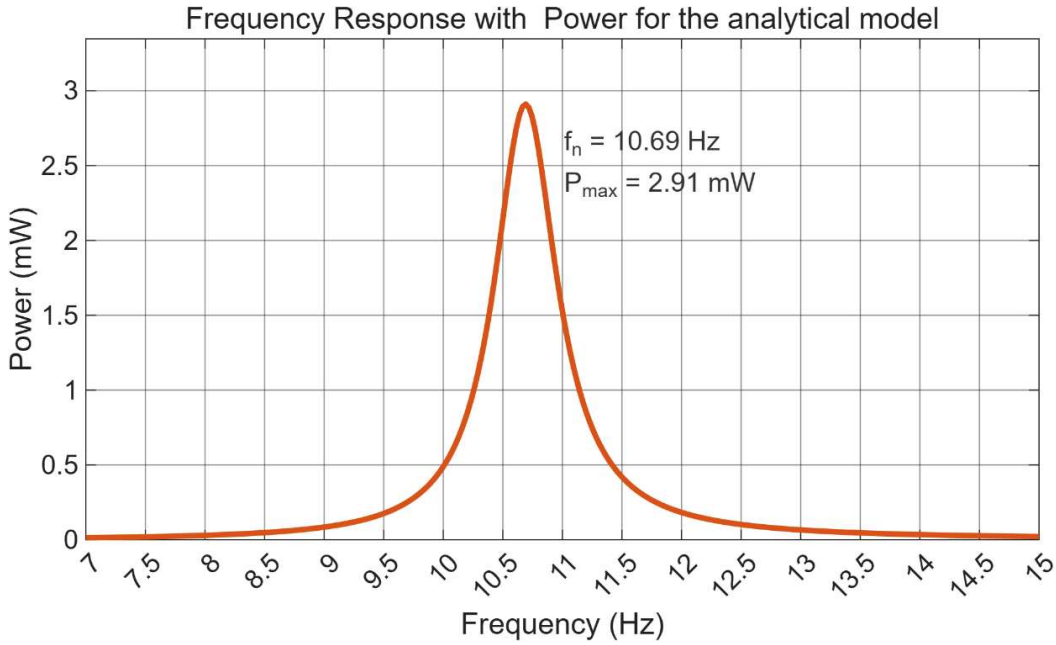


Figure 3-4 Analytical power and resonance frequencies of energy harvester

Figure 3-3 and Figure 3-4 shows the analytical model gives Vmax=0.265V and P_{max}=2.91μW at the fundamental resonant frequency of fn=10.69Hz, respectively. The power response is sharper at the resonance peak than the voltage response because power is proportional to the square of the voltage. Clearly, the harvested power is very sensitive to resonance tuning, which plays an important role in practical energy harvesting applications.

Chapter conclusion

The analysis indicates that the electrical output of the piezoelectric energy harvester is strongly governed by the mechanical behaviour of the cantilever beam. As the beam curvature increases, the axial strain in the Macro Fiber Composite (MFC) layer also rises. This, in turn, enhances the electric displacement, causing more electric charge to accumulate on the electrodes. Consequently, the generated output voltage grows with increasing strain. The peak strain and maximum beam deflection occur at the fundamental resonance frequency, where the vibration amplitude is highest, and therefore the output voltage reaches its maximum at resonance. Since the power generated depends on both the voltage and the load resistance, the power output increases markedly as the voltage rises.

At the same time, the output power is influenced by the electrical load and is inversely related to the load resistance, in accordance with the power relationship. Thus, even a modest increase in output voltage can yield a substantial rise in harvested power when the load is appropriately selected. Furthermore, the analytical model demonstrates that maximum power transfer is obtained only when the external load resistance is close to the optimal electrical load of the piezoelectric transducer. Satisfying this load-matching condition promotes efficient energy transfer from the piezoelectric element to the electrical circuit and maximises the harvested power. Hence, the analytical model serves as a valuable tool for predicting the dynamic performance of the piezoelectric energy harvester and for guiding the design and optimization of its geometric and electrical parameters before undertaking numerical simulations and experimental testing.

Chapter 4 Finite Element Modelling

In this chapter, the FEM-based model was based on an MFC piezoelectric harvester that consists of a piezoelectric sheet, epoxy resin, and an aluminium substrate layer, which are joined together with a contact layer. MFC-P2 Mode d_{31} PEH is integrated with a unimorph cantilever beam, clamped at one end and free at the other end. The vibration acts on the harvester as a harmonic point load applied at the free end, which experiences large-deflection vibrations. The mode d31 piezoelectric energy harvester generates electrical voltage from a transverse load applied (concentrated force applied at the cantilever tip). The output wires from the positive and negative poles are connected to an electrical load of R for generating electrical power [100,184]. In this section, a finite element model for modelling MFC-P2 types of piezoelectric materials and an aluminium substrate with rectangular geometrical configurations is modelled. The aluminium beam and MFC transducer interface were assumed to be perfectly mechanically bonded, i.e. the displacement field is continuous across the interface. However, a mechanical bond does not imply an electrical connection between the two materials. In the current energy harvesting scheme, the aluminium substrate was not used as an electrical electrode and thus the Al–MFC interface was considered to be electrically insulating. Therefore, the electrical current was not allowed to flow between the aluminium beam and MFC layer. The electrical response of MFC was decided by two electrode surfaces of MFC. The aluminium substrate does not provide any electrical degrees of freedom for the coupled system, and the entire electromechanical coupling and thus the harvested electrical output are determined solely by the potential and charge conditions at the two MFC electrode surfaces. This assumption is consistent with the experimental configuration and decouples the mechanical load transfer function of the aluminium substrate from the electrical circuit of the piezoelectric transducer.

The numerical model was implemented in COMSOL Multiphysics 6.3 Figure 4-1 based on the Piezoelectric Devices interface, a predefined multiphysics coupling of the Solid Mechanics and Electrostatics interfaces, together with an Electrical Circuit interface to represent the external resistive load connected across the MFC terminals . This enables the mechanical strain field generated by vibration to be transformed, using the piezoelectric constitutive relations, to a distributed electric potential along the patch and then to an accessible terminal voltage and power dissipated in the load resistance.

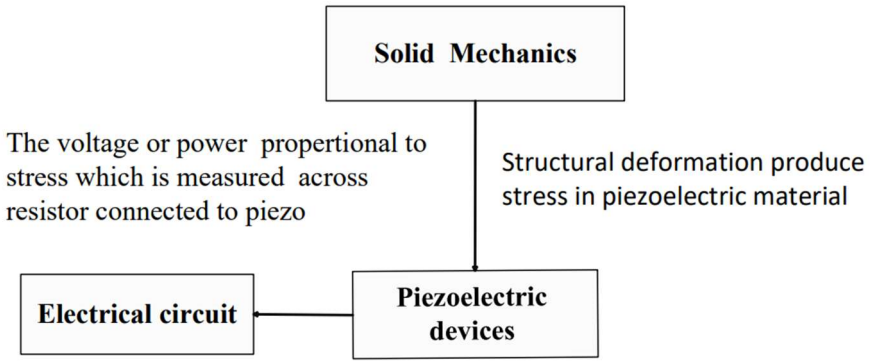


Figure 4-1 COMSOL Multiphysics coupling for simulation

The Solid Mechanics interface the deformation of a cantilever beam under vibration, which induces mechanical stress in the piezoelectric material. This stress is transferred to the interface of the piezoelectric device and is converted to proportional output voltage or power.

4.1 Numerical modelling using finite element method

The coupled mechanical electrical behaviour of the piezoelectric energy harvesting device was numerically investigated using finite element analysis (FEA). Unlike a traditional structural analysis, in which only the mechanical displacement and stress fields are considered, the piezoelectric analysis involves the simultaneous study of mechanical and electrical fields. The direct piezoelectric effect generates an electric displacement when the piezoelectric material is deformed, and an applied electric field can produce the mechanical deformation by the converse piezoelectric effect. Therefore, the finite element formulation has to include the linked electromechanical constitutive relations of the piezoelectric material. To determine the energy generation ability of the MFC, a finite element model using COMSOL Multiphysics software was used to determine the resonance frequency ,the voltage and power output from the MFC integrated with AL cantilever beam substrate. The Finite Element Method (FEM) is regarded as effective for illustrating the dynamic operations of the harvester, particularly when the structural arrangement is more elaborate for complex structures [14,42,100,113,142,185–188].This method is a robust computer-aided method for the analysis of complex structures, which (correctly used) can be in high agreement with experimental methods. Natural frequency and mode shape are important parameters for designing structures under dynamic loading conditions. It also serves as a starting point for dynamic analysis, such as harmonic analysis, transient analysis, or spectrum analysis [42,100,142,185,188,189].The natural frequency of a structure is the frequency at which the structure naturally vibrates if it is subjected to a

disturbance. When the vibrating frequency of the source matches the resonant frequency of the device, an optimum condition of maximum displacement is obtained.. The first key element in modelling piezoelectric transducers for energy harvesting using COMSOL Multiphysics modelling in 2D or 3D is t to determine eigen frequency and frequency analysis. Eigenfrequency is used to determine the resonance frequency and vibration mode shape analysis. The harvester plate consists of one substrate layer and one Macro Fiber Composite layer, as shown Figure 4-2. MFC transducers are placed on the side of the aluminium cantilever beam on opposite sides. MFC P2 was placed 65 mm from the clamped end of the Al beam to harness the most active stress region. The dimensions of the active area of the MFC with epoxy resin are 85 mm length (l_p), 14 mm width (w_p) and thickness ($\mathrm{h_p}$) of about 0.38 mm. Dimensions of the beam are 400 mm length (l_b), 300 mm width (w_b) and 2 mm thickness and 2 mm height (t_b) (Figure 4-2). The volumetric fraction of MFC in epoxy resin is approximately 60%, with 40% epoxy resin, which balances electromechanical performance, flexibility, and durability. The Macro Fiber Composite (MFC) is not a monolithic PZT plate; it is a composite of piezoelectric fibers embedded in epoxy. PZT fibers with epoxy resins filling in the gaps. MFCs are comprised of very thin fibers that are unidirectionally aligned and sandwiched between two sets of electrode patterns printed on a polyimide film (Figure 4-3). The fibers are made of PZT-5A material, and the matrix is made of epoxy resin for which the built-in materials from the COMSOL Multiphysics material library are used. Compared to monolithic piezoelectric materials, composite piezoelectric material offers superior mechanical and thermal properties along with customisation. Electrode layers sandwiched the MFC generator, and electrical circuit physics was used to model a resistance load across the MFC terminals, as shown in Figure 4-3. In the finite element study, eigenfrequency and frequency-domain modal analyses were employed. For the simulation, varied materials were used, and each one had a set Young's modulus and Poisson's ratio from COMSOL's library of materials. The eigenfrequency solver was set up to use the ARPACK algorithm, which looks for a shift of about 1 Hz without any geometric nonlinearity. The physics interfaces encompassed solid mechanics, electrostatics, deformed geometry, and parametric optimisation. Standard COMSOL solver settings were used, and physics-controlled linearisation was used. After that, the top and bottom surfaces of the piezoelectric layers were defined as ground and terminal in the boundary conditions of electrostatics physics. The rest of the faces were labelled as zero charge. In the next step, a tetrahedral mesh with extremely fine element size was used for the discretisation of the beams. Finally, eigenfrequency and electric potential analysis were performed to determine eigenvalues, voltage, and power output potential of the harvesters. These setups made sure that

the model worked quickly while still giving accurate results, which made it useful in the real world.

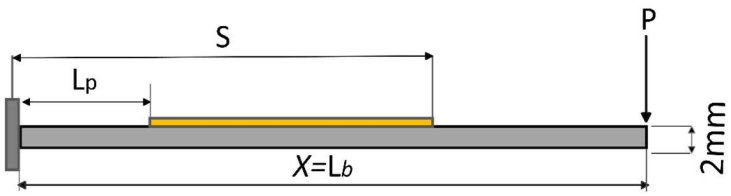


Figure 4-2 schematic Aluminium cantilever beam unimorph patched with MFC

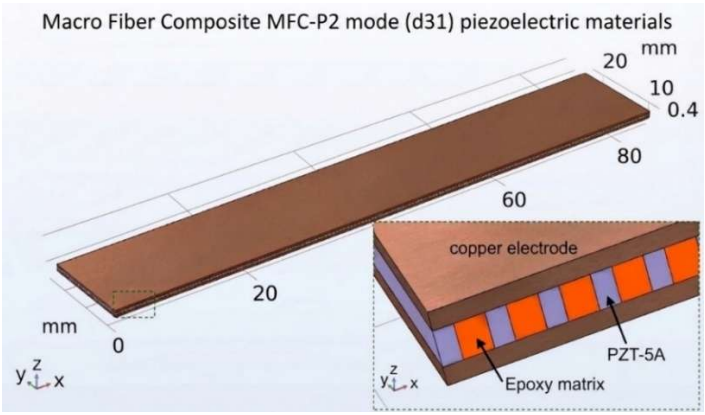


Figure 4-3 The components of Macro fiber Composites from model on COMSOL Multiphysics

Figure 4-2 physical geometry of the whole harvester) and internal material architecture of the active patch (Figure 4-3), giving a top-down view of how the model for the governing equations and mesh/solver settings works.

4.2 Geometric and material properties of the Substrate and energy harvester

The geometric and material properties of the substrate and piezoelectric transducer of a cantilever-based piezoelectric energy harvester strongly affect its performance, as they define the stiffness, mass distribution, resonant frequency and electromechanical coupling of the beam. The energy harvester is defined as a bonded MFC-P2 patch and the substrate as an aluminium beam. The dimensions, densities and elastic properties are given and used as inputs in the analytical and finite element models developed in this work.The MFC transducer and the aluminium cantilever beam were treated as a coupled electromechanical system in this thesis. The MFC layer was described using the material characteristics of the M8514-P2 piezoelectric composite, while the aluminium substrate was depicted as an elastic, electrically inert substance. The two main dependent variables chosen were the electric potential and the mechanical displacement field. The link between the mechanical strain/stress field and the electric field/electric displacement field was established using the piezoelectric constitutive

equations. The piezoelectric multiphysics formulation was used in COMSOL Multiphysics to create the finite element model. While the electrical boundary conditions were applied to the MFC electrodes in accordance with the experimental electrical configuration, the mechanical continuity between the aluminium beam and the MFC layer was enforced through the bonded interface. The natural frequencies, mode shapes, voltage response, and harvested electrical power were then ascertained by eigenfrequency and frequency-domain analysis of the resulting coupled system.

4.2.1 Design parameter of substrate and energy harvester

A rectangular cantilever beam with a unimorph MFC-P2 type geometric configuration is chosen, which can produce large deformation under vibration. The bottom of the MFC layer is grounded, and a floating potential or voltage condition is applied to the top surface of the piezoelectric layer. The substrate layer of a VEH is typically not entirely covered by piezoelectric materials due to their prohibitive cost, particularly for larger VEHs with lower resonance frequencies intended for environmental vibrations. The parameters used for the mechanical energy harvester and substrate material are listed Table 4-1. The homogenised electromechanical properties of the MFC piezoelectric materials are computed based on the individual properties of the fiber and matrix, the fiber volume fraction, and the poling directions. In M8514-P2 MFC, the piezoelectric fibers are poled through the thickness (z-axis), and mechanical deformation occurs along the in-plane axis (x-axis) where bending-dominant strain is applied. [1,100]. For this study, the fiber in the composite material is made of PZT-5A, while the matrix comprises epoxy resin. The MFC8514-P2 (Smart Material Corporation) piezoelectric patch has been integrated with the cantilever beam, positioned at 65 mm from the fixed support end. The patch has overall dimensions of 85 mm × 14 mm × 0.38 mm and operates according to the d_{31} electromechanical coupling mechanism (directional dependence of material properties).The dimensions of both the electrode and adhesive are the same dimensions as the MFC patch, except for its thickness, which is 0.1 mm. It is important to note that the design was aimed at maintaining equal mass for fair comparison. Based on this model, the effects of fiber width for a single cell, 0.25 mm, and height, 0.38 mm, on the stress field distribution and output potential were systematically modelled.

In the length dimension, the fiber length of 85 mm and fixed to the beam at 65 mm from the fixed end support. Too short fibers will reduce the effective piezoelectric polarization volume and weaken the electromechanical coupling capability, while too long fibers are prone to stress concentration in periodic arrangement and flexible encapsulation, which may lead to

fracture failure under long-term dynamic loads, affecting the device's reliability. The entire top and bottom surfaces of the P_2-type MFC are covered by electrodes. The voltage load on the P2-type MFC harvester is applied by setting the potential on the bottom electrode to be zero and imposing the sinusoidal electrical potential on the top electrode. The fiber in the composite material is made of PZT-5A material, while the matrix is made of epoxy resin (epoxy matrix).The substrate material (Figure 4-2 and Table 4-1), with a density of 2700 kg/m³, along with the isotropic elastic material model, the Poisson's ratio of 0.33, and an elastic modulus of 70 GPa. The material properties of the MFC piezoelectric composite layer and the substrate layer are shown in Table 4-1.

Table 4-1 Geometric parameters and material properties of unimorph beam PEH

Item	Parameter	Unit
Aluminium substrate		
Length	400	mm
width	30	mm
Thickness	2	mm
Density (ρ_{Al})	2700	kg/m^3
Poisson Ratio	0.345	-
Elasticity	70×109	Pa
MFC		
Length	85	mm
width	14	mm
Thickness	0.38	mm
Young's Modulus E_1	30.35×109	Pa
Young's Modulus $E_2 = E_3$	15.85×109	Pa
Shear Modulus $G12 = G_{13} = G_{23}$	5.52×109	Pa
Poisson Ratio $v12$	0.3	-
Poisson Ratio $v_{13} = v_{23}$	0.16	-
Piezoelectric constant d_{33}	4.6×10^{-10}	C/N
Piezoelectric constant d_{31}	-2.1×10^{-10}	C/N

The material properties of the MFC piezoelectric composite and the substrate layer are shown in Table 4-1.

4.2.2 Mechanical damping model

Rayleigh damping assumes the damping matrix is a linear combination of mass and stiffness. In FEA, the Rayleigh damping effect was considered; otherwise, the calculation would be terminated because of the convergence problem near the beam resonance. Both the energy extracted from the MFC harvesters and the damping from the structural material contribute to the entire damping effect of the system. However, in FEA, only the open circuit voltage of the MFC harvester is calculated, and no energy is removed from the system, in which case it is assumed that the damping of the system is only attributed to the damping of the Al beam material can be described by the equation [125,190]:

$$\xi_i = \frac{1}{2}\left(\frac{\alpha}{\omega_i} + \omega_i\beta\right). \tag{4.1}$$

where α and β are the unknown parameters and ω_i is the frequency of the i^{th} vibration mode. To obtain α and β, the damping ratios for the first and second resonance modes should be experimentally determined [190]. The damping ratios for the first and second modes are obtained as $\xi 1 = 0.0064$ and $\xi 2 = 0.0077$. Applying $\xi 1$ and $\xi 2$ to the damping equation, the two parameters of the Rayleigh damping can be determined as $\alpha = 0.66$ and $\beta = 3.544 \times 10^5$ [125,191].

4.3 Analysis of simulation results for the finite element method model

Figure 4-4 3D models and mesh for finite element (FE) model of cantilever beam integrated with a MFC piezoelectric energy harvester (PEH) were developed with COMSOL Multiphysics software, operating in transverse d_{31} mode.

To calculate power output, FEM is a powerful tool to model complex PEH systems. Aluminium beams within un-morph MFC are employed for VEH when driven at the resonance frequency. In the particular case of 31-mode piezoelectric coupling, with mechanical stress along the 1-axis (x-direction) and the electric field/polarisation along the 3-axis (z-direction) the general 3D constitutive equations reduce to the following scalar forms. The equation is now presented in its proper scalar form for the 1D 31-mode reduction, using standard IEEE notation. Such a reduction is valid for the MFC-P2 patch used in this work, where vibrational forces are only acting along the z-axis and the electrodes are perpendicular to the poling direction:

$$S_1 = \sigma_1 s^{\mathrm{E}}{}_{11} + d^{\sigma}\mathrm{E}_3, \tag{4.2}$$

$$D_3 = d\sigma_1 + \epsilon^{\sigma}{}_{33}E_3. \tag{4.3}$$

Where S_1 represents the strain component along the beam axis, and σ_1 is the corresponding stress component. D_3 denotes the electric displacement component, and E_3 the electric field component, both along the poling direction. The term $s^E{}_{11}$ refers to an element of the 6×6 elastic compliance matrix, evaluated under a constant electric field. d_{31} is the relevant element in the 3×6 piezoelectric strain matrix, linking stress along the beam axis to the electric field along the poling direction. Finally, $\epsilon^\sigma{}_{33}$ is the element of the 3 by 3 dielectric permittivity matrix, assessed at constant stress.

4.4.1 Natural Frequencies and modal analysis of a Cantilever Beam

Natural frequency is when the system vibrates without external forces, and modal analysis determines the mode shapes (patterns of deformation). The cantilever beam has many different vibration modes, each with different resonance frequencies. The identification of the natural frequency of the energy harvester beam is extremely important since this will determine the frequency range for which the energy model will be performed. The resonant energy harvester is most used when the input vibrations are regular, the frequencies are high, and the input vibration amplitude is smaller than the device's critical dimensions, such as vibrations on machinery or vehicles.

The first vibration modes have the lowest frequency of resonance and usually provide the most vibration and therefore the most energy. The lower frequency is close to the natural frequency, and the power is produced at lower frequencies [28,39,137]. Thus, optimum energy can be harvested efficiently when the harvester is driven at resonant frequencies.

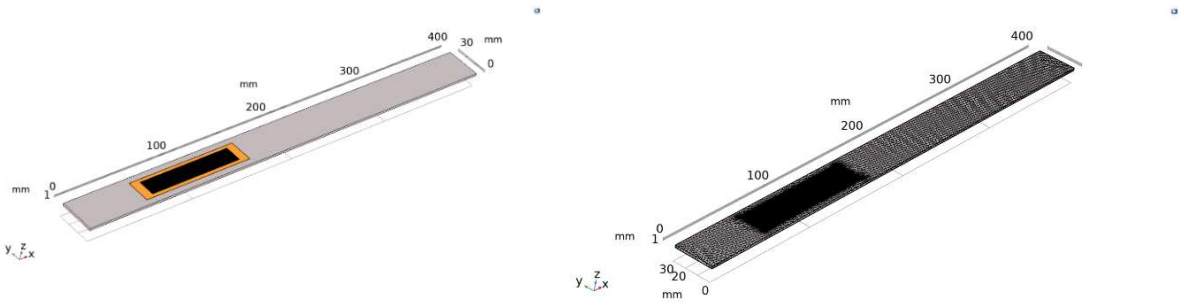
Figure 4-5 shows the first four vibration modes, eigenfrequencies, and displacements of the rectangular-shaped cantilever beam harvesters, respectively. The real part is the natural (resonant) frequency of that mode, and the imaginary part is the damping present in the eigenvalue solution. A non-zero imaginary component appears because the piezoelectric-circuit coupling (and/or the Rayleigh damping I was defined in in equation 4.1) makes the system matrices non-symmetric/damped, so COMSOL's eigenvalue solver returns complex conjugate pairs instead of purely real eigenvalues. This is expected and normal for a coupled electromechanical eigenfrequency extraction. The results show that the free end of the rectangular-shaped harvester beam was displaced and reached a maximum value of 0.075 mm at a fundamental resonance frequency of 10.976 Hz. This fundamental frequency, used in closed-circuit conditions as the frequency of excitation, induces peak tip response. It is important to note that there is a decrease in natural frequencies of the proposed harvester over

the rectangular beam harvester in all three modes of vibration considered. This advantage is highly desirable in designing vibration-based energy harvesters since most vibration sources have lower excitation frequencies. The first four natural frequencies and mode shapes of PEH are obtained by model analysis in COMSOL FEM simulation. Rectangular cantilever beams with a uniform point load at the free end of the cantilever beam considered. The resonant frequency errors obtained from impedance analysis are less than 2.47% for mode one, mode 2 (2%) and mode 4 (0.64%).

The eigenfrequency analysis produced complex eigenfrequencies, expressed as (f_n = f{n,r} + $f_{\{n,i\}}$). The real part ($f_{\{n,r\}}$) represents the system's damped natural frequency (in Hz), while the imaginary part ($f_{\{n,i\}}$) indicates the frequency decay rate (in Hz), which reflects energy loss. This energy dissipation comes from both mechanical damping modelled using Rayleigh damping coefficients and electrical losses in the MFC, represented by the dielectric loss tangent.

The imaginary part is much smaller than the real part, as seen in the fundamental mode shown in Figure 4-5, which implies a low damping ratio. The damping ratio for each mode can be estimated by the ratio of the imaginary part to the real part of the eigenfrequency. The fundamental mode has only slight damping, demonstrated by its very small imaginary component. In contrast, higher modes show increased imaginary parts, indicating stronger modal attenuation under the model's damping assumptions. Therefore, the complex eigenfrequencies listed in the legend of Figure 4-5 convey not only the natural frequencies of the structure but also the damping and energy dissipation characteristics of each vibration mode.

.



(a) Al beam withMFC model (b) Mesh model

Figure 4-4 Schematic of the EH MFC with a unimorph rectangular substrate model and mesh

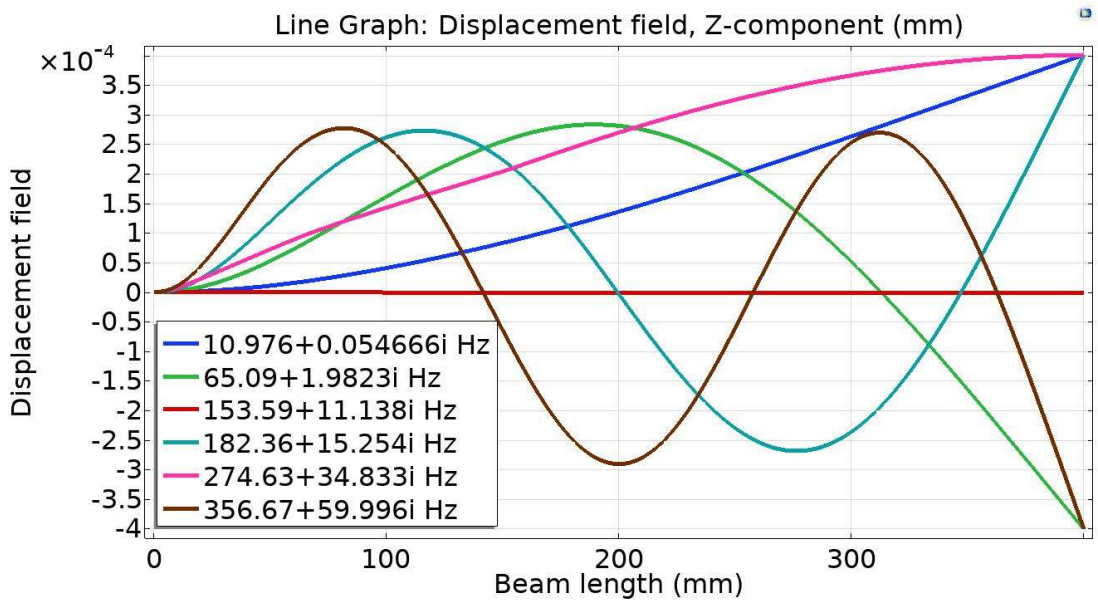


Figure 4-5 The mode shapes and natural frequencies for numerical model

From the Figure 4-5:

- The eigen frequency 10.976 Hz: This is the basic bending mode, with a monotonically increasing deflection from the clamped end (x = 0) to the free tip (x = 400 mm) without any internal nodes. This classic first-mode cantilever shape for energy harvesting, since the MFC patch placed near the root (high strain region) couples most strongly to this mode.
- 65.09Hz eigenfrequency: The Second bending mode. One internal node (change of sign) at x =280-300 mm.
- 182.36 Hz: The third bending mode and has two internal nodes.
- 274.63 Hz: Does not have the normal bending pattern which for a higher bending mode (torsion mode) and oscillations along the beam length.
- 356.67 Hz: The fourth bending mode (three internal node).
- 153.59 Hz: This is a flat curve at zero over the entire length of the beam (not a true bending mode shape or zero Z displacement).

One of the fundamental factors influencing the charge generation of a piezoelectric cantilever is the amount of stress generated when loaded. Therefore, a cantilever PEH subjected to basic excitation in the first vibration mode generates voltage as a function of the stress experienced in the material [175,191]:

$$V_{31} = \sigma_{xx} g_{31} t_{xx}, \tag{4.4}$$

where:

- V_{31} electric voltages produced between the electrodes of the piezoelectric layer ("31" subscript indicates the mode: mechanical stress along the direction 1 leads to an electric field along the direction 3).
- g_{31} the piezoelectric voltage constant (units: $\mathrm{V} \cdot \mathrm{m/N}$), a property of the piezoelectric fibres. It relates an applied mechanical stress in the 1-direction (in-plane, along the length of the beam/fibre axis) to the electric field generated in the 3-direction (through the thickness of the patch, where the electrodes reside).
- σ_{xx} (or σ_1) mechanical stress in the x-direction (along the length of the beam) caused when the cantilever bends. In your situation, this is the axial/bending stress at the patch location based on the beam curvature.
- t_p thickness of the piezoelectric layer, over which the electric field is integrated to give a voltage rather than a field.

The structural and piezoelectric properties significantly influence the dynamic behaviour of the cantilever beam. The primary objective of mechanical vibration energy harvesting is to operate the system at natural frequency, where stress and strain are maximised, thereby high electrical output voltage and power. In energy harvesting systems operating under low-frequency excitation, the cantilever beam undergoes damped free vibration at its first natural frequency. As shown in Figure 4-6, at resonance the beam reaches its maximum displacement, causing the MFC harvester to experience the highest strain and therefore generate the maximum output voltage and power. Consequently, the efficiency of energy harvesting at resonance is crucial. Figure 4-7 illustrates that the resonance frequency plays a key role, and the efficiencies of MFC harvesters are evaluated at the first natural frequency while accounting for damping effects.

Figure 4-8 Von Mises stress distribution of the rectangular cantilever beam with MFC. The maximum stress (σ_{max}) of the order of $12.5 \times 10^6\ N/(m)^2$ is observed at the fixed end of the beam where bending curvature is maximum. Thus, this region is the most suitable due to the maximum strain experienced by the piezoelectric material for the conversion of mechanical-to-electrical energy. On the other hand, the stress reduces towards the free end of the beam and reaches around $0.002 \times 10^6 \mathrm{N/m^2}$ which indicates a much lower contribution to the electrical energy generation. The distribution of the stress is the reason that the partially covered piezoelectric cantilever beam is widely used in the literature with the piezoelectric layer near

the clamped end to improve the utilisation of materials with high energy harvesting performance.

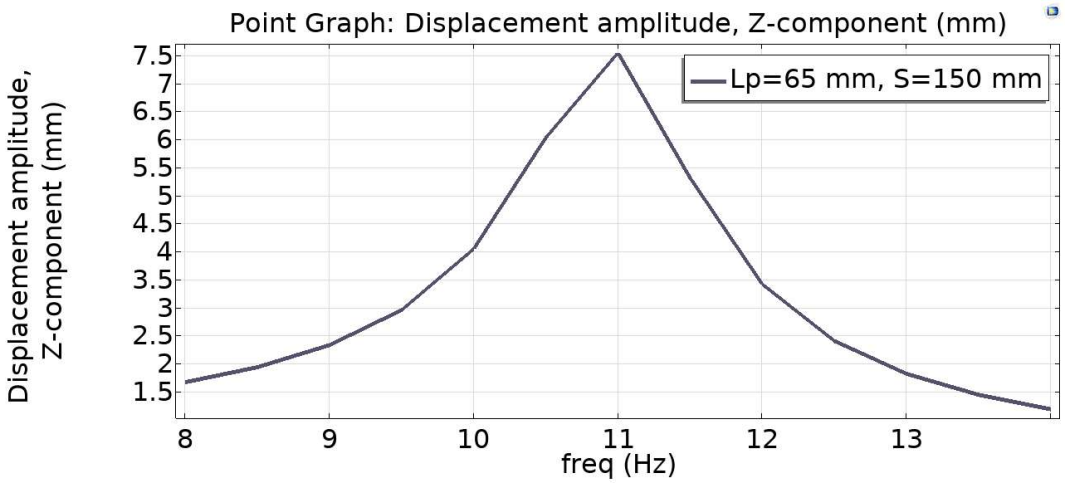
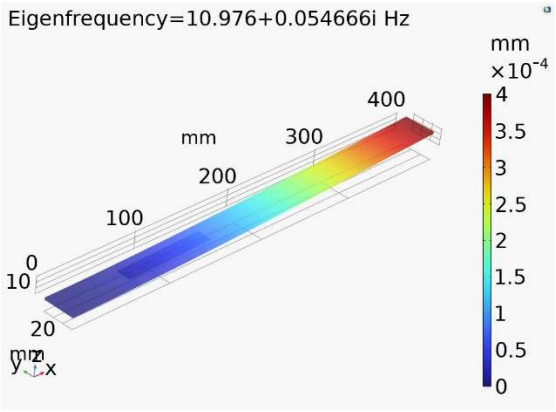


Figure 4-6 Displacement amplitude versus frequency for analytical model

Note

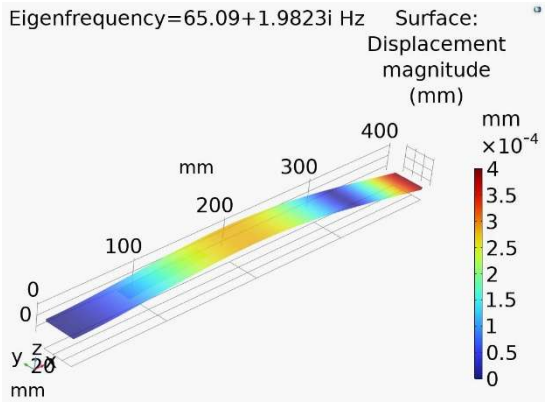
- *L*p: initial placement of MFC piezoelectric from the fixed support end at 65 mm.
- *S* (segment): the total line segment over which MFC is placed from the fixed support of the beam.

Mode 1

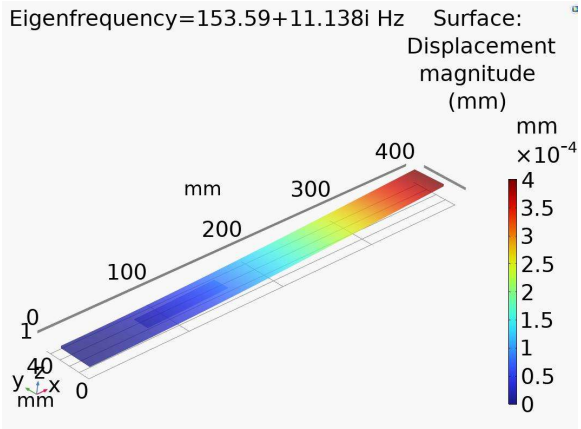


Mode shape 1 with natural frequency

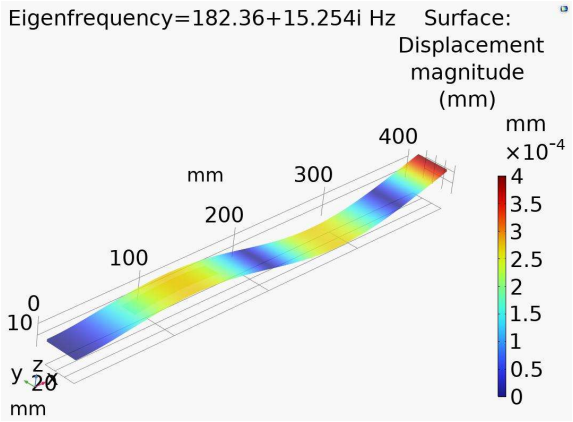
Mode 2



Mode shape 2 with natural frequency



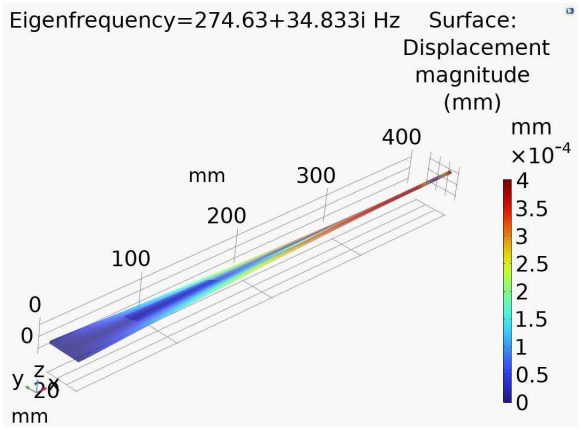
Mode shape 3 with natural frequency



Mode shape 4 with natural frequency

Mode shape 5 with natural frequency

Mode shape 6 with natural frequency



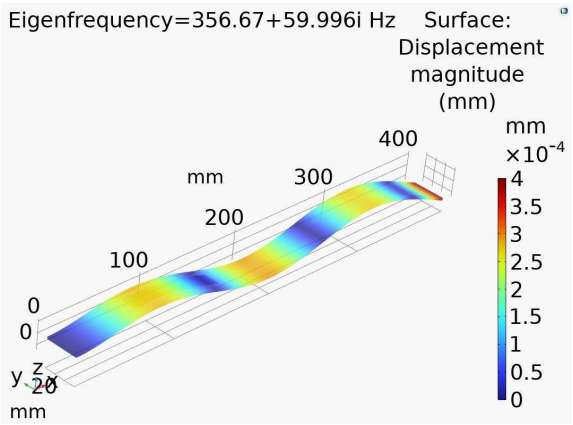


Figure 4-7 3D mode shape and natural frequency, COMSOL Multiphysics modelled

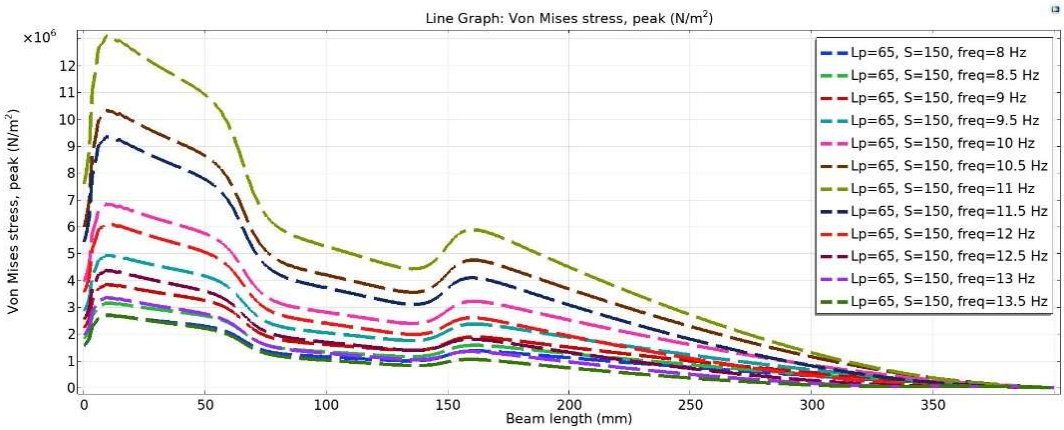
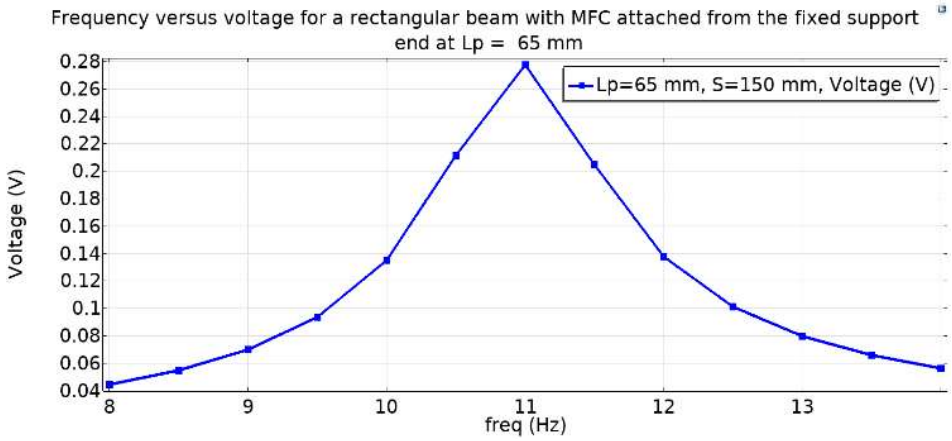
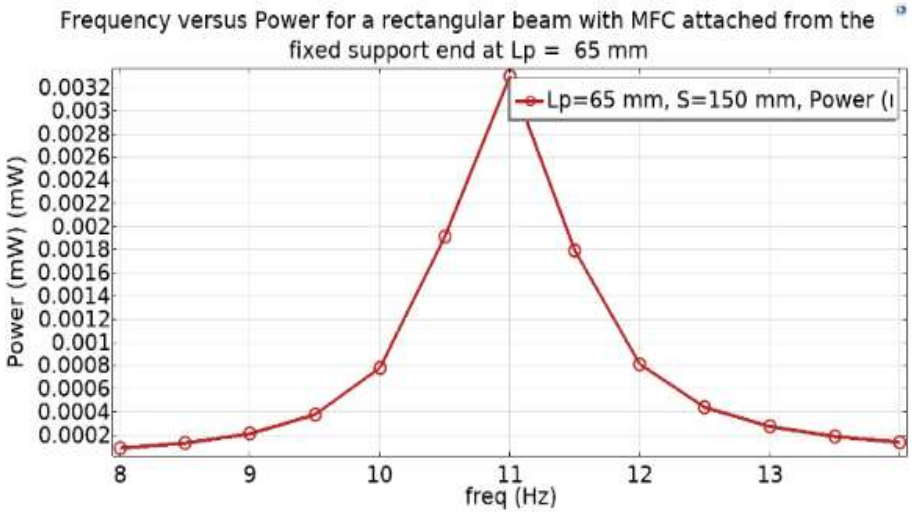


Figure 4-8 Von Mises stress of EH at MFC is 65 mm from the fixed support end



(a) voltage harvested by rectangular beam with MFC



b) power output harvested by rectangular beam with MFC

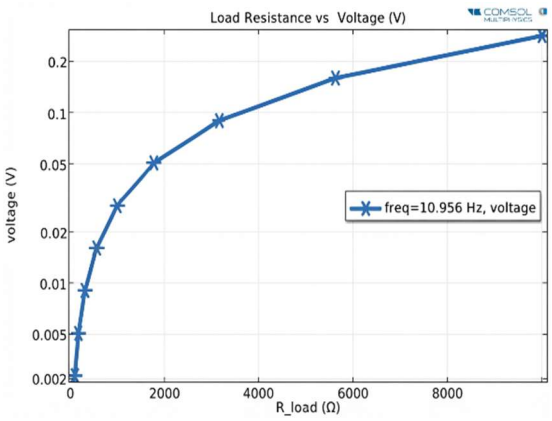
Figure 4-9 Voltage and Power versus Eigen frequency of the for rectangular EH

The generated voltage and power depend on the resonance frequency for maximum power harvesting, as shown in the Figure 4-9 (a). In the first mode, the natural frequency obtained from simulation is 10.976 Hz, and the corresponding output voltage is 0.28 V. Figure 4-9 (b)

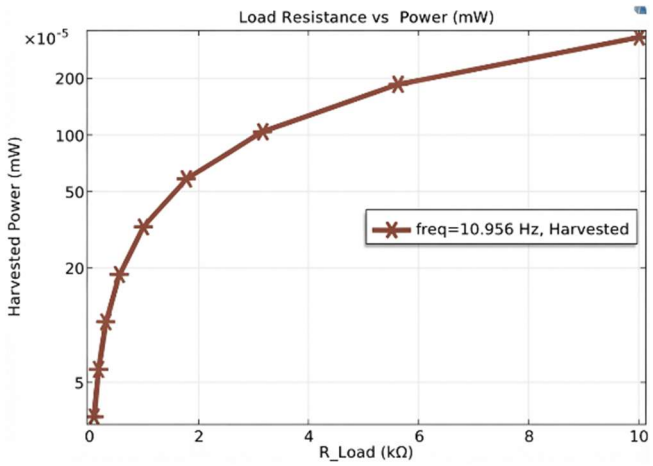
shows the electric power output in milliwatts of the setup at its fundamental resonance frequency of 10.976 Hz. For series connection, generated power is 0.0032 mW with load resistance between 10 and 12 kΩ, and beam displacement is 7.5 mm. For the rectangular substrate harvester, the power output was obtained in the range of 0.0002 mW to 0.0032 mW in the resonance frequency range of 7-15 Hz with a frequency step size of 0.5 Hz.

Load resistance versus voltage and power at fundamental frequency

The harvested power also increases continuously across the entire simulated range, reaching a maximum of approximately 0.0032 mW at a load resistance of 10-12 kΩ, as shown in Figure 4-10 for a range of small electrical loads. When the electrical load is in this range, the peak power occurs at a frequency of 10.976 Hz, which is close to the beam's pure structural natural frequency. As the load increases beyond this range, the peak power drops. Therefore, it can be concluded that the frequency at which the power is maximum depends on the electrical load.



(a) Load resistance versus h voltage at the resonance frequency



(b) Load resistance versus harvested

Figure 4-10 Voltage and power under with different external resistances

At the fundamental frequency of 10.976 Hz, both voltage and harvested power increase monotonically with load resistance over the simulated range (up to 12 kΩ). At the high end of the tested range, voltage is approaching its open circuit asymptote, but power continues to increase, suggesting the optimal (power-maximising) load resistance is at or above 12 kΩ.

4.4 Comparison between theoretical and numerical models

The comparison was made between natural frequencies, voltage, and output power for analytical and finite element method results, which are in good agreement. In the Table 4-2 results of the numerical analysis of the resonant frequencies and the corresponding mode shapes are compared with the analytical model. Modal analysis is used to examine the different vibration modes and the frequencies at which they occur. The analytical mode shape and natural frequency are compared with the numerical model using COMSOL Multiphysics. The first mode's present FEM results show a negligible difference from the analytical models. However, for the 2nd and 3rd modes, this difference becomes immense. There are good agreements between the FEM model and the analytical one. For the 2nd and 3rd modes, the effect of load on the resonant frequency is small. However, for the 4th mode, the effect is slightly higher than the rest of the other mode shapes, with a percentage less than 5%. It is indicated in these table that the resonant frequencies of both models are very close, and the result differences of impedance analysis are very small for each mode.

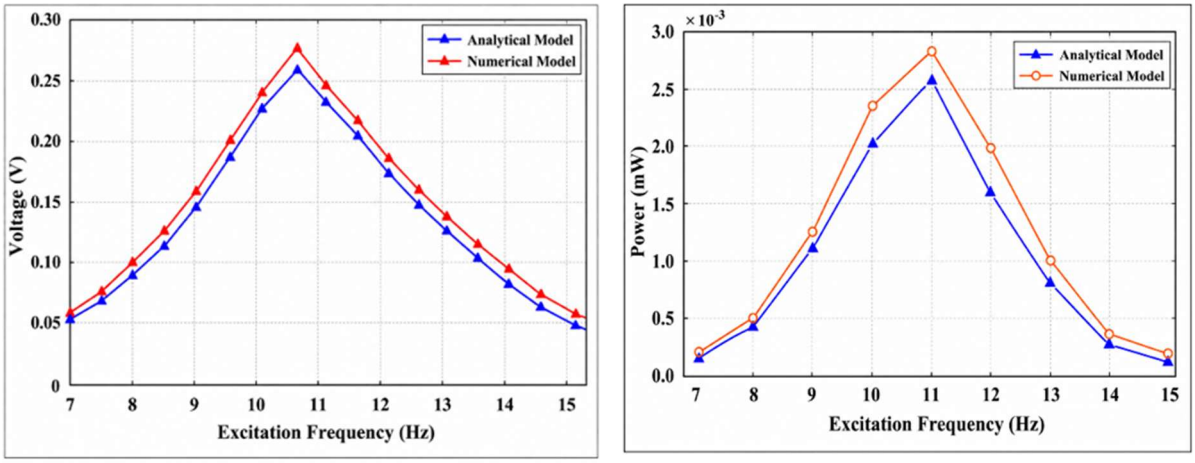
The fundamental natural frequency obtained by the finite element method (FEM) is 10.976 Hz, which is 2.42% higher than the analytical value (10.69 Hz). The variation of the analytical and FEM natural frequencies is less than 5% for all four vibration modes analysed. Table 4-2 Comparison of analytical and finite element results for the first four natural frequencies. The results are in good agreement. The percentage differences are in the range of about 0.4% to 0.5%.To produce maximum voltage and power from piezoelectric elements that are attached to vibrating structures, the structures should be excited at their first natural frequency, where they experience the largest deflections. Figure 4-11 (a) shows the output voltage and power for a 10kΩ for both the analytical and numerical models. The open circuit voltage response and power output response are also important for assessing the performance of a piezoelectric energy harvester. Typically, a resistor is connected to the harvester as an electrical load to evaluate its power output performance. To achieve the maximum power output, the optimal resistor value should be selected based on impedance matching techniques. These optimal values slightly vary at each frequency point. However, the most significant interest lies in the peak values around the resonance frequencies for power output research from a piezoelectric

energy harvester. Therefore, for simplicity, instead of determining every optimal 10 kΩ resistor at each frequency, the focus is on the optimal resistor at the resonances, because responses at off-resonance frequencies are considerably lower. An approximate value of the optimal resistor should be chosen for further analysis. When the resistor value is around 12 kΩ, the PEH had a maximum response for voltage and power output for both peaks, as shown in Figure 4-11peak voltage response of the harvester was 0.28 V at the excitation frequency of 10.97 Hz when the harvester was simulated in open-circuit conditions, as shown in Figure 4-10.The results had a 1.02% difference from the theoretical model. Figure 4-9 presents the output voltage and power responses of the analytical and numerical models with a load resistance of 10 kΩ.

The open circuit voltage response and the power output are important indicators to evaluate the performance of a piezoelectric energy harvester. To evaluate the power output performance of the harvester, a load resistor is typically connected to the harvester. Impedance matching should be used to select the optimum load resistance for maximum power output. However, the optimum load resistance varies slightly with the excitation frequency, and the greatest interest is in the peak response at the resonance frequency where the harvested power is maximised. Thus, the approximate optimum load resistance value of 10 kΩ is used for the study instead of finding the optimum load resistance at each frequency since the responses at the off-resonance frequencies are significantly lower. As shown in Figure 4-10 (a) and (b), the piezoelectric energy harvester (PEH) generated maximum voltage and power output at the load resistance of about 10 kΩ. As can be seen from Figure 4-11(a) and (b), the peak voltage response of the harvester in open-circuit condition is 0.28 V for the excitation frequency of 10.976 Hz. The result is 1.02% deviation from the theoretical prediction, indicating an excellent consistency of the analytical and numerical models.

Table 4-2 The natural frequencies for analytical and numerical

Vibration mode	Natural frequency (Hz)		Difference in %
	Analytical	Numerical	
The 1st bending mode	10.69	10.976	2.675
The 2nd mode	63.96	65.09	1.767
The 3rd bending mode	175.41	182.36	3.96
4th bending mode	355.02	356.67	0.46



(a) Frequency vs Voltage (b) Frequency vs power

Figure 4-11 The theoretical and numerical models of voltage and power

The magnitude of the voltage at the resonance frequency for both models increases within the resistor load, as shown in Figure 4-11 (a). For the case of a cantilever beam with small damping, the results of [192] can be used. It must, however, be noted that the model represents the system behaviour only in the small vibration of a single eigenmode.

Small deviations are due to modelling assumptions, e.g., neglecting the shim layer or the assumption of ideal boundary conditions. Also, nonlinear effects of the material behaviour are not considered in the analytical model, but these are present in the experimental results. For small mechanical excitation, dielectric losses are neglected, and the electrical load is modelled by a resistive load as beams have small vibrations. Maximum power transfer is achieved if the load resistance matches the internal resistance of the energy harvester.

The power produced using the theoretical method is lower than the numerical method. The main reason for the Euler-Bernoulli method is correctly assuming that the MFC does not bend on its own neutral axis but bends on another shifted neutral axis. The average power models from classical PZT piezoelectric energy harvesters usually lie in the tens or hundreds of μW, while the optimum load impedance is a hundred kΩ, as mentioned in literature reviews. Thanks to the non-classical MFC piezo with low frequency, the MFC energy harvester can reduce the optimum load impedance to 10 kΩ and generate an average power of up to 0.0032 mW. It indicates that MFC piezoelectric energy harvesters have a few tens of milliwatts of power generation potential for low-electronic material applications.

Chapter 5 Experimental validation

Chapters 3 and 4 outlined, respectively, the theoretical (mathematical) and numerical models of the aluminium cantilever beam bonded with a unimorph Macro Fiber Composite (MFC-P2) piezoelectric energy harvester were developed. These models were formulated to predict the energy harvester's mechanical and electrical responses under vibrational excitation and to assess electromechanical energy conversion performance. The mathematical model offers an analytical representation of the system's behaviour, whereas the numerical model, based on finite element analysis, allows a more detailed exploration of its dynamic response.

Validating the developed models against experimental measurements is essential to establishing their accuracy and reliability. This experimental verification serves as a critical step in assessing how well both models capture the physical behaviour of the piezoelectric energy harvester under real operating conditions. Accordingly, Chapter five focuses on the experimental investigation conducted to validate the mathematical and numerical models. The experimental setup, measurement procedures, instrumentation, and testing conditions are described in detail, followed by a comparison of the experimental results with the corresponding theoretical and numerical predictions. Initially, the energy harvester consists of a mechanical substrate, a piezoelectric material, and an electrical interface. Frequency response functions of the energy harvester beam were obtained by applying an actuation voltage to the beam to compare the natural frequency obtained from both mathematical and numerical models versus the experimental frequency. The unimorph MFC-P2 is bonded to a cantilever beam of length 400 mm when mounted on the clamping fixture. The dimensions and material properties are shown in Table 5.1. In this chapter the experimental results of applying harmonic actuation voltage and measuring the frequency response functions in the neighbourhood of the fundamental resonance of the unimorph are presented.

5.1. Sample preparation

In Figure 5-1 shows the setup of the unimorph energy-harvesting system. The MFC8514-P2 piezoelectric transducer was attached to the upper surface of the aluminium substrate, and the MFC8514-P1 transducer was bonded to the bottom surface near the clamped end. The cantilever beam was assumed to have only bent vibrations, with no torsional modes, according to the Euler–Bernoulli beam theory. An aluminium cantilever beam is used as the host structure for the energy-harvesting system, which is equipped with MFC piezoelectric material patches, as shown in Figure 5-1 (a) and (b). The MFC8514-P2 and MFC8514-P1 transducers (Smart

Material Corporation) were installed at 65 mm from the fixed end of the beam. The piezoelectric patches were bonded to the aluminium beam by a standard epoxy adhesive and assumed to be perfectly bonded to the host structure. According to the manufacturer's datasheet, the bonded assembly requires 24 hours of cure time at room temperature (approximately 23°C) to achieve handling strength after application of the epoxy adhesive. The surface of the MFC layers was coated with a copper electrode, and the electric field was poled along the thickness direction of the energy harvester.



(a) Macro Fiber Composite piezoelectric material prior to being bonded to the beam



(b) MFC bonded to the aluminium beam

Figure 5-1 Unmorphed MFC-P2 sample prepared for experimental testing

Figure 5-2 Presents the schematic diagram and the experimental the setup used in the laboratory experiments. The diagram illustrates the entire signal pathway. The function generator excites the MFC-$P1$ patch, resulting in the beam flexing through the piezoelectric d33 effect. The flexing of the beam induces a strain in the MFC-P2 patch, which produces a voltage across the load resistor through the d_{31} effect. This voltage signal is also simultaneously recorded by the oscilloscope, multimeter and DAQ; recorded in LabVIEW; and then processed in MATLAB to generate the voltage and power vs frequency plots used in your results chapter. The setup consists mainly of an aluminium cantilever beam with an MFC piezoelectric patch bonded on it, a signal generator, and a data acquisition unit. The MFC is composed of piezoelectric ceramic fibres, epoxy resin, electrodes, and organic binder. The MFC piezoelectric material was bonded to the aluminium cantilever beam at 65 mm from the clamped end of the fixed fixture.

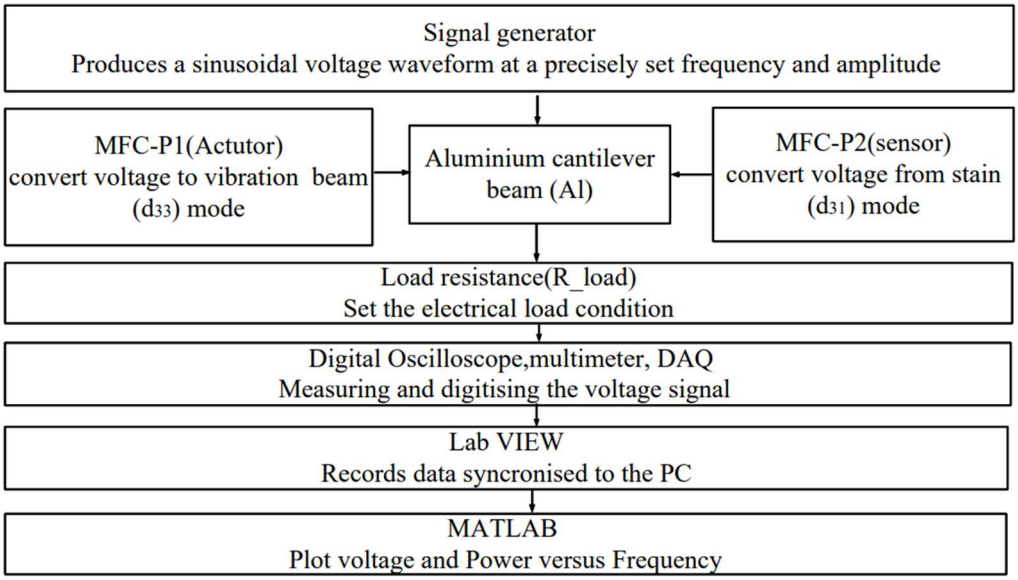


Figure 5-2 Schematic model of the experiment for validation

Again, from the Figure 5-2 the data acquisition system for measuring the electrical output of the MFC piezoelectric energy harvester comprised an NI cDAQ-9191 Compact DAQ chassis and an NI-9215 analogue input module . The NI-9215 contains four differential analogue input channels with a ±10 V range, 16-bit resolution, and a maximum sampling rate of 100 kS/s per channel. It allows for simultaneous sampling so you can take synchronous voltage measurements at multiple points. The cDAQ-9191 is a single-slot chassis that manages timing, synchronisation and data transfer between the C Series module and the host computer over Ethernet or IEEE 802.11 Wi-Fi. In theses , the voltage signals generated by MFC were collected by the NI-9215 and transmitted to the computer through the cDAQ-9191 for processing and analysis. The data collected were used to calculate the output voltage, the frequency response and the electrical power delivered to the external load.

Table 5-1 The physical dimensions, geometric characteristics, and material properties

Category	Property	Symbol/unit	Substrate (aluminium beam)	Piezoelectric materials (MFC (M8514-P2))
Geometry	Length	L [mm]	400	85
	Width	b [mm]	30	14
	Thickness	h [mm]	2	0.38
	Placement (from clamp)	x [mm]	–	65 (cantered on width)
Mechanical property	Density	ρ [kg/m^3]	2700 (Al 6061)	5400
	Young's modulus	E [GPa]	69	15–30 (effective, along fiber)
	Poisson's ratio	ν [-]	0.33	~0.3
	Bending stiffness	EI [N·m^2]	E b h^3 / 12	included in FE patch stiffness
Piezoelectric	Coupling mode	–	–	d_{31} mode (polarised along z, strain along x)
	Piezoelectric constant	d_{31} [pm/V]	–	2.1×10^{-10}
	Permittivity ($\varepsilon_{33}^{T}/\varepsilon_0$)	–	–	1700
	Dielectric constant	ε_{33}^{T} [F/m]	–	1.5×10^{-8}
	Capacitance	Cp [nF]	–	120–160 (at 1 kHz, 1 Vrms)
	Electromechanical coupling coefficient	$K3_1$	–	0.35–0.4
Electrical	Resistance load (varied)	RL [kΩ]	–	12 kΩ
	Max operating voltage	Vmax [V]	–	±1500 V (blocking), ±360 V (operating)
Environmental	Operating temperature	[°C]	–	25
	Adhesive (epoxy layer) thickness added to MFC	[mm]	Very small 0.05	–

The material properties and geometric configuration are important for the analysis of the energy harvesting capability of cantilevered piezoelectric unimorph beams. The material properties and their dimensions were provided in Table 5-1.

5.2. Description of experimental procedures and system identification

The MFC-based piezoelectric vibration energy harvester was experimentally validated using a unimorph aluminium cantilever beam with a Macro Fibre Composite; both MFC-P2 and MFC-P1 were patch-bonded near the fixed end of the beam. The MFC patch in the experimental setup is used as an vibration actuator to excite the beam to simulate the ambient mechanical vibration and as a sensor to measure the electrical output due to the direct piezoelectric effect, as shown in Figure 52. The experimental setup was used to measure the voltage produced by the MFC-P2 patch in response to an actuation voltage applied to the MFC-P1, which was used to vibrate the beam configuration. The voltage generated by the MFC transducer was acquired using an NI-9215 analogy input module installed in an NI cDAQ-9191 Compact DAQ chassis and recorded through LabVIEW software. The output Power was then calculated from the measured voltage with the resistive load.

An actuation voltage was applied to the MFC-P1 to generate transverse vibrations in the beam. In addition, the MFC can serve as a highly sensitive strain sensor, capable of detecting deformation, noise, and vibration, as well as harvesting energy from these sources. The M8514-P2 piezoelectric transducer was attached to the right side of the substrate, while the M8514-P1 transducer was bonded to the left side to excite the beam. The P2-type transducer works in the d_{31} mode; using the piezoelectric strain constant d_{31} as a basis, the device was designed and manufactured with electrodes of identical polarity on both sides of the piezoelectric fiber layer and was poled through its thickness [23,179]. In contrast, the P1-type MFC exploits the d_{33} piezoelectric effect as an actuator to produce harmonic excitation in the aluminium beam coated with piezoelectric material, with the resulting vibration amplitude controlled by adjusting the voltage applied to the actuator. The selection of the $P1$-type MFC as the vibration actuator was based on the following considerations: (1) Its d_{33} coefficient is greater than d_{31}; (2) its operating voltage range of −500 V to +1500 V makes it well suited to actuation, whereas the P_2-type is limited to a range of −60 V to +360 V; and (3) the interdigitated electrode configuration used in the P_1-type MFC limits the achievable current, reducing its suitability for energy harvesting applications [14,23] . The beam's vibration amplitude could therefore be tuned by varying the voltage applied to the MFC-P1 as vibration actuator.

A resistor was connected through the MFC-P2 patch to measure the output voltage, which was acquired using high-precision NI data acquisition modules (DAQ). The $NI\ DAQ$ system was connected to a PC, and all data was recorded using LabVIEW software to capture both the output voltage and the beam displacement. The DAQ system had an output range of ±10 V and

an output current drive of ±5 mA, and it recorded voltage signals in the time domain synchronised with the excitation frequency. LabVIEW software was used to drive the beam near its resonance frequency and to perform a series of frequency sweeps from 7 to 15 Hz, in increments of 0.5 Hz. During testing, the excitation amplitude was manually adjusted using the power amplifier control until the maximum beam vibration amplitude was achieved. The voltage output generated by the MFC sheets was recorded using a digital multimeter, while the mechanical vibration response was measured across a 10 kΩ resistive load. The output sinusoidal voltage waveform was also recorded using a digital oscilloscope, from which the output power was calculated. Finally, the voltage and power output of the energy-harvesting device, as functions of frequency, were plotted using MATLAB software [23].



1. wave form generator
2.Digital Oscilloscope
3. High-Voltage Amplifier
4. Digital Multimeter
5. NI cDAQ-9191
6. MFC with beam
7. Computer with LabVIEW

Figure 5-3 The overall experimental setup for MFC vibration energy harvester

In the case of a cantilever-type piezoelectric energy harvester (PEH), the voltage output and strain of the MFC were measured, and the corresponding output power was calculated. The first step was to conduct experimental tests to validate the mathematical model that estimates the electrical power output by measuring the voltage at different excitation frequencies and load resistances. An important parameter of the energy harvester beam is the first natural frequency because it shows the frequency band in which the experiment was conducted and the maximum

energy can be extracted. Dynamic characteristics of the system were obtained by measuring the frequency response functions of the system by applying an actuation voltage to the MFC-P1 patch, as shown in the experimental setup in Figure 5-3.

The natural frequency of the unimorph MFC-P2 energy harvester was measured to be approximately 10.2 Hz. In the experiment, a harmonic actuation voltage was applied to the MFC-P1 vibration actuator, as summarised in Table 5-2, while the harvested voltage from the MFC-P2 patch was measured across the connected load resistance. The vibration amplitude of the beam was found to be maximum at this frequency of approximately 10.2 Hz, confirming it as the system's resonance frequency. The natural frequencies obtained from the analytical, numerical, and experimental approaches were found to be in close agreement, with a maximum difference of 5.4% between the experimental results and the theoretical and numerical models. This discrepancy can be attributed to experimental uncertainties and to simplifying assumptions inherent in the theoretical and numerical models. The device's electrical performance was characterised by using two key parameters: output voltage and generated power. The output voltage was measured directly across the load resistor. After data acquisition using LabVIEW, the recorded voltage signals were post-processed in MATLAB, where they were transformed from the time domain to the frequency domain using the Fast Fourier Transform (FFT). Voltage–frequency response functions were subsequently generated using MATLAB's plotting routines. Figure 5-4 presents a representative frequency response function of the recorded voltage signal, showing a pronounced peak corresponding to the first bending mode at a resonance frequency of 10.2 Hz. Because multiple datasets were acquired across different excitation frequency ranges and at different measurements, a comparative analysis was conducted to identify the dataset that most accurately represented the system's natural frequency. The voltage obtained from the harvester corresponds to a condition of constant acceleration amplitude maintained across the entire frequency range. The output voltage, denoted V, was measured across an electrical load resistance $R\mathrm{Load}$ while the system was excited at its resonance frequency under a constant vibration amplitude.

5.3 Result and discussion of experimental model

This section presents the results of the experiment divided into three subsections. In the first subsection, an initial estimation of the experimental voltage output is performed. The following two subsections study the variation of output power with the magnitude and frequency of excitation and compare the experimental results with theoretical and numerical models. In the experimental setup described in the previous section, the voltage output response of the MFC

integrated with the cantilever beam was recorded for different input frequencies by applying an actuation voltage to the MFC-P1 patch and measuring the output voltage via the MFC-P2 patch. The output voltage of the energy harvesting device was measured over a range of excitation frequencies. This was then used to determine the mean output power using Equation (5.1), based on the peak voltage measured across the load resistor, as summarised in Table 5-2 .

$$p_{ave} = \frac{{V_R}^2}{2R}, \tag{5.1}$$

Where P_{ave}. denotes the power output, R represents the load resistance, and V_R. is the output voltage amplitude (peak voltage) of the energy harvesting device measured across the load resistor. As can be seen from the Table 5-2, the output power decreases gradually with the increase of the frequency difference from the resonant frequency, even if the frequency difference is relatively small.

Table 5-2 Voltage and output power from experiments with frequencies

No.	Frequency (Hz)	Measured Voltage (V)	Calculated Power (mW)
1	7	0.0105	2.72094e-04
2	7.5	0.0362	0.00035
3	8	0.078	0.000709584
4	8.5	0.1201	0.001205
5	9	0.162	0.0016219
6	9.5	0.208	0.002078
7	10	0.21345	0.0023128
8	10.5	0.2450	0.002720
9	11	0.19567	0.002045
10	11.5	0.16406	0.001804
11	12	0.12801	0.00148
12	12.5	0.10306	0.001162
13	13	0.0751	0.000852
14	13.5	0.0508	0.000532
15	14	0.0261	0.000376
16	14.5	0.0092	0.0001627
17	15	0.00343	0.0000852

The output voltage when the beam was excited from 7 Hz to 15 Hz with a constant MFC-P1 actuation voltage and a load resistor of 10 kΩ in series is shown in Figure 5-4. The voltage

increases smoothly from approximately 0.012 V at 7 Hz to a maximum of 0.245 V at around 10.2 Hz, which is essentially the fundamental natural frequency of the cantilever (10.165 Hz), and then decreases, following the classical bell-shaped resonance curve. This peak corresponds to the maximum mechanical strain in the piezoelectric layer and the maximum charge generated by the direct piezoelectric effect. This frequency-dependent behaviour of the experimental voltage closely tracked what the theoretical and numerical models had predicted, with all three approaches converging on very similar voltage values.

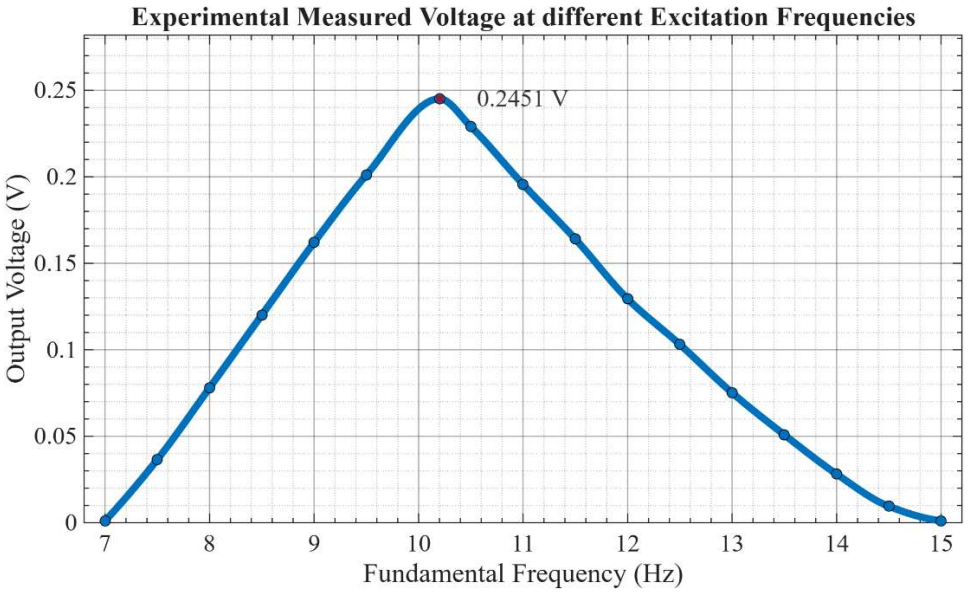


Figure 5-4 Experimental voltage versus frequency response at constant resistance load

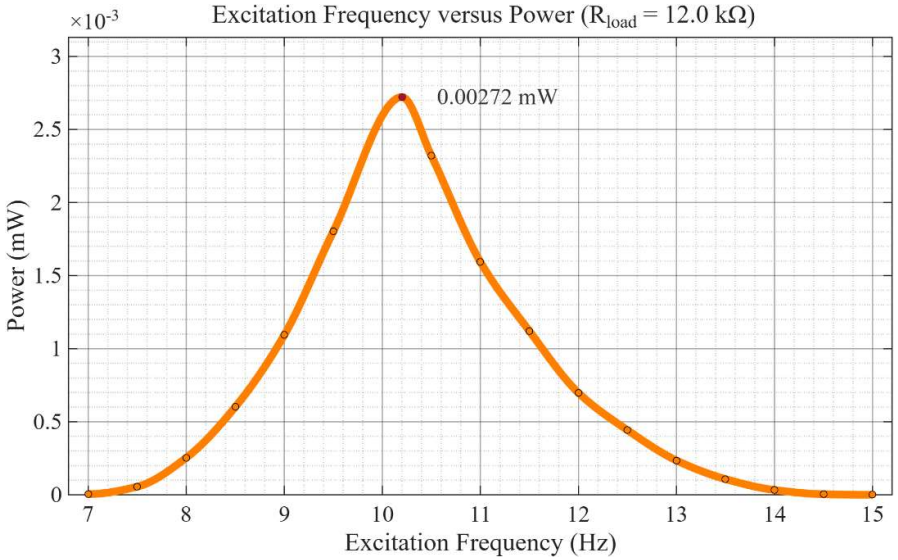


Figure 5-5 The experimental frequency responses vs power harvester with a load resistor

From the measured voltage, the electrical power output derived from the MFC piezoelectric structure was calculated using the mathematical model outlined in Equation 5.1. The resonance

frequency of the cantilever harvester determines both the peak power and the highest open-circuit voltage, resulting in the harvester's output reaching its maximum at this frequency. When power output is graphed against excitation frequency in Figure 5-5the peak power is approximately 2.720 μW, observed at the fundamental frequency of the energy-harvesting structure with a 10 kΩ resistive load attached.

5.4. Comparison of the theoretical, FEM and experimental model

The numerical solution is first validated by comparing the calculated voltage and fundamental frequency for a rectangular uniform beam. As discussed in the previous chapter, both the mathematical and FEM models of the energy harvester were validated. In this chapter, the focus shifts to validating the experimental results against the theoretical and numerical predictions, comparing the resonance frequency, voltage, and harvested power of the unimorph piezoelectric energy harvester. This validation is limited to the first resonance mode since the higher modes not only lie far from the fundamental frequency but also generate considerably lower power output. Piezoelectric energy harvesters are generally designed to operate near the fundamental frequency of the mechanical structure and are rarely intended for high-mode operation, as at higher modes positive and negative charges are generated simultaneously and tend to cancel each other out. The measured deflection of the cantilever beam at 0.4 m from the clamped end, with the MFC transducer integrated, was 6.57 mm. By comparison, the analytical model predicted a deflection of 6.75 mm, and the numerical simulation predicted 6.4 mm. While a discrepancy of this size might normally seem significant, given how small the absolute deflections are, a difference of around 0.5 mm is considered acceptable. In the experiment, the maximum voltage output occurred at approximately 10.2 Hz, compared with 10.693 Hz and 10.976 Hz for the theoretical and numerical models, respectively, as shown in Table 6-3.

The resonance frequencies predicted by the simulation and theoretical model were close to one another, differing by only 6.9%. As shown in Figure 5-6 presents , the theoretical, numerical, and experimental voltages were approximately 0.265 V, 0.281 V, and 0.249 V, respectively, corresponding to a percentage error of around 3.74%. Similarly, Table 5-4 and Figure 5-7 show that all three models predicted a power output of approximately 0.0032 mW a result that is promising for potential broadband energy-harvesting applications. Overall, the resonance (natural) frequency obtained experimentally showed reasonably good agreement with both the mathematical and numerical models, and the displacement results followed the same pattern. In Figure 5.7, the maximum power output as a function of frequency was also determined using all three methods, applying the optimal load resistance in each case. The three

sets of results were found to be broadly consistent with one another, both in resonance frequency and in magnitude.

Table 5-3 The comparison of the 1st natural frequencies of the model.

Type of model	First natura frequency (Hz)
Experimental	9.159≅10.2
Theoretical	≅ 10.69
Numerical	≅10.976

Table 5-4 Comparison of EHM for the theoretical, numerical, and experimental

S. No	Experimental model			Theoretical model			Numerical model
	Excitation Frequency (Hz)	Voltage (V)	Power (mW)	Voltage (V)	Power (mW)	Voltage (V)	Power (mW)
1	7	0.0105	2.72094e-04	0.05902	2.42E-4	0.05902	1.41E-04
2	7.5	0.0362	0.00035	0.07260	4.38E-4	0.0726	2.14E-04
3	8	0.078	0.000709584	0.08430	7.44E-4	0.0843	2.89E-04
4	8.5	0.1201	0.001205	0.108	1.08E-3	0.0990	4.73E-04
5	9	0.162	0.0016219	0.12966	1.63E-3	0.12966	6.83E-04
6	9.5	0.208	0.002678	0.16821	2.25E-3	0.15821	1.25E-03
7	10	0.21345	0.003128	0.21601	2.7E-3	0.21601	1.89E-03
8	10.5	0.24503	0.002715	0.26522	2.91E-3	0.26422	2.94E-03
9	11	0.19567	0.002345	0.24640	2.05E-3	0.27894	0.003196
10	11.5	0.16406	0.001804	0.20887	1.52E-3	0.21950	0.002356
11	12	0.12801	0.00148	0.15723	9.47E-4	0.18446	0.001581
12	12.5	0.10306	0.001162	0.12857	6.8E-4	0.15723	8.50E-04
13	13	0.0751	0.000852	0.12857	4.7E-4	0.12557	6.40E-04
14	13.5	0.0508	0.000532	0.11074	3.59E-4	0.11074	4.98E-04
15	14	0.0261	0.000376	0.09401	2.83E-4	0.09401	3.59E-04
16	14.5	0.0092	0.0001627	0.08242	2.23E-4	0.08542	2.96E-04
17	15	0.00343	0.0000852	0.06831	2.05E-4	0.07831	2.30E-04

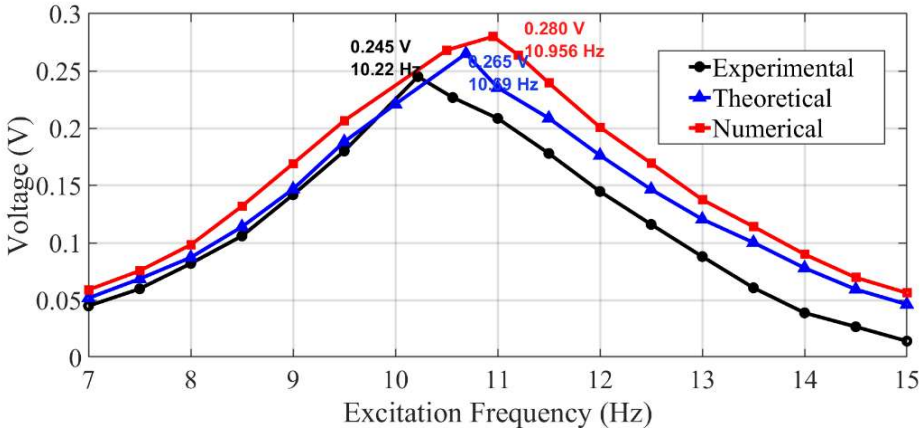


Figure 5-6. Experimental, theoretical, and numerical voltage with frequency

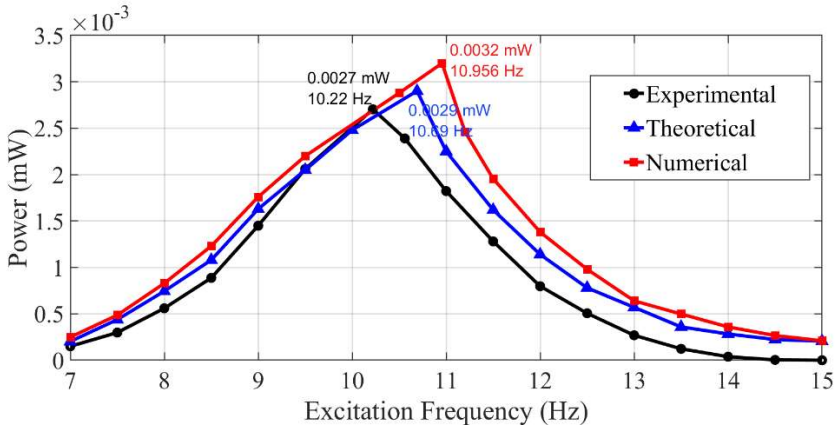


Figure 5-7 Comparison of power for experimental, theoretical, and numerical model

The RMSE was computed for the main response characteristics discussed in this chapter, providing a quantitative measure of agreement across the entire frequency range rather than comparing individual peak values. The relatively low error values confirm strong consistency between the experimental measurements and the analytical and finite element results. However, the remaining differences can be attributed to measurement uncertainty, variations in material properties, imperfect bonding between the MFC and the aluminium beam, damping assumptions, and deviations from the idealised boundary conditions used in the analytical and numerical models. Despite some discrepancies in resonance frequency, voltage magnitude, and power output between the three datasets, the mathematical, FEM, and experimental models were found to be generally consistent in predicting the energy-harvesting performance of the piezoelectric cantilever beam. All three approaches proved effective for modelling piezoelectric energy harvesting; however, FEA simulation stands out as the more robust method, particularly for modelling more complex structures, such as those with varying geometric cross-sections.

Chapter five conclusion

The experimental setup included a signal/function generator, which generated a sinusoidal excitation signal to actuate the MFC patch and induce vibration in the cantilever beam; a digital oscilloscope, which was used to display and measure the time-domain voltage response of the harvester in real time; a digital multimeter, which was used to take accurate voltage and/or current measurements across the load resistor to quantitatively determine the harvested electrical power; and a National Instruments (NI) Data Acquisition (DAQ) module, which was used to connect the sensor output to a computer for synchronised, high-resolution digital recording of the voltage signal for subsequent post-processing and analysis.

Table 5-5 Comparison of voltage and power at fundamental frequency for all model

Model	Frequency (Hz)	Generated voltage (V)	Power (mW)
Theoretical model	10.69	0.265	0.00291
FEM	10.976	0.28	0.0032
Experimental	10.2	0.245	0.00272

Table 5-5 compares the theoretical, simulation and experimental results of the responses of the MFC piezoelectric unimorph beam. The theoretical modelling was based on coupled electromechanical equations and analysis of a unimorph cantilever beam using Euler-Bernoulli beam theory. The resulting natural frequency, voltage and power output were then verified by finite element analysis in COMSOL Multiphysics and experimentally. The fundamental frequency (first modal frequency) from theoretical, simulation and experimental analysis were 10.69 Hz, 10.956 Hz and 10.2 Hz, respectively. Good agreement was found among all three methods. The measured open circuit voltage of the Macro Fibre Composite cantilever beam device, at fundamental frequency, with a point force of 0.5 N, was 0.265 V. The theoretical model was calculated with a load resistance of 10 kΩ, which gave a peak power of 0.00291 mW. The FEM simulation provides a resonance frequency of 10.956 Hz with a voltage output of 0.28 V and a power output of 0.0032 mW. The experimental results at a resonance frequency of 10.2 Hz give a voltage output of 0.245 V and a power output of 0.00272 mW. These results are in good agreement with the theoretical and numerical ones. In general, the results indicated that the resonance frequency, voltage, and power output were consistent for all three methods under the applied load resistances. The small differences, especially the slightly lower experimental values, were due to effects such as damping, losses in the bonding layer between the MFC patch and the beam, fabrication tolerances and other experimental uncertainties that

were not fully accounted for in the idealised analytical and numerical models. This consistency between theoretical, numerical, and experimental approaches confirms the validity and reliability of the developed modelling methodology for predicting the performance of MFC-based piezoelectric vibration energy harvesters.

Chapter 6 Parametric optimisation of piezoelectric harvesters

This chapter models and simulates key parameters to maximize the efficiency of energy output from mechanical vibrational energy harvesters. It focuses on geometrical parameters (mechanical parameter optimization), MFC patch location (x_p), and tip mass(t_m), which influence the mode shape, frequency, voltage, and power output of the energy harvester.

Another goal of this thesis is to optimize the efficiency of piezoelectric energy harvesting using cantilever beams with various geometries. It is essential to optimize the substrate's geometric configuration, the placement of the PEM, and the dimensions of the tip mass to mechanically affect the system through resonant frequency and electrically through voltage and power. To improve the efficiency, a model is needed to analyse mode shapes and the frequency domain, which are critical. Cantilever beams with different structural geometries and MFC placements are simulated using finite element software to determine natural frequencies, vibration modes, and output voltages of PEH. These simulations involve the cantilever beam as a deformed structure under an external dynamic vibration force. The advancement of self-powered and wireless electronic devices has increased interest in energy harvesting. To power small electronic devices, energy can be harvested from ambient sources using piezoelectric energy harvesting (PEH) materials, enabling a self-sustaining electronic system. This innovative research concept, increasing performance efficiency, has attracted significant research attention [15,193].

6.1. Improving the efficiency of the piezoelectric energy harvesting systems

The main goal is geometric optimisation, during which the system vibrates around the first resonance frequency region to maximise electrical power generated by the system. To improve power output efficiency, structural configuration is a major factor that influences the efficiency of piezoelectric energy harvesting. Under this section, the effect of each geometric optimisation variable on both the voltage amplitude and power is analysed separately. The optimised geometric parameters of the MFC were determined using finite element analysis software, which is COMSOL Multiphysics software, to estimate the output voltage and power of the MFC harvester [100,194].

Classical piezoceramic materials, such as lead zirconate titanate (PZT), are recognised for their strong electromechanical coupling. However, they have drawbacks of brittleness and limited flexibility, making them less suitable for applications on lightweight or curved surfaces. In PEHs, the properties of piezoelectric materials are crucial and influential factors that can

enhance their output capability. The maximum power output depends on the maximum permissible stress of the materials, the geometric configuration, and the working frequency of the device. [53,148]. The direct piezoelectric effect is the ability of piezoelectric substances to generate an electric potential under mechanical stimuli and external vibrations. But the rate range and magnitude of force of environmental vibration sources are usually below the operational mode of a PEH system. Furthermore, most of the literature on vibration-based power generation of PEH devices is limited by the input energy sources, their output performance, and operation bandwidth [195–197].

Among the various MFC types, the M8514-P2 variant has garnered significant attention due to its optimised performance when subjected to transverse vibration. It's polarized along the 3-axis and engineered to generate strain along the 1-axis, which maximizes energy conversion through the d_{31} coupling mechanism. The composite structure consists of MFC, which is about 60% piezoceramic fibers and 40% epoxy, striking a balance between flexibility, mechanical strength, and electromechanical efficiency. Piezoelectric transversely oriented piezoelectric fibers in an epoxy matrix are developed as a means for large-scale structural actuation and sensing, as well as for energy harvesting [40,198].

One of the challenges for piezoelectric energy harvesting is that they generate low power at the off-resonant frequency, especially for low frequencies. The design and optimization of a vibration-based piezoelectric energy harvester is the first step in envisioning a self-healing energy harvester capable of returning function and increasing efficiency of power generation [131,193]. In this chapter, the performance efficiency of the piezoelectric energy harvester and the optimum working conditions are determined to optimize the electrical voltage and power output. Piezoelectric energy harvesting, enhancing efficiency, requires multilevel approaches such as geometric configuration, resonance frequency, and electrical boundary conditions to make energy conversion more effective [23]. Shape optimization, or geometry modification, is an effective approach because it can enhance the deflection of the free end of the cantilever beam by using diverging beams, resulting in a uniform strain distribution along the beam's length and higher power extraction [199]. Optimization of these parameters is essential for enhancing energy conversion efficiency and ensuring system reliability [77,115]. While several analytical and numerical models have been proposed to predict the electromechanical response of MFC-integrated structures, finite element modelling (FEM) remains the most powerful tool for accurately capturing the coupled dynamic and electrical behaviour [28,200]. FEM provides insights into strain distribution, modal characteristics, and voltage generation under various

excitation and boundary conditions. For the parametric study of the optimal configuration, a finite element analysis (FEA) model is established to estimate the resonance frequency, output voltage, and power of the MFC harvester.

This optimization-based finite element simulation of an M8514-P2 Composite piezoelectric transducer integrated within an aluminium cantilever beam. An aluminium substrate is selected due to its high stiffness and low mass density compared to steel. The key parameter to examine is how design parameters such as the geometry of the beam, patch placement, and tip mass affect the output voltage and harvested power. The analytical and computational findings are compared to validate the model and identify optimal configurations for maximum energy extraction. The outcomes aim to support the development of efficient, dependable, and structurally adaptive MFC-based energy harvesters capable of powering low-power sensing and monitoring devices. In general, the resonant frequency, the shape of the beam, the resistivity load, and the shape of the proof mass affect the voltage and power of the PE vibration energy harvesting. The output power also depends on the overall stress distribution on the beam or the piezoelectric layer. As output power is directly proportional to the amount of stress exerted, the geometry that allows maximum stress within the fracture limit gives the maximum output power [201]. For geometrical optimization, the width, thickness, beam shape, and free end tip mass can be the important parameters to increase the vibration amplitude and to improve the strain-induced energy output [23,109,202]. Here, only the geometric shape, adding tip mass, patch placement of MFC on the beam, and thickness are considered for optimization.

6.1.1 Geometric parametric optimization

Modifying the geometric shape of harvesting substrate materials is one of the effective ways to increase efficiency. This method alters the internal strain distribution along the beam length and shifts the resonance frequency to the ambient vibration. This optimization method is the cornerstone of piezoelectric energy harvesting because these systems are highly tuned resonators. According to the uniform-strength criterion, a rectangular cantilever beam carries its highest stress at the fixed end, with that stress dropping linearly to zero at the free tip. In contrast, a tapered cantilever beam is shaped so that stress stays essentially uniform along its entire length [203,204]. Rectangular Cantilever beam with piezoelectric energy harvesters currently faces the issue of low energy conversion efficiency, which can be increased by altering their shape and structure [50]. The best-known optimization method is to vary the harvester geometry to improve the energy harvesting efficiency of PEHs. The rectangular cantilever beam geometric configuration is most frequently employed in the design of piezoelectric energy

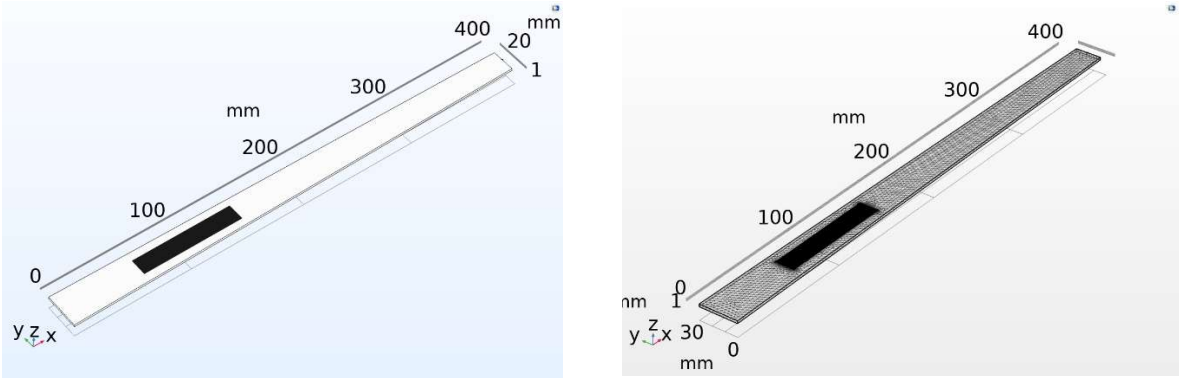
harvesting devices. However, the power output from a rectangular cantilevered beam integrated with MFC piezoelectric materials is limited by significant stress concentration at the fixed end and non-uniform strain distribution and relatively low energy efficiency, which can be improved by modifying its shape and structure [50]. Another method for rectangular and tapered unimorph cantilever beam with and without proof mass is designed using COMSOL by having aluminium as a substrate energy harvester and MFC-*P*2 as a piezoelectric material of 0.38mm thickness.

Compared to a rectangular cantilever beam, a tapered cantilevered (TC) beam with a larger clamped end and smaller free tip produces a higher strain distribution in the first mode, which can significantly increase the power output. Tapered geometry increases the strain distribution throughout the beam, increasing by more than 50% the output power per unit volume. For a rectangular beam carrying a mass at its free end, the mass generates the highest bending moment at the fixed support. As a result, the base of the beam experiences a strong concentration of stress, while the stress near the free end is minimal [109,202,205,206]. In the configuration of a tapered beam instead of a uniform rectangular beam, perfect bonding is performed such that there is no slip between the piezoceramic layers and the substrate layer. The power output of a cantilever beam is directly related to its shape. A piezoelectric MFC of length L_p is attached to the top surface of the tapered beam near the fixed end. The maximum voltage and power are generated from the energy harvester when the beam is made to vibrate at resonance with its fundamental natural frequency. It was designed and simulated using the finite element method, based on the direct piezoelectric effect, which includes electrostatic physics and mechanical physics. In this study, an aluminium tapered cantilever beam was used as a substrate, and MFC (Smart Materials Corp., model: M8514-P2) was used as the piezoelectric material.

Figure 6-1 shows the configuration. One end of the model is fixed as a boundary condition, and the other end is free to vibrate. External force is applied to the free end of the cantilever beam. The electrostatic boundary conditions were defined as the top surface of the piezoelectric layer as ground and the bottom surface (interface between the electrode and MFC) as the terminal voltage. The electrical response was obtained by coupling the electrostatics and electrical circuit physics interfaces.[142]. The simulation was conducted using COMSOL Multiphysics 6.3 with a medium mesh size to balance computational efficiency and accuracy in capturing key features like stress distribution and displacement in the cantilever beam. Then, for meshing, a tetrahedral mesh with an appropriate element size was used to discretize the model. Finally, a frequency domain analysis was performed on the piezoelectric harvester to

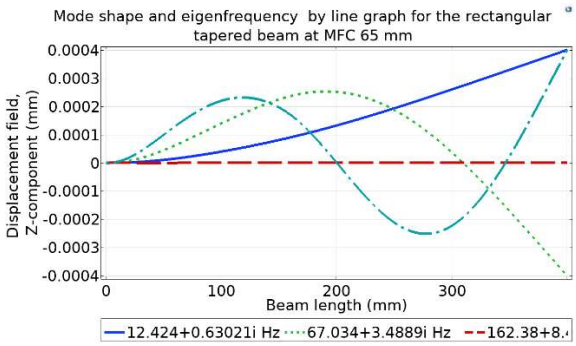
obtain output voltage and power. Figure 6-2 (a) and (b) show the natural frequency and mode shape for a tapered cantilever beam. The first mode occurs at 12.42 Hz, followed by frequencies of 67.034, 162.38, and 187.17 Hz, respectively. Due to the uniform strain produced over the surface of the beam by the tapered section, the fundamental natural frequency of the tapered rectangle was increased from 10.976 Hz to 12.42Hz as the width of the beam was decreased from 30 mm to 20 mm compared to a conventional rectangular beam.

From Figure 6-3 (a), the results from the simulation show that the free end of the tapered beam-shaped harvester was simulated and reached a maximum displacement of 8 mm at a fundamental resonance frequency of 12.42 Hz. The frequency is affected by the position and geometry (i.e., same volume but different shape). Figure 6-3 (b), A voltage output of about 0.45 V was achieved from the simulated harvester with a rectangular tapered beam, while 0.28 V was obtained from the conventional rectangular cantilever energy harvester. Therefore, the rectangular tapered beam demonstrated a higher voltage conversion efficiency of 37.78% than the normal rectangular beam. As shown in Figure 6-3 (c), shows the output power increased from 0.003 to 0.0065 mW, corresponding to an increase of about 53.85% compared with the rectangular beam design. The convergent tapered cantilevered beam designs with partial coverage of the MFC piezoelectric layer can generate a higher electromechanical coupling coefficient than conventional rectangular cantilevered designs. The rectangular tapered beam produces more than twice the output power of the rectangular beam, as the strain can be more evenly distributed throughout the structure.

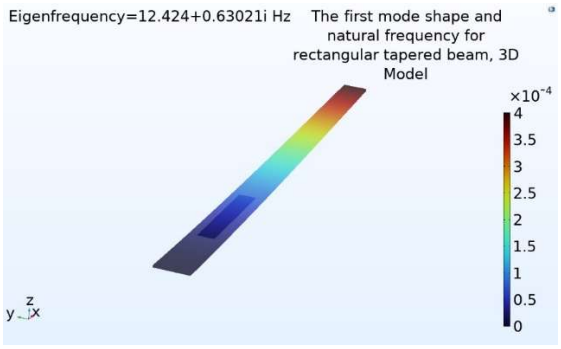


(a) Rectangular tapered beam geometric shape (b) Free tetrahedral mesh

Figure 6-1 Schematic of a tapered beam with unimorph MFC energy harvester geometry

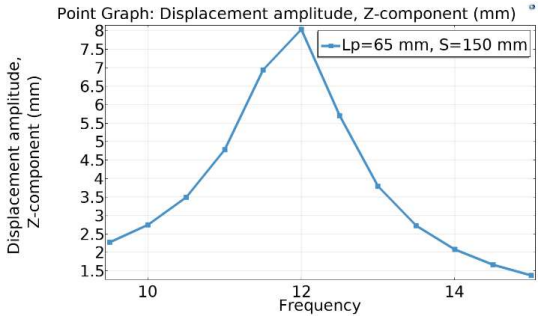


(a) Mode shape and eigen frequency

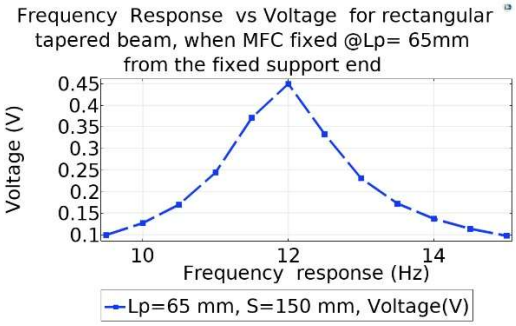


(b) Model bending mode shape and eigen

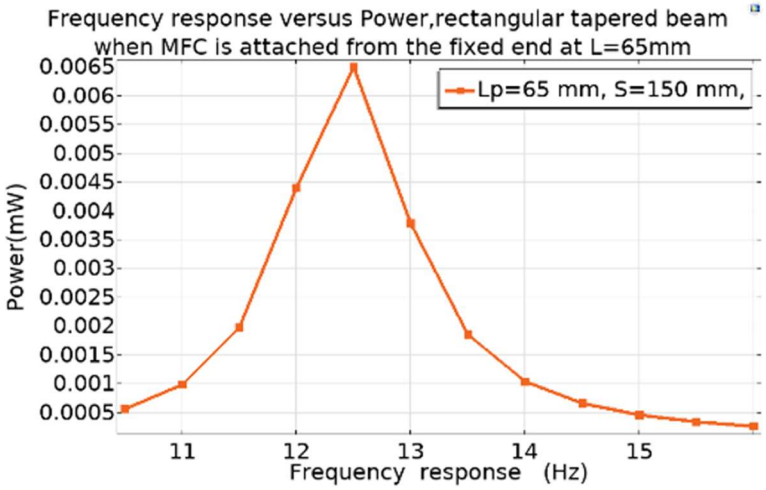
Figure 6-2 Mode shape and eigenfrequency and 3D Model for tapered beam EH



(a) Displacement versus resonance frequency



(b) Output voltage versus frequency



(c) Frequency versus Power with MFC

Figure 6-3 The FE simulation of the MFC with the tapered beam

6.1.2 The effect of adding tip mass at the free end of the energy harvester

Typically, a cantilever-type piezoelectric energy harvester is attached with a separate tip (proof) mass at its free end for two reasons. Since most environmental and structural vibration sources of interest are below 5-100 Hz [207,208], it first lowers the fundamental natural frequency of the harvester without the need to make the beam itself longer or more compliant. This enables the tuning of the device to match the low frequency ambient vibration sources, which is a typical requirement in practical energy harvesting applications. Second, when the harvester is operating at resonance, tip mass addition often increases the harvested voltage and power for a given input acceleration as the added inertia increases the bending curvature (and strain) of the piezoelectric layer under base excitation [208–211].

6.1.2.1 Tip mass with rectangular beam

The most important improvement of energy harvesting efficiency can be achieved by the energy harvesting geometry structure, and the second method is using an optimized energy harvesting circuit. Energy harvesters generally consist of a substrate and a piezoelectric material bonded to it and produce electrical energy by converting the applied mechanical energy. To select a cantilever beam design with a wide variety of cantilever beam shapes, while the beam is partially coated with the piezoelectric material to maximize the power output capacity of the harvester [1,138]. Under this section, the optimization was done by numerical simulation using the COMSOL Multiphysics software, understanding the effects of geometric parameters on performance. The system was modelled and parameterized as a unimorph cantilever beam piezoelectric energy harvester, consisting of a substrate structure (aluminium), piezoelectric material (PZT-5A) with epoxy resin material, and a rectangular tip mass made from tungsten material attached to the free end of the substrate, as shown in Figure 6-4.

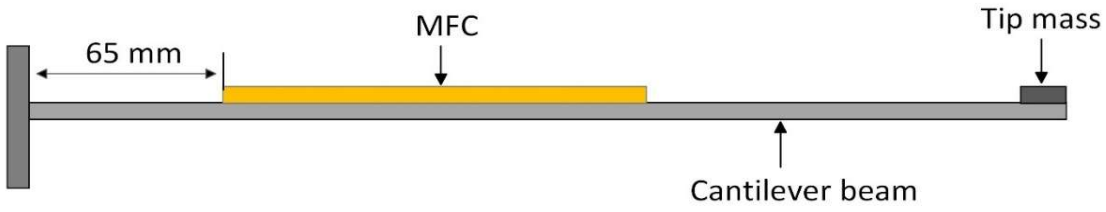


Figure 6-4 A schematic representation of EH integrated with a tip mass

The portion of the aluminium beam with the patch of MFC will be referred to as the composite section during operation, and the MFC patch undergoes axial deformation in the longitudinal x-direction. The patch is bonded to the substrate using epoxy adhesive is used for

bonding the MFC to the substrate. The top surface of the piezoelectric material was assigned as the terminal surface, and the bottom of the lower piezoelectric material was assigned as the ground. The cantilever structure with a proof mass was primarily examined because this design can produce greater strain and can be readily tuned to oscillate at low frequencies, which typically range from 5 to 200 Hz [8].In Figure 6-4 the tip mass is bonded to the top of the free end of a rectangular cantilever beam to tune the natural frequency. Adding the tip mass modifies it and is likely to have some influence on the natural frequency, mode shape, and strain acting in the structure compared to the beam without tip mass. Hence, the resonance frequency can be decreased by adding a mass at the free end of the cantilever, which is easier to achieve, and hence, the output power will increase. A resistor is connected across the MFC to measure the output voltage. A piezoelectric material 85mm in length, 30 mm in width, and 0.38 mm in thickness, was attached at 65mm from the fixed end of the cantilever beam [28,100].Table 6-1 Mechanical properties of the tip mass and its dimensions. The tip mass is made up of tungsten metal, having a size of 5 mm x 30 mm x 2 mm, and is fixed at 395 mm from the fixed support of the cantilever beam. The density of tungsten is $19.3\,\frac{\mathrm{g}}{\mathrm{cm}^3}$. The mass of the tip mass is 2.89 grams. A larger tip mass is beneficial for performance; however, this statement is inaccurate due to significant changes in fundamental frequency between designs.

Table 6-1 Mechanical properties of the tip mass and its dimensions

Parameter	Value
Material	Tungsten
Length (mm)	5
Width (mm)	30
Thickness (mm)	1
Volume (mm^3)	1.5×10^{-7}
Density of tip mass ($\frac{g}{mm^3}$)	1.925×10^{-5}
Mass (g)	2.89

Tip masses are essential in micro-scale devices to decrease the reducing the fundamental frequency and increase the strain along the beam to increase both the voltage output and power output [131,212].

Figure 6-4 shows that adding tip mass (tip mass) at the free end of the cantilever beam reduces natural frequency (f_n) and crucially increases the strain near the clamped end, increases the voltage and the power output where MFC is located, which eventually affects the VEH

performance. In resonant frequency tuning methods, the resonant frequency of the harvester is matched with the excitation frequency to achieve dynamic flexibility and higher power output. Without causing excessive strain or defection, or an excessively large mass, causes over-damping, nonlinear deformation, and may reduce overall bandwidth [138]. Tuning added mass is the most practical method; however, one should be careful because it may increase the viscous air damping and reduce the harvester's fatigue life.

For the maximum power harvesting using the tip mass, the resonance frequency (fn)can be calculated as follows [208,210,211]:

$$f_n = \frac{1}{2\pi}\sqrt{\frac{k_{eff}}{m_{eff}+m_{Tungsten}}}. \tag{6.1}$$

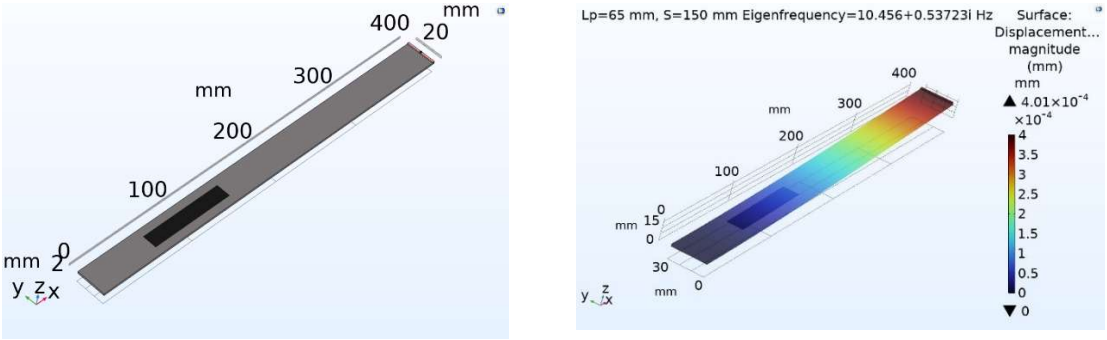
Figure 6-6 and Table 6-2 show the natural frequency variations when a 5.79-gram tip mass is added. The added tip mass reduces the first natural frequency by 4.42%, which is a substantial. It has been shown from the above equation (6.1) that increasing the mass at the tip of the cantilever beam increases the output power, and the resonance frequency is inversely proportional to the mass at the tip of the cantilever beam. Hence, the resonance frequency can be decreased by adding a mass at the free end of the cantilever, which is easier to achieve, and hence, the output power will increase.

Table 6-2 The natural frequencies' variation due to tip mass added at the free end beam

Mode shape	Frequency without tip mass (Hz)	Frequency with tip mass (Hz)	Frequency ratio (%)
1	10.976	10.456	4.73
2	65.09	62.001	3.06
3	182.36	177.44	2.69
4	356.67	350.11	1.83

For this model, a rectangular proof mass is attached to the free end of a cantilever beam and is made to vibrate under a harmonic small force of 0.5N. As shown in Figure 6-5 (a), a geometric model of a cantilever beam with a tip mass, and Figure 6-5(b), the first four mode shapes and resonance frequency when a tip mass is added at the free end of the energy harvester substrate. Adding tip mass or reducing the beam dimension reduces the resonant frequency and increases the harvested voltage and output power. It also modifies the mode shape, mass, and strain distribution, which ultimately affect VEH performance. The rectangular cantilever beam with proof mass is designed to have the same volume as the one in the earlier case. Adding a mass also increases the mechanical strain (bending) at the fixed end of the beam for a given

acceleration, which can increase the voltage output from piezoelectric harvesters, provided the frequency is matched to the fundamental natural frequency of the structure. In Figure 6-6 frequency is decreased from 10.976 Hz to 10.456 Hz, then the first mode resonance frequency shifts by 1.049. The resonant frequency for the tip mass model was 10.46 Hz, which is slightly higher than the experiment (10.2 Hz) and theoretical (10.69 Hz) models. In other configurations with different tip masses, the resonant frequencies obtained from the distributed model are also very close to the finite element method model. From the result of the finite element simulation method, the electrical voltage and power output frequency responses are shown in Figures Figure 6-7 (a) and (b) the voltage for the first mode at the resonance is 0.385 V, which is 1.48 times greater than the rectangular beam without mass. Numerically, the maximum output power increases from 0.0032 mW to 0.004 mW, which is 1.25 times greater than the rectangular beam without mass or a percentage increase of 25%. Thus, the added tip mass increases the voltage and power more prominently because it is stiffer, and then the tip mass causes more significant deflection than without the tip mass. The size and tip mass material are key factors and govern the performance of a piezoelectric energy harvester. Even though the frequency is lower, the mode shape curvature concentrates more near the clamp, which can increase strain there. However, this must be taken with caution, as the major differences in fundamental frequency reduce the credibility of this test. The use of a tip mass to control the fundamental frequency of an energy harvester in a justified way.



(a)Geometric model of EH with a tip mass (b) mode shape and eigenfrequency

Figure 6-5 The model and the first mode shape and eigenfrequency when a tip mass is applied

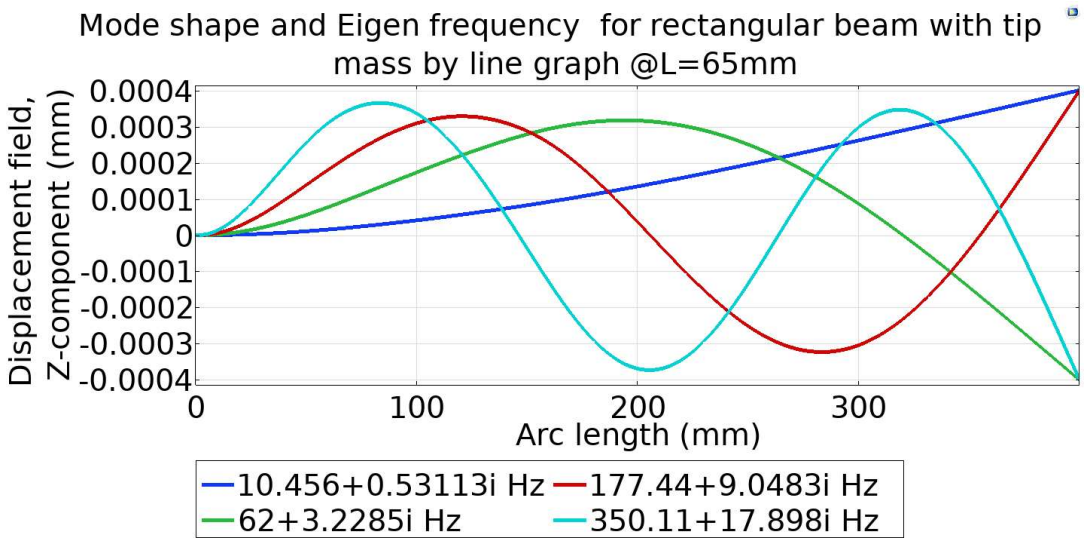
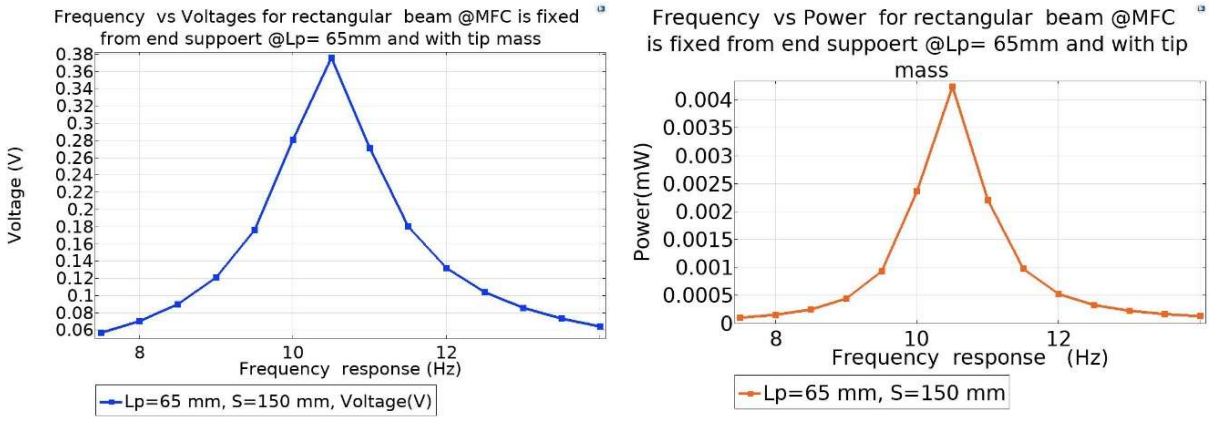


Figure 6-6 Mode shape and natural frequency by line graph with tip mass



(a)Frequency versus voltage (b) Frequency versus power

Figure 6-7 The effect of adding tip mass on the voltage and power

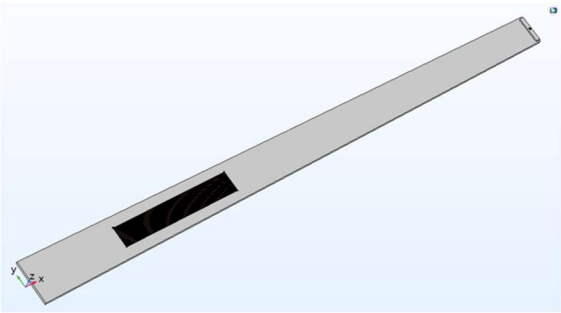
The maximum voltage of 0.39 V was generated using a MFC piezoelectric material attached to cantilever beam with a tip mass, in comparison with the configuration without a tip mass which produced 0.28 V as shown in Figure 6-7.

6.1.2.2 Tip mass with tapered rectangular beam

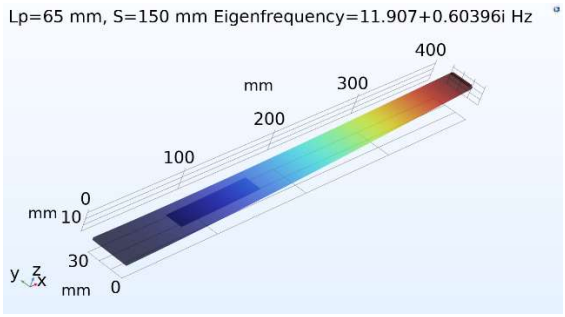
Rectangular cantilever beams are used in piezoelectric energy harvesting applications because of their simple geometry and the ease with which they can be fabricated and modelled analytically. However, this configuration has an inherent drawback. When a force is applied at the free end, the bending strain is highest at the clamped end and decreases linearly along the beam, becoming zero at the tip. Consequently, the average strain experienced by the beam is only about half of the maximum strain at the fixed boundary. To address this limitation, cantilevers with non-uniform geometries, such as triangular or trapezoidal shapes, have been

proposed. Trapezoidal cantilever results in more evenly distributed strain along the beam length compared to rectangular geometry These profiles promote a more uniform strain distribution along the beam length, resulting in a higher average strain under the same loading conditions and, therefore, improved electrical power generation in piezoelectric energy harvesters. A triangular beam geometry can deliver up to 50% higher power output compared with a conventional rectangular beam. For a rectangular cantilever beam with a tip mass, the bending moment generated by the mass reaches its maximum at the clamped end, causing a high stress concentration at the clumped end, while the stress near the free end remains minimal. The triangular geometry provides a clear advantage by allowing the piezoelectric material to be stressed more uniformly, with the stress level kept just below the yield threshold. As a result, strain is effectively maximized across the material, enhancing its energy conversion efficiency [199,213].

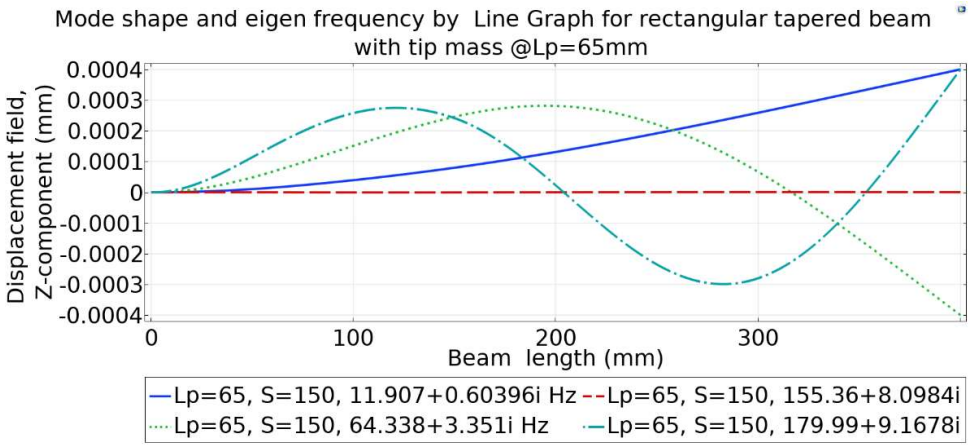
The structure shown in Figure 6-8 (a), (b) and (c) with a rectangular-shaped proof mass with a tapered beam is simulated and natural frequency of 11.907Hz. This frequency improvement is obtained due to the varying geometric shape of the beam with a tip mass added at the free end. The strain and the charge generation become uniform over the length of piezoelectric material, which is the effective way of maximizing the strain in the material. The maximum voltage of 0.61V is obtained with 2 mm length and 20mm with tip mass fixed at 398mm from the fixed support end as shown Figure 6-9 (a). distribution in the first mode, which can increase the power output significantly.



(a) Model of taper beam with tip mass

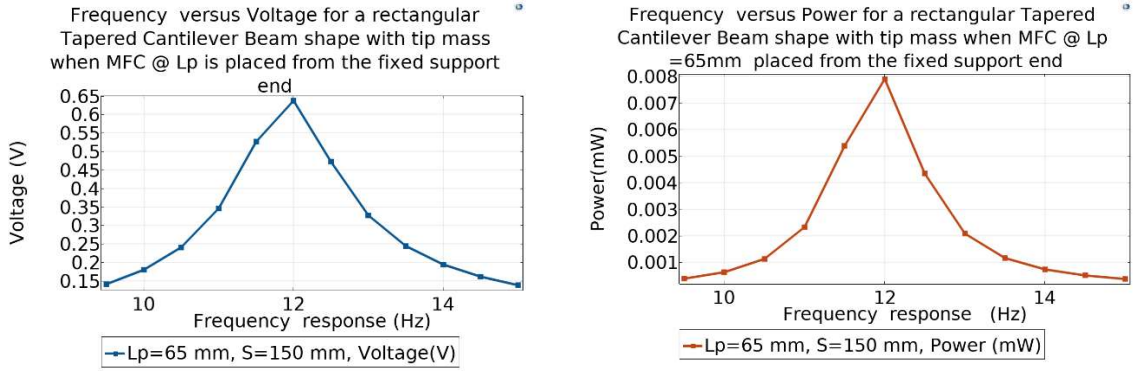


(b) The first mode shape and eigen frequency



(c)Mode shape and eigen frequency for tapered beam with proof mass

Figure 6-8 Geometrical model and resonance frequency of tapered beam with the tip mass



(a) Voltage (b) Power

Figure 6-9 Voltage and output power for tapered EH within tip mass added free end

As shown in Figure 6-9, the voltage and power are compared to the rectangular tapered beam without tip mass; the proposed PVEH generates 44.4% more voltage for an input point force of 0.5N, and the power on the device is evenly distributed, with the maximum power near the root increasing by more than 50% compared to a normal rectangular beam energy harvester. The optimum size of the tapered beam with proof mass was obtained through simulation, which produces 1.356 times greater voltage compared to a rectangular tapered beam without mass and 1.56 times more compared to a rectangular beam with mass. With respect to the increase in length and a decrease in width of the proof mass, the fundamental natural frequency of the structure is found to decrease, which can be seen from. A tapered cantilever (RC) beam with a larger clamped end and smaller rectangular tip produces a higher strain.

6.2. The effect of MFC patch location on energy harvesting efficiency

The output efficiency of the piezoelectric energy harvester is influenced by several factors. The placement or location of piezoelectric material on the harvester beam is one of the crucial factors which affect the output of the energy harvester [214]. The location of the piezoelectric patch is one of the optimisation method variables that has a direct impact on the voltage amplitude. However, the voltage amplitude is not a direct measure of the other three variables related to optimisation of attachment.

The position of the patch is directly visible because the generated charge is obtained by the integration of the strain over the region of the piezoelectric patch. The other optimisation variables, the attachment position, the attachment mass and the mass moment of inertia, are not usually included explicitly, as they affect the voltage indirectly via the beam dynamics [75,206,214,215].To improve the efficiency of the piezoelectric energy harvester, place the piezoelectric material as the dominant design variable controlling the harvested power. Furthermore, the optimal placement maximizes electromechanical damping and voltage output. The optimal placement of piezoelectric material for the smart structure is based upon the boundary conditions. As piezoelectric material placed near the fixed end produces more power compared to the other locations due to more strain concentration near the fixed. The power produced by the piezoelectric materials is directly related to the strain of the beam.

The amount of energy harvested from vibrating structures through piezoelectricity depends on the properties of the piezoelectric material and the mechanical strain that occurs in the material. This section model MFC patch location for Energy harvesting analysis was implemented by using COMSOL Multiphysics finite element analysis program. The natural (eigen) frequency varies about 5-25% when the MFC patch is moved towards the clamped end of a cantilever beam, depending on the size of the MFC piezoelectric material in relation to the size of the beam and the stiffness of the beam. This is because the fundamental mode has the maximum curvature (maximum bending strain) at the fixed end region. The voltage produced by the harvester is directly proportional to the strain in the patch location region for both rectangular and tapered beams.

6.2.1 MFC placement for the rectangular beam without tip mass

From Figure 6-9 and Figure 6-11, the harvester's eigenfrequency significantly increased from 10.27 Hz to 11.48 Hz when the MFC was placed from 200 mm to 0 mm. The

eigenfrequency variation by placement of MFC on the near-end support of the substrate can be used as an approach for frequency-matching design, positively affecting the power output.

In a cantilever clamped-free condition, the stresses near the clamped line are considerably higher. Figure 6-12 shows the von Mises stress for a cantilever beam that is clamped-free with an MFC integrated at a location of 0 mm to 200 mm. The simulation also predicts that the maximum bending stress, occurring at the root of the cantilever beam, is 6.5 N/m², while the minimum bending stress at the free end is 0.5 N/m², indicating that the stress is reduced by about 92.3%. Thus, in the piezoelectric cantilever beam, the high-stress regions generate considerably higher power than the other regions. The stress is distributed along the length of the beam, and the poling of the piezoelectric material is in the z-direction, which corresponds to the direction of the input vibration. Therefore, a substantial portion of the piezoelectric sheet does not contribute to power generation as it is far from the fixed support end of the beam. The stress near the clamped region is high, so the power generation around the clamped regions is considerably larger than in other regions.

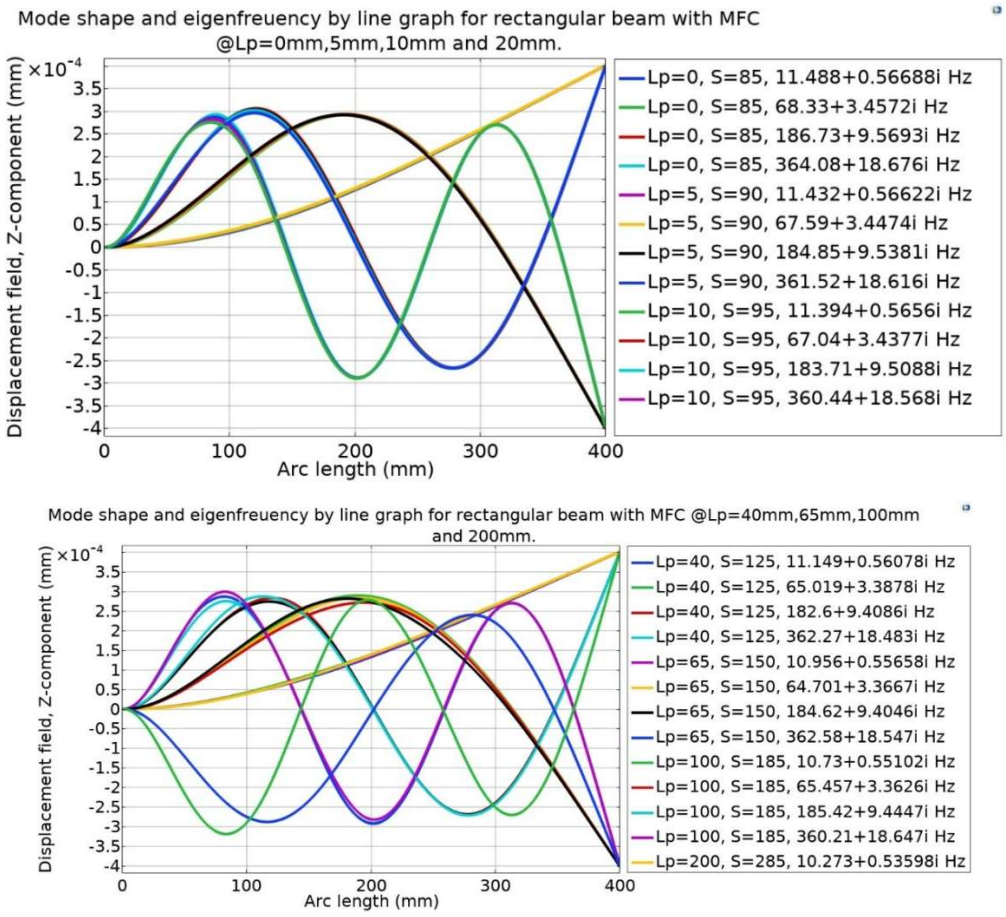
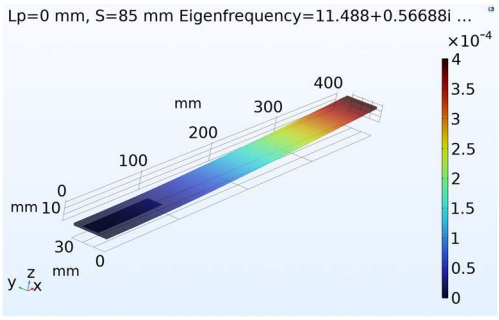
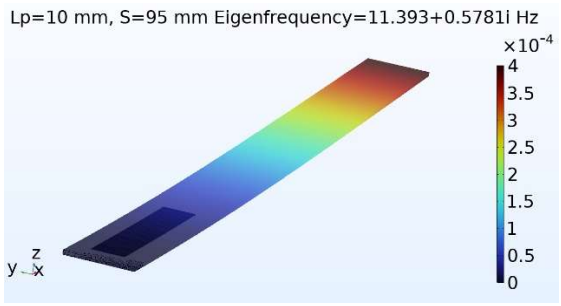


Figure 6-10 Mode shape and natural frequency when MFC attached at different place

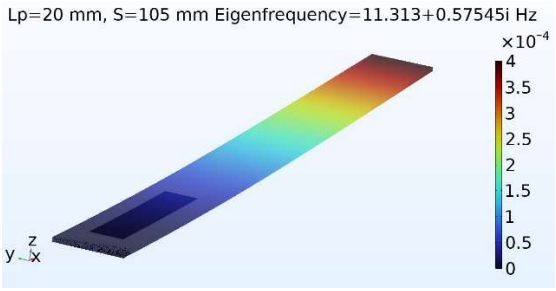
Mode 1for MFC at fixed support Mode1 for MFC at 10mm



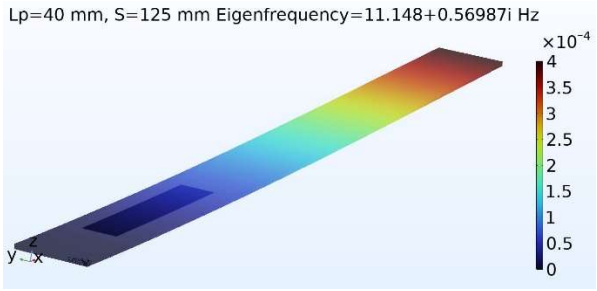
Mode1 for MFC at 20mm



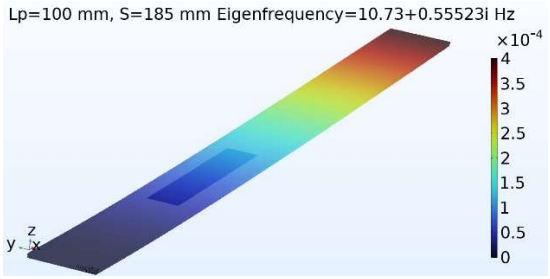
Mode1for MFC at 40mm



Mode1for MFC at 100mm



Mode1for MFC at 200mm



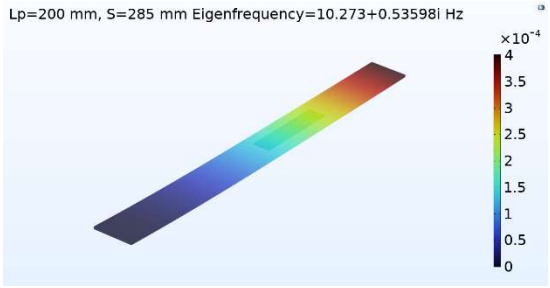


Figure 6-11 3D mode shape and natural frequency when MFC placed at different location

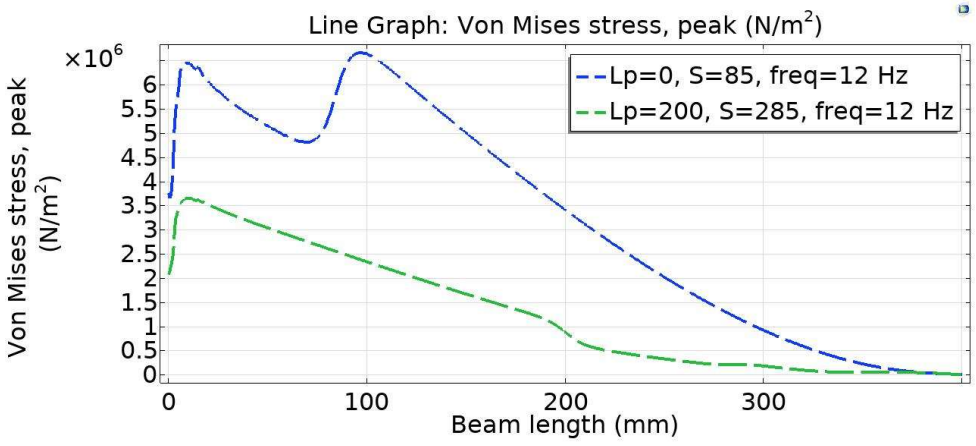


Figure 6-12 The von Mises stress along the rectangular cantilever energy harvester

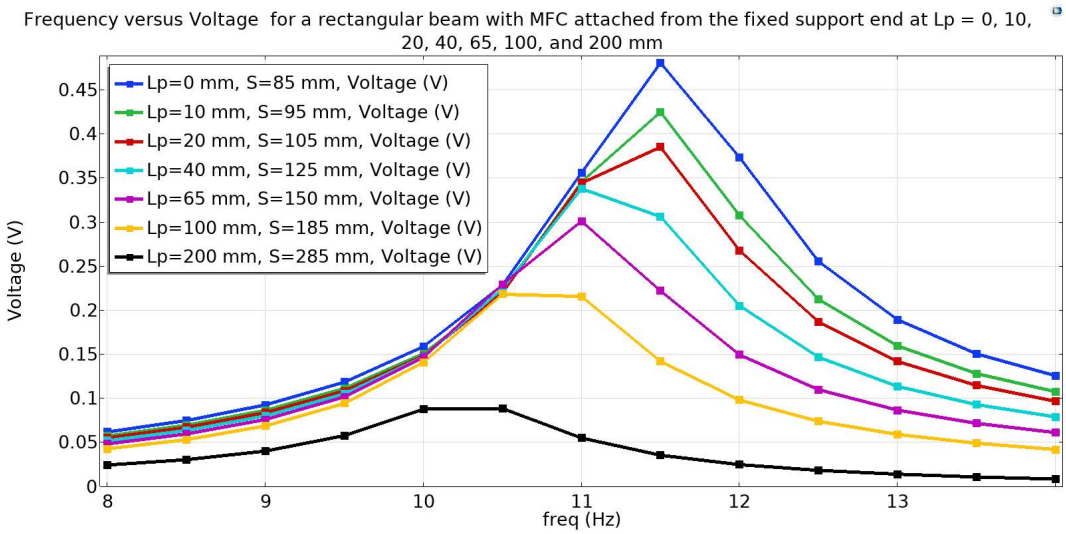


Figure 6-13 The voltage versus frequency response for various placements of MFC

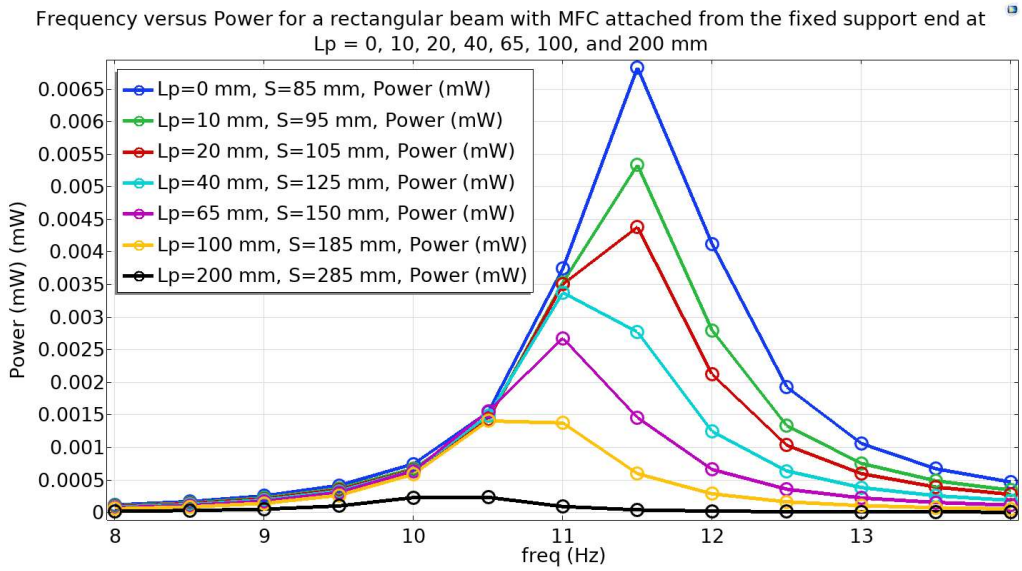


Figure 6-14 The power output and resonance frequency with various placements of the MFC

As shown in Figure 6-13 and Figure 6-14, the maximum voltage and power output are achieved at L_p = 0 mm and 11.488 Hz. The voltage and power outputs are 0.45 V and 0.0065 mW, respectively, at the optimal condition, which are 77.77% and 92.3% higher than those obtained when the MFC is placed 200 mm from the fixed support end. The optimal MFC placement for maximum peak power and resonance frequency occurs between L = 0 mm and 65 mm. Therefore, larger strain can cause charge-cancellation effects, leading to a decrease in power output. Positioning the patch too close to high-stress areas can also heighten the risk of damage to either the piezoelectric patch or the supporting structure, especially under long-term vibration.

6.2.2 MFC placement on the rectangular beam with tip mass

It is well known that a mass at the free tip produces the lowest frequency, and by moving the MFC position from 200 mm to 0 mm near the clamped end, the tuned frequency increases due to the longer strain length of the beam. The extra mass not only increases the volume but also modifies the mode shape, mass distribution, and strain distribution, which eventually affects the VEH performance. The dimensions of the rectangular tip masses are 2 mm, 10 mm, and 1 mm; the volume of the tip mass is $50mm,^{3}$its mass weight is 0.368g, and the ratio of the tip mass/beam mass is 0.0149, ≈1.5%. There is a need to find out the differences in the mass ratio when using tip masses with altered locations of MFC.

Figure 6-15 Shows that when the MFC position is close to the clamped area, the strain increases rapidly. Besides, the resonance frequencies of the beam models with bulky tip masses can become even smaller than the original natural frequency of the beam without mass. For the clamped end and the tip mass at the free condition, the strains close to the clamp end are substantially larger than in other areas. Therefore, most of the power output in a piezoelectric cantilever is generated from the near clamp regions. Therefore, as the MFC bonding area is close to the clamp region, it leads to significant influences on the piezoelectric beam performance.

From the Figure 6-16,the voltage results show a strong dependence of the piezoelectric output on the location of the MFC patch along the cantilever beam. The maximum voltage output (0.62 V) was found for the patch position at Lp = 0 mm, i.e., nearest to the fixed support, where the bending strain due to the tip mass excitation is maximum. With the patch location moving progressively towards the free end (Lp = 10, 20, 65, 100, and 200 mm), the peak voltage decreased steadily to about 0.55 V, 0.47 V, 0.40 V, 0.30 V, and 0.13 V, respectively.

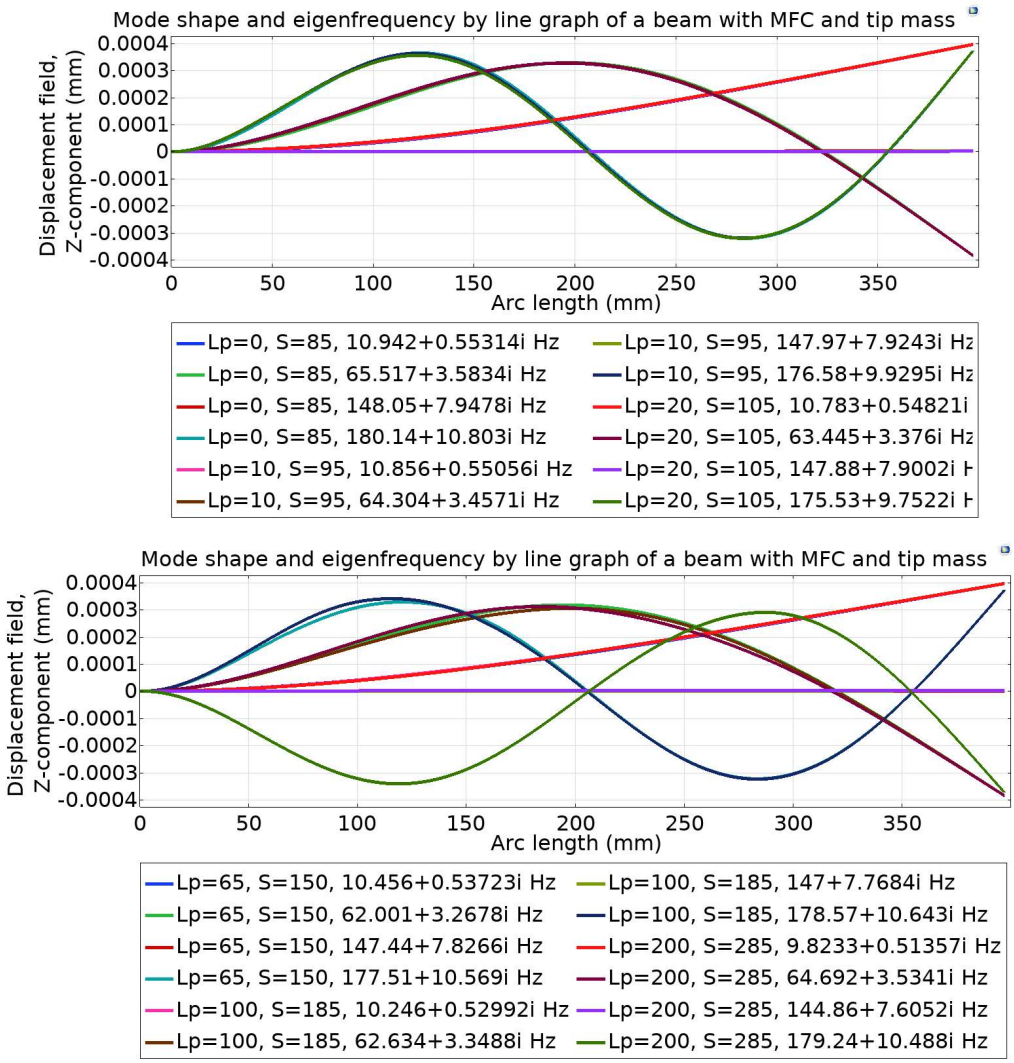


Figure 6-15 Mode shape versus resonance frequency with tungsten tip mass

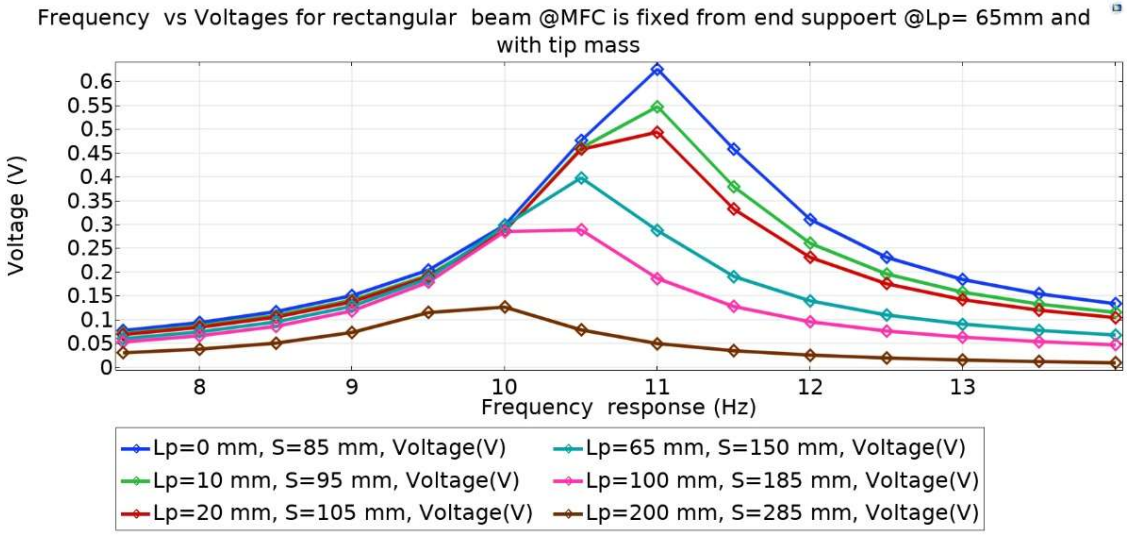


Figure 6-16 Frequency versus Voltage for a rectangular cantilever beam shape with a tip mass

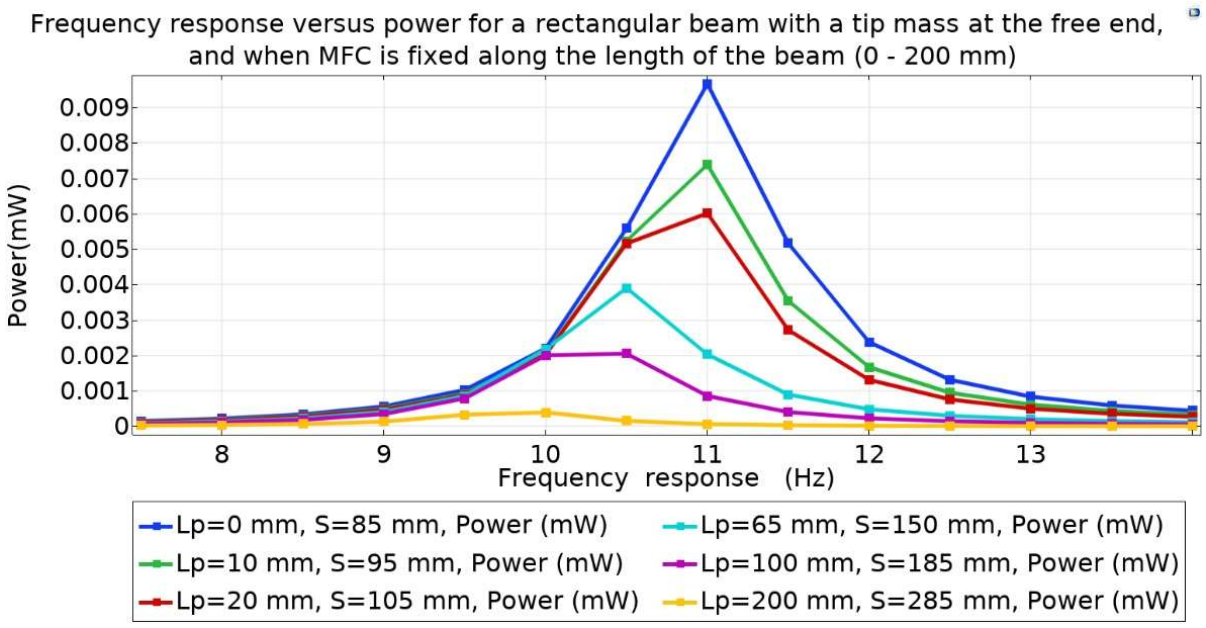


Figure 6-17 Frequency versus power for a rectangular cantilever beam with a tip mass

Figure 6-17 The graph shows the frequency response vs. the output power for a rectangular cantilever beam with a tip mass and MFC (Macro Fibre Composite) piezoelectric patch at six different positions (Lp = 0, 10, 20, 65, 100 and 200 mm) along the beam length, measured from the fixed support. From the figure, the maximum power for the rectangular beam with a tip mass of 0.0095 mW was obtained.

6.2.3 MFC placement on the tapered rectangular beam without tip mass

Figure 6-18 show the mode shapes of the tapered rectangular beam (with MFC patch, no tip mass) for patch positions L_p = 0, 10, 20,65, 100, 200 mm (patch length L_p) from fixed support end , starting offset S = 85, 95, 105 150, 185, 285 mm (the total distance of MFC from the fixed support). Each placement shows the first four bending mode shapes (four line-colour groups per plot, each tagged with its complex eigenfrequency).The fundamental frequency decreases steadily as the patch moves further from the clamped end and towards the tip of beam, from 12.967 Hz at L_p=0/S=85 to 11.552 Hz at L_p=200/S=285, consistent with standard cantilever beam theory where added mass/stiffness near the low-curvature, high-displacement tip region lowers the fundamental natural frequency more than an equivalent addition near the high-curvature root .

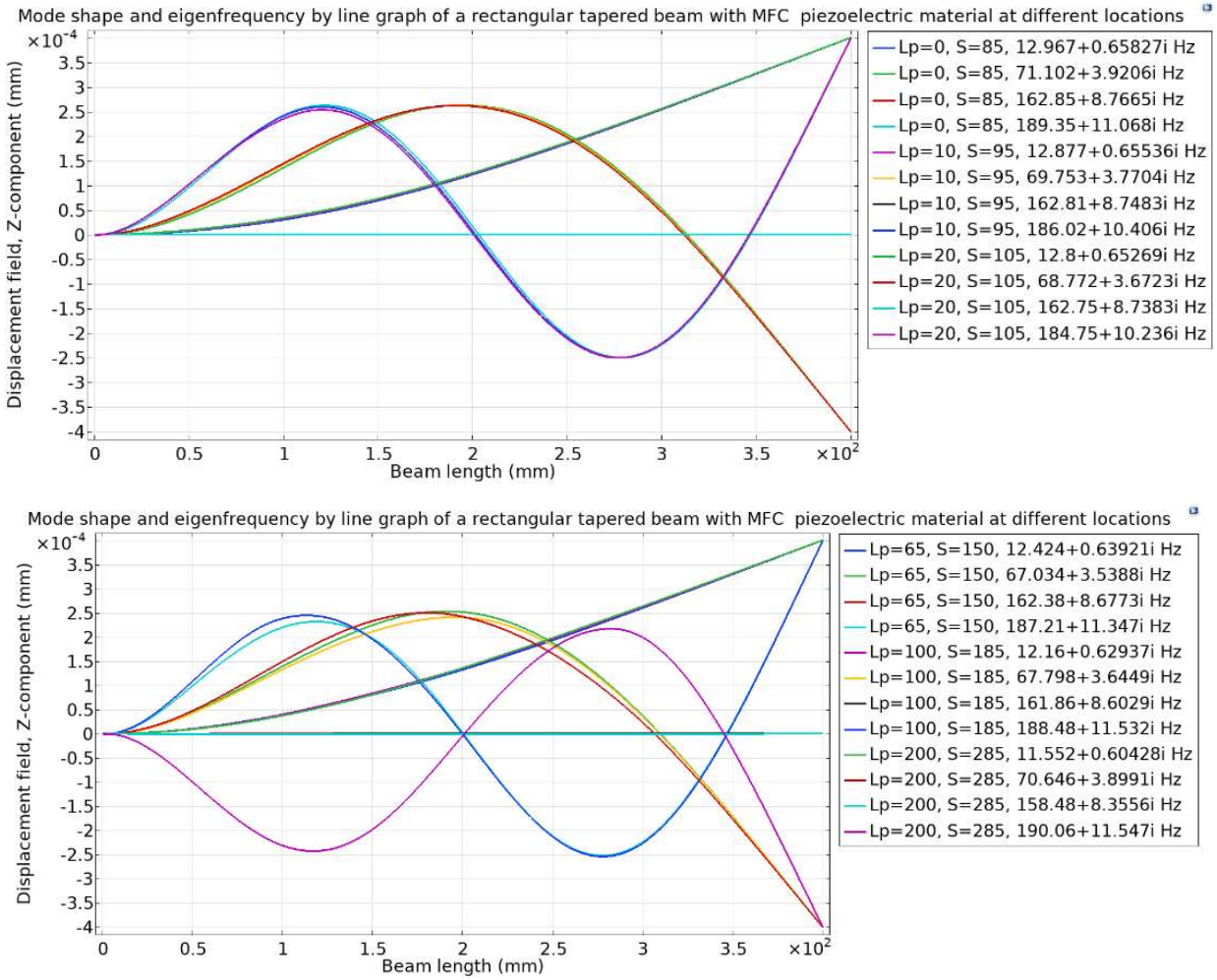


Figure 6-18 Mode shape and natural frequency by line graph for tapered beam

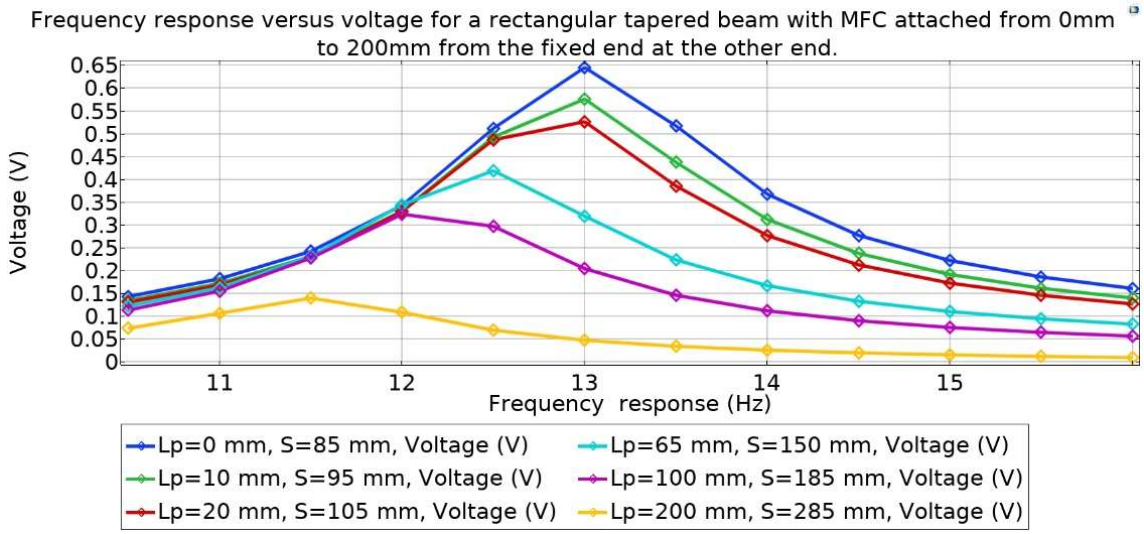


Figure 6-19 Frequency and voltage magnitude at the resonance modes for tapered beam

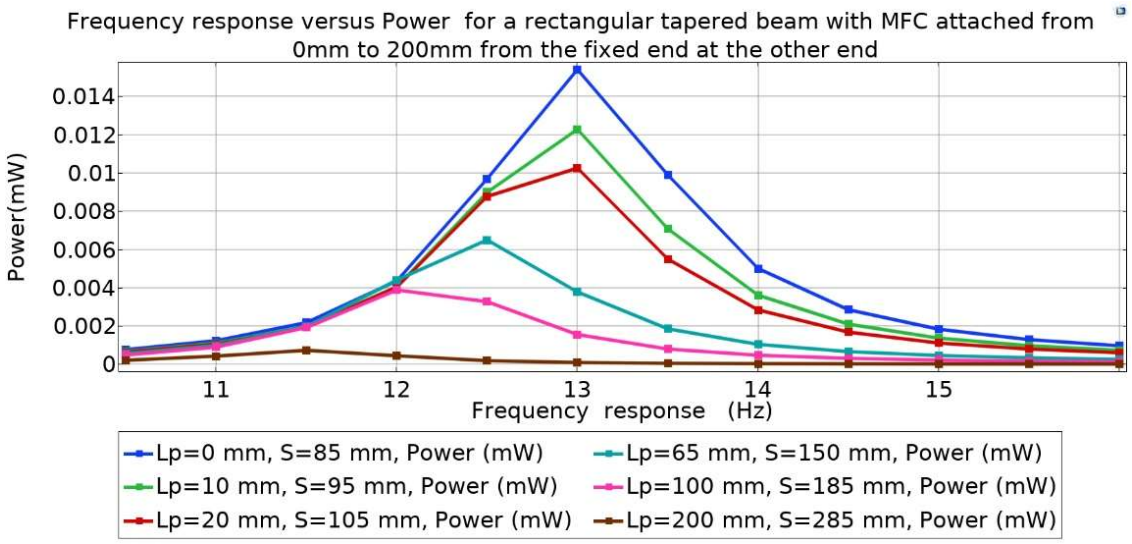


Figure 6-20 Frequency and power for the tapered beam

As shown in Figure 6-19 and Figure 6-20 mode shape with frequency, the maximum voltage and power output are achieved at L_p = 0 mm and 12.97Hz. The voltage and power outputs are 0.65 V and 0.015 mW, respectively, at the optimal condition, which are 86.667% and 93.44% higher than those obtained when the MFC is placed near 200 mm from the fixed support end. The optimal MFC placement for maximum peak power and resonance frequency occurs between L = 0 mm and 65 mm.

6.2.4 MFC Pach placement on the tapered rectangular beam with tip mass

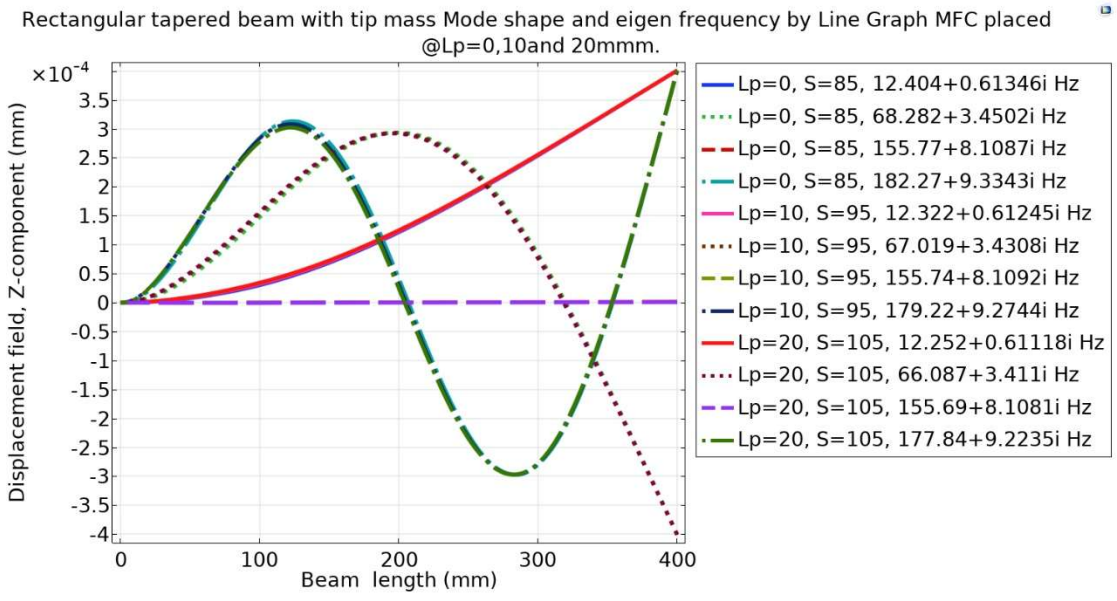
From the results, it is observed that the trapezoidal beam with a rectangular shape has a high eigenfrequency as the MFC is attached near the fixed support end. Which generates a high output voltage for a given applied force compared to the rectangular beam due to the increased bending moment produced near the fixed end due to the mass of the MFC and uniform strain distribution produced by the tapered section. Figure 6-21,Figure 6-22, and Figure 6-23 show how the MFC will be sequentially moved along the beam from position 200 mm to 0 mm, and COMSOL Multiphysics 6.3 simulated the resonance frequency, voltage, and output power for each location.As MFC patches close to the clamped end of a cantilever beam, it stiffens the beam much more than it adds mass. That pushes the first natural frequency upward. It's the opposite of putting a proof mass at the tip, which mainly adds mass and drives the frequency down. Figure 6-21 shows the frequency response of a tapered cantilever with tip mass, the structure with respect to the variations of the MFC placement, and the frequency decreases from 12.4 to 11.1 Hz as the MFC is placed from 0 mm to 200 mm along the length of the beam. As

the MFC approaches fixed support, end power and strain are directly proportional to the resonance frequency increase along the length L_2 from 200 mm to L_1 to 0 mm.

This structure is more suitable for low-frequency energy harvesting due to the slenderness of the beam. The optimal energy efficiency for a proof mass of a given volume is simulated by varying the position of the MFC, keeping the length, width of the proof mass, and thickness constant. From the results in Figure 6-22, the voltage and power gradually decreasefrom 0.91 V to 0.015 V as the MFC is moved beyond 200 mm from the fixed support end, and the voltage is minimum at the free end of the energy harvester. The maximum voltage of 0.91 V is obtained with an MFC close to the end support, a 0 mm width of the beam tapered towards the free end, and a rectangular tip mass.

$$V \propto \int d_{31} \times \sigma(x) dx \tag{6.2}$$

In Figure 6-23, the simulation output power results of the harvester with a tapered cantilever with tip mass are presented. The uniform strain produced over the surface of the tapered beam by the tapered section and tip mass results in an increase in strain along the beam. Hence, piezoelectric produces more voltage for a given applied force. This modelled structure produces 0.2 mW, which is 25% more than a tapered beam without a tip mass energy harvester and 94.5% greater than a rectangular beam piezoelectric energy harvester with tip mass.



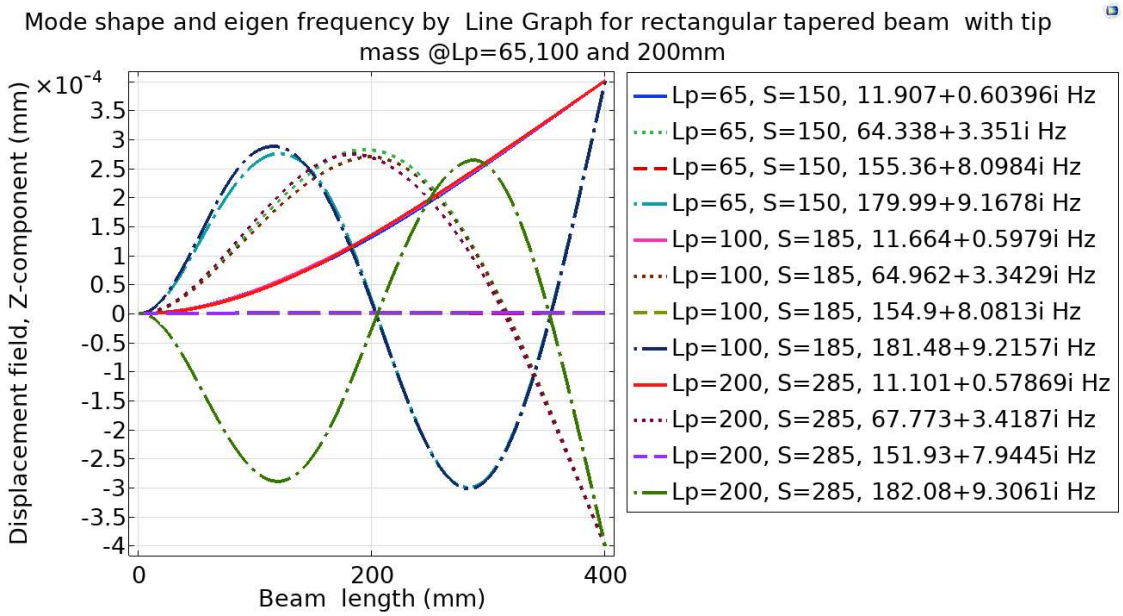


Figure 6-21 Mode shape and eigen frequency by Line Graph for tapered beam with tip mass

Figure 6-22 and Figure 6-23 show the effect of the patch location and tip-mass attachment on the rectangular tapered beam in terms of the voltage amplitude and output power versus frequency. The maximum voltage and power outputs of 0.009 mW and 0.022 mW were obtained for the tapered rectangular beam with tip mass configuration, representing increases of approximately 28.57% and 33.33%, respectively, compared to the tapered rectangular beam without tip mass.

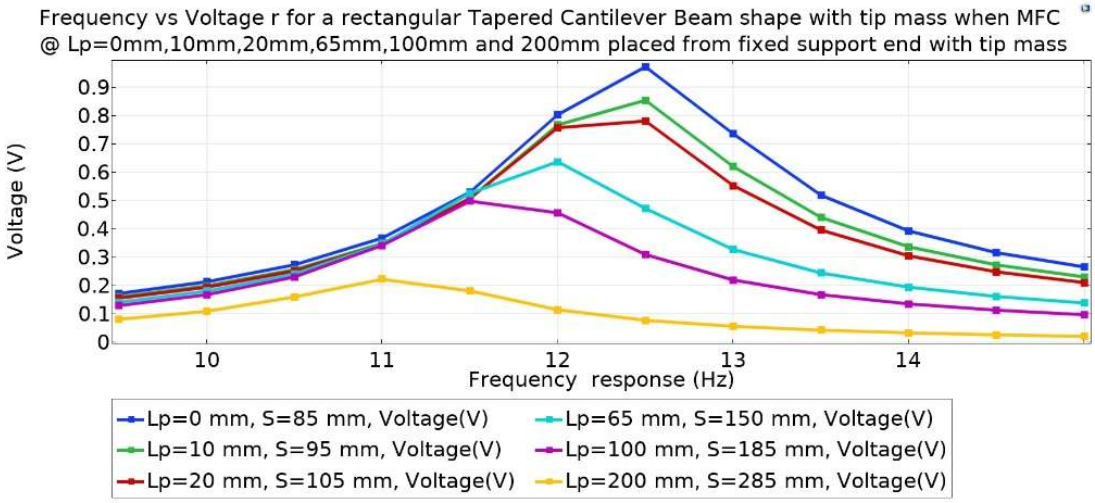


Figure 6-22 Frequency versus Voltage, for tapered beam with tip mass

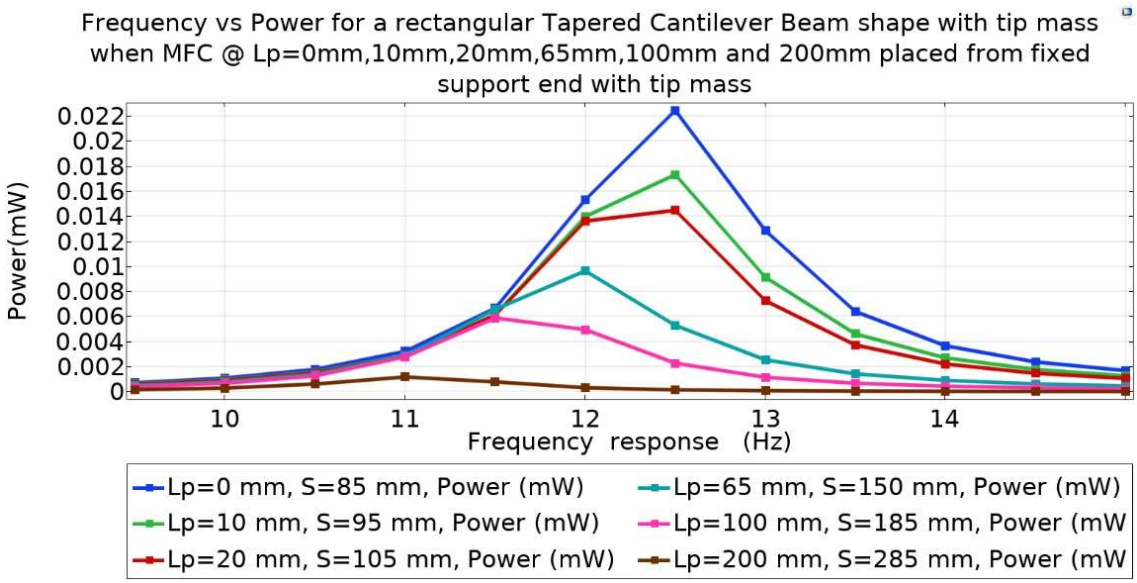


Figure 6-23 Power output versus frequency for tapered beam with tip mass

As shown in this figure, when the excitation frequency is close to the first natural frequency, and the piezoelectric patch is placed near the clamped end, the first vibration mode shape and the largest strain are near the clamped end of the beam. The optimum position of the attachment can be explained by its proximity to the maximum strain which occurs near the fixed support while the excitation force is applied at the free end of the beam. Generally, the largest strains in the beam are near the clamped end and the highest voltage and power outputs are obtained when the piezoelectric patch is placed in this region.

6.3. Parametric optimization EH based on the variable thickness of the substrate

Another design for the parametric optimisation process of cantilever beams involves a substrate energy harvester with variable thickness. This optimised shape illustrates how the cantilever beam adapts to best fit boundary conditions, balancing size, and frequency performance for real-world applications. Adding tip mass allows you to adjust the frequency of a specific vibration by reducing the natural frequency to a suitable level for low-frequency vibrations. The final compact design is easy to integrate into existing wearable devices and can be attached to various energy sources, demonstrating its flexibility. In this section, the effects of substrate thickness on natural frequency, voltage, and power output are analysed for rectangular and tapered beams. Simulations were conducted to predict the output voltage (V) and power (W) across the MFC piezoelectric material for different substrate energy harvester thicknesses and various geometric shapes of cantilever beams. Most energy harvesting devices are designed to operate at their fundamental natural frequency, as most power is generated in

the first mode compared to higher modes. An aluminium rectangular beam measuring 400 mm x 30 mm x 2 mm and a rectangular tapered beam with matched length, but varying width and thickness are examined.

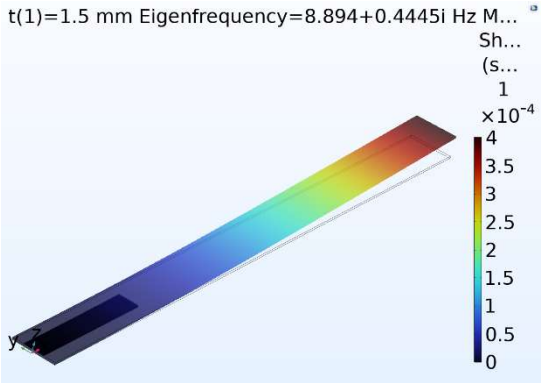
6.3.1 Effect of substrate thickness on the efficiency of EH from a rectangular beam

The model was first used to investigate the effect of varying the cantilever beam thickness on the natural frequency, voltage, and power generated. The substrate thickness was increased while the piezoelectric thickness was kept constant (Figure 6-24). The layer thickness was swept from approximately 1.5 mm to 2.8 mm, with the MFC fixed near the clamped support end. This configuration yielded a higher natural frequency but lower voltage and power output, as shown in Figure 6-25 and Figure 6-26 respectively. With the MFC placed near the fixed support end and six thickness values simulated, the optimised power was obtained at a thickness between 1.8 mm and 2.2 mm. For each MFC, the voltage and power output were evaluated by direct connection to a resistive load, while the other MFCs remained in an open-circuit condition.

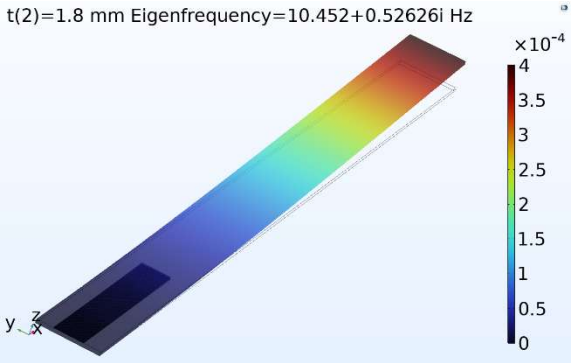
As shown in Figure 6-24, the natural frequency varies slightly from 11.48 Hz to 8.894 Hz when thickness varies from 2 mm to 1.5 mm. Depending on the energy-harvesting dimensions of the substrate, the natural frequency can be increased or decreased. Small frequency-power output shifts due to electromechanical coupling. As the thickness decreased and the curvature increased, the natural frequency increased and the electrical output increased accordingly. The voltage outputs of all the MFCs at the excitation frequency are shown in Figure 6-25. It can be seen from the figure that the voltage varies with different thicknesses. The maximum output voltage at the first resonance peak, at a frequency of approximately 8.89 Hz for a substrate thickness of t (1) = 1.5 mm, is 0.75 V. At very small thicknesses, the beam experiences higher deflection and a reduced resonance frequency. In this case, the deflection of the beam under a point load of 0.5 N is 14 mm, which is very high. In general, the deflection of the cantilever beam depends on the beam's dimensions length, width, and thickness as well as the material properties used to construct the cantilever energy harvester.

Therefore, large deflections are not recommended for thinner, longer beams. Figure 6-25 and Figure 6-26 show the analysis performed at thicknesses of 1.8 mm, 2 mm, and 2.2 mm, where the output voltage and power increase optimally, with an average deflection of 7 mm to 10 mm. Beyond a thickness of 2.5 mm, increasing the beam's thickness raises the natural frequency indicating higher beam stiffness while reducing the output electrical power. It was found that changes in width do not significantly affect the output voltage and natural frequency

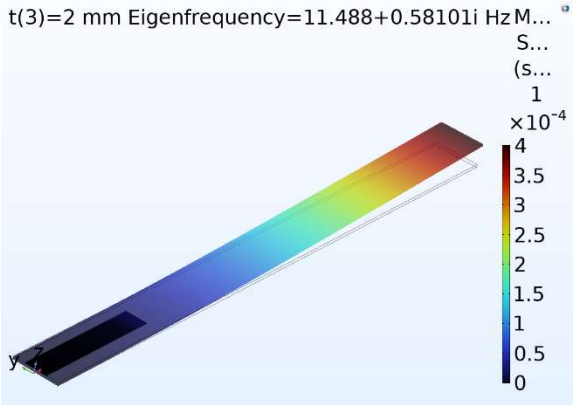
of a rectangular cantilever beam, unlike changes in length and thickness. Based on this parametric analysis, a thickness of 1.8 mm to 2.2 mm is recommended for the MFC beam dimensions to achieve optimal energy-harvesting performance. The minimum and maximum power harvested for this configuration range between 0.005 mW and 0.014 mW when the beam vibrates at its first natural frequency, as shown in Figure 6-26. A thicker substrate makes the beam stiffer, shifting the resonant frequency higher and resisting bending, which results in lower average strain in the MFC for a given base excitation. The results indicate that as the beam's thickness increases, power output decreases. Conversely, decreasing the thickness results in higher power output but with larger deflections, which can cause structural degradation of the beam. Additionally, since resonance must be induced at low excitation frequencies, the first natural frequency of the energy-recovery device was limited to 15 Hz or below. Overall, increasing the substrate thickness from 2 mm to 2.8 mm raises the first natural frequency to 15.63 Hz; however, the voltage and power harvested were reduced by 46.49% and 67.86%, respectively, as shown in Table 6-3 from the initial design of the beam thickness. The Variations in substrate thickness therefore significantly affect the resonant frequency, voltage, and power output. Given the inherently low voltage and power output of MFCs, the associated losses are substantial. Overall, considerable output energy is lost due to electromechanical coupling and mechanical damping. Consequently, more efficient modelling approaches for such harvesters are highly desirable, requiring further improvements in modelling techniques.



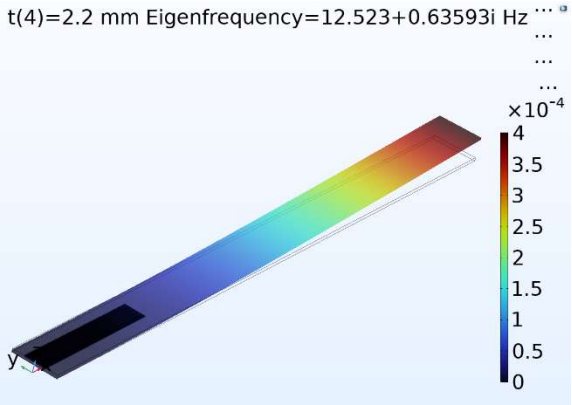
Mode shape and eigen frequency t=1.5mm



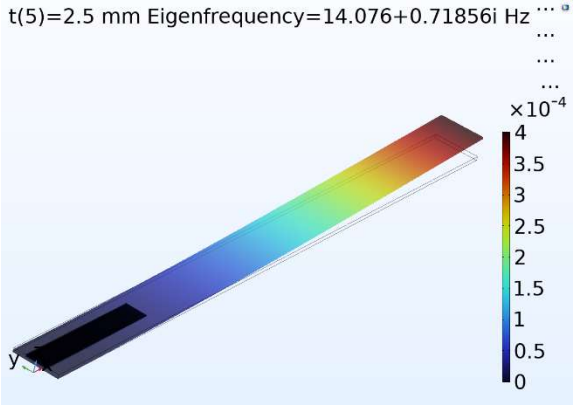
Mode shape and eigen frequency t=1.8mm



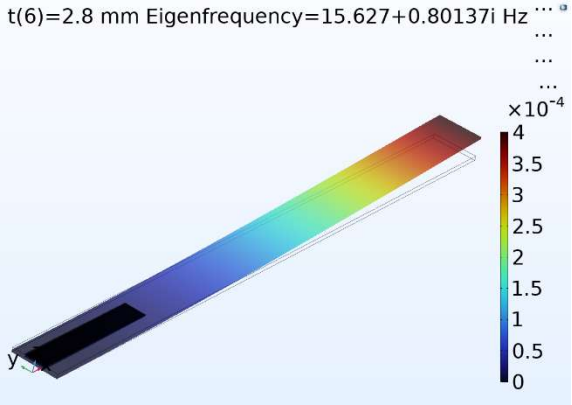
Mode shape and eigen frequency t=2mm



Mode shape and eigen frequency t=2.2mm



Mode shape and eigen frequency t=2.5mm



Mode shape and eigen frequency t=2.8mm

Figure 6-24 The mode shape, natural frequency, and displacement with different thickness

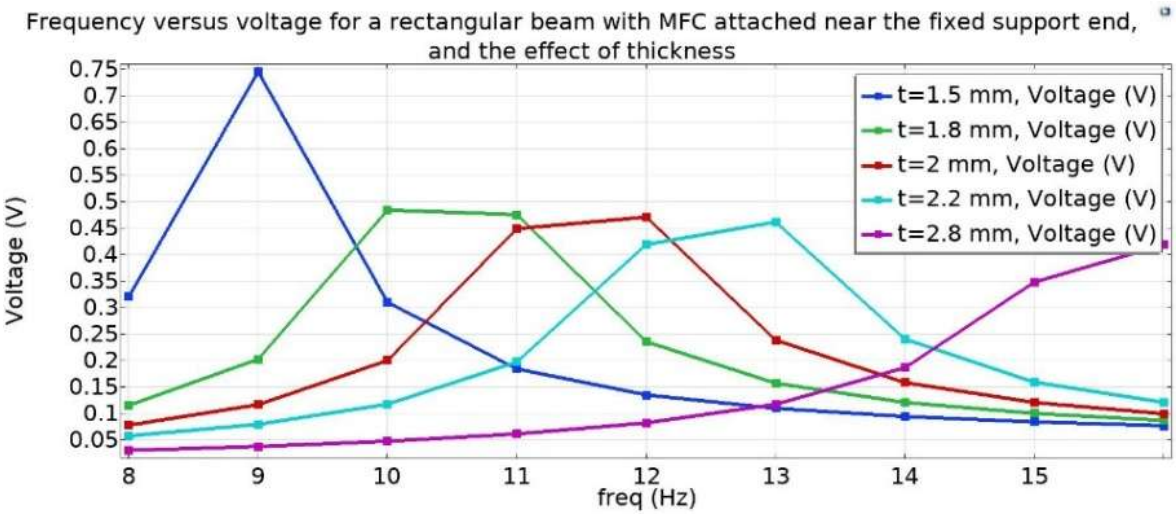


Figure 6-25 Variation of voltage over frequency for different substrate thicknesses

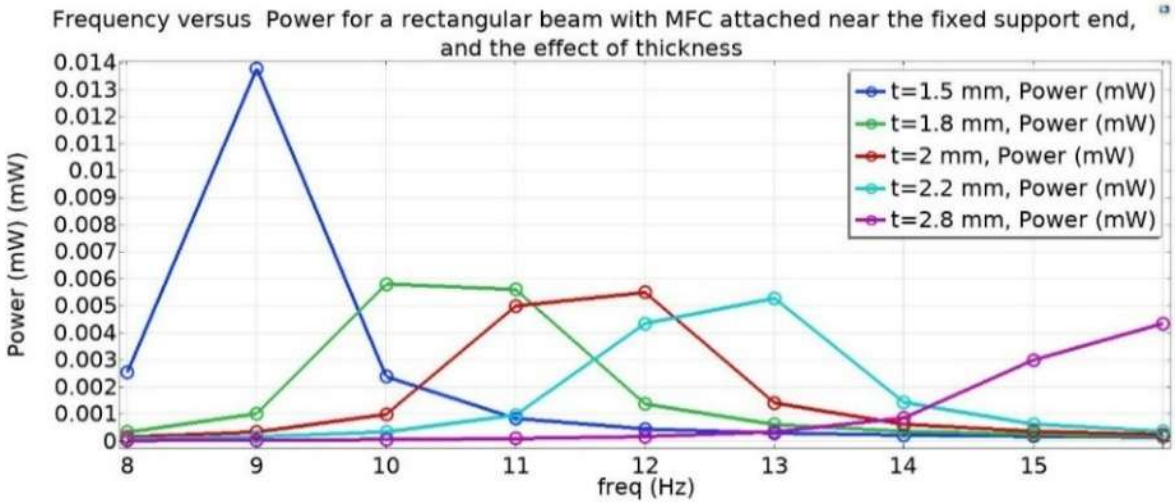


Figure 6-26 The power versus excitation frequency for different thicknesses

Table 6-3 EH performance of a rectangular beam at different substrate thicknesses

Beam Size	Output value		
Thickness (mm)	The 1st Resonance Frequency (Hz)	Peak output voltage (V)	Output power(mW)
1.5	8.894	0.753	0.014
1.8	10.45	0.49872	0.006
2	11.488	0.4725	0.0057
2.2	12.52	0.46275	0.0052
2.8	15.627	0.4013	0.0045

Table 6-3 compares the energy harvesting performance of the rectangular cantilever beam at resonance for different substrate thicknesses from 1.5 mm to 2.8 mm. As the thickness

increases, the first resonance frequency increases considerably from 8.894 Hz for 1.5 mm to 15.627 Hz for 2.8 mm which indicates the increased stiffness with the thicker beams. The maximum output voltage and output power, however, decrease sharply with increasing thickness from 0.753 V and 0.014 mW at 1.5 mm to 0.4013 V and 0.0045 mW at 2.8 mm, respectively. beams yielding higher voltage and power output at the cost of a lower resonance frequency.

6.3.2 Influence of variable substrate thickness on a tapered beam

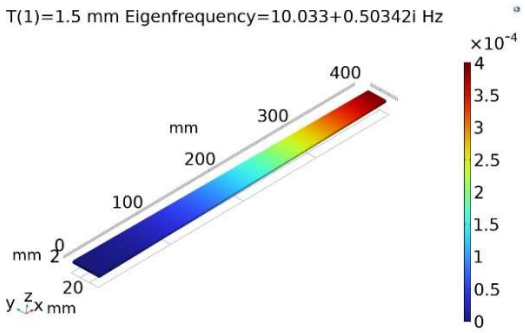
Another way to improve the performance of the PEH is by altering the thickness of the energy harvester. This is a very effective way to greatly increase its power output and efficiency. Thickness affects stiffness, strain distribution, natural frequency, and electrical output. Here, the length and width are fixed and six thicknesses are considered. Figure 6-27, Figure 6-28,Figure 6-29,Figure 6-30 and Figure 6-31 show the frequency, amplitude-displacement, voltage, and power respectively, which indicate that the beam thickness has a significant effect on the efficiency of the MFC harvester. The aluminium substrate is 30 mm wide and 400 mm long . The thickness of the tapered beam was swept from 1.5 mm to 2.8 mm in steps of 0.25 mm while the thickness of the MFC piezoelectric material was kept constant .

Then, finite element analysis was performed to determine the resonance frequencies, peak voltage outputs and power. The results are summarised in Figure 6-30 and Figure 6-31. As the result shows, the resonance frequency increased from 10.03 Hz to 17.65 Hz with the thickness increased from 1.5 mm to 2.8 mm. Note that the resonant frequency can be tuned by modifying the thickness of the beam energy harvester. In contrast, the peak voltage output decreased from 1.067V to 0.613V. As the cantilever thickness increases slowly, the resonant frequency increases, while the voltage and power both decrease. If the thickness is too thin, the beam has a large strain but less structural stability and frequency mismatch.

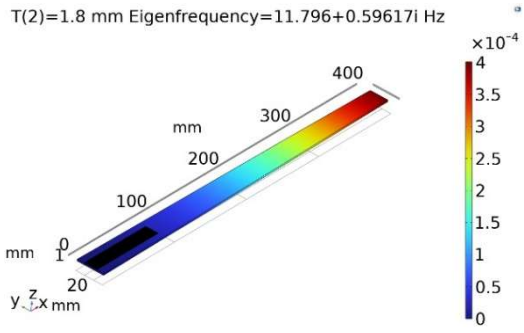
Increasing the thickness of the aluminium substrate resulted in a continuous increase in the resonance frequency of the PEH. The peak voltage and power output of the PEH decreased initially with increasing thickness, achieving a maximum of 0.72 V at a thickness of 1.5 mm, and then increased again with increasing thickness. Hence, the optimum thickness of the aluminium substrate for maximum voltage and power output was found to be in the range of 1.8 mm to 2.2 mm. Thus, the final optimised dimensions of the aluminium substrate for the piezoelectric rectangular tapered cantilever beam were obtained as 400 mm ×30 mm × (1.8~2.2) mm.

For better comparison, the results of varying the thickness of the beam PEH at constant beam lengths and width are also summarized in Table 6-4. The maximum output Voltage reached up to 0.9V for the thickness of 1.5 mm with a load resistance of 10 kΩ when a 0.5 N point force was applied at 10.033 Hz at the beam length when the MFC was placed near the fixed support end of the rectangular tapered cantilever beam. The maximum average power has become 25% greater than that of the previously normal rectangular cantilever beam with constant thickness and width. The peak power can be optimized to 0.024mW when the beam vibrates at the 1st natural frequency. The variation of frequency with variable thickness and width of the beam is shown in Figure 6-27,Figure 6-28 and Figure 6-29 which depicts that as the rectangular tapered cantilever beam length increases, the frequency decreases when the width and thickness are fixed at a minimum. Again, this figure shows that the frequency slowly increases with the thickness of the beam.

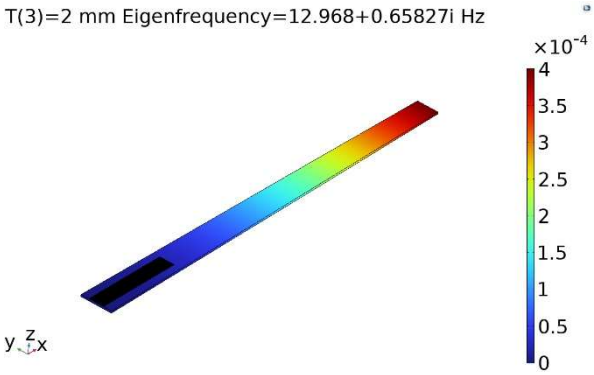
Mode shape and eigenfrequency for t_b=1.5mm



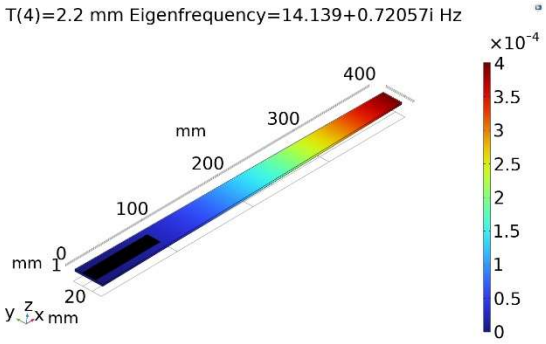
Mode shape and eigenfrequency t_b=1.8mm



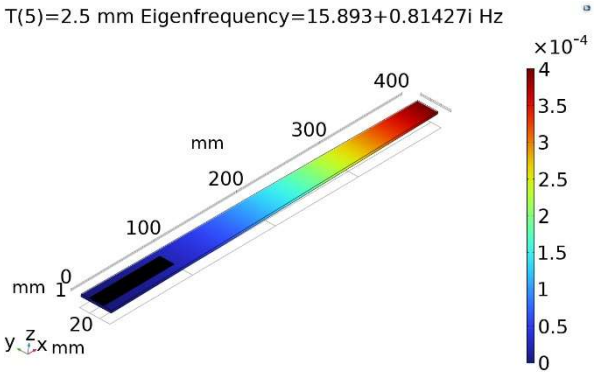
Mode shape and eigenfrequency for t_b=2mm



mode shape and eigenfrequency t_b=2.2mm



Mode shape and eigenfrequency for t_b=2.5mm



Mode shape and eigenfrequency t_b=2.8mm

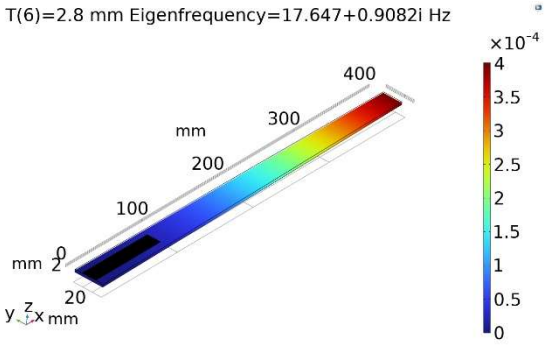


Figure 6-27 Mode shapes and eigenfrequencies of tapered beams with variable thickness

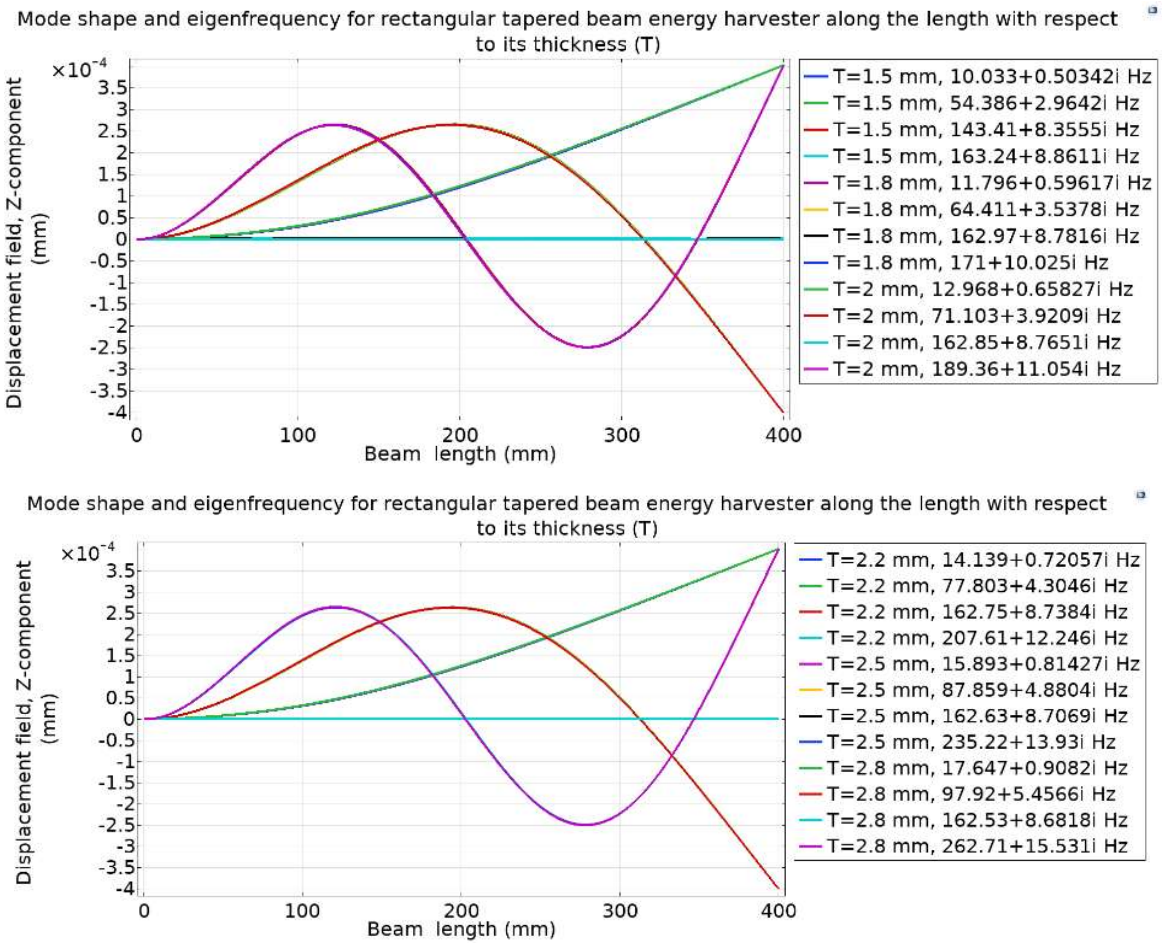


Figure 6-28 Eigenfrequency with the variable thickness for a tapered rectangular beam

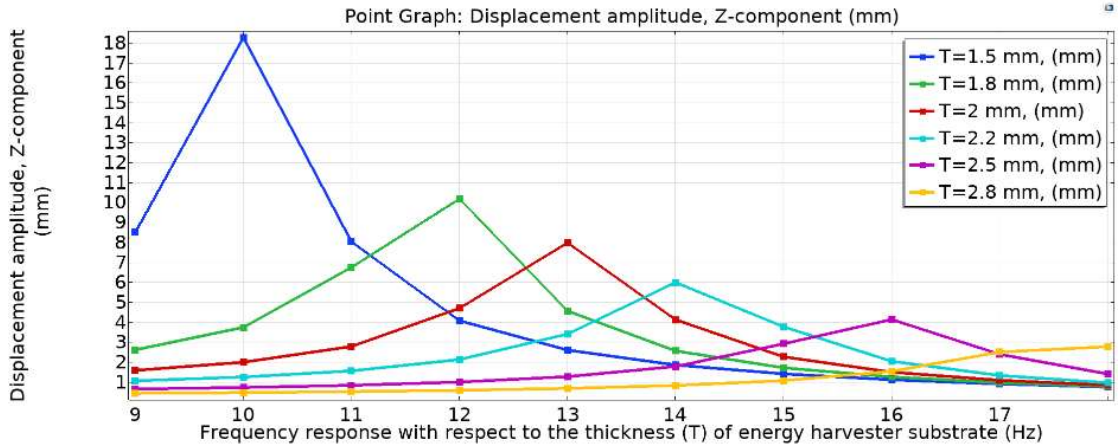


Figure 6-29 Parametric study for displacement varying thickness for a cantilever beam EH

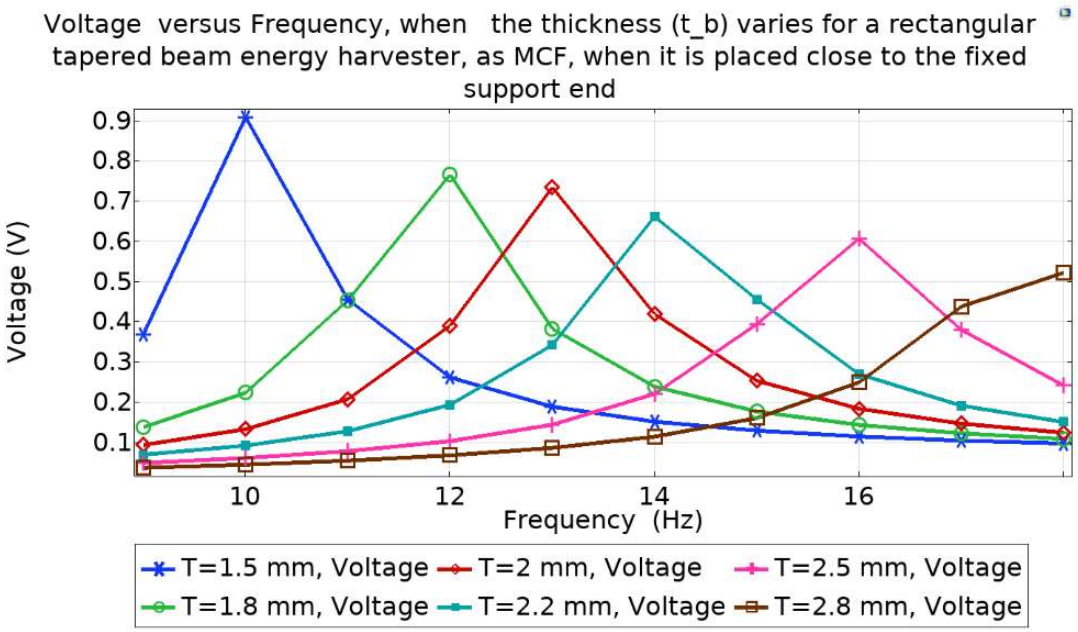


Figure 6-30 Parametric study for varying the thickness on Voltage and frequency

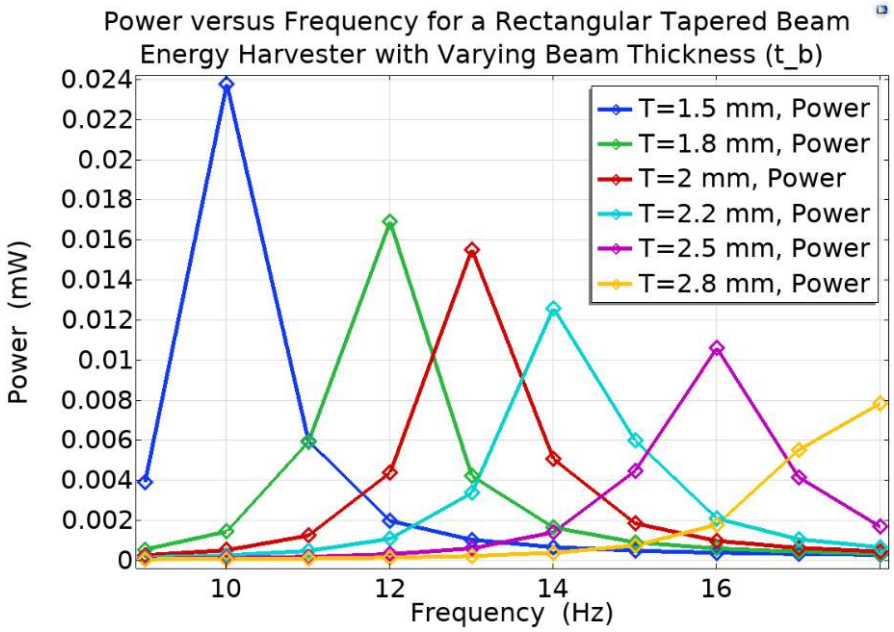


Figure 6-31 The effect of parametric study for varying the thickness of tapered beam EH

In Table 6-4, provides the resonance frequency, the peak output voltage and the output power of the tapered cantilever beam energy harvester for six different substrate thickness values from 1.5 mm to 2.8 mm. Results show clear and consistent trends in the relation between substrate thickness and electromechanical performance. The resonance frequency increased from 10.033 Hz to 17.647 Hz (about 76%) with the increase of the substrate thickness from 1.5 mm to 2.8 mm. This is expected behaviour because increasing the substrate thickness increases the bending stiffness of the beam, which directly increases the beam's natural frequency. This

trend confirms that the thicker the substrate the stiffer the structure and the higher the resonance frequencies.

From the Figure 6-30 and Figure 6-31,the output voltage decreased from 0.9 V at 1.5 mm to 0.52 V at 2.8 mm, a decrease of 42%, and the output power decreased from 0.024 mW to 0.0078 mW, a decrease of 67.5%. This inverse relation is because the thicker the substrate, the more resistant it is to be bending. Hence, for a given excitation, the maximum displacement amplitude and the strain induced in the piezoelectric layer are reduced. The MFC patch produces voltage and power proportional to the strain it is subjected to; thus, the greater the deformation of a beam, the higher the voltage and power it can generate. Thicker beams deform less and therefore generate less voltage and power.

The harvester is well balanced in terms of structural stiffness and electromechanical output in the recommended design range of 1.8 mm to 2.2 mm. Within this range, the resonant frequency increases moderately from 11.976 Hz to 14.139 Hz (18%), whereas the voltage and power output decrease more gradually (13.3% and 29.4%, respectively) than the more significant losses at larger thicknesses. This range is therefore a practical compromise, thin enough to keep enough beam flexibility and strain transfer to the MFC patch, but thick enough to maintain sufficient structural stiffness and a stable, high enough resonance frequency for reliable low frequency vibration harvesting.

Table 6-4 Voltage and power versus frequency for tapered beam EH with substrate thickness

Al Size	Output value		
Thickness (mm)	Resonance Frequency (Hz)	Peak output voltage (V)	Output power(mW)
1.5	10.033	0.9	0.024
1.8	11.976	0.75	0.017
2	12.968	0.72	0.015
2.2	14.139	0.65	0.012
2.25	15.893	0.60	0.0104
2.28	17.647	0.52	0.0078

Table 6-4 summarises the effect of substrate (aluminium) thickness on the resonance frequency, peak output voltage and output power of tapered cantilever beam energy harvesters. The resonance frequency increases gradually from 10.033 Hz to 17.647 Hz as the thickness of the aluminium substrate increases from 1.5 mm to 2.28 mm. This is due to the increase in stiffness of the beam for a thicker substrate which causes the natural frequency to shift higher.

Instead, the maximum output voltage and power output both decrease monotonically with the increasing thickness from 0.9 V and 0.024 mW at 1.5 mm to 0.52 V and 0.0078 mW at 2.28 mm. This negative correlation shows that the thinner substrate is exposed to larger bending strain under vibration, which can improve the piezoelectric effect and lead to larger voltage and power generation. Therefore, the results suggest that decreasing the substrate thickness is favourable for maximising energy harvesting output. However, this must be balanced with the concomitant shift in resonance frequency to match the target excitation source.

6.4. Optimisation by algorithm including parameters and constraints

The electrical output of a vibration-based piezoelectric energy harvester is strongly dependent on the interaction between the mechanical characteristics of the host structure and the electromechanical properties of the piezoelectric transducer [77]. The finite element model developed in the previous chapters can accurately predict the dynamic response of the M8514-P_2 Macro Fiber Composite (MFC) integrated with an aluminium cantilever beam; however, the baseline design does not necessarily provide the maximum electrical power output. The amount of power harvested depends on several design parameters, such as the position of the piezoelectric transducer, the stiffness of the supporting beam, and the inertial loading at the free end. Therefore, a systematic optimisation procedure is required to find the combination of design parameters that maximises the energy harvesting performance while maintaining the structural integrity and practical design limitations. The optimisation is implemented by combining the validated finite element model with the optimisation module, which allows for an automatic variation of selected design variables while repeatedly solving the electromechanically coupled system. The optimisation procedure considers the interaction of the structural dynamics of the cantilever beam and the electrical response of the piezoelectric transducer under harmonic excitation.

In the previous chapter, while the fundamental physics of piezoelectric cantilever energy harvesting is well modelled, the performance of these devices is critically dependent on their geometric design. The key parameters, including the geometric shape of the substrate, the position of the piezoelectric patch along the beam, the thickness of the substrate beam, and the magnitude of a tip mass, significantly influence the resonant frequency, strain distribution, and, ultimately, the harvested power. The operation of these devices is controlled by a complex interaction between the spatial position of the active piezoelectric element, the structural stiffness of the host beam, and the inertial properties introduced by the tip mass loading. The influence of this key parameter on output energy is determined by parametric sweep and

optimisation algorithms. Parametric sweep or parametric estimation, which models a discrete set of values for one or more parameters. This method is well-suited for finding approximate optimal regions and for making publication-quality parametric plots. It systematically varies one or more input parameters over a predefined range and solves the model for each distinct parameter configuration. In addition, a parametric sweep does not require an optimisation module and identifies all local and global optimum values [216]. The limitation of the parametric sweep method is to miss the optimum point. This does not find the exact optimum between points. An optimisation study automatically varies the design variables to either maximise or minimise a selected objective function, subject to specified constraints. The method uses multiple parameters simultaneously (Xp + tip mass + beam thickness + load resistance) and then switches to the optimisation module, using different algorithms.

This optimisation model was based on the BOBYQA algorithm (Bound Optimisation BY Quadratic Approximation) in the COMSOL Multiphysics Optimisation module. BOBYQA is a derivative-free optimisation algorithm particularly well-suited to this application, as it efficiently manages bound-constrained problems without requiring gradient information. The objective function is a peak power output from a frequency domain solution and is non-smooth and not amenable to easy differentiation [217–219].

6.4.1 Algorithm optimisation rectangular cantilever beam with MFC

For the rectangular beam with an MFC integrated to optimise the energy harvester, three design variables are chosen since they directly influence the strain distribution within the MFC and the electrical output. The first variable is the position of the MFC patch from the fixed end of the cantilever beam (x_{p}). This is because bending strain is maximum at the clamped support and decreases towards the free end. Hence, the position of the transducer plays a key role in the induced electric field and harvested power. The second variable is the thickness of the aluminium cantilever beam (t_{b}), which affects the structural stiffness, natural frequency, bending deformation, and strain transferred to the piezoelectric layer. The third variable is the tip mass (t_{m}), which changes the effective mass of the system, shifts the resonant frequency, and changes the vibration amplitude and strain energy available for conversion into electrical energy. The methods for energy harvesting optimisation on COMSOL are shown in Figure 6-32 and Table 6-5 Constraints of the optimisation parameter. It is a constraint that the input driving vibration frequency, should be within the range of 4 Hz to 20 Hz.

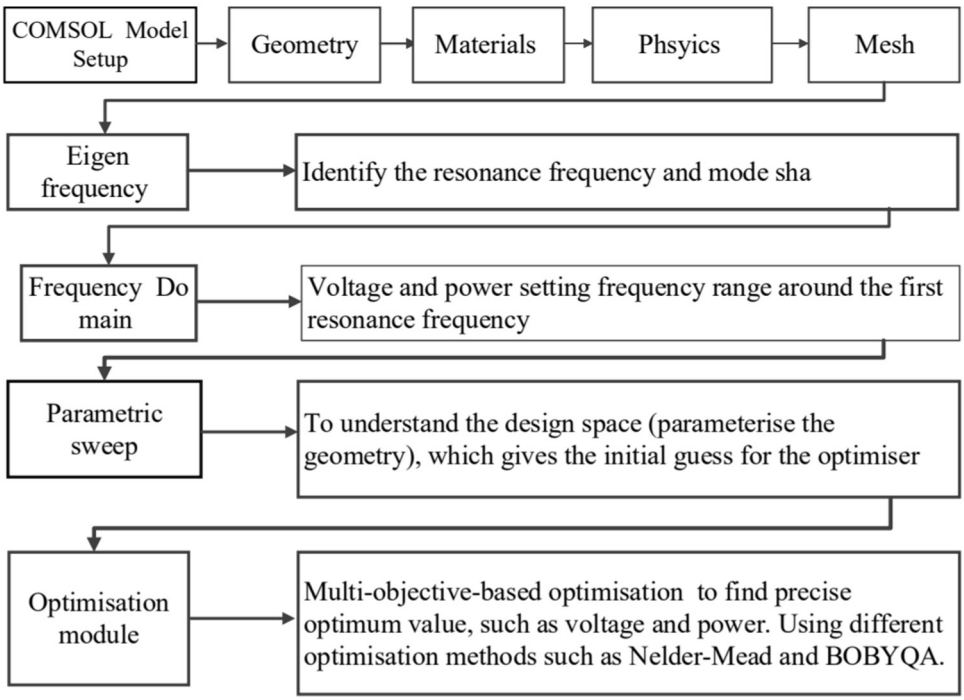


Figure 6-32 Flowchart for Optimisation of Energy Harvesting in COMSOL Multiphysics

Figure 6-32 shows the workflow of COMSOL Multiphysics for optimisation of an energy harvester. The first step in the COMSOL Multiphysics workflow is to set up the model, including the geometry, materials, physics settings and mesh for the piezoelectric energy harvester. Then the COMSOL Multiphysics workflow is used to perform an eigenfrequency study to determine the resonance frequency and the mode shape of the energy harvester. Then the COMSOL Multiphysics workflow runs a frequency domain study to compute the voltage and power output at the resonance frequency of the piezoelectric energy harvester. The COMSOL Multiphysics workflow proceeds with a sweep to explore the design space and provide a good first guess for the piezoelectric energy harvester. Finally, the COMSOL Multiphysics workflow enters an optimisation stage using methods such as Nelder-Mead and BOBYQA to find the best geometry and parameters that maximise voltage and power output for the piezoelectric energy harvester. The feedback of each stage into steps is indicated by the blue arrows, such that the COMSOL Multiphysics workflow can be considered as an iterative pipeline from setup through to resonance identification, response mapping, design-space exploration and final optimisation.The design variables were chosen from the geometric and operational parameters that directly affect the electromechanical performance of the MFC-based energy harvester. Which include the MFC patch position (x_p), the beam thickness (t_b), and the tip mass (t_m). All other geometric and material properties are fixed parameters (see Table 6-5). The goal is to maximize the output power at the optimal load resistance identified in

Chapter 5. The optimization is subject to several constraints: a stress constraint to ensure structural integrity, a geometric constraint to keep the patch within the beam length and bounds on the design variables. The problem is solved using a method based on the BOBYQA algorithm.

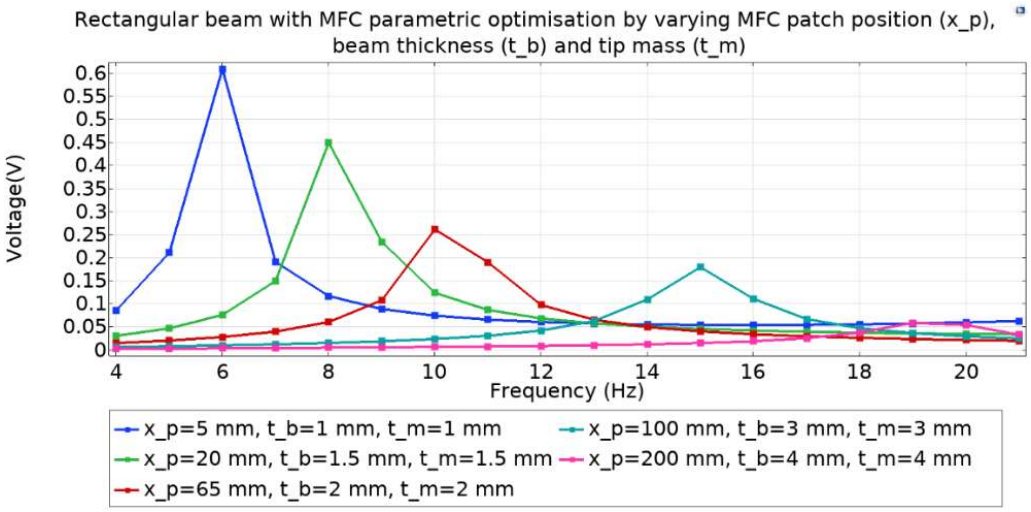
Table 6-5 Optimisation Parameters and Control Variables rectangular beam

Category	Symbol	Description	Initial value	Scale	Lower bound	Upper bound
Design variable	x_p	Distance from fixed end to MFC attached	65 mm	10 mm	5 mm	300 mm
Design variable	t_b	Aluminium beam thickness	2mm	1 mm	1 mm	4 mm
Design variable	t_m	Tip mass thickness	1 mm	1 mm	1 mm	1 mm
			1.5 g	2 g	2 g	15 g
Design variable	R_{load}	Load resistance	12kΩ	10kΩ	1	100kΩ
Fixed parameter	w_b	The width of beam	30mm	-		
Fixed parameter	Wp	The width of MFC	14mm	-		
Fixed parameter	L_b	Length of the beam	400 mm	-		

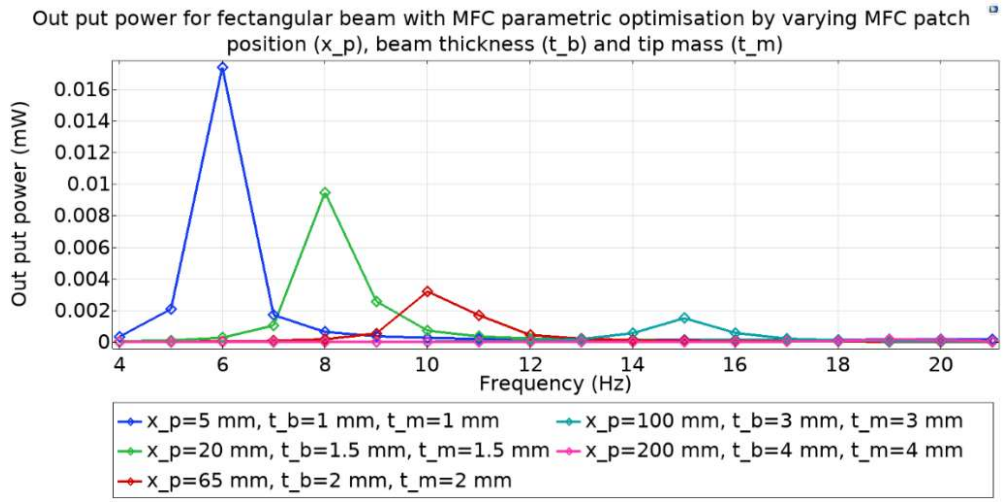
Figure 6-33, The initial parametric optimization aimed to determine the electrical outputs, specifically voltage and power, to enhance the peak power output during a frequency sweep ranging from 4 to 20 Hz. This frequency range encompasses many values around the first resonance frequency for optimising geometric parameters, including the varied positions of the MFC patch, alterations in beam thickener dimensions, and changes in tip mass thickness.

The initial optimisation concentrated on the primary parametric algorithm, as it frequently provides a comprehensive perspective of the design space. For problems involving precision or multiple variables, the next phase involved algorithm optimisation through multifunctional parameter design. Prior to numerical optimisation, a parametric optimisation analysis is conducted to assess the individual impact of each design variable on factors such as resonance frequency, stress distribution, output voltage, and harvested power. This preliminary analysis offers an understanding of the energy harvester's physical behaviour, identifies the most significant parameters, and sets appropriate limits for the optimisation variables. The following optimisation employs the Method of Bound Optimization BY Quadratic Approximation within the COMSOL Optimisation Module to determine the parameter combination that maximises

harvested power. The BOBYQA optimisation module, which is a derivative-free method, is particularly well-suited for this application. This optimisation resulted in an increase in power output from 0.017 mW in the parametric optimisation design to 0.028 mW in the optimised BOBYQA algorithm optimisation module configuration, with an improvement of 64.70%, as shown in Figure 6-34 (b) and (c), respectively.

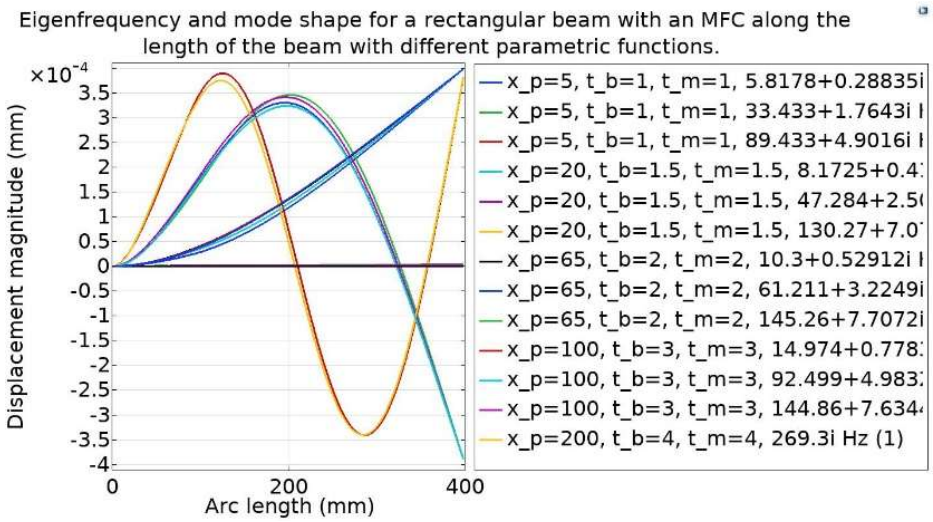


a) Voltage

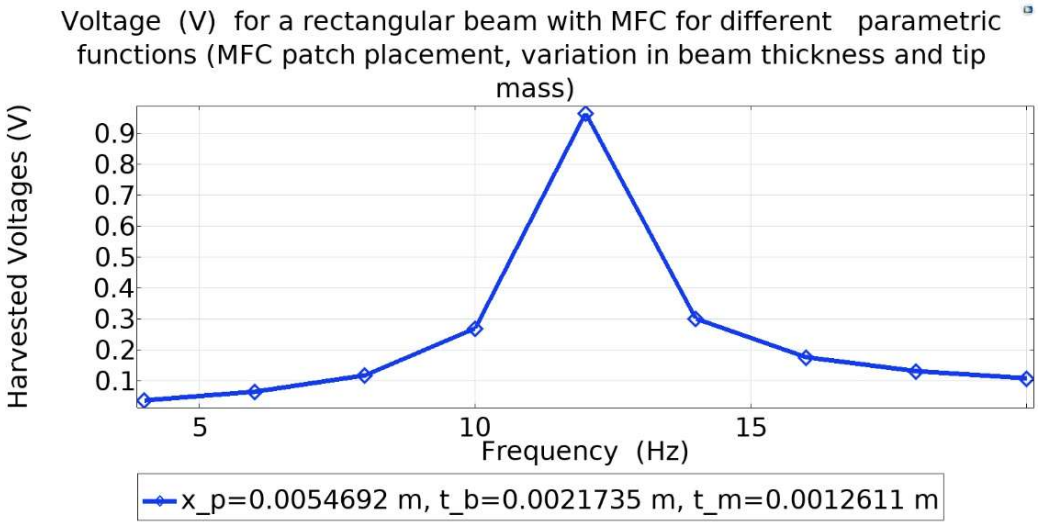


(b) Power

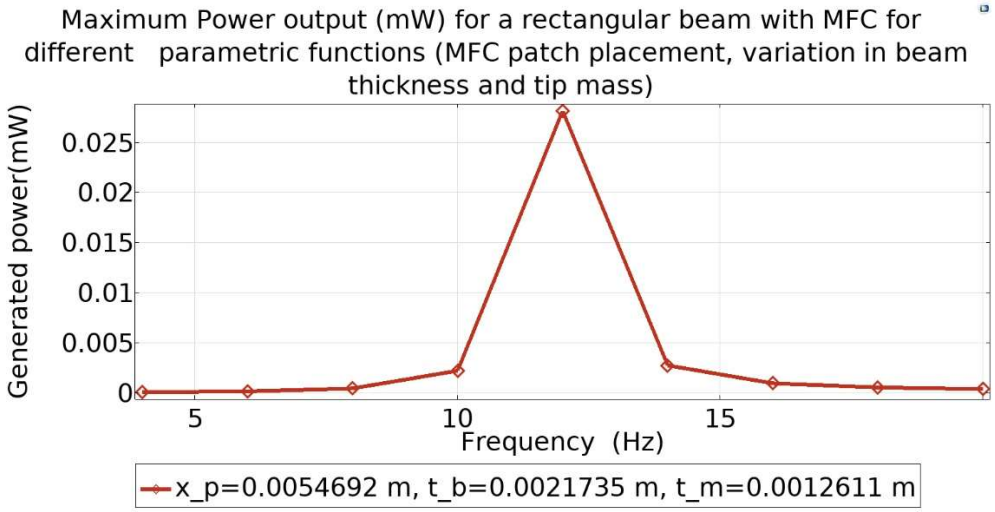
Figure 6-33 The influence of geometric parameters on voltage and output power



(a) Eigen frequency and mode shape



(b) The maximum Voltage r as a function of frequency for different parametric functions



c) The maximum power for different parametric functions

Figure 6-34 The optimum amplitude, voltage and outputs power

From Figure 6-34, the maximum optimisation of MFC position of (x_p = 5) mm, which is the lower bound defined in the task. Thus, over the range of designs investigated, the gathered power increases with the position of the MFC closer to the fixed end of the cantilever. This is consistent with the bending-strain distribution of the first vibration mode where the longitudinal strain is maximal close to the clamped end. As the MFC mostly functions in the d_{31} mode, the increase of strain results in a more significant electromechanical response, and consequently, an increased electrical power output.

Table 6-6 Optimisation result analysis for rectangular harvester

Quantity	Initial parametric design (mm)	Optimized design (mm)	Effect on the system	The effect on the output power harvested
MFC patch position (XP)	65	5	Increase the bending strain on MFC patch	As general increases voltage and power,
Beam thickness	2	2.2	Increases stiffness and natural frequency but reduces strain	Increases power until the beam becomes too compliant
Tip mass	1	1.26	Lowers resonance frequency and increases vibration amplitude	Improves power up to an optimum value before excessive stress or detuning occurs
Comparison of initial optimum approximation by parametric sweep and optimisation by algorithm module for rectangular beam with MFC				
Energy form	Initial design	Optimum design	Comparison	
Voltage (V)	0.6	0.95	58.33% higher	
Power (mW)	0.017	0.028	64.705% higher	

Table 6-6 shows the optimisation of the rectangular MFC based harvester design. When the MFC patch position changed from 65 mm to 5 mm, the bending strain of the harvester increased. When the beam thickness changed from 2 mm to 2.2 mm, the stiffness and natural frequency increased without excessively increasing the compliance of the beam. The increase of tip mass from 1 g to 1.26 g reduced the resonance frequency and optimised the vibration amplitude. A further increase in tip mass would generate excessive stress or detuning. The combined parametric modifications resulted in an improvement of the harvester output voltage from 0.6 V to 0.95 V (58.33% increase) and power from 0.017 mW to 0.028 mW (64.7% increase), demonstrating that the precise control of patch location, beam thickness and tip mass may significantly improve the energy harvesting efficiency. The optimisation led to an optimal MFC location of x_p= 5 mm, that is, the lower bound specified in the optimisation issue. The answer

for this limit has a clear physical interpretation. In the first bending mode of the cantilever beam the bending moment and longitudinal strain are maximum in the region adjacent to the fixed end and decrease towards the free end. Because the MFC mostly works in the d_{31} mode, its electromechanical behaviour is heavily dependent on the longitudinal strain in the host beam. Therefore, pushing the MFC towards the fixed end increases the strain imparted to the piezoelectric layer and subsequently increases the generated voltage and captured electrical power. That the optimum lies at the lower bound that, over the design interval of $5 \leq x_p \leq 300$ mm, the harvested power rises as the MFC is placed nearer to the fixed end. Therefore, $x_p = 5$ mm should be regarded as a boundary (active constraint) optimum within the defined design space, rather than as proof that 5 mm is intrinsically the global best location. This lower limit was chosen to avoid interference separation from the clamped region and to prevent conflicts with the mechanical fastening and bonding area.

6.4.2 Optimisation of a tapered rectangular cantilever beam with MFC configuration

Table 6-7 Design variables for the optimisation for the tapered beam

Design Variables					
Description	Symbol	Initial value (mm)	Lower bound (mm)	Scale (mm)	Upper bound (mm)
MFC position	x_p	65	5	10	100
Beam thickness	b_m	2	1	1	3
Tip mass thickness (mm) or gram(g)	t_m	1	1	1	3
		2	2	2	15
Load resistance (kΩ)	R_{load}	12	1	10	100 k
Frequency range (Hz)	f_n	10.61	4	2	22
Applied force (N)	F	0.2	0.1	0.2	0.5

For the tapered rectangular cantilever beam, the optimisation problem includes both geometric and operational design variables. Unlike the uniform beam (Table 6-6), the load resistance R_L and the applied force amplitude F are treated as design variables to account for the varying electrical impedance matching and excitation conditions inherent to the tapered geometry. Table 6-8 and Figure 6-35 show that the optimisation results showed that the maximum electrical power was achieved when the MFC patch was placed at approximately 5 mm from the fixed end of the cantilever beam. At this position, the MFC is under a large bending

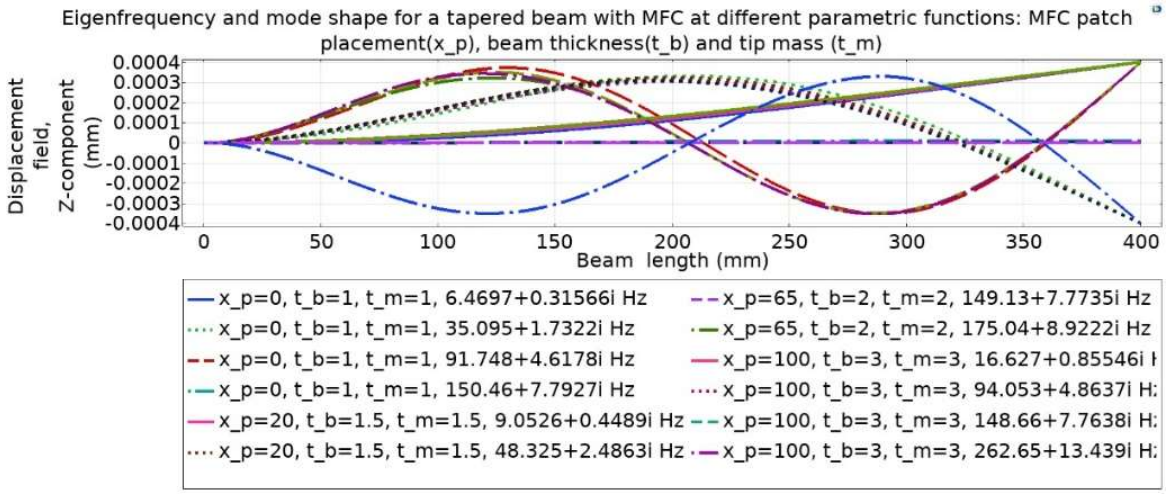
strain and still exhibits appreciable deformation, thereby making the conversion of electromechanical energy more efficient.

The optimum beam thickness was increased slightly from 2.00 mm to 2.17 mm. This change is quite small (about 7.83%), but it indicates that a slight increase in stiffness gives a more favourable balance between bending deformation and strain transfer to the piezoelectric layer. Overly thin beams lead to larger deflections and less structural stability, while overly thick beams reduce both bending strain and electrical output. Thus, the optimum thickness is a compromise between flexibility and stiffness.

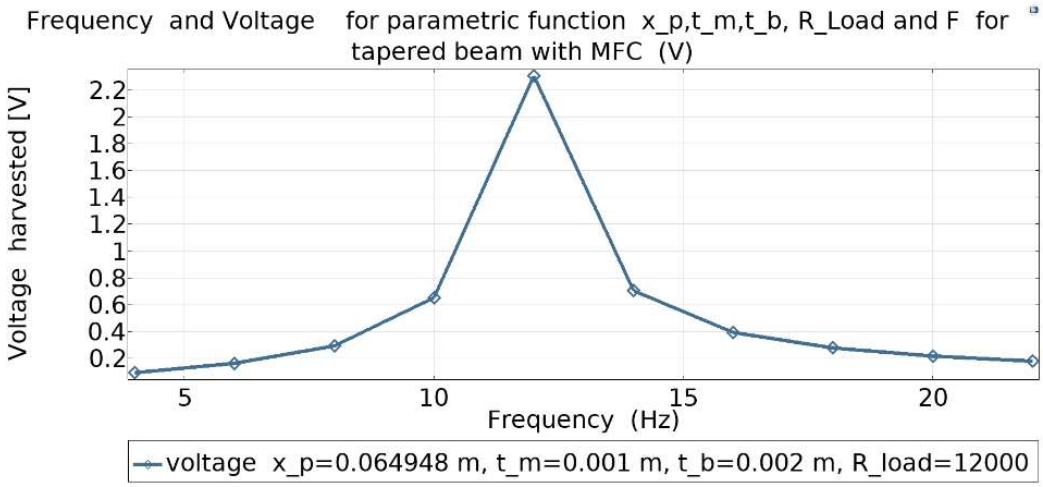
Finally, the optimised excitation force was increased from 0.20 N to 0.26 N, resulting in a larger vibration amplitude and thus higher strain in the MFC. However, the excitation force is an external operating condition and not a structural design parameter and should therefore be generally treated as a fixed input rather than an optimisation variable when evaluating the harvester design. The optimised design gave a maximum output voltage of around 2.30 V in Figure 6-35 (b) and harvested power of around 0.065 mW at a resonance frequency of 12 Hz as shown in Figure 6-35 (c). These results show that the appropriate choice of the placement of the MFC, tip mass, beam thickness, applied force, and load resistance for the structural parameters can significantly improve the performance of the piezoelectric energy harvester while meeting the design constraints.

Table 6-8 Optimisation result for tapered rectangular beam with MFC

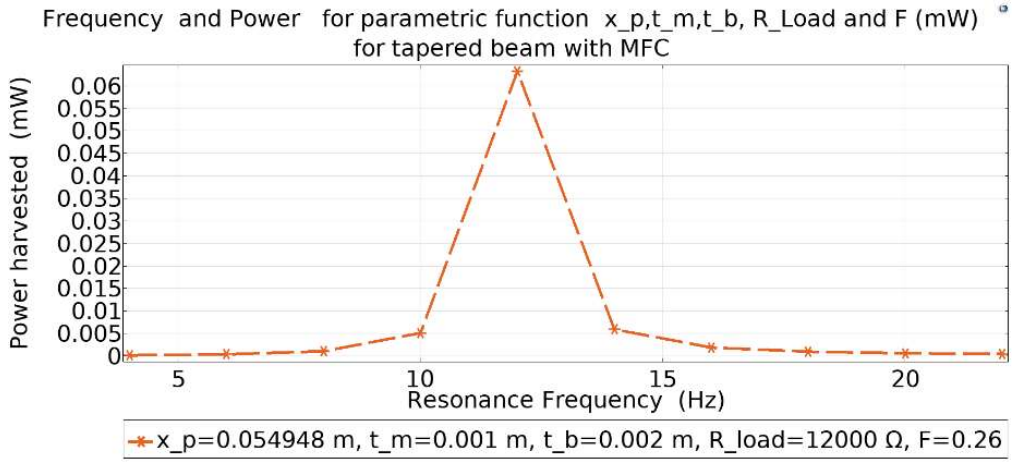
Output parameter		Parametric optimised	Design module optimised algorism	Change
1	Resonance frequency (Hz)	10.61	12	13.1%
2	Maximum output voltage (Vmax) (V)	1.15	2.3	100%
3	Maximum harvested power (Pmax) (mW)	0.028	0.065	132.14%
4	Beam thickness (tb) (mm)	2	2.17	8.5%
5	MFC patch placement (mm)	65	5.46	91.6%
6	Tip mass (mm)	1	1.12	12%
7	Resistance load (kΩ)	10	12	20%
8	Applied external force (N)	0.2	0.26	30%



(a)Eigen frequency and mode shape



(b) Voltage



(c) Power

Figure 6-35 Amplitude displacement and the optimised energy for tapered beam

Table 6-9 Comparison of Algorism optimised EH by rectangular and tapered models

Output Parameter	Rectangular beam	Tapered beam	Change (%)
Resonance frequency [Hz]	10.61	12	13.1
Voltage output [V]	0.95	2.3	142.1
Power Output [mW]	0.028	0.065	132.14

From the above models the optimisation study of the uniform rectangular cantilever beam with the integrated MFC patch showed significant improvements in the energy harvesting performance by tuning simultaneously three key design parameters.

MFC patch position (x_p), beam thickness (t_b), and tip mass dimension (t_m). The initial parametric design (Xp = 65 mm, t_b = 2 mm, tm = 1 mm) yielded an initial output voltage of 0.6 V and harvested power of 0.017 mW. After the optimisation, the MFC patch was found to be 5 mm from the fixed support, the beam thickness was increased to 2.2 mm, and the tip mass dimension was refined to 1.26 mm. The optimised output voltage and the peak harvested power were 0.95 V and 0.028 mW, respectively. This represented an enhancement of 58.33% and 64.7% respectively over the initial values. The tapered rectangular beam, which has a width profile that tapers from 30 mm at the fixed support to 20 mm at the free end, showed a significantly improved energy harvesting performance for all the output metrics compared to the uniform rectangular beam as can be seen from the results in Table 6-8 and the comparative summary on Table 6-9. From Table 6-8 parametric optimisation of the tapered beam resulted in a resonant frequency of 10.61 Hz, maximum output voltage of 1.15 V and peak harvested power of 0.028 mW. The resonant frequency was shifted to 12Hz, the maximum output voltage increased to 2.3V and a peak harvested power of 0.065mW was achieved following further significant improvements through optimisation with the BOBYQA design module algorithm. The results show change of 13.1%, 100% and 132.1% for the resonance frequency, voltage, and power, respectively, with the parametric optimisation baseline for the tapered rectangular configuration.

From Table 6-9: Comparison of Algorithm-Optimized Rectangular and Tapered Beam Models; The tapered rectangular beam after BOBYQA optimisation outperforms the conventional rectangular beam for all the three key performance parameters: resonance frequency, output voltage, and output power. The frequency of the tapered beam was 12 Hz which is an improvement of about 13.1% over the rectangular beam (10.61 Hz). This increase is attributed to the variation of mass and stiffness along the beam length due to the tapered

geometry, which leads to an increase in the fundamental natural frequency as compared to the uniform rectangular beam.

The output voltage saw the most substantial improvement, 2.3 V for the tapered beam versus 0.95 V for the rectangular beam, an increase of 142.1%. Such increase in voltage output is more than two-fold, indicating the better ability of the tapered geometry to concentrate the strain energy within the MFC patch region. The output power also showed a similar trend, where the tapered beam generated 0.065 mW against 0.028 mW for the rectangular beam which is an improvement of 132.14%. The power output is proportional to the voltage squared for a fixed load resistance. This is consistent with and supports the large voltage gain seen above.

The low resonant frequency of 12 Hz, the harvester is particularly suited to structural health monitoring (SHM) and machine condition monitoring applications on slow rotating or low frequency equipment such as conveyors, large motors, pumps and civil infrastructure where vibration frequencies of this order are typical [220]. These applications can use the harvester with strain gauges, MEMS accelerometers, or vibration sensors for self-powered wireless condition monitoring without any need of wired power infrastructure or periodic battery maintenance [3].

Chapter six conclusion

This chapter has presented a local parametric and algorithmic optimisation modelling approach for MFC-P2 piezoelectric energy harvesters. The efficiency and applicability of the proposed optimised output energy and fundamental frequency were demonstrated by comparing the rectangular and tapered rectangular beam configurations as summarised in Table 6-9. From the performance of energy harvesting devices based on MFC-P2 type piezoelectric materials was studied and evaluated using four criteria. First, a rectangular and tapered unimorph configuration with the MFC fixed at 65 mm from the fixed support was considered. Second, the same volume of beam and MFC piezoelectric materials with the tip mass fixed at the free end of the beam was used. Third, the same geometry with the MFC placed at various positions on the beam was examined. Lastly, the thickness of the cantilever beam was changed while keeping the same materials and geometry.

In the design of two cantilever beams, featuring both normal rectangular and tapered shapes, the tapered configuration yields the highest output voltage of 0.45 V when using the same MFC-P_2 piezoelectric material. Thus, altering the beam's shape and ensuring uniform strain along the cantilever's length are crucial for maximizing voltage from vibrations in piezoelectric energy harvesting (PEH). The process of optimizing the geometrical shape is essential for creating a

compact and efficient energy harvester capable of functioning across various frequencies. The rectangular 3D unimorph cantilever beam, both with and without a proof mass, is constructed using aluminium as the substrate and MFC as the piezoelectric material, with a thickness of 0.38 mm. Simulations were conducted to assess displacement, resonant frequency, changes in generated voltage, and output power. The fundamental resonance frequency, voltage, and power of the rectangular beam without tip mass are 10.976 Hz, 0.28 V and 0.0032 mW, respectively. The harvester with the same geometric structure and small tip mass was simulated to generate a voltage of 0.347 V at the fundamental frequency of 10.456 Hz. The maximum output power in this simulation is 0.004 mW. The power is 1.24 times the power of a rectangular beam without tip mass

The third method is variation of the substrate thickness. The fundamental resonance frequency of the MFC unimorph with Al substrates increases from 10 Hz to 17.6 Hz as the substrate thickness increases from 1.5 mm to 2.8 mm. The maximum voltage and power outputs for a 10 kΩ resistive load are achieved at an Al substrate thickness of 1.8 mm. This numerical optimisation is in good agreement with both theoretical and experimental results. The algorithm optimisation results presented in this thesis demonstrate that local optimisation methods can be used to achieve meaningful performance gains in MFC-based piezoelectric energy harvesters, specifically the BOBYQA algorithm applied through COMSOL's parametric optimisation framework.

The conventional rectangular beam and the tapered rectangular beam configurations were optimised using the Bound Optimisation BY Quadratic Approximation (BOBYQA) algorithm available in COMSOL Multiphysics to further improve the performance of the piezoelectric energy harvester. BOBYQA was chosen as it is good at solving nonlinear optimisation problems with multiple coupled design variables, without the need for analytical derivatives. The harvested power and voltage output was significantly improved for both the rectangular and tapered beam configurations, with the tapered geometry outperforming the conventional design for all optimisation criteria [103,121]. For the conventional rectangular beam, BOBYQA optimisation produced a maximum harvested power of 0.028 mW and an output voltage of 0.95 V at a resonant frequency of 10.61 Hz, representing improvements of 58.33% and 64.7% over the parametric design, respectively. The optimal configuration placed the MFC patch 5 mm from the clamped end, with a beam thickness of 2.2 mm and a tip-mass dimension of 1.26 mm.

Using the same optimisation approach, the tapered beam achieved a maximum power of 0.065 mW and a voltage of 2.3 V at 12 Hz, increases of 100% and 132.1% over its parametric

baseline. From the tapered geometry, the energy is optimised in comparison to the rectangular geometry, also corresponding to increases of more than 132% in power and 142% in voltage, thus confirming the mechanical superiority of the tapered geometry. For the tapered design, the MFC patch was placed at a distance of 5.46 mm from the fixed end with a beam thickness of 2.17 mm, a tip-mass size of 1.12 mm, a load resistance of 12 kΩ and an excitation force of 0.26 N. The sensitivity analysis indicated that the most influential parameter was the MFC patch location, followed by the excitation force, the tip-mass dimensions, the beam thickness, and the load resistance.

the overall model result and improvement in the performance of the harvester through the successive stages of the study, from the initial validated model to the final algorithm-optimised design. The analytical, finite element and experimental models of the baseline rectangular unimorph configuration, with resonance frequencies clustering between 10.2 Hz and 10.96 Hz and power outputs in the range of 0.0027 - 0.0032 mW, confirming the validity of the modelling approach prior to optimisation starting. The addition of a tip mass increased the maximum voltage to 0.39V and power to 0.0045mW, and the combination of a tapered geometry with a tip mass further increased these figures to 0.65V and 0.0082mW, also confirming that geometric tailoring alone, without the need for algorithmic optimisation, already produces substantial gains compared to the baseline unimorph design. The biggest improvements, however, are made by the BOBYQA-optimized models. The optimised rectangular beam reached 0.95 V and 0.028 mW, while the optimised tapered beam provided the best overall performance in the study with a maximum voltage of 2.3 V and power output of 0.065 mW at a resonance frequency of 12 Hz. Overall, there is around 8.7 times increase in voltage, and more than 22 times increase in power output between the initial analytical model and the final BOBYQA-optimised tapered beam design. This clearly shows that the combined effect of tapered geometry and systematic algorithm-based optimisation of MFC patch placement, tip mass, beam thickness and load resistance is significantly more effective than relying on geometric modification or parametric variation alone.

Table 6-10 Summary of the results from the initial model to the fully optimised design

Model	Geometric configuration	Resonance frequency(Hz)	Maximum Voltage (V)	Maximum Power(mW)
Analytical model	Rectangular beam with rectangular unimorph MFC	10.69	0.265	0.00291
Finite element model	Rectangular unimorph	10.976	0.28	0.0032
Experimental method	Rectangular unimorph	10.2	0.245	0.00272
Finite element method	Rectangular beam with tip mass	10.45	0.39	0.0045
Finite element method	Tapered rectangular beam with tip mass	12.42	0.65	0.0082
BOBYQA optimisation	Rectangular beam (optimum)	10.61	0.95	0.028
BOBYQA optimisation	Tapered beam (optimum)	12	2.3	0.065

Table 6-10 summarises the evolution of the piezoelectric energy harvester performance through the seven modelling stages of progressively increasing refinement, from the initial analytical model to the fully optimised design. For the analytical model with a rectangular beam and rectangular unimorph MFC, the resonance frequency was 10.69 Hz, the maximum voltage was 0.265 V, and the maximum power was 0.00291 mW. This was validated by a finite element model and an experimental method, both of which demonstrated reasonably consistent results (10.976 Hz/0.28 V/0.0032 mW and 10.2 Hz/0.245 V/0.00272 mW respectively), confirming the baseline modelling approach as dependable.

The inclusion of a tip mass in the rectangular finite element model significantly enhanced the output, raising the maximum power to 0.0045 mW and voltage to 0.39 V, thus illustrating the positive impact of inertial loading at the free end. The rectangular beam was tapered for further improvement with the tip mass kept. The power output and voltage were increased to 0.0082 mW and 0.65 V, respectively, indicating the advantage of geometric shaping in strain distribution and energy conversion. However, the biggest improvements were achieved with the BOBYQA optimisation algorithm. By optimisation of the rectangular beam configuration, the maximum power and voltage were increased to 0.028 mW and 0.95 V respectively, nearly ten times that of the original analytical model. The tapered beam optimised by BOBYQA exhibited the best overall performance throughout the entire study with a resonance frequency of 12 Hz, a peak voltage of 2.3 V and a maximum power of 0.065 mW.

Overall, the results highlight a distinct and progressive enhancement in the energy harvesting performance as the model transitioned from a simple analytical representation to a fully optimised tapered beam design. The final BOBYQA-optimised tapered beam configuration resulted in power output and voltage increase of 22 and 8.7 times respectively in comparison to the initial analytical model, demonstrating that the combination of geometric tapering and tip mass loading with the algorithm-based optimisation (BOBYQA) is very effective in maximising the electrical output of MFC-based piezoelectric energy harvesters.

Chapter 7 Conclusions and Future Work

This thesis has presented an integrated framework to design and optimise MFC-P2 based piezoelectric vibration energy harvesters. . In future work, this framework can be extended to consider the effect of the tip (proof) mass on the resonant tuning and strain distribution, the development of multi-modal and broadband harvesting configurations to increase the effective operating bandwidth of the harvester, and further experimental validation of the tapered-beam and multi-patch configurations for realistic, variable-frequency ambient vibration sources.

7.1. Conclusion

The framework has integrated analytical modelling (Euler–Bernoulli beam theory with electromechanical coupling), finite element simulation (COMSOL Multiphysics) and gradient-free optimisation (BOBYQA/COBYLA) for rectangular and tapered cantilever beam configurations. The model has been validated with experimental measurements throughout. The good consistency between theoretical, numerical and experimental results for natural frequency, generated voltage and harvested power confirms the validity of the proposed modelling and optimisation approach. Systematic optimisation of the position of the MFC patch and the load resistance led to measurable improvements in harvested power when compared to the baseline (non-optimised) configurations. The analytical, finite element method, experimental, and optimisation studies detailed in this thesis offer a validated and increasingly refined comprehension of the behaviour of an MFC-based piezoelectric cantilever harvester, how its performance can be greatly enhanced through geometric design. Initially,
a thorough review of recent portable devices for vibration-based energy harvesting was conducted. Piezoelectric energy harvesting techniques have garnered considerable interest in the development of vibration-based energy harvesters due to their compatibility with standard micromachining processes and their ability to function without an external voltage supply, unlike other vibration energy harvesting methods. Over the past few decades, piezoelectric energy harvesting from vibration sources has become prevalent, leading to numerous studies in this area. The focus of this thesis has been theoretical and numerical modelling, experimental investigation, and geometric efficiency enhancement or optimisation of geometric-based energy vibration harvesters using non-classical Macro Fiber Composite (MFC) piezoelectric materials.

Since the early development of energy harvesting technologies, classical PZT-based harvesters have demonstrated that ambient vibrations can be effectively converted into useful electrical energy, particularly in cantilever beam configurations. However, PZT materials are

very stiff and difficult to apply, especially to curved structures. The design of PZT energy harvesters requires careful adaptation to each targeted vibration source to achieve maximum efficiency. Non-classical MFC piezoelectric materials (PEMs) offer greater flexibility, environmental compatibility, lightweight design, and easier integration into wearable devices, biomedical applications, and smart structural systems. The use of this material for energy harvesting is expanding because it can convert clean energy into electrical energy to power small electronic devices.

In Chapter Three, piezoelectric Macro Fiber Composite (MFC) and aluminium (Al) substrate materials were used along with MFC patches as substrates to harvest energy from vibrating sources and excitation caused by an externally applied point load. A theoretical unimorph linear model was developed for an aluminium cantilever beam integrated with a Macro-Fiber Composite (MFC) piezoelectric patch. Mathematical models were analysed and developed based on Euler–Bernoulli and Rayleigh beam theory, composite beam bending stiffness, piezoelectric constitutive relations, modal analysis, and a resistive electrical load model. It was used to predict the beam displacement, strain in the MFC patch, resonance frequency, generated voltage, and harvested electrical power.

The analysis of the results indicates that the beam is sufficiently flexible and well-suited to low-frequency energy harvesting applications. The findings reveal that the harvester operates at a resonant frequency of about 10.69 Hz. Under excitation at this frequency, the output voltage and power generated by the harvester were measured as 0.265 V and 0.0028 mW, respectively.

Chapter Four introduces the numerical model developed for the same substrate materials and MFC piezoelectric layer. While the numerical analysis and simulations focus on the fundamental vibration mode, the model is formulated using linear constitutive equations and incorporates the mode-dependent locations of strain nodes. The energy harvesting behaviour of piezoelectric transducers under external mechanical loading was investigated using Multiphysics finite element (FE) simulations in the commercial package COMSOL Multiphysics, and the accuracy of the analytical models was confirmed.

Finite element analysis enabled an in-depth investigation of vibration mode shapes, stress distributions, electric potential fields, and power output behaviour that cannot be directly captured using simplified analytical models. The simulations produced a maximum power output of approximately 0.0032 mW at a resonant frequency of 10.96 Hz, in very close agreement with the analytical prediction. This strong consistency between the two modelling approaches confirms the validity of the theoretical assumptions and enhances confidence in the

proposed electromechanical representation. Consequently, the combined application of analytical and finite element methods provides a robust framework for predicting the performance of vibration energy harvesters prior to prototype fabrication. This modelling approach significantly reduces development time and experimental expenses, while also enabling rapid evaluation of alternative structural configurations. In addition, the validated numerical model forms the basis for the optimisation investigations presented in the subsequent chapters of this thesis, where the influences of beam geometry, tip mass, MFC patch location, beam thickness, and electrical load resistance on energy harvesting effectiveness are systematically analysed.

The analytical and finite element models were additionally validated through experiments conducted on an MFC-P2 unimorph piezoelectric energy harvester bonded to an aluminium cantilever beam. A dedicated experimental setup was developed to record the harvester's voltage and power output under controlled harmonic excitation. The experimental results were then compared with the analytical solutions and finite element results to assess the precision and robustness of the proposed modelling approach. The experimental study verified the accuracy of both the analytical and numerical models. The measured resonance frequency of the harvester was about 10.2 Hz, closely matching the analytically predicted 10.69 Hz and the finite element prediction of 10.96 Hz. Under external actuation voltage, the unimorph device produced an output voltage of roughly 0.245 V and an electrical power of 0.00272 mW across a maximum 12 kΩ load. The strong correlation among analytical, numerical, and experimental findings indicates that the proposed modelling framework reliably represents the coupled electromechanical response of the MFC-based vibration energy harvester. This validation supports the use of the developed models for design, analysis, and optimisation, reducing the dependence on extensive and expensive experimental testing.

The study concentrated on enhancing the vibration energy harvester's performance through methodical parametric optimization after the model was validated. The electrical output of piezoelectric harvester is strongly dependent on structural and electrical characteristics. Therefore, a detailed analysis was conducted to establish the effect of important design parameters on the harvested voltage, power output, and resonance frequency.

Several significant design factors, including beam geometry, MFC patch position, beam thickness, tip-mass dimensions, electrical load resistance, and excitation force, were considered during optimization. These factors affect the piezoelectric layer's strain distribution, which in turn affects the electromechanical energy conversion efficiency. In COMSOL Multiphysics, a

coupled Multiphysics optimization model was created to assess how the structural and electrical domains interact and find configurations that maximise the harvested power output.

The energy harvesting performance by the size or density of the tip mass, adding a large tip mass to a cantilever-based piezoelectric energy harvester poses several challenges. Overloading may lead to a decline in stability, performance, and durability of the system. So, for the proper optimization, a balance between the tip mass and the beam stiffness is required so that the harvester can well match the ambient vibration conditions without exceeding the mechanical and electrical limits of the piezoelectric material. Another method of optimization approach is MFC patch placement. From this method, the results obtained from the variable MFC placement show that the maximum power value of the first resonance mode is achieved at the MFC location between 0 mm and 65 mm. The strain is near zero at the MFC near the free end of the cantilever, and the voltage at this point is near zero.

A suitable and effective approach for many real industrial energy-harvesting scenarios is to use an off-resonance strategy that utilizes MFC patches directly attached to areas of maximum strain. The MFC's flexibility, conformability, and anisotropic force coupling make it an ideal component for such an approach. Based on the results of this thesis, areas of high strain or strain nodes can almost always be identified on a structure, machine, or vehicle oscillating in a bending mode. Attaching the MFC directly to these areas allows the available vibration energy from the structure to be harvested independently of specific resonance constraints. Applying the MFC directly to the structure first requires identifying the area with the highest strain. The efficiency of energy harvesting cannot be maximized by selecting
a high piezoelectric coefficient alone. Successful harvesters require the right material in the right structure, operating at the right frequency. Improving energy harvester performance for different vibration sources will enable the design of more efficient application-specific devices adapted to a variety of environmental conditions.

In the optimisation part, this study has shown that the systematic multi-variable optimisation of the MFC-integrated cantilever beam energy harvesters using the derivative-free BOBYQA algorithm within the finite element framework of COMSOL Multiphysics leads to appreciable and quantifiable improvements in the harvested electrical power and output voltage. The MFC patch position was identified as the dominant design parameter for both geometric configurations with its optimisation relative to the fixed support boundary providing the biggest single contribution to performance improvement. The tapered beam geometry further improved

the strain distribution more uniformly and obtained the maximum harvested power of 0.065 mW and output voltage of 2.3 V at resonant frequency of 12 Hz under optimised conditions.

7.2. Future work recommendation

The work presented in this thesis provides a good basis for further development of modelling accuracy and efficiency of piezoelectric energy harvesters for powering small electronic devices. The findings suggest a number of directions for future work. From a modelling point of view the thesis considered linear deformation of the harvester, which is a reasonable assumption as the ambient vibrations considered are at low resonance frequencies. However, if the excitation frequency varies to a larger extent, nonlinear deformation, temperature effects, and losses of the circuit should be included in future models. The effects of mechanical damping in combination with other geometrical changes such as change in piezoelectric thickness are out of the scope of this work but are worth further investigation. More detailed knowledge of the behaviour of mechanical damping would be useful in particular in two situations: when varying several geometric parameters simultaneously, as damping was fixed in the parametric analysis of this study, and at higher acceleration levels where damping was found to increase with base excitation at a rate that was markedly different between samples. A better understanding of this variation would improve the reliability of the theoretical models developed here. Also note that since this thesis focused on a unimorph configuration, a natural next step is to extend the modelling and optimisation work to bimorph harvesters was recommended.

Further , optimise the added mass by varying its location and dimensions and test the model at a range of electrical load resistances to find where maximum energy harvesting system is also recommended. A particularly promising direction is data-driven optimisation, where COMSOL is used in conjunction with MATLAB to perform faster response-surface based optimisation. Such an approach could significantly reduce the time and cost of exploring large design spaces, whether it's trying out new materials, geometries, or circuit configurations. That said, any machine learning or surrogate-modeling used for this purpose should be based on physical principles and validated against experimental data rather than being a black box. Additive manufacturing and printed electronics also provide interesting opportunities in this direction, as they can produce piezoelectric structures with spatially varying properties, embedded electrodes, or even integrated circuitry, all of which are compatible with newer materials and flexible device designs. The results of this thesis demonstrate that the simultaneous optimisation of beam geometry and transducer location can result in a significant

improvement in the electrical power output of tapered cantilever harvesters and that this improvement can be achieved without sacrificing the structural integrity of the design.

In addition, this thesis can be extended to the development of multi-modal and broadband harvesting configurations to increase the effective operating bandwidth of the harvester, and further experimental validation of the tapered-beam and multi-patch configurations for realistic, variable-frequency ambient vibration sources

The methodology developed here should be a useful starting point for this future work and, more generally, for continued progress towards efficient, dependable, and sustainable piezoelectric energy harvesting.

List of scientific achievements

A. Publication related with my PhD thesis:

1. **D.G. Wakshume** and M.Ł. Płaczek, Optimizing Piezoelectric Energy Harvesting from Mechanical Vibration for Electrical Efficiency: A Comprehensive Review, *Electronics (Switzerland)* 13 (5) (2024). DOI: 10.3390/s25103071

2. **Wakshume DG**, Płaczek MŁ. Mathematical Modelling and Finite Element Simulation of the M8514-P2 Composite Piezoelectric Transducer for Energy Harvesting. Sensors 2025; 25:3071. https://doi.org/10.3390/s25103071.

B. Book chapter/ monograph and international conference participation

1. **Wakshume Demeke**, Płaczek Marek: Composite piezoelectric materials for mechanical vibration energy harvesting: modeling and application, In: Materiały i technologie XXI wieku. XXVI Międzynarodowa studencka konferencja naukowa, 22 maj 2025, Katowice. Materiały konferencyjne. Książka abstraktów / Maciąg Tomasz (eds.), 2025, pp.56-56, ISBN 978-83-68390-18-6

2. **Wakshume Demeke,** Płaczek Marek: Composite piezoelectric materials for mechanical vibration energy harvesting: modeling and application, In: Mechanical Engineering for Future Development. MT2025 / Bonek Mirosław (eds.), 2025, Wydawnictwo Politechniki Śląskiej, pp.132-135, ISBN 978-83-68390-24-7

3. **Wakshume Demeke:** Piezoelectric energy harvesters' contribution to sustainable energy transformation, In: Zrównoważony rozwój i Europejski Zielony Ład dyktatami doskonalenia warsztatu naukowca / Buzek Jerzy, Kretek Henryk, Staniszewski Michał (eds.), Monografia / Politechnika Śląska, 2024, no. 1032, Wydawnictwo Politechniki Śląskiej, pp.369-378, ISBN 978-83-7880-962-3

4. **Wakshume D**, Płaczek M. Mathematical modelling and analysis of unmorph non-classical piezoelectric transducer for energy harvesting. In: Duda S, Jureczko P, Machoczek T, editors. XV Warsztaty Naukowe Studenckiego Koła Mechatroniki (15th Scientific Workshop of the Mechatronics Student Club). Gliwice, Poland: Wydawnictwo Katedry Mechaniki Teoretycznej i Stosowanej, Politechnika Śląska; 2024. p. 79–88. ISBN: 978-83-601028-2-4.

5. **Wakshume D**, Płaczek M. Development of a numerical simulation model of systems containing piezoelectric Macro Fiber Composite transducers. In: Duda S, Jureczko P, Machoczek T, editors. XIV Warsztaty Naukowe Studenckiego Koła Mechatroniki (14th

Scientific Workshop of the Student Mechatronics Club). Gliwice, Poland: Wydawnictwo Katedry Mechaniki Teoretycznej i Stosowanej, Politechnika Śląska; 2023. p. 113–120. ISBN: 978-83-601028-0-0

6. **Wakshume Demeke**, Płaczek Marek: Simulation of advanced MFC piezo electric materials for energy harvesting from mechanical vibration of beam, In: The 12th International Conference on Modern Manufacturing Technologies in Industrial Engineering. ModTech 2024. Book of abstracts, 2024, ModTech Publishing House, pp.81-81

7. Płaczek Marek, Degefa Tolera, Wakshume Demeke, Molla Dessalew: Mathematical and computer aided modelling of systems for energy harvesting and technical condition monitoring witch MFC piezoelectric transducers, 2023, 5th Polish Congress of Mechanics. 25th International Conference on Computer Methods in Mechanics 2023, paper presented.

8. **Wakshume Demeke**, Płaczek Marek: Optimizing the performance of MFC-based piezoelectric for energy harvesting under trans-verse vibration excitation (ModTech-2025)

9. **Wakshume Demeke**, Płaczek Marek: Mathematical and computer aided modelling of systems for energy harvesting and technical condition monitoring witch MFC piezoelectric transducers (5th Polish Congress of Mechanics. 25th International Conference on Computer Methods in Mechanics (PCM - CMM 2023), 2023, 04-09-2023 - 07-10-2023, Gliwice, Polska).

C. Internship and mobility participation

1. Demeke Wakshume. Short mobility: Think Innovation Week (ORION seminar) held from 1 to 9 July 2026 at ENSGSI (École Nationale Supérieureen Génie des Systèmes et de innovation), Nancy, France. It combines creativity, entrepreneurship, and prototyping through three complementary blocks, designing a business model for an international market; and Block 3, prototyping innovative ideas.

2. Demeke Wakshume. The 2026 Edition of the summer school CEAD_Circular Engineering Across Disciplines: Rethinking Electrification: Powering the Electrified Everything. By Hasselt University and KU Leuven University, Belgium. on site from 3 May to 8 May 2026virtually from 9 May to 20 May 2026. The training school can count for up to 3 ECTS.my Final grade: 16/20 - ECTS-grade: B.

3. Demeke Wakshume. Doctoral Internships: Differential Geometry of Classifiers participation in the Bell-type experiment with human involvement (EEG + serious game). From April 19.04.2026 to June 20.05.2026. Austria, Vienna. After the internship, I registered for one course

as part of my PhD. Then I obtained an award of five (5) marks after the completion of the internship.

4.Demeke Wakshume: Poster presentation on the title of Piezoelectric energy harvesters' contribution to sustainable energy transformation: In recognition of the participation in different lectures, field trips and workshops, PhD Journey 2024, which was held at the Montan university Leoben from 5-18 November and 25 - 29 November 2024, in Leoben, Austria.

References

1. D.G. Wakshume and M.Ł. Płaczek, Optimizing Piezoelectric Energy Harvesting from Mechanical Vibration for Electrical Efficiency: A Comprehensive Review, Electronics (Switzerland) 13 (5) (2024).
2. C. Covaci and A. Gontean, Piezoelectric energy harvesting solutions: A review, Sensors (Switzerland) 20 (12) (2020) 1–37.
3. R. Mohamed et al., Design of Piezoelectric Energy Harvester Single Cantilever Beam for IoT applications and Micro-electronic devices, Jurnal Kejuruteraan 37 (1) (2025) 489.
4. S. Roundy, P.K. Wright, and J. Rabaey, A study of low level vibrations as a power source for wireless sensor nodes, Comput. Commun. 26 (11) (2003) 1131–1144.
5. S.R. Anton and H.A. Sodano, A review of power harvesting using piezoelectric materials (2003–2006), Smart Mater. Struct. 16 (3) (2007) R1.
6. J. Ghazanfarian, M.M. Mohammadi, and K. Uchino, Piezoelectric Energy Harvesting: A Systematic Review of Reviews, Actuators 10 (12) (2021).
7. A. Erturk and D.J. Inman, Mechanical considerations for modeling of vibration-based energy harvesters, (2007).
8. D. Shen, S.Y. Choe, and D.J. Kim, Analysis of piezoelectric materials for energy harvesting devices under high-g vibrations, Japanese Journal of Applied Physics, Part 1: Regular Papers and Short Notes and Review Papers 46 (10 A) (2007) 6755–6760.
9. Y. Zhang, Piezoelectric based energy harvesting on low frequency vibrations of civil infrastructures, Louisiana State University and Agricultural & Mechanical College, (2014).
10. M. Bassetti et al., Analysis and modeling of a piezoelectric energy harvester for powering a wireless sensor, in Active and Passive Smart Structures and Integrated Systems 2013, SPIE, (2013): p. 86882A.
11. M. Matak and P. Šolek, Harvesting the Vibration Energy, American Journal of Mechanical Engineering 1 (7) (2013) 438–442.
12. H.S. Kim, J.-H. Kim, and J. Kim, A review of piezoelectric energy harvesting based on vibration, International Journal of Precision Engineering and Manufacturing 12 (6) (2011) 1129–1141.
13. Y. Zhang, Piezoelectric based energy harvesting on low frequency vibrations of civil infrastructures, Louisiana State University and Agricultural & Mechanical College, (2014).
14. Y. Yang, L. Tang, and H. Li, Vibration energy harvesting using macro-fiber composites, Smart Mater. Struct. 18 (11) (2009).
15. S. Khan et al., Modeling and Parametric Investigation of Vibration Energy Harvesting using Bimorph Piezoelectric Beam with a Tip Mass, in 2022 International Conference on Emerging Trends in Electrical, Control, and Telecommunication Engineering, ETECTE 2022 - Proceedings, Institute of Electrical and Electronics Engineers Inc., (2022).
16. S. Roundy, P.K. Wright, and J. Rabaey, A study of low level vibrations as a power source for wireless sensor nodes, Comput. Commun. 26 (11) (2003) 1131–1144.

17. K. Tungpimolrut et al., Design of energy harvester circuit for a MFC piezoelectric based on electrical circuit modeling, in 2011 International Symposium on Applications of Ferroelectrics (ISAF/PFM) and 2011 International Symposium on Piezoresponse Force Microscopy and Nanoscale Phenomena in Polar Materials, IEEE, (2011): pp. 1–4.
18. S. Roundy and P.K. Wright, A piezoelectric vibration based generator for wireless electronics, Smart Mater. Struct. 13 (5) (2004) 1131–1142.
19. S.R. Anton and H.A. Sodano, A review of power harvesting using piezoelectric materials (2003-2006), Smart Mater. Struct. 16 (3) (2007).
20. S. Das Mahapatra et al., Piezoelectric Materials for Energy Harvesting and Sensing Applications: Roadmap for Future Smart Materials, Advanced Science 8 (17) (2021).
21. M. Smith and S. Kar-Narayan, Piezoelectric polymers: theory, challenges and opportunities, International Materials Reviews 67 (1) (2022) 65–88.
22. V. Bhavanasi, Piezoelectric energy harvesting using poly (Vinylidene Difluoride-Trifluoroethylene), Nanyang Technological University, 2016.
23. L. Tang, Y. Yang, and H. Li, Optimizing efficiency of energy harvesting by macro-fiber composites, in Smart Structures, Devices, and Systems IV, SPIE, (2008): p. 726808.
24. J.M. Lloyd, Electrical Properties of Macro-Fiber Composite Actuators and Sensors, (2004).
25. S.Q. Zhang, Y.X. Li, and R. Schmidt, Modeling and simulation of macro-fiber composite layered smart structures, Compos. Struct. 126 (2015) 89–100.
26. Z. Dong, Dynamic Modeling of Macro-Fiber Composite Transducers integrated into Composite Structures, (2018).
27. A. Pandey and A. Arockiarajan, Actuation performance of macro-fiber composite (MFC): Modeling and experimental studies, Sens. Actuators A Phys. 248 (2016) 114–129.
28. M.T. Mhiri et al., Optimization of a macrofiber piezoelectric energy harvester using artificial neural networks, Compos. Struct. 367 (2025).
29. A. Erturk et al., Piezoelectric energy harvesting from macro-fiber composites with an application to morphing-wing aircrafts, in Proceedings of the 19th International Conference on Adaptive Structures and Technologies, Citeseer, (2008): pp. 6–9.
30. H. Li, C. Tian, and Z.D. Deng, Energy harvesting from low frequency applications using piezoelectric materials, Appl. Phys. Rev. 1 (4) (2014).
31. Y.C. Shu and I.C. Lien, Efficiency of energy conversion for a piezoelectric power harvesting system, Journal of Micromechanics and Microengineering 16 (11) (2006) 2429–2438.
32. T. Takenaka and H. Nagata, Current status and prospects of lead-free piezoelectric ceramics, J. Eur. Ceram. Soc. 25 (12 SPEC. ISS.) (2005) 2693–2700.
33. X. Xiong, Development of vibration-based multi-resonance energy harvesters using piezoelectric materials, The University of Manchester (United Kingdom), (2015).

34. S.P. Beeby, M.J. Tudor, and N.M. White, Energy harvesting vibration sources for microsystems applications, Meas. Sci. Technol. 17 (12) (2006).
35. S. Priya, Advances in energy harvesting using low profile piezoelectric transducers, J. Electroceram. 19 (1) (2007) 165–182.
36. W.J. Choi et al., Energy harvesting MEMS device based on thin film piezoelectric cantilevers, in J. Electroceram., (2006): pp. 543–548.
37. X. Pan et al., Mechanical energy harvesting based on the piezoelectric materials: Recent advances and future perspectives, Chemical Engineering Journal 497 (2024).
38. O. Garg et al., Piezoelectric energy harvesting: a developing scope for low-power applications, in Lecture Notes in Electrical Engineering, Springer Verlag, (2019): pp. 763–776.
39. A. Babaei, Mechanical energy harvester for powering RFID mechanical energy harvester for powering RFID systems components: modeling, analysis, optimization systems components: modeling, analysis, optimization and design and design, 2022.
40. A. Koszewnik, Assessment of Parameters of the Vibration-Based Energy Harvesting System Located in the Micro-Power Generator, Acta Mechanica et Automatica 18 (2) (2024) 223–232.
41. M.N. Hasan, M.A. Muktadir, and M. Alam, Comparative Study of Tapered Shape Bimorph Piezoelectric Energy Harvester via Finite Element Analysis, Forces in Mechanics 9 (2022).
42. P. Asthana and G. Khanna, Finite-element modeling of piezoelectric energy harvesters using lead-based and lead-free materials for voltage generation, Journal of Asian Ceramic Societies 6 (4) (2018) 394–400.
43. S. Rafique, Piezoelectric Vibration Energy Harvesting: Modeling & Experiments, Springer International Publishing, (2017).
44. A.S. Bojesomo, Piezoelectric Energy Harvester Design and Characterization, (2016).
45. P. Carneiro et al., Electromagnetic energy harvesting using magnetic levitation architectures: A review, Appl. Energy 260 (2020) 114191.
46. A. Erturk et al., Electromechanical Modeling of Piezoelectric Energy Harvesters, (2009).
47. C. Wei and X. Jing, A comprehensive review on vibration energy harvesting: Modelling and realization, Renewable and Sustainable Energy Reviews 74 (2017) 1–18.
48. M. Li et al., Recent Progress on Mechanical Optimization of MEMS Electret-Based Electrostatic Vibration Energy Harvesters, Journal of Microelectromechanical Systems 31 (5) (2022) 726–740.
49. B. Maamer et al., A review on design improvements and techniques for mechanical energy harvesting using piezoelectric and electromagnetic schemes, Energy Convers. Manag. 199 (2019).
50. J. Liao et al., Advances in mechanical energy harvesting using piezoelectric ceramics, Mater. Sci. Semicond. Process. 206 (2026).
51. S.X. Long et al., Numerical and Experimental Investigation of a Compressive-Mode Hull Piezoelectric Energy Harvester under Impact Force, Sustainability (Switzerland) 15 (22) (2023).

52. J. Song et al., Design optimization of PVDF-based piezoelectric energy harvesters, Heliyon 3 (2017) 377.
53. A.K. Batra, B.B. Bohara, and J.R. Currie, Design, Fabrication, and Testing of Piezoelectric Energy Harvesters, SPIE, (2018).
54. Y. Xiao, Q. Han, and N. Wu, Piezoelectric energy harvesting: a review of energy sources, structures, and working mechanisms in high-frequency excitations and operations, Smart Mater. Struct. 34 (2) (2025).
55. M. Umeda, K. Nakamura, and S. Ueha, Analysis of the transformation of mechanical impact energy to electric energy using piezoelectric vibrator, Jpn. J. Appl. Phys. 35 (5S) (1996) 3267.
56. M. Askari, E. Brusa, and C. Delprete, Vibration energy harvesting via piezoelectric bimorph plates: An analytical model, Mechanics of Advanced Materials and Structures 30 (23) (2023) 4764–4785.
57. S. Kim, Low power energy harvesting with piezoelectric generators, (1992).
58. W.U. Hao, Multi-modal vibration energy harvesting using the piezoelectric effect, (2015).
59. S.P. Beeby, M.J. Tudor, and N.M. White, Energy harvesting vibration sources for microsystems applications, Meas. Sci. Technol. 17 (12) (2006).
60. A. Muscat, S. Bhattacharya, and Y. Zhu, Electromagnetic Vibrational Energy Harvesters: A Review, Sensors 22 (15) (2022).
61. P. Li, S. Gao, and H. Cai, Modeling and analysis of hybrid piezoelectric and electromagnetic energy harvesting from random vibrations, Microsystem Technologies 21 (2) (2015) 401–414.
62. M. Lo Monaco, C. Russo, and A. Somà, Identification Procedure for Design Optimization of Gravitational Electromagnetic Energy Harvesters, Applied Sciences (Switzerland) 13 (4) (2023).
63. M. Iqbal et al., Vibration-based piezoelectric, electromagnetic, and hybrid energy harvesters for microsystems applications: a contributed review, Int. J. Energy Res. 45 (1) (2021) 65–102.
64. K.T. Prajwal, K. Manickavasagam, and R. Suresh, A review on vibration energy harvesting technologies: analysis and technologies, European Physical Journal: Special Topics 231 (8) (2022) 1359–1371.
65. R. Patel, S. McWilliam, and A.A. Popov, A geometric parameter study of piezoelectric coverage on a rectangular cantilever energy harvester, Smart Mater. Struct. 20 (8) (2011) 085004.
66. Z. Hadas, J. Smilek, and O. Rubes, Analyses of electromagnetic and piezoelectric systems for efficient vibration energy harvesting, in Smart Sensors, Actuators, and MEMS VIII, SPIE, (2017): p. 1024619.
67. M. Li et al., Recent Progress on Mechanical Optimization of MEMS Electret-Based Electrostatic Vibration Energy Harvesters, Journal of Microelectromechanical Systems 31 (5) (2022) 726–740.
68. N. Kumari and A. Trivedi, A review on modelling and techniques used for piezoelectric power generation from vibration of geo-structures, E-Prime - Advances in Electrical Engineering, Electronics and Energy 2 (2022).
69. S. Bairagi et al., Mechanical energy harvesting and self-powered electronic applications of textile-based piezoelectric nanogenerators: A systematic review, Nano Energy 111 (2023).

70. Md.N. Hussain et al., A Comprehensive Review on Techniques and Challenges of Energy Harvesting from Distributed Renewable Energy Sources for Wireless Sensor Networks, Control Systems and Optimization Letters 2 (1) (2024) 15–22.
71. S. Roundy, P.K. Wright, and J. Rabaey, A study of low level vibrations as a power source for wireless sensor nodes, Comput. Commun. 26 (11) (2003) 1131–1144.
72. G.H. Haertling, Ferroelectric ceramics: History and technology, Journal of the American Ceramic Society 82 (4) (1999) 797–818.
73. R. Ahmed, F. Mir, and S. Banerjee, A review on energy harvesting approaches for renewable energies from ambient vibrations and acoustic waves using piezoelectricity, Smart Mater. Struct. 26 (8) (2017) 085031.
74. M. Kim, J. Dugundji, and B.L. Wardle, Effect of electrode configurations on piezoelectric vibration energy harvesting performance, Smart Mater. Struct. 24 (4) (2015).
75. M. Mallouli and M. Chouchane, Piezoelectric energy harvesting using macro fiber composite patches, Proc. Inst. Mech. Eng. C J. Mech. Eng. Sci. 234 (21) (2020) 4331–4349.
76. A.A. Bent and N.W. Hagood, Piezoelectric fiber composites with interdigitated electrodes, J. Intell. Mater. Syst. Struct. 8 (11) (1997) 903–919.
77. A. Erturk and D.J. Inman, Piezoelectric Energy Harvesting, John Wiley & Sons, (2011).
78. H.A. Sodano, D.J. Inman, and G. Park, A review of power harvesting from vibration using piezoelectric materials, Shock and Vibration Digest 36 (3) (2004) 197–205.
79. S. Priya and D.J. Inman, Energy Harvesting Technologies, Springer, Boston, MA, (2009).
80. A. Lendlein and S. Kelch, Shape-memory polymers, Angew. Chem. Int. Ed. 41 (12) (2002) 2034–2057.
81. M.J. Adams, Smart materials: Definitions and applications, J. Intell. Mater. Syst. Struct. 15 (3) (2004) 189–197.
82. R.E. Rosensweig, Ferrohydrodynamics, Dover Publications, New York, (2014).
83. A. Raza, S. Mahato, and R. Rimašauskienė, Actuation Performance of Macro Fibre Composite (MFC) as Actuator in Vibration Reduction of Cantilever Beams, Mechanika 29 (1) (2023) 42–50.
84. L.M. Swallow et al., A piezoelectric fibre composite based energy harvesting device for potential wearable applications, Smart Mater. Struct. 17 (2) (2008).
85. H. Li, C. Tian, and Z.D. Deng, Energy harvesting from low frequency applications using piezoelectric materials, Appl. Phys. Rev. 1 (4) (2014) 41301.
86. Y. Cao and H. Huang, Performance optimization and broadband design of piezoelectric energy harvesters based on isogeometric topology optimization framework, European Journal of Mechanics, A/Solids 97 (2023).
87. H. Liang, G. Hao, and O.Z. Olszewski, A review on vibration-based piezoelectric energy harvesting from the aspect of compliant mechanisms, Sens. Actuators A Phys. 331 (2021).

88. N. Almarri et al., Piezoelectric Energy Harvesting and Ultra-Low-Power Management Circuits for Medical Devices, Nano Energy (2024) 110196.
89. S. Wada, H. Kakemoto, and T. Tsurumi, Enhanced piezoelectric properties of piezoelectric single crystals by domain engineering, Mater. Trans. 45 (2) (2004) 178–187.
90. P.A. Wlodkowski, K. Deng, and M. Kahn, The development of high-sensitivity, low-noise accelerometers utilizing single crystal piezoelectric materials, Sens. Actuators A Phys. 90 (1–2) (2001) 125–131.
91. H.A. Sodano, Macro-Fiber Composites for Sensing, Actuation and Power Generation, (2003).
92. S. Wada, H. Kakemoto, and T. Tsurumi, Enhanced piezoelectric properties of piezoelectric single crystals by domain engineering, Mater. Trans. 45 (2) (2004) 178–187.
93. N. Ahbab et al., A Comprehensive Review of Piezoelectric PVDF Polymer Fabrications and Characteristics, Micromachines (Basel). 16 (4) (2025).
94. H.A. Sodano, G. Park, and D.J. Inman, An investigation into the performance of macro-fiber composites for sensing and structural vibration applications, Mech. Syst. Signal Process. 18 (3) (2004) 683–697.
95. K. Tungpimolrut et al., Design of energy harvester circuit for a MFC piezoelectric based on electrical circuit modeling, in 2011 International Symposium on Applications of Ferroelectrics (ISAF/PFM) and 2011 International Symposium on Piezoresponse Force Microscopy and Nanoscale Phenomena in Polar Materials, IEEE, (2011): pp. 1–4.
96. S.M. Purushothaman et al., A review on electrospun PVDF-based nanocomposites: Recent trends and developments in energy harvesting and sensing applications, Polymer (Guildf). 283 (2023).
97. A. Veved, G.W. Ejuh, and N. Djongyang, Review of emerging materials for PVDF-based energy harvesting, Energy Reports 8 (2022) 12853–12870.
98. Y. Yang, L. Tang, and H. Li, Vibration energy harvesting using macro-fiber composites, Smart Mater. Struct. 18 (11) (2009).
99. C. Zhu et al., High Performance KNN-Based Macro Fiber Composites for Human Motion Monitoring Applications, Small (2025).
100. D.G. Wakshume and M.Ł. Płaczek, Mathematical Modeling and Finite Element Simulation of the M8514-P2 Composite Piezoelectric Transducer for Energy Harvesting, Sensors 25 (10) (2025) 3071.
101. M. Askari et al., Design, fabrication and evaluation of a Quad-Finger multimodal vibration energy harvester utilizing MFC generators, Mechanics of Advanced Materials and Structures (2025).
102. M.P. Saravanan, K. Marimuthu, and K. Jayabal, Characteristic investigation of macro fiber composite structure using FE model, Archives of Metallurgy and Materials 66 (4) (2021) 1059–1066.
103. M. Khazaee, A. Rezaniakolaie, and L. Rosendahl, A broadband macro-fiber-composite piezoelectric energy harvester for higher energy conversion from practical wideband vibrations, Nano Energy 76 (2020) 104978.

104. K. Tungpimolrut et al., Design of Energy Harvester Circuit for a MFC Piezoelectric based on Electrical Circuit Modeling, (n.d.).
105. M. Płaczek and Ł. Dulat, Supporting the Design of Systems for Energy Recovery from Mechanical Vibrations Containing MFC Piezoelectric Transducers, Applied Sciences (Switzerland) 15 (10) (2025).
106. MACRO FIBER COMPOSITE-MFC Actuator, Sensor, Energy Harvester Energy Harvesting Systems Piezo Powering and Instrumentation Engineering Services, (n.d.).
107. M. Płaczek and G. Kokot, Modelling and laboratory tests of the temperature influence on the efficiency of the energy harvesting system based on MFC piezoelectric transducers, Sensors (Switzerland) 19 (7) (2019).
108. J. Liu et al., The influence of piezoelectric fibers on energy harvesting characteristics in piezoelectric composite MFC, AIP Adv. 15 (7) (2025).
109. P. Hajheidari, Performance Enhancement of Cantilever Beam Piezoelectric Energy Harvesters, Montreal, QC, Canada, (2020).
110. X. Shan et al., Novel energy harvesting: A macro fiber composite piezoelectric energy harvester in the water vortex, in Ceram. Int., Elsevier Ltd, (2015): pp. S763–S767.
111. Y.C. Lin, K.S. Tseng, and C.C. Ma, Investigation of resonant and energy harvesting characteristics of piezoelectric fiber composite bimorphs, Mater. Des. 197 (2021).
112. Vibration and Flow Energy Harvesting using Piezoelectric, (2011).
113. Y. Jia et al., Multiphysics vibration FE model of piezoelectric macro fibre composite on carbon fibre composite structures, Compos. B Eng. 161 (2019) 376–385.
114. T. Li and P.S. Lee, Piezoelectric Energy Harvesting Technology: From Materials, Structures, to Applications, Small Struct. 3 (3) (2022).
115. M. Płaczek, Modelling and production process of the energy harvesting system based on MFC piezoelectric transducers, (2020).
116. M.G. Kang et al., Recent progress on PZT based piezoelectric energy harvesting technologies, Actuators 5 (1) (2016).
117. S. Yang and J. Kim, Low-Frequency Vibration Damping Using Ecoflex-Reinforced Fabric Composite and Macro-Fiber Composite Actuators, Fibers and Polymers 26 (12) (2025) 5713–5724.
118. M.Y. Gao et al., A rail-borne piezoelectric transducer for energy harvesting of railway vibration, Journal of Vibroengineering 18 (7) (2016) 4647–4663.
119. T. Li and P.S. Lee, Piezoelectric energy harvesting technology: from materials, structures, to applications, Small Struct. 3 (3) (2022) 2100128.
120. A. Erturk and D.J. Inman, Piezoelectric Energy Harvesting, Wiley, (2011).
121. Z. Hasan, H. Hammoudeh, and G. Atmeh, Design and analysis of a smart composite wing, in ASME International Mechanical Engineering Congress and Exposition, (2011): pp. 213–222.
122. H.D. Akaydın, N. Elvin, and Y. Andreopoulos, Flow-induced vibrations for piezoelectric energy harvesting, in Advances in Energy Harvesting Methods, Springer, (2013): pp. 241–267.

123. D.A. Aldahiry et al., Piezoelectric Transducer as an Energy Harvester: A Review, Yanbu Journal of Engineering and Science 19 (1) (2022).
124. H.A. Sodano, G. Park, and D.J. Inman, Estimation of electric charge output for piezoelectric energy harvesting, Strain 40 (2) (2004) 49–58.
125. A. Erturk, Assumed-modes modeling of piezoelectric energy harvesters: Euler-Bernoulli, Rayleigh, and Timoshenko models with axial deformations, Comput. Struct. 106–107 (2012) 214–227.
126. A. Erturk and D.J. Inman, Piezoelectric Energy Harvesting, John Wiley & Sons, (2011).
127. T.G. Degefa, M.Ł. Płaczek, and G. Kokot, The Study of the Influence of Temperature and Low Frequency on the Performance of the Laminated MFC Piezoelectric Energy Harvester, Applied Sciences (Switzerland) 12 (23) (2022).
128. D.S. Ibrahim et al., On geometrical configurations of vibration-driven piezoelectric energy harvesters for optimum energy transduction: A critical review, Mechanics of Advanced Materials and Structures 30 (7) (2023) 1340–1356.
129. S. Gu et al., High-performance piezoelectric energy harvesting system with anti-interference capability for smart grid monitoring, Renew. Energy 221 (2024).
130. R. Patel, S. McWilliam, and A.A. Popov, A geometric parameter study of piezoelectric coverage on a rectangular cantilever energy harvester, Smart Mater. Struct. 20 (8) (2011).
131. Q. Xu et al., Design and Optimization of Piezoelectric Cantilever Beam Vibration Energy Harvester, Micromachines (Basel). 13 (5) (2022).
132. P. Hajheidari, Performance Enhancement of Cantilever Beam Piezoelectric Energy Harvesters, (2020).
133. H. Elahi et al., Characterization and Implementation of a Piezoelectric Energy Harvester Configuration: Analytical, Numerical and Experimental Approach, Integrated Ferroelectrics 212 (1) (2020) 39–60.
134. X. Liu and J. Wang, Performance Exploration of A Radially Layered Cymbal Piezoelectric Energy Harvester under Road Traffic Induced Low Frequency Vibration, in IOP Conf. Ser. Mater. Sci. Eng., Institute of Physics Publishing, (2019).
135. X.R. Chen et al., Vibration energy harvesting with a clamped piezoelectric circular diaphragm, in Ceram. Int., (2012).
136. K. Mou et al., Using piezoelectric technology to harvest energy from pavement: A review, Journal of Traffic and Transportation Engineering (English Edition) 12 (1) (2025) 68–86.
137. A. Koszewnik, Assessment of Parameters of the Vibration-Based Energy Harvesting System Located in the Micro-Power Generator, Acta Mechanica et Automatica 18 (2) (2024) 223–232.
138. M. Mohiuddin et al., Optimizing Power Density in Partially Coated Cantilever Beam Energy Harvesters: A Cost-Effective Design Strategy, Energies (Basel). 17 (22) (2024).
139. A. Erturk and D.J. Inman, Piezoelectric Energy Harvesting, John Wiley & Sons, (2011).

140. J.R. Liang and W.H. Liao, Piezoelectric energy harvesting and dissipation on structural damping, J. Intell. Mater. Syst. Struct. 20 (5) (2009) 515–527.
141. Design, modeling, and optimization of nonlinear piezoelectric energy harvesters, Nanyang Technological University, 2017.
142. H. Rejdali et al., Simulation of a piezoelectric energy harvester using finite element method, Mater. Today Proc. 66 (2022) 125–129.
143. Pritam Ramchandra Shinde and Sandip Patil, Towards Sustainable Energy Solutions: A Comprehensive Analysis of Piezoelectric Sensors for Power Generation, International Journal of Advanced Research in Science, Communication and Technology (2024) 151–161.
144. L. V. Duong, Finite element modeling of piezoelectric cantilever-beam energy harvester, J. Adv. Dielectr. 14 (5) (2024).
145. S. Ravi and A. Zilian, Monolithic modeling and finite element analysis of piezoelectric energy harvesters, Acta Mech. 228 (6) (2017) 2251–2267.
146. A. Homayouni-Amlashi, A. Mohand-Ousaid, and M. Rakotondrabe, Analytical modelling and optimization of a piezoelectric cantilever energy harvester with in-span attachment, Micromachines (Basel). 11 (6) (2020).
147. T.R. Kandukuri, C. Liao, and L.G. Occhipinti, Modeling and Optimization of Energy Harvesters for Specific Applications Using COMSOL and Equivalent Spring Models, Sensors 24 (23) (2024).
148. P. Kurt and S. Orhan, Improving Energy Harvesting from Cantilever-like Structures Based on Beam Geometry, Journal of Vibration Engineering and Technologies 12 (7) (2024) 7781–7797.
149. A.A. Hashim, K.I. Mahmoud, and H.M. Ridha, Geometry and shape optimization of piezoelectric cantilever energy harvester using COMSOL multiphysics software, International Review of Applied Sciences and Engineering 12 (2) (2021) 103–110.
150. A. Homayouni-Amlashi, A. Mohand-Ousaid, and M. Rakotondrabe, Multi directional piezoelectric plate energy harvesters designed by topology optimization algorithm, IEEE Robot. Autom. Lett. 5 (2) (2019) 462–469.
151. A. Homayouni, A.M. Ousaid, and M. Rakotondrabe, “Multi directional piezoelectric plate energy harvesters designed by topology optimization algorithm,” IEEE Robot. Autom. Lett. 5 (2019) 8.
152. M. Mallouli and M. Chouchane, Selection of piezoeloectric material and fiber volume fraction to maximize the electrical power produced by macro-fiber composite energy harvesters, J. Compos. Mater. 57 (2) (2023) 273–295.
153. K. Zhao et al., Topological optimization of a variable cross-section cantilever-based piezoelectric wind energy harvester, Front. Mater. 9 (2022) 956182.
154. A.H. Amlashi et al., Topology optimization of micro piezoelectric actuators and energy harvesters at femto-st institute: summary andMATLAB code implementation, J. Microbio Robot. 20 (2) (2024) 1–27.

155. A. Homayouni-Amlashi et al., Topology optimization of piezoelectric structures: micro-actuators and energy harvesters, in 2023 International Conference on Manipulation, Automation and Robotics at Small Scales (MARSS), IEEE, (2023): pp. 1–6.

156. A. Homayouni-Amlashi, A. Mohand-Ousaid, and M. Rakotondrabe, Topology optimization of 2dof piezoelectric plate energy harvester under external in-plane force, J. Microbio Robot. 16 (1) (2020) 65–77.

157. M. He et al., Topology optimization of piezoelectric energy harvesters for enhanced open-circuit voltage subjected to harmonic excitations, Materials 15 (13) (2022) 4423.

158. M.J.D. Powell, The BOBYQA algorithm for bound constrained optimization without derivatives, Cambridge NA Report NA2009/06, University of Cambridge, Cambridge 26 (26–46) (2009) 1.

159. S. Roundy, P.K. Wright, and J. Rabaey, A study of low level vibrations as a power source for wireless sensor nodes, Comput. Commun. 26 (11) (2003) 1131–1144.

160. H.-S. Kim, J.-H. Kim, and J.-S. Kim, A review of piezoelectric energy harvesting based on vibration, International Journal of Precision Engineering and Manufacturing 12 (6) (2011) 1129–1141.

161. Z.L. Wang, Self-powered nanosensors and nanosystems, Advanced Materials 24 (2) (2012) 280–285.

162. T. Wacharasindhu and J.W. Kwon, A micromachined energy harvester from a keyboard using combined electromagnetic and piezoelectric conversion, Journal of Micromechanics and Microengineering 18 (10) (2008) 104016.

163. M. Renaud et al., Harvesting energy from the motion of human limbs: the design and analysis of an impact-based piezoelectric generator, Smart Mater. Struct. 18 (3) (2009) 035001.

164. E.-J. Kim et al., High output performance of piezoelectric energy harvesters using epitaxial Pb(Zr, Ti)O3 thin film grown on Si substrate, Appl. Phys. Lett. 121 (16) (2022) 161901.

165. E. Brusa, A. Carrera, and C. Delprete, A Review of Piezoelectric Energy Harvesting: Materials, Design, and Readout Circuits, Actuators 12 (12) (2023).

166. S. Das Mahapatra et al., Piezoelectric Materials for Energy Harvesting and Sensing Applications: Roadmap for Future Smart Materials, Advanced Science 8 (17) (2021) 2100864.

167. P. Aela et al., Vibration energy harvesting from railway tracks via a magnetic–piezoelectric system, Smart Mater. Struct. 34 (11) (2025) 115030.

168. A. Batra, A. Alomari, and D. Brown, Hybrid Energy Harvester Using Piezoelectric and Pyroelectric Properties of PVDF Nanocomposite Films, ECS Meeting Abstracts MA2016-02 (1) (2016) 102.

169. H. Ucar, Piezoelectric energy harvesting from vortex-induced vibrations on a GFRP beam with embedded piezoelectric patch, International Journal of Energy Studies 7 (2) (2022) 157–177.

170. R. Song et al., A novel piezoelectric energy harvester using the macro fiber composite cantilever with a bicylinder in water, Applied Sciences 5 (4) (2015) 1942–1954.

171. A. Erturk and D.J. Inman, A distributed parameter electromechanical model for cantilevered piezoelectric energy harvesters, J. Vib. Acoust. 130 (4) (2008) 41002.

172. F. Biscani, Modelling-based design of anisotropic piezocomposite transducers and multi-domain analysis of smart structures, (2012).
173. Design, modeling, and analysis of piezoelectric energy harvesters, Aalborg University, 2021.
174. Design, modeling, and optimization of nonlinear piezoelectric energy harvesters, Nanyang Technological University, 2017.
175. D.S. Ibrahim et al., Modeling and simulation of a gauge shaped beam coupled with macro fiber composite for energy harvesting application, in IOP Conf. Ser. Mater. Sci. Eng., Institute of Physics Publishing, (2020).
176. M. Płaczek, Conception of the system for traffic measurements based on piezoelectric foils, in IOP Conf. Ser. Mater. Sci. Eng., Institute of Physics Publishing, (2016).
177. S. Kundu and H.B. Nemade, Modeling and Simulation of a Piezoelectric Vibration Energy Harvester, in Procedia Eng., Elsevier Ltd, (2016): pp. 568–575.
178. M.N. Fakhzan and A.G.A. Muthalif, Harvesting vibration energy using piezoelectric material: Modeling, simulation and experimental verifications, Mechatronics 23 (1) (2013) 61–66.
179. S.Q. Zhang, Y.X. Li, and R. Schmidt, Modeling and simulation of macro-fiber composite layered smart structures, Compos. Struct. 126 (2015) 89–100.
180. Y. Wang et al., State-of-the-art review on evaluation indicators of integrated intelligent energy from different perspectives, Renewable and Sustainable Energy Reviews 189 (2024) 113835.
181. H. Luo et al., Dynamic Modeling and Active Vibration Control of Piezoelectric Laminated Structure Based on Macrofiber Composite, Struct. Control Health Monit. 2024 (2024).
182. M.T. Mhiri et al., Modeling and analysis of a macro-fiber piezoelectric bimorph energy harvester operating in d33-Mode using Timoshenko theory, Mechanics of Advanced Materials and Structures (2024).
183. J. Rencis, Mechanics of materials: An introductory course with integration of theory, analysis, verification and design, in 2005 Annual Conference, (2005): pp. 10–931.
184. D. Emad et al., Low-Computational-Cost Technique for Modeling Macro Fiber Composite Piezoelectric Actuators Using Finite Element Method, Materials 14 (15) (2021).
185. A. Kumar et al., Finite element analysis of vibration energy harvesting using lead-free piezoelectric materials: A comparative study, Journal of Asian Ceramic Societies 2 (2) (2014) 138–143.
186. T.S. Plagianakos et al., Finite element-based assessment of energy harvesting in composite beams with piezoelectric transducers, Proceedings of the Institution of Mechanical Engineers, Part L: Journal of Materials: Design and Applications 236 (3) (2022) 473–488.
187. A. Nechibvute, A. Chawanda, and P. Luhanga, Finite Element Modeling of a Piezoelectric Composite Beam and Comparative Performance Study of Piezoelectric Materials for Voltage Generation, ISRN Materials Science 2012 (2012) 1–11.
188. M.A.F. Muhammad Yazid et al., Finite element analysis of hybrid energy harvesting of piezoelectric and electromagnetic, in MATEC Web of Conferences, EDP Sciences, (2016): p. 01039.

189. A. Melro and K. Liu, Evaluation and validation of a multiphysics finite element model for a piezoelectric energy harvester, Transactions of the Canadian Society for Mechanical Engineering 45 (4) (2021) 562–572.
190. A. Erturk and D.J. Inman, An experimentally validated bimorph cantilever model for piezoelectric energy harvesting from base excitations, Smart Mater. Struct. 18 (2) (2009) 25009.
191. X. Wang et al., Performance Correction and Parameters Identification Considering Non-Uniform Electric Field in Cantilevered Piezoelectric Energy Harvesters, Sensors 24 (15) (2024).
192. B. Richter, J. Twiefel, and J. Wallaschek, Piezoelectric equivalent circuit models, in Energy Harvesting Technologies, Springer, (2009): pp. 107–128.
193. M. Farnsworth, A. Tiwari, and R. Dorey, Modelling, simulation and optimisation of a piezoelectric energy harvester, in Procedia CIRP, Elsevier B.V., (2014): pp. 142–147.
194. R. Huang et al., Research and Design of Energy-Harvesting System Based on Macro Fiber Composite Cantilever Beam Applied in Low-Frequency and Low-Speed Water Flow, Materials 17 (12) (2024).
195. H. Liu et al., A comprehensive review on piezoelectric energy harvesting technology: Materials, mechanisms, and applications, Appl. Phys. Rev. 5 (4) (2018).
196. E. Varadha and S. Rajakumar, Performance improvement of piezoelectric materials in energy harvesting in recent days – A review, Journal of Vibroengineering 20 (7) (2018) 2632–2650.
197. I. Izadgoshasb et al., Optimizing orientation of piezoelectric cantilever beam for harvesting energy from human walking, Energy Convers. Manag. 161 (2018) 66–73.
198. N.W. Hagood and A.A. Bent, Development of piezoelectric fiber composites for structural actuation, in Collection of Technical Papers - AIAA/ASME Structures, Structural Dynamics and Materials Conference, Publ by AIAA, (1993): pp. 3625–3638.
199. J. Baker, S. Roundy, and P. Wright, Alternative geometries for increasing power density in vibration energy scavenging for wireless sensor networks, in 3rd International Energy Conversion Engineering Conference, (2005): p. 5617.
200. A. Pandey and A. Arockiarajan, Performance studies on Macro fiber composite (MFC) under thermal condition using Kirchhoff and Mindlin plate theories, Int. J. Mech. Sci. 130 (2017) 416–425.
201. A. Nisanth, K.J. Suja, and V. Seena, Design and optimization of MEMS piezoelectric energy harvester for low frequency applications, Microsystem Technologies 27 (1) (2021) 251–261.
202. A. Homayouni-Amlashi, A. Mohand-Ousaid, and M. Rakotondrabe, Analytical modelling and optimization of a piezoelectric cantilever energy harvester with in-span attachment, Micromachines (Basel). 11 (6) (2020).
203. E. Brusa, A. Carrera, and C. Delprete, A Review of Piezoelectric Energy Harvesting: Materials, Design, and Readout Circuits, Actuators 12 (12) (2023).
204. S. Srinivasulu Raju et al., An effective energy harvesting in low frequency using a piezo-patch cantilever beam with tapered rectangular cavities, Sens. Actuators A Phys. 297 (2019).

205. J. Baker, S. Roundy, and P.P. Wright, Alternative Geometries for Increasing Power Density in Vibration Energy Scavenging for Wireless Sensor Networks, (n.d.).
206. P. Asthana and G. Khanna, Characterization and Optimization of Piezoelectric Bimorph Cantilever Structure for Ambient Vibration-Based Energy Harvesting Application, Integrated Ferroelectrics 211 (1) (2020) 45–59.
207. P. Aceti et al., Optimization of an Impact-Based Frequency Up-Converted Piezoelectric Vibration Energy Harvester for Wearable Devices, Sensors 23 (3) (2023).
208. L. Tang and J. Wang, Size effect of tip mass on performance of cantilevered piezoelectric energy harvester with a dynamic magnifier, Acta Mech. 228 (11) (2017) 3997–4015.
209. M. Liu et al., Research on frequency bandwidth and phase difference of piezoelectric resonant cantilever based on mass, Microsystem Technologies 27 (10) (2021) 3667–3677.
210. M.G. Greeshma and S.P. Rajeev, Optimising proof mass for cantilever based piezoelectric energy harvester, Mater. Today Proc. 59 (2022) 623–627.
211. M.I. Badrin et al., Tip mass effect of piezoelectric energy harvester on power generation, (2022).
212. A.H. Alameh et al., Effects of proof mass geometry on piezoelectric vibration energy harvesters, Sensors (Switzerland) 18 (5) (2018).
213. E. Worthington, Piezoelectric energy harvesting: Enhancing power output by device optimisation and circuit techniques, (2010).
214. F. Ksica et al., Homogenized model of piezoelectric composite structure for sensing purposes, in Advances in Intelligent Systems and Computing, Springer Verlag, (2020): pp. 358–365.
215. P. Hajheidari, I. Stiharu, and R. Bhat, Performance enhancement of cantilever piezoelectric energy harvesters by sizing analysis, Int. J. Smart Nano Mater. 11 (2) (2020) 93–116.
216. M.A. Karami and D.J. Inman, Parametric study of zigzag microstructure for vibrational energy harvesting, Journal of Microelectromechanical Systems 21 (1) (2011) 145–160.
217. M.J.D. Powell, The BOBYQA algorithm for bound constrained optimization without derivatives, Cambridge NA Report NA2009/06, University of Cambridge, Cambridge 26 (26–46) (2009) 1.
218. C. Cartis et al., Improving the flexibility and robustness of model-based derivative-free optimization solvers, ACM Transactions on Mathematical Software (TOMS) 45 (3) (2019) 1–41.
219. A. Homayouni-Amlashi, A. Mohand-Ousaid, and M. Rakotondrabe, Analytical modelling and optimization of a piezoelectric cantilever energy harvester with in-span attachment, Micromachines (Basel). 11 (6) (2020) 591.
220. F.U. Khan and T. Ali, A piezoelectric based energy harvester for simultaneous energy generation and vibration isolation, Int. J. Energy Res. 43 (11) (2019) 5922–5931.

Appendix :1 MAT LAB script

MATLAB script for the analytical mode shapes and natural frequencies

```
clear; clc; close all;
L_b = 400e-3;      % total beam length [m]
Lp      = 65e-3;       % patch start position [m]
S      = 150e-3;      % patch end position (65+85 mm) [m]
Eb     = 70.02e9;
rho_Al = 2700;
b      = 30e-3;
tb     = 2e-3;
Ab     = b*tb;
Ib     = b*tb^3/12;
EI_bare = Eb*Ib;
mA_bare = rho_Al*Ab;
EI_patch = 1.798e6 * 1e-6;
mA_patch = 0.190728;
nElemPerSeg = 20;
x_nodes = unique([linspace(0, Lp, nElemPerSeg+1), ...
                  linspace(Lp, S, nElemPerSeg+1), ...
                  linspace(S, Lb, nElemPerSeg+1)]);
nNode  = length(x_nodes);
nElem  = nNode - 1;
nDof   = 2*nNode;
K = zeros(nDof, nDof);
M = zeros(nDof, nDof);
for e = 1:nElem
    xL = x_nodes(e);  xR = x_nodes(e+1);
    Le = xR - xL;      xc = 0.5*(xL+xR);
    if xc >= Lp && xc <= S
        EI = EI_patch;  mA = mA_patch;
    else
        EI = EI_bare;   mA = mA_bare;
    end
    Ke = (EI/Le^3) * [ 12,      6*Le,   -12,     6*Le;
                       6*Le,   4*Le^2, -6*Le,   2*Le^2;
                      -12,    -6*Le,    12,    -6*Le;
                       6*Le,   2*Le^2, -6*Le,   4*Le^2];

    Me = (mA*Le/420) * [156,     22*Le,   54,    -13*Le;
                        22*Le,  4*Le^2, 13*Le,  -3*Le^2;
                        54,     13*Le,  156,   -22*Le;
                       -13*Le, -3*Le^2,-22*Le,  4*Le^2];
    dofIndex = [2*e-1, 2*e, 2*e+1, 2*e+2];
    K(dofIndex, dofIndex) = K(dofIndex, dofIndex) + Ke;
    M(dofIndex, dofIndex) = M(dofIndex, dofIndex) + Me;
end
fixedDof = [1, 2];
freeDof  = setdiff(1:nDof, fixedDof);
```

```
Kr = K(freeDof, freeDof);
Mr = M(freeDof, freeDof);
[Phi, Omega2] = eig(Kr, Mr);
omega2 = diag(Omega2);
[omega2_sorted, idx] = sort(omega2, 'ascend');
Phi_sorted = Phi(:, idx);
omega_n = sqrt(omega2_sorted);
f_n     = omega_n / (2*pi);
fprintf('First 4 Natural Frequencies:\n');
for i = 1:4
   fprintf('  Mode %d: f_%d = %.3f Hz\n', i, i, f_n(i));
end
colours = { [0.635 0.078 0.184], ...   % dark red   - Mode 1
          [0     0.208 0.741], ...   % blue       - Mode 2
          [0.100 0.100 0.100], ...   % near-black - Mode 3
          [0.494 0.184 0.702] };     % purple     - Mode 4
nModes = 4;
xq = linspace(0, Lb, 2000);   % dense grid for smooth curves
fig = figure('Color','w', 'Units','centimeters', ...
           'Position',[2 2 22 15]);
ax = axes(fig); hold(ax,'on'); box(ax,'on');
yl = [-1.15, 1.15];
legendEntries = cell(1, nModes);
for i = 1:nModes
   modeVec_free = Phi_sorted(:, i);
   modeVec_full = zeros(nDof,1);
   modeVec_full(freeDof) = modeVec_free;
   w_mode = modeVec_full(1:2:end);
   w_mode = w_mode / max(abs(w_mode));
   % Ensure tip deflection is positive for odd modes (sign convention)
   if mod(i,2) == 1 && w_mode(end) < 0
      w_mode = -w_mode;
   end
   % Smooth (spline) interpolation for a visually cleaner curve
   w_smooth = interp1(x_nodes, w_mode, xq, 'pchip');

   plot(ax, xq, w_smooth, '-', 'Color', colours{i}, 'LineWidth', 2.6);
   legendEntries{i} = sprintf('Mode %d (%.2f Hz)', i, f_n(i));
end
% Baseline
plot(ax, [0 Lb], [0 0], '-', 'Color', [0.5 0.5 0.5], ...
    'LineWidth', 0.75, 'HandleVisibility','off');
xlabel(ax, 'Beam Length (m)', 'FontSize', 16, 'FontWeight','bold');
ylabel(ax, 'Normalized Displacement', 'FontSize', 16, 'FontWeight','bold');
title(ax, 'Mode Shapes and Natural Frequencies of Composite Al-MFC Cantilever Beam', ...
     'FontSize', 15, 'FontWeight','bold');
lgd = legend(ax, legendEntries, 'Location', 'southwest');
set(lgd, 'Box','on', 'FontSize', 12);
xlim(ax, [0, Lb]);
ylim(ax, yl);
set(ax, 'FontSize', 14, 'FontName','Helvetica', ...
```

```
    'LineWidth', 1.1, 'TickDir','out', ...
    'XMinorTick','on', 'YMinorTick','on', ...
    'GridAlpha', 0.25, 'MinorGridAlpha', 0.12);
grid(ax, 'on');
ax.GridLineStyle = '-';
ax.MinorGridLineStyle = ':';
set(fig, 'Renderer', 'painters');   % vector renderer -> crisp lines/text
% PNG (raster, high DPI) for slides/Word; PDF/EPS (vector) for
% publication-quality print use.
exportgraphics(fig, 'ModeShapes_AlMFC_Beam.png', 'Resolution', 600);
exportgraphics(fig, 'ModeShapes_AlMFC_Beam.pdf', 'ContentType', 'vector');
% print(fig, 'ModeShapes_AlMFC_Beam', '-depsc', '-painters'); % optional EPS
```

Analytical Voltage and Eigenfrequencies Model

```
clear; clc; close all;
fn      = 10.69;       % natural frequency, Mode 1 [Hz] (from your FEM)
wn      = 2*pi*fn;   % natural angular frequency [rad/s]
zeta    = 0.01;        % mechanical damping ratio (0.05-0.02 range)
Meff    = 0.0372;      % effective modal mass [kg] (adjust to your model, or fold into eta scaling)
theta   = 1e-4;        % modal electromechanical coupling coefficient [N/V]
Cp      = 4.5e-8;      % piezoelectric patch capacitance [F] - REPLACE with your value
R       = 12e5;         % load resistance [Ohm] - REPLACE with your chosen/optimised value
f  = linspace(7, 15, 300);   % excitation frequency sweep [Hz], adjust range as needed
w  = 2*pi*f;                  % angular frequency [rad/s]
%   eta(w) = (Y0) / sqrt( (wn^2 - w.^2).^2 + (2*zeta*wn.*w).^2 )
eta = Meff*Y0 ./ sqrt( (wn^2 - w.^2).^2 + (2*zeta*wn.*w).^2 );
Vomega = (theta .* w .* eta) ./ sqrt( (1/R)^2 + (w*Cp).^2 );
[Vpeak, idxPeak] = max(Vomega);
fig = figure('Color','w', 'Units','centimeters', ...
           'Position',[2 2 22 15]);
ax = axes(fig); hold(ax,'on'); box(ax,'on');
plot(ax, f, Vomega, '-', 'Color', [0 0.208 0.741], 'LineWidth', 5);
% Mark resonance point
plot(ax, f(idxPeak), Vpeak, 'o', 'MarkerFaceColor', [0.635 0.078 0.184], ...
    'MarkerEdgeColor', [0.635 0.078 0.184], 'MarkerSize', 1, ...
    'HandleVisibility','off');
text(ax, f(idxPeak)+0.3, Vpeak*0.95, ...
    sprintf('f_n = %.2f Hz\nV_{max} = %.3f V', f(idxPeak), Vpeak), ...
    'FontSize', 24, 'Color', [0.2 0.2 0.2], ...
    'VerticalAlignment','top');
xlabel(ax, 'Frequency (Hz)', 'FontSize', 20, 'FontWeight','normal');
ylabel(ax, 'Voltage (V)', 'FontSize', 20, 'FontWeight','normal');
title(ax, 'Frequency Response with Voltage for the analytical model ', ...
     'FontSize', 20, 'FontWeight','normal');
xlim(ax, [f(1), f(end)]);
ylim(ax, [0, Vpeak*1.15]);
set(ax, 'FontSize', 24, 'FontName','Helvetica', ...
   'LineWidth', 1, 'TickDir','in', ...
   'XMinorTick','off', 'YMinorTick','off', ...
   'GridAlpha', 0.5, 'MinorGridAlpha', 0.12);
```

```
grid(ax, 'on');
ax.GridLineStyle = '-';
ax.MinorGridLineStyle = ':';
set(fig, 'Renderer', 'painters');   % vector renderer -> crisp lines/text
fprintf('Resonance frequency (voltage peak): %.3f Hz\n', f(idxPeak));
fprintf('Peak voltage: %.4f V\n', Vpeak);
exportgraphics(fig, 'FreqResponse_Voltage.png', 'Resolution', 600);
exportgraphics(fig, 'FreqResponse_Voltage.pdf', 'ContentType', 'vector');
```

Voltage and frequency obtained from the experimental work

```
clear; clc; close all;
frequency = [ ...
    7, 7.5, 8, 8.5, 9, 9.5, 10.2, 10.5, 11, ...11.5, 12, 12.5, 13, 13.5, 14, 14.5,15];

voltage = [ ...0.00105, 0.0365, 0.0780, 0.1201, 0.1620, 0.201, ...0.24509, 0.2290,
0.1956, 0.1640, 0.12941, ...0.1030600, 0.07510, 0.0508, 0.0281, 0.00945, 0.00113];
f_smooth = linspace(min(frequency), max(frequency), 6000);
v_smooth = interp1(frequency, voltage, f_smooth, 'pchip');
[v_max, idx] = max(voltage);
f_max = frequency(idx);
fprintf('Peak measured voltage: %.4f V at %.2f Hz\n', v_max, f_max);
fig = figure('Units','centimeters', 'Position',[5 5 20 14], 'Color','w');
ax = axes(fig); hold(ax,'on'); box(ax,'on');
plot(ax, f_smooth, v_smooth, '-', ...
     'LineWidth', 7, ...
     'Color', [0 0.4470 0.7410]);
% Experimental points
plot(ax, frequency, voltage, 'o', ...
     'MarkerSize', 10, ...
     'MarkerFaceColor', [0 0.4470 0.7410], ...
     'MarkerEdgeColor', 'black', 'LineWidth', 0.75);

plot(ax, f_max, v_max, 's', 'MarkerFaceColor', [0.635 0.078 0.184], ...
     'MarkerEdgeColor', [0.635 0.078 0.184], 'MarkerSize', 8);
text(ax, f_max+0.3, v_max, sprintf(' %.4f V', v_max), ...
     'FontName','Times New Roman', 'FontSize', 24, 'Color', [0.2 0.2 0.2]);

xlabel(ax, 'Fundamental Frequency (Hz)', ...
    'FontName','Times New Roman', 'FontSize', 24, 'FontWeight','normal');
ylabel(ax, 'Output Voltage (V)', ...
    'FontName','Times New Roman', 'FontSize', 24, 'FontWeight','normal');
title(ax, 'Experimental Measured Voltage at different Excitation Frequencies', ...
    'FontName','Times New Roman', 'FontSize', 20, 'FontWeight','bold');
xlim(ax, [6.8 15.2]);
ylim(ax, [0, max(v_smooth)*1.15]);

grid(ax, 'on');
grid(ax, 'minor');
set(ax, 'GridAlpha', 0.4, 'MinorGridAlpha', 0.25, ...
        'FontName','Times New Roman', 'FontSize', 24, ...
        'LineWidth', 1.1, 'TickDir','in', ...
        'XMinorTick','on', 'YMinorTick','on');

set(fig, 'Renderer', 'painters');   % vector renderer -> crisp lines/text
exportgraphics(fig, 'Voltage_Frequency_MFC.pdf', 'ContentType','vector');
exportgraphics(fig, 'Voltage_Frequency_MFC.png', 'Resolution', 600);
```

Experimental, theoretical, and numerical voltage and power with Eigenfrequency

```
clear; clc; close all;
f_exp = [7 7.5 8 8.5 9 9.5 10.22 10.56 11 11.5 12 12.5 13 13.5 14 14.5 15];
f_the = [7 7.5 8 8.5 9 9.5 10 10.69 11 11.5 12 12.5 13 13.5 14 14.5 15];
f_num = [7 7.5 8 8.5 9 9.5 10.5 10.976 11.2 11.5 12 12.5 13 13.5 14 14.5 15];
V_exp = [0.045 0.0599 0.0820 0.10601 0.1420 0.1801 ... 0.24506 0.2268 0.2086 0.1780
0.14480 ... 0.11608 0.08800 0.0608 0.0389 0.026798 0.0143];
V_the = [0.0518 0.06860 0.08730 0.114 0.14689 0.18821 ... 0.22101 0.26502 0.23540 0.20874
0.1763 ... 0.14657 0.12057 0.100274 0.07801 0.05942 0.04631];
V_num = [0.05902 0.0756 0.0983 0.1320 0.16916 0.20661 ... 0.2681 0.28002 0.26394 0.23950
0.20086 ...0.16943 0.1377 0.11414 0.09001 0.06972 0.05631];
P_exp = [0.00015 0.000298 0.000560 0.000887 0.001450 ... 0.002061 0.002704 0.002390
0.001822 ... 0.001281 0.000798 0.000506 0.000269 ... 0.000123 0.000038 0.000004
0.00000006];
P_the = [2.02E-4 4.38E-4 7.44E-4 1.08E-3 1.63E-3 ... 2.05E-3 2.48E-3 2.901E-3 2.25E-3 ...
1.62E-3 1.14E-3 7.8E-4 5.7E-4 ...3.59E-4 2.83E-4 2.23E-4 2.05E-4];
P_num = [2.49E-4 4.86E-4 8.29E-4 1.23E-3 1.76E-3 ...2.20E-3 2.88E-3 3.20E-3 2.4626E-3 ...
 0.001956 0.001381 9.80E-4 6.40E-4 ... 4.98E-4 3.59E-4 2.66E-4 2.10E-4];
% Power values above are in mW already per the original data set
plotComparison(f_exp, V_exp, f_the, V_the, f_num, V_num, ...
   'Voltage (V)', 'V', ...
   'Voltage Comparison: Experimental vs Theoretical vs Numerical', ...
   'Voltage_Comparison_MFC');
plotComparison(f_exp, P_exp, f_the, P_the, f_num, P_num, ...
   'Power (mW)', 'mW', ...
   'Power Comparison: Experimental vs Theoretical vs Numerical', ...
   'Power_Comparison_MFC');
function plotComparison(f1, y1, f2, y2, f3, y3, yLabelStr, unitStr, titleStr, fileStem)
   % Consistent color palette (matches other figures in this series)
   colExp = [0.10 0.10 0.10];    % near-black
   colThe = [0    0.2078 0.7412];% blue
   colNum = [0.635 0.078 0.184]; % dark red
   fig = figure('Units','centimeters', 'Position',[5 5 22 15], 'Color','w');
   ax = axes(fig); hold(ax,'on'); box(ax,'on');
   plot(ax, f1, y1, '-o', 'LineWidth', 2, 'MarkerSize', 6, ...
       'Color', colExp, 'MarkerFaceColor', colExp);
   plot(ax, f2, y2, '-^', 'LineWidth', 2, 'MarkerSize', 6, ...
       'Color', colThe, 'MarkerFaceColor', colThe);
   plot(ax, f3, y3, '-s', 'LineWidth', 2, 'MarkerSize', 6, ...
       'Color', colNum, 'MarkerFaceColor', colNum);
   % Peak values
   [y1max, id1] = max(y1);  f1max = f1(id1);
   [y2max, id2] = max(y2);  f2max = f2(id2);
   [y3max, id3] = max(y3);  f3max = f3(id3);
   plot(ax, f1max, y1max, 'o', 'MarkerFaceColor', colExp, ...
       'MarkerEdgeColor', colExp, 'MarkerSize', 9, 'HandleVisibility','off');
```

```
    plot(ax, f2max, y2max, '^', 'MarkerFaceColor', colThe, ...
        'MarkerEdgeColor', colThe, 'MarkerSize', 9, 'HandleVisibility','off');
    plot(ax, f3max, y3max, 's', 'MarkerFaceColor', colNum, ...
        'MarkerEdgeColor', colNum, 'MarkerSize', 9, 'HandleVisibility','off');
    text(ax, f1max+0.2, y1max, sprintf(' %.4g %s\n %.2f Hz', y1max, unitStr, f1max), ...
       'FontName','Times New Roman', 'FontSize', 11, 'Color', colExp);
    text(ax, f2max+0.2, y2max, sprintf(' %.4g %s\n %.2f Hz', y2max, unitStr, f2max), ...
       'FontName','Times New Roman', 'FontSize', 11, 'Color', colThe);
    text(ax, f3max+0.2, y3max, sprintf(' %.4g %s\n %.3f Hz', y3max, unitStr, f3max), ...
       'FontName','Times New Roman', 'FontSize', 11, 'Color', colNum);
    xlabel(ax, 'Excitation Frequency (Hz)', ...
       'FontName','Times New Roman', 'FontSize', 17, 'FontWeight','bold');
    ylabel(ax, yLabelStr, ...
       'FontName','Times New Roman', 'FontSize', 17, 'FontWeight','bold');
    title(ax, titleStr, ...
       'FontName','Times New Roman', 'FontSize', 15, 'FontWeight','normal');
    legend(ax, {'Experimental', 'Theoretical', 'Numerical'}, ...
       'FontName','Times New Roman', 'FontSize', 13, ...
       'Location','best', 'Box','on');
    xlim(ax, [f1(1)-0.3, f1(end)+0.3]);
    grid(ax, 'on');
    grid(ax, 'minor');
    set(ax, 'GridAlpha', 0.3, 'MinorGridAlpha', 0.15, ...
          'FontName','Times New Roman', 'FontSize', 14, ...
          'LineWidth', 1.2, 'TickDir','out', ...
          'XMinorTick','on', 'YMinorTick','on');
    set(fig, 'Renderer', 'painters');   % vector renderer -> crisp lines/text
    % Export: EMF (vector, editable in Word — Windows only) + high-res TIFF
    exportgraphics(fig, [fileStem '.emf'], 'ContentType','vector');
    exportgraphics(fig, [fileStem '.tiff'], 'Resolution', 600);
    exportgraphics(fig, [fileStem '.pdf'], 'ContentType','vector');
end
```